LABRADOR – ISLAND TRANSMISSION LINK ENVIRONMENTAL ASSESSMENT

Marine Environment and Effects Modelling Component Study

November 2011

nalcor energy
LOWER CHURCHILL PROJECT

LABRADOR – ISLAND TRANSMISSION LINK ENVIRONMENTAL ASSESSMENT
Environmental Component Studies: Introduction and Overview

Nalcor Energy is proposing to develop the *Labrador – Island Transmission Link* (the Project), a High Voltage Direct Current (HVdc) electrical transmission system extending from Central Labrador to the Avalon Peninsula on the Island of Newfoundland.

The Project was registered under the Newfoundland and Labrador *Environmental Protection Act* (*NLEPA*) and the *Canadian Environmental Assessment Act* (*CEAA*) in January 2009 (with subsequent amendments and updates), in order to initiate the provincial and federal environmental assessment (EA) processes. Following public and governmental review of that submission, an Environmental Impact Statement (EIS) was required for the Project. The EIS is being developed by Nalcor Energy, in accordance with the requirements of both *NLEPA* and *CEAA* and the *EIS Guidelines and Scoping Document* issued by the provincial and federal governments.

In support of the Project's EIS, Nalcor Energy has undertaken a series of environmental studies to collect and/or compile information on the existing biophysical and socioeconomic environments and to identify and assess potential Project-environment interactions. This environmental study program has included field surveys, associated mapping and analysis, environmental modeling, and the compilation and analysis of existing and available information and datasets on key environmental components. This report comprises one of these supporting environmental studies.

A general guide to these Environmental Component Studies, some of which are comprised of multiple associated reports, is provided on the opposite page.

The information reported herein will be incorporated into the Project's EIS, along with any additional available information, to describe the existing (baseline) environmental conditions and/or for use in the assessment and evaluation of the Project's potential environmental effects and in the identification and development of mitigation.

This study focuses on the relevant aspects of the proposed Project – including the proposed and alternative HVdc transmission corridors, marine cable crossings, and/or other Project components and activities – as known and defined at the time that the EA process was initiated and/or when the study commenced. Project planning and design are ongoing, and as is the case for any proposed development, the Project description has and will continue to evolve as engineering and EA work continue. The EIS itself will describe and assess the specific Project components and activities for which EA approval is being sought, and will also identify and evaluate other, alternative means of carrying out the Project that are technically and economically feasible as is required by EA legislation.

The EIS and these Component Studies will be subject to review by governments, Aboriginal and stakeholder groups and the public as part of the EA process.

Nalcor Energy – Lower Churchill Project

LABRADOR-ISLAND TRANSMISSION LINK: ENVIRONMENTAL COMPONENT STUDIES (CSs)		
1) Vegetation CS	**Report 1a** **Ecological Land Classification**	**Report 1b** **Wetlands Inventory & Classification**
	Report 1c **Regionally Uncommon Plants Model**	**Report 1d** **Timber Resources**
	Report 1e **Vegetation Supplementary Report**	
2) Avifauna CS		
3) Caribou & Other Large Mammals CS	**Report 3a** **Caribou & Their Predators**	**Report 3b** **Moose & Black Bear**
4) Furbearers & Small Mammals CS		
5) Marine Environment: **Fish & Fish Habitat, Water Resources CS**	**Report 5a** **Marine Fish: Information Review**	**Report 5b** **Marine Flora, Fauna & Habitat Survey**
	Report 5c **Marine Habitats (Geophysical) Survey**	**Report 5d** **Water, Sediment & Benthic Surveys**
	Report 5e **Marine Surveys: Electrode Sites**	**Report 5f** **Marine Surveys: Supplementary**
6) Freshwater Environment: **Fish & Fish Habitat, Water Resources CS**		
7) Marine Environment: **Marine Mammals, Sea Turtles & Seabirds CS**	**Report 7a** **Marine Mammals, Sea Turtles & Seabirds: Information Review**	**Report 7b** **Marine Mammal & Seabird Surveys**
	Report 7c **Ambient Noise & Marine Mammal Surveys**	
8) Species of Special Conservation Concern CS		
9) Marine Environment & Effects Modelling CS	**Report 9a** **Strait of Belle Isle: Oceanographic Environment & Sediment Modelling**	**Report 9b** **Strait of Belle Isle: Marine Sound Modelling - Cable Construction**
	Report 9c **Electrodes: Environmental Modelling**	
10) Historic & Heritage Resources CS		
11) Socioeconomic Environment: **Communities, Land & Resource Use, Tourism & Recreation CS**	**Report 11a** **Communities, Land & Resource Use, Tourism & Recreation**	**Report 11b** **Current Levels of Accessibility Along the Transmission Corridor**
12) Socioeconomic Environment: **Aboriginal Communities & Land Use CS**		
13) Socioeconomic Environment: **Marine Fisheries in the Strait of Belle Isle CS**		
14) Viewscapes CS		

Environmental Component Study Required Under the EIS Guidelines: Comprising Reports (Shaded cells above)	
Avifauna: 2, 7a, 7b	Furbearers: 4
Caribou (and Predators): 3a	Timber Resources: 1d
Water (Quality and Quantity): 5a, 5d, 5e, 5f, 6	Marine and Freshwater Fish and Fish Habitat: 5, 6, 7, 13
Species at Risk: 8	Historic Resources: 10
Viewscapes: 14	Socioeconomics: 11, 12, 13
Environmental study reports submitted as additional background information: 1a, 1b, 1c, 1e, 3b, 9	

Labrador – Island Transmission Link

Marine Environment and Effects Modelling Component Study

Preface

This *Marine Environment and Effects Modelling Component Study* has been prepared and submitted as part of the Environmental Assessment (EA) of the proposed **Labrador-Island Transmission Link** (the Project).

This submission (November 2011) is comprised of three (3) study reports:

1) **Strait of Belle Isle: Oceanographic Environment and Sediment Modelling** (June 2011): A study to model the likely characteristics of sedimentation that may occur as a result of marine construction activities associated with the Strait of Belle Isle submarine cable crossing.

2) **Sound Modelling: Proposed Strait of Belle Isle Cable Installation Activities** (June 2011): A study to estimate and describe potential sound levels resulting from the proposed construction activities associated with underwater cable installation in the Strait of Belle Isle.

3) **Environmental Modelling: Proposed Shore Electrodes** (August 2011): A study to estimate the emissions associated with monopolar and bipolar operations of the electrodes for two HVdc system voltages, 320 kV and 400 kV.

The environmental modelling presented in this *Marine Environment and Effects Modelling Component Study* will be incorporated and used in the Project's eventual Environmental Impact Statement (EIS), which will provide a summary description of the existing environment and an environmental effects assessment for the Project.

Labrador – Island Transmission Link

Strait of Belle Isle:
Oceanographic Environment and Sediment Modelling

Prepared for:

Nalcor Energy
Hydro Place, 500 Columbus Drive, PO Box 12800
St. John's, Newfoundland and Labrador
Canada A1B 0C9

Contract #LC-EV-018

Prepared by:

AMEC Earth & Environmental
A division of AMEC Americas Limited
133 Crosbie Road
St. John's, Newfoundland and Labrador
Canada A1B 4A5

AMEC Project #TN09210180

June 17, 2011

EXECUTIVE SUMMARY

Nalcor Energy is proposing to develop the *Labrador – Island Transmission Link* (the Project), a high voltage direct current (HVdc) transmission system extending from Central Labrador to the Island of Newfoundland's Avalon Peninsula.

The Strait of Belle Isle submarine cable crossing component of the Project will likely see the installation of three mass impregnated cables under and across the Strait of Belle Isle. Cable installation will initially involve the development of three horizontal directionally drilled holes from on-land, potentially at Forteau Point on the Labrador side and at Shoal Cove on the Newfoundland side, extending underground for up to several kilometres. Three cables will then be installed through the drill holes and along the seabed and each will be protected by a dedicated rock berm, approximately 30 to 35 km long (depending their specific routings). The three rock berms will each be approximately 0.8 to 1.5 m high and 8 to 12 m wide at the base, and will be comprised of approximately 1 million tonnes of rock in total placed by a fall pipe vessel. The rock size has been specified to be 2-8" graded.

In preparation for, and in support of, the Project's environmental assessment, this Study has been completed to model and describe key aspects of the existing oceanographic environment, as well as model the likely characteristics of sedimentation that may occur as a result of marine construction activities associated with the Strait of Belle Isle submarine cable crossings.

The first step of the study involved the creation of a hydrodynamic model to simulate the current fields and other hydrodynamic processes (such as water elevation). The second step involved creating a sediment transport model that used the current fields output of the hydrodynamic model to simulate the dispersion of the sediment material that may be released as a result of construction activities.

The hydrodynamic model was based on bathymetric data previously acquired by Nalcor Energy and forced by tidal water level variations. Tidal measurements were obtained from four tidal gauges installed in the Strait of Belle Isle specifically for this study. A tide-only simulation was performed initially and then validated against historical data. A second simulation of currents associated with the Strait as a result of atmospheric forcing was conducted using information from the scientific literature. Overall, the output and validation process was successful and demonstrated the ability of the model to reproduce water level and current fluctuations associated with tides and atmospheric forcing.

The sediment dispersion model was developed using information from surficial sea-bottom survey results previously acquired by Nalcor Energy and the output of the hydrodynamic tidal simulation. Available information regarding the proposed construction activities in the marine environment (i.e., rock placement) was also compiled to provide a hypothetical scenario of bottom sediment release.

The key results of the sediment dispersion model demonstrated:

- the most noticeable effect, specifically, that of suspended sediment concentrations over 100 mg/L, following the rock placement activities was found to be relatively limited to within a few hundred metres of the activity location;

- the maximum thickness of material potentially deposited was found to be very small with values ranging from about 0.1 mm to a maximum of 1.5 mm; and
- the duration of elevated suspended sediment concentration (over 100 mg/L) was found to range from 1 hour for various locations along and near the corridor with total area 10.9 km^2, to 100 hours or more for fewer locations totaling 1.3 km^2 in area.

Table of Contents

List of Figures

List of Tables

1.0 INTRODUCTION

Nalcor Energy is proposing to develop the *Labrador – Island Transmission Link*, a High Voltage Direct Current (HVdc) transmission system extending from Central Labrador to the Island of Newfoundland's Avalon Peninsula, that will include the construction and operation of marine cables across the Strait of Belle Isle.

The environmental assessment (EA) process for the Project was initiated in January 2009 and is in progress. An Environmental Impact Statement (EIS) is being prepared by Nalcor Energy, which will be submitted for review by governments, Aboriginal and stakeholder groups and the public.

In preparation for and support of the EA of the Project this *Oceanographic Environment and Sediment Modelling Study* has been completed with the objective to model and describe key aspects of the existing oceanographic environment, as well as model the likely characteristics of sedimentation that may occur as a result of marine construction activities associated with the Strait of Belle Isle submarine cable crossings.

1.1 Project Overview

The proposed *Labrador – Island Transmission Link* (the Project) involves the construction and operation of transmission infrastructure within and between Labrador and the Island of Newfoundland. Nalcor Energy is proposing to establish an HVdc transmission system extending from Central Labrador to Newfoundland's Avalon Peninsula.

The proposed transmission system, as currently planned, will include the following key components:

- an ac-dc converter station near the lower Churchill River in Central Labrador, adjacent to the switchyard for the Lower Churchill Hydroelectric Generation Project;
- an HVdc transmission line extending across Southeastern Labrador to the Strait of Belle Isle. This overhead transmission line will be approximately 400 km in length with a cleared right-of-way averaging approximately 60 m wide, and consist of single galvanized steel lattice towers;
- cable crossings of the Strait of Belle Isle with associated infrastructure, including cables placed across the Strait through various means to provide the required cable protection;
- an HVdc transmission line (similar to that described above) extending from the Strait of Belle Isle across the Island of Newfoundland to the Avalon Peninsula, for a distance of approximately 700 km;
- a dc-ac converter station at Soldiers Pond on the Island of Newfoundland's Avalon Peninsula; and
- electrodes at each end of the HVdc transmission line in Labrador and on the Island, with overhead lines connecting them to their respective converter stations.

Project planning and design are currently at a stage of having identified a 2 km wide corridor for the on-land portions of the proposed HVdc transmission line and a 500 m wide corridor for the proposed Strait of Belle Isle cable crossings. The proposed cable crossing corridor is shown in Figure 1.1-1. The proposed transmission corridor reaches the Strait of Belle Isle shores at Forteau Point in Labrador, and resumes at Shoal Cove in Newfoundland.

It is these proposed transmission corridors and components that were the subject of Nalcor Energy's environmental study program. Project planning is in progress, and it is anticipated that the Project description will continue to evolve as engineering and design work continue. The EA of the Project will also identify and evaluate alternative means of carrying out the Project that are technically and economically feasible. In conjunction and concurrent with the EA process, Nalcor Energy will be continuing with its technical and environmental analyses of the corridors, in order to identify and select a specific routing for the Project. The eventual transmission routes and locations will be selected with consideration of technical, environmental and socioeconomic factors.

The Strait of Belle Isle submarine cable crossing component of the Project will likely see the installation of three mass impregnated (MI) cables under and across the Strait of Belle Isle. Cable installation will initially involve the development of three horizontal directionally drilled (HDD) holes from on-land, potentially at Forteau Point on the Labrador side and at Shoal Cove on the Newfoundland side, extending out and under the Strait on both sides for up to several kilometres. These HDD holes will each extend for a distance of approximately 1.5 to 2.5 km, out to a water depth of approximately 80 m. Three cables will then be installed through the HDD holes and from there across the seabed and each will be protected by a dedicated rock berm, approximately 30 to 35 km long (depending on their specific routings). The three rock berms will each be approximately 0.8 to 1.5 m high and 8 to 12 m wide at the base, and be comprised of approximately 1 million tonnes of rock in total placed by a fall pipe vessel. The rock has been specified to be 2-8" graded.

A detailed description of the Project, including the key components and construction activities associated with the Strait of Belle Isle cable crossings, will be provided in the EIS.

1.2 Study Purpose and Objectives

In preparation for and support of the EA of the Project, this *Strait of Belle Isle: Oceanographic Environment and Sediment Modelling Study* was completed to model and describe key aspects of the existing oceanographic environment, as well as the likely characteristics of sedimentation that may occur as a result of proposed marine construction activities associated with the Strait of Belle Isle submarine cable crossings, for use in the eventual marine environmental effects analyses in the EIS.

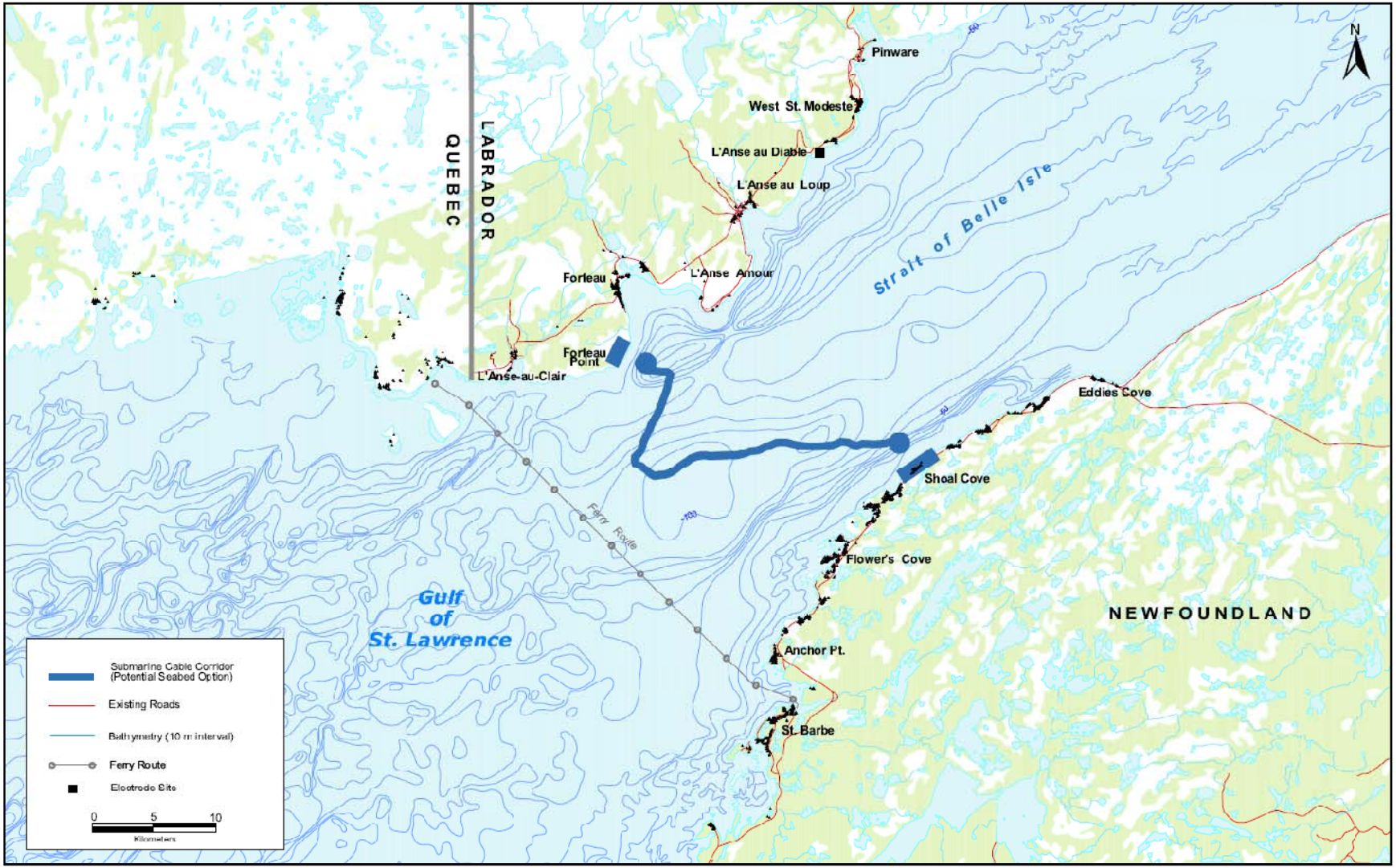

Figure 1.1-1: Study Area and Strait of Belle Isle Submarine Cable Crossing Corridor.

2.0 APPROACH AND METHODS

To assess the nature and zone of influence of marine construction operations and sediment release in a marine environment, the environment setting of the study area must be characterized, including weather (or atmospheric forcing conditions), water stratification, waves, tides, ocean currents and circulation, and sediment bottom characteristics. The activities involved, including techniques to be used, and the rate of sediment release also need to be understood.

Based on this analysis and on available site-specific data, a model can then be developed and refined and the limits of available data and model limitations can be determined. Two numerical models were created for this study:

1) a *Hydrodynamic Model*: a model able to simulate the current fields associated with water level variations (tidal or atmospheric forcing); and

2) a *Sediment Transport Model* using the above to simulate the transportation and dispersal of the sediment material released by the proposed marine construction activities.

Section 2.1 describes the atmospheric and oceanographic environmental settings of the study area, based on a literature review and on the site-specific measurements that were collected. Section 2.2 describes the setup and implementation of the two numerical models.

2.1 Environmental Setting

The Strait of Belle Isle and Cabot Strait connect the Gulf of St. Lawrence to the North Atlantic Ocean. Although the Cabot Strait is wider and deeper, the Strait of Belle Isle significantly influences the oceanography of the Gulf, as discussed in Section 2.1.2. As shown in Figure 1.1-1, the Strait of Belle Isle is approximately 17 km wide at the narrowest point and about 125 km long, lying between the Labrador coast to the north and the Newfoundland coast to the south. The deepest water in the Strait is about 125 m (Figure 2.1-1).

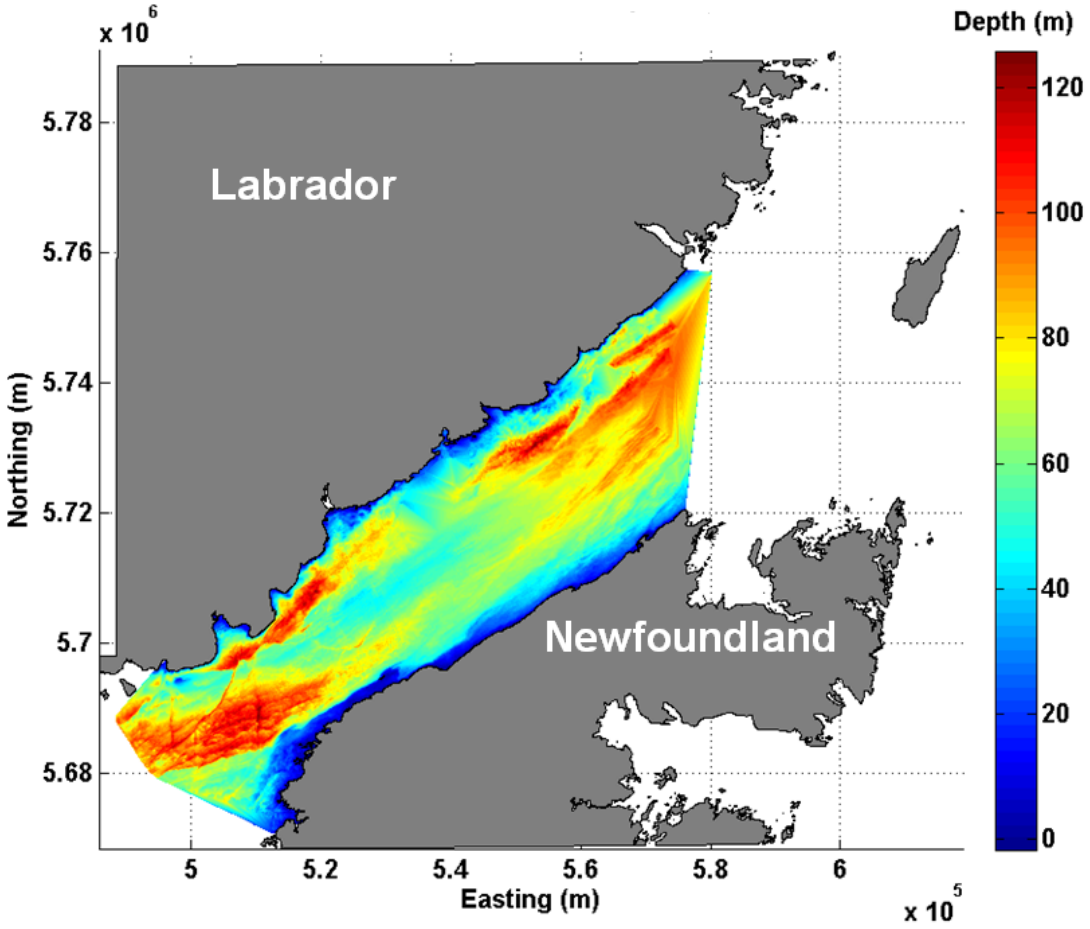

Figure 2.1-1: Strait of Belle Isle, Bathymetry (based on CHS and Fugro GEOS 2007a and 2007b data).

2.1.1 Atmospheric Setting

Weather in the Strait of Belle Isle is greatly influenced by atmospheric pressure trends and wind direction, the distribution of which depends on the prevailing storm tracks in the region. Monthly and annual weather statistics are presented in the following subsections. In addition to these factors, the presence of sea ice in the area can contribute toward the observed weather conditions in the area.

2.1.1.1 Atmospheric (Sea Level) Pressure

Atmospheric pressure gradients contribute to large-scale wind fields over the Strait area and near-surface ocean currents.

The Strait surface currents are correlated with cross-Strait pressure gradients and are uncorrelated with along-Strait pressure gradients (Garrett and Toulany, 1981). Generally, the pressure difference between Gander and Goose Bay is a measure of the cross-Strait pressure gradient while the difference between the average Gander/Goose Bay axis (Figure 2.1-2) and Grindstone Island is a measure of the along-Strait pressure gradient.

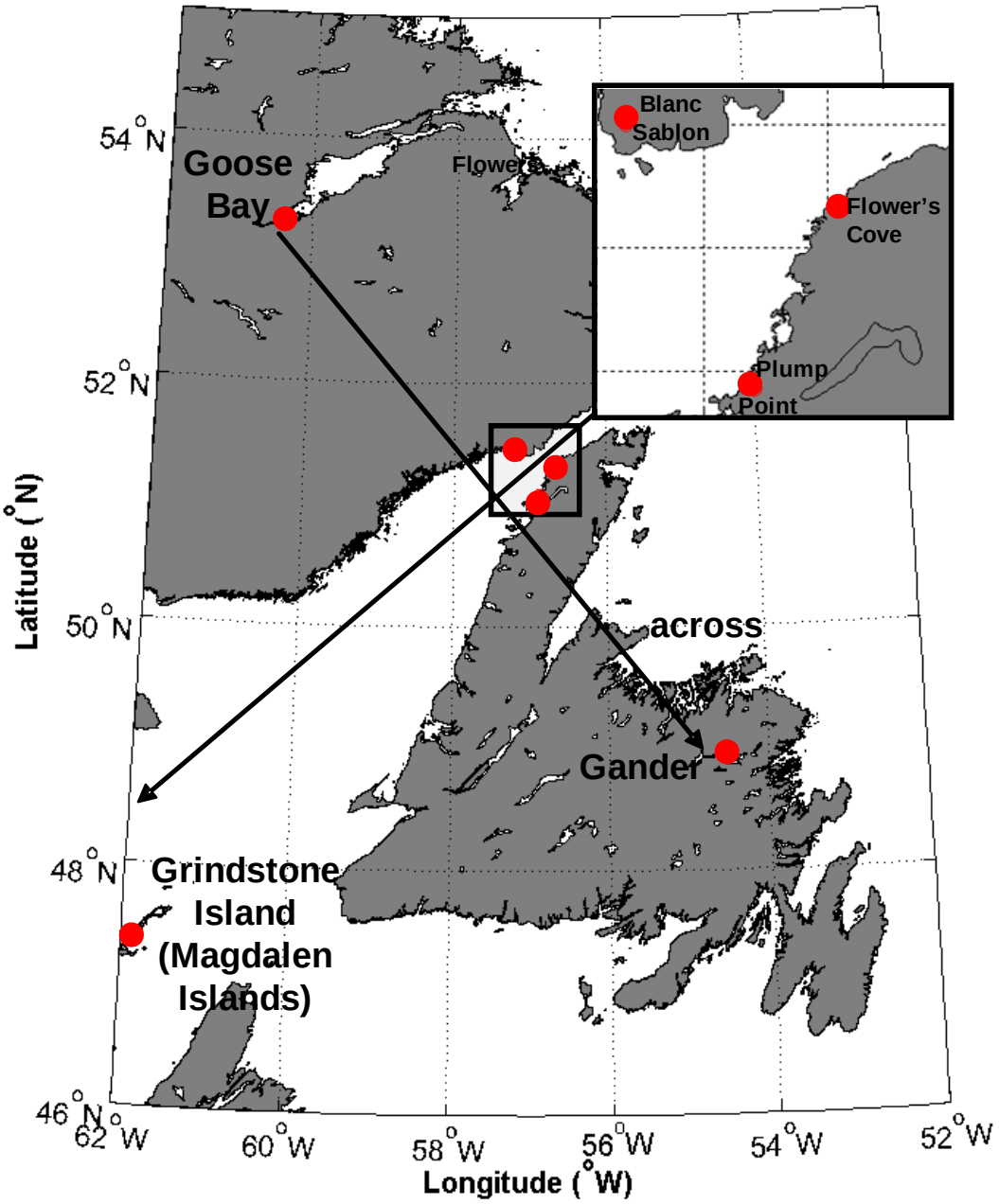

Figure 2.1-2: Strait of Belle Isle, Weather Stations and Coordinate System.

Average monthly atmospheric pressures of the three stations, Gander, Goose Bay, and Grindstone Island (30 year Canadian Climate Normals, Environment Canada, 2010a, 2010b) were therefore used to study the pressure gradients over the Strait and are presented in Table 2.1-1. The difference between Gander and Goose Bay monthly average values divided by the distance between those two stations (645 km) provides the monthly averaged cross-Strait pressure gradient. For the along-Strait, the average of Gander and Goose Bay monthly mean values were subtracted from the monthly averaged pressure of Grindstone Island and then divided by the distance between the midpoint of the Goose Bay-Gander axis and Grindstone Island (523 km).

As illustrated in Table 2.1-1, the cross-Strait gradient is negative all winter and spring (from December to April), and becoming positive during summer (June to October). The along-Strait gradient is negative from January to June, increasing in strength to a maximum in April, and then decreasing toward the summer months. The along-Strait gradient could be expected to be positive during summer but only the September value is available. In the fall, this gradient is null.

Table 2.1-1: Atmospheric Pressure Gradients in the Strait of Belle Isle.

		Jan	Feb	Mar	Apr	May	Jun	Jul	Aug	Sep	Oct	Nov	Dec	Year
A	**Gander (kPa)**	100.8	100.9	101.1	101.2	101.4	101.3	101.3	101.4	101.4	101.4	101.1	100.9	101.2
B	**Goose Bay (kPa)**	100.9	101.1	101.2	101.4	101.4	101.1	100.9	101.1	101.1	101.2	101.1	101.1	101.1
C	**Grindstone Island (kPa)**	100.8	100.9	100.9	101.0	101.2	101.1	N	N	101.4	101.3	101.1	N	N
D = (A+B)/ 2	**Average Gander– Goose Bay (kPa)**	100.85	101.0	101.15	101.3	101.4	101.2	101.1	101.25	101.25	101.3	101.1	101.0	101.15
1000x (A-B) /645	**Cross-Strait Gradient (Pa/km)**	-0.155	-0.310	-0.155	-0.310	0	0.310	0.620	0.465	0.465	0.310	0	-0.310	0.155
1000x (C-D) /523	**Along-Strait Gradient (Pa/km)**	-0.096	-0.191	-0.478	-0.574	-0.382	-0.191	N	N	0.287	0	0	N	N

Sources are Canadian Climate Normals: 1971-2000 for Gander, Goose Bay, and 1961-1990 for Grindstone Island
N = data exist, but not enough to derive a value

2.1.1.2 Temperatures and Precipitation

Climate statistics were derived using three Environment Canada weather stations located near the Strait of Belle Isle: Blanc Sablon, Flower's Cove and Plum Point (AMEC, 2007) (Figure 2.1-2). Monthly air temperature and precipitation statistics from that study are presented in Table 2.1-2, Figure 2.1-3, and Figure 2.1-4 (AMEC, 2007). Daily maximum temperatures drop below zero in December and remain below zero through early spring. Maximum temperatures peak above 15 °C during July and August, while minimum temperatures reach their lowest values in January and February at between -15 and -20 °C. The daily minimum temperature is, on average, below freezing from November through April.

Average total precipitation amounts are quite similar through each month of the year, while the first measurable snowfall generally occurs during October. On average, rainfall amounts in this region are twice as much as snowfall amounts during the year (assuming 1 cm of snowfall is roughly equivalent to 1 mm of rainfall).

Table 2.1-2: Monthly Climate Averages for the Strait of Belle Isle (1971-2000).

	Jan	Feb	Mar	Apr	May	Jun	Jul	Aug	Sep	Oct	Nov	Dec	Year
Temperature:													
Daily Average (°C)	-11.4	-11.7	-6.7	-0.8	4.0	8.5	12.7	13.3	9.7	4.2	-0.8	-6.9	1.2
Daily Maximum (°C)	-6.9	-7.2	-2.6	2.6	7.7	12.5	16.5	17.0	13.3	7.4	2.3	-3.1	5.0
Daily Minimum (°C)	-16.0	-16.1	-10.8	-4.1	0.1	4.4	8.9	9.7	6.0	1.0	-3.9	-10.7	-2.6
Precipitation:													
Rainfall (mm)	16.1	10.5	20.0	28.8	68.8	104.5	109.8	104.5	101.2	90.8	58.4	29.9	743.3
Snowfall (cm)	91.1	71.4	63.6	32.9	8.7	1.1	0.0	0.0	0.0	7.2	26.6	67.6	370.1
Precipitation (mm)	107.2	82.0	83.7	61.9	77.4	105.6	109.8	104.5	101.2	97.9	85.0	97.5	1113.5
Days with Rainfall:													
>= 0.2 mm	3.0	2.5	4.7	7.3	13.5	16.4	17.3	15.7	15.8	15.9	10.3	4.8	127.2
>= 5 mm	1.1	0.9	1.5	2.1	4.7	6.8	6.8	6.6	6.4	6.5	3.9	2.0	49.3
>= 10 m	0.5	0.2	0.6	0.8	2.0	3.5	3.3	3.4	3.6	3.0	1.6	1.0	23.5
>= 25 mm	0.0	0.0	0.0	0.0	0.2	0.6	0.7	0.7	0.7	0.3	0.3	0.1	3.6
Days With Snowfall:													
>= 0.2 cm	17.1	14.9	13.5	8.9	2.6	0.3	0.0	0.0	0.0	2.2	8.3	15.1	82.8
>= 5 cm	7.2	5.6	4.9	2.5	0.5	0.1	0.0	0.0	0.0	0.4	1.7	5.6	28.6
>= 10 cm	2.7	2.1	1.9	0.8	0.2	0.0	0.0	0.0	0.0	0.2	0.5	1.7	10.0
>= 25 cm	0.2	0.1	0.2	0.1	0.0	0.0	0.0	0.0	0.0	0.0	0.0	0.0	0.6
Days with Precipitation:													
>= 0.2 mm	18.2	16.2	16.1	14.3	15.3	16.4	17.4	15.7	15.8	16.7	16.5	17.7	196.3
>= 5 mm	8.2	6.5	6.5	4.7	5.2	6.8	6.8	6.6	6.4	7.0	5.9	7.8	78.3
>= 10 mm	3.5	2.3	2.6	1.7	2.3	3.6	3.3	3.4	3.6	3.2	2.3	3.1	34.8
>= 25 mm	0.2	0.1	0.2	0.1	0.2	0.6	0.7	0.7	0.7	0.3	0.4	0.2	4.5

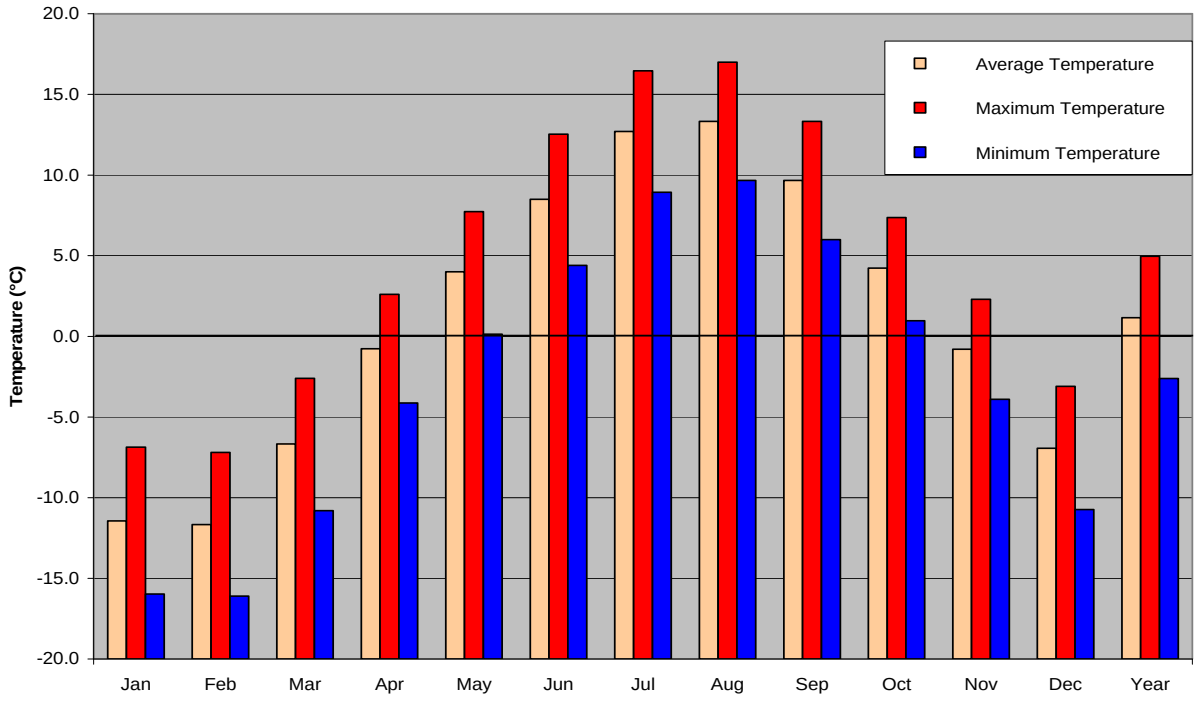

Figure 2.1-3: Strait of Belle Isle, Monthly Average, Maximum, and Minimum Air Temperatures.

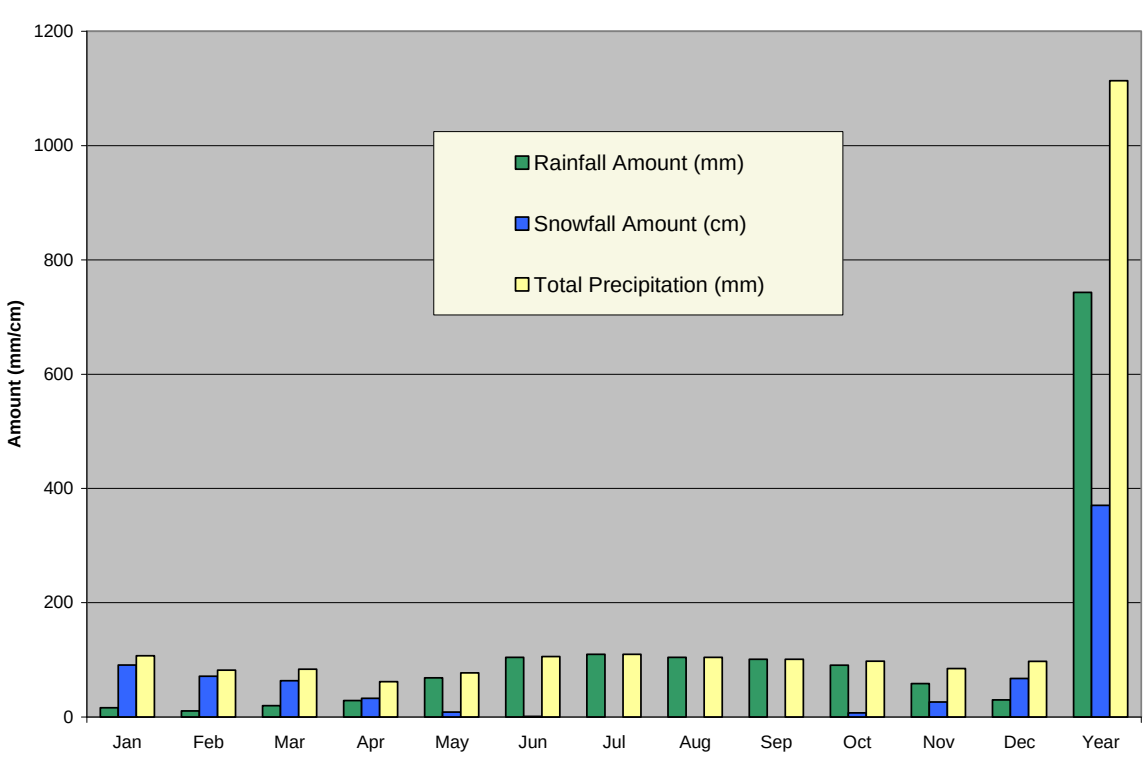

Figure 2.1-4: Strait of Belle Isle, Monthly Rainfall, Snowfall and Total Precipitation Amounts.

2.1.1.3 Winds

Directional wind statistics were calculated by AMEC (2007) using the MSC50, a wind and wave hindcast of hourly data of the North Atlantic Ocean provided by the Meteorological Services of Canada (Swail et al., 2006). The data cover the years 1954 to 2005, inclusive, and include consideration of periods with sea ice cover.

Annual and monthly wind roses for the MSC50 node #18071 (51.4° N, 56.8° W) are presented in Figure 2.1-5 and Figure 2.1-6. They indicate that winds are frequently aligned with the Strait, with predominant winds from the southwest. On average, the predominant flow is from the west or northwest during January to March, while a blend of northeast and southwest winds are expected from April to June. These wind directions are highly dependent on the two major storm tracks; one track takes lows through Labrador, while the other low which produces northeast winds passes through Newfoundland. Wind roses for July to December show that the majority of winds during the summer and early fall originate from the southwest, then begin to veer to westerlies in late October and November.

This is consistent with the earlier discussion of pressure gradients: a positive gradient south-north during summer and winds from the southwest, and a negative gradient during winter and more frequent winds from the north.

Wind speeds are on average of comparable strength from May to August (mostly less than the 10 to 15 m/s range), and increase markedly, on average, in September and October (with more occurrence of winds of 10 to 15 m/s range and above). Maximum wind speeds reach 25 m/s, mostly from November to January.

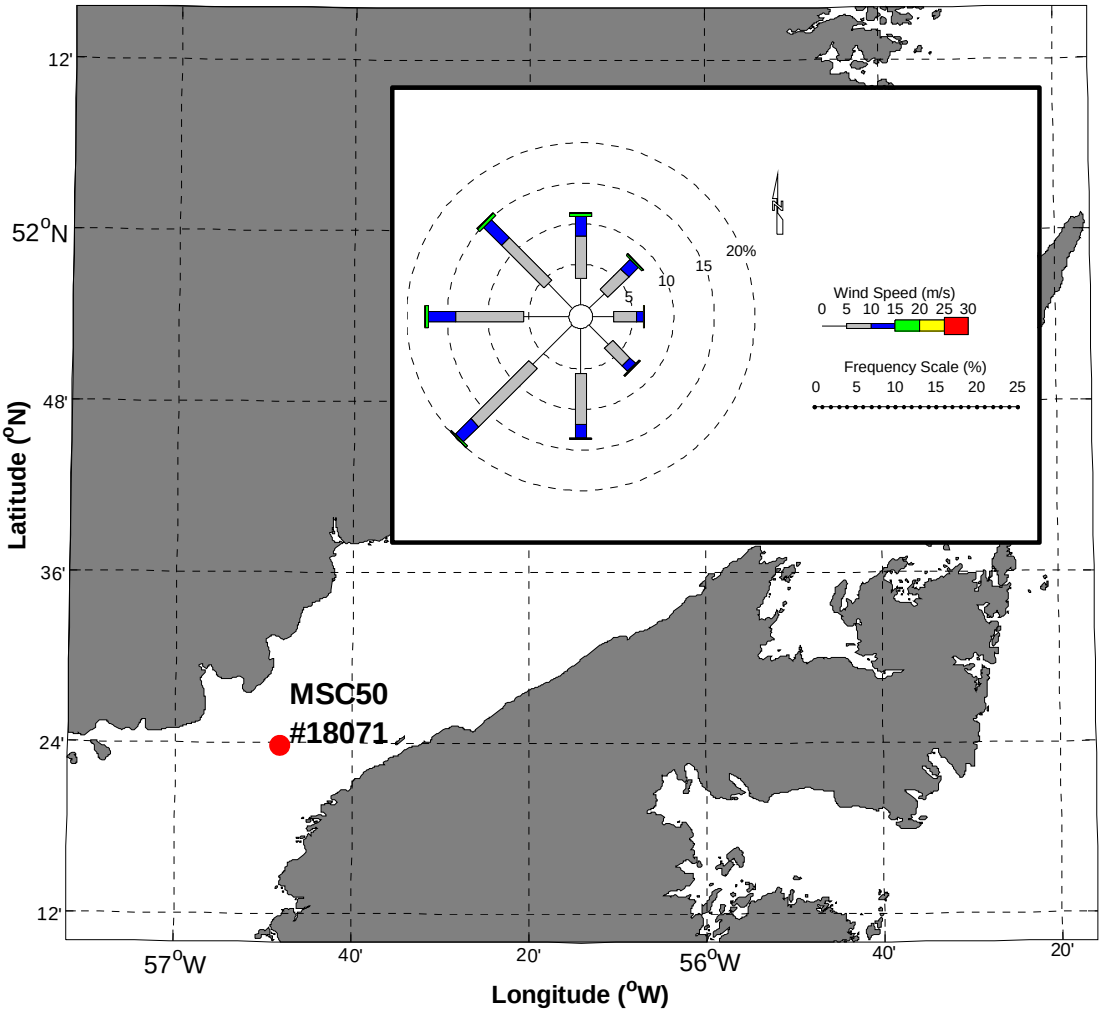

Figure 2.1-5: Strait of Belle Isle, MSC50 Node #18071, Location and Annual Wind Rose.

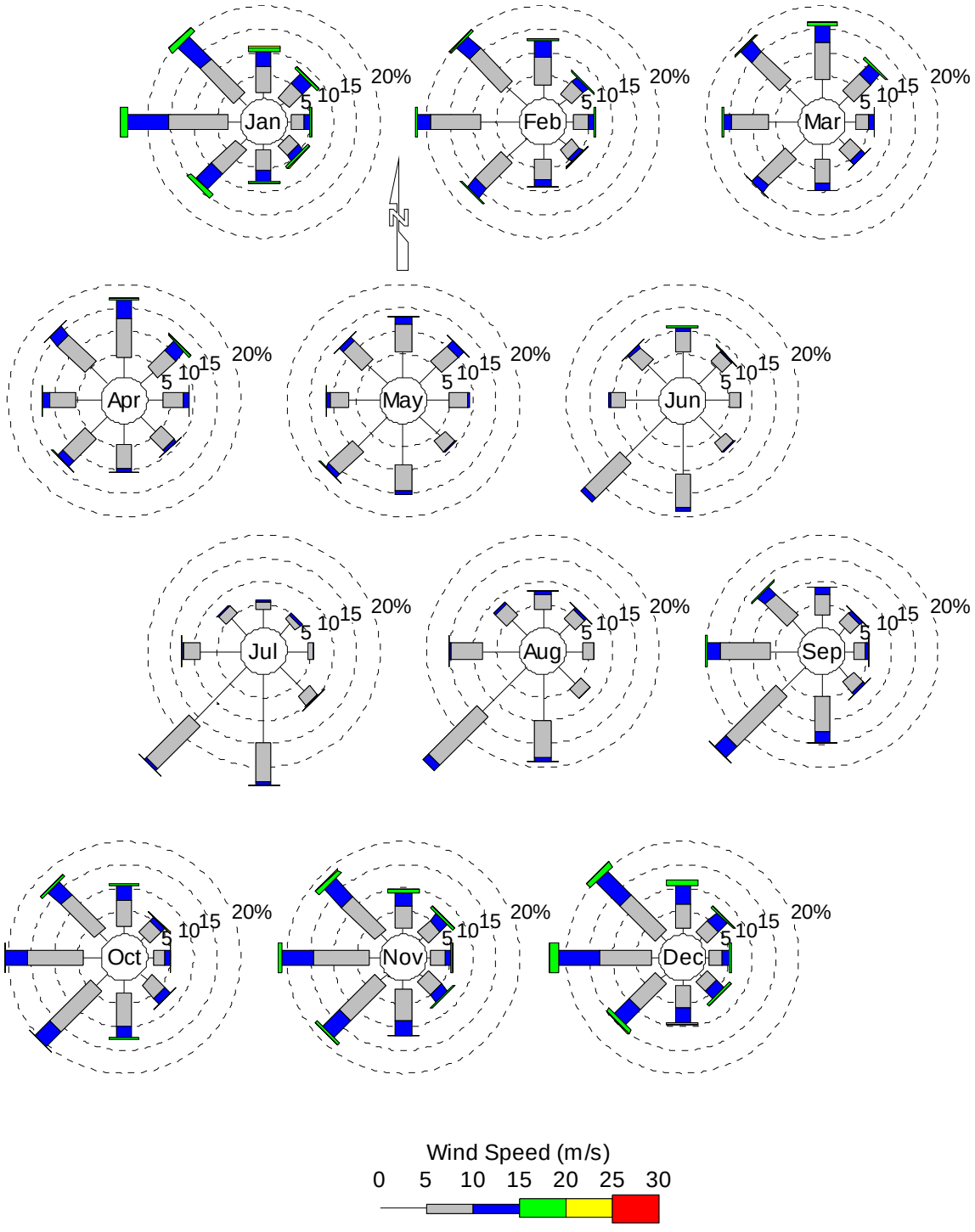

Figure 2.1-6: Strait of Belle Isle, MSC50 Node #18071, Monthly Wind Roses.

2.1.2 Oceanographic Setting

2.1.2.1 General Circulation Pattern

The Strait of Belle Isle is within the Cabot Strait, one of the two straits that connect the Gulf of St. Lawrence to the North Atlantic Ocean, and is therefore very much influenced by the conditions of the Gulf as well as the Labrador Current which characterizes most of the Eastern Canadian shelf oceanography.

The circulation of the Continental Shelf waters off Eastern Canada is dominated by a general southward flow. From the Hudson Strait to the Grand Banks (Figure 2.1-7), the waters are transported southward by the Labrador Current. As first described by Smith et al. (1937), the current is a continuation of the Baffin Island Current, which transports the cold, and relatively low salinity waters flowing out of Baffin Bay, and the warmer and more saline waters of a branch of the West Greenland Current, which turns westward in the Davis Strait. At Hamilton Bank, on the southern Labrador Shelf, the current appears as two branches: a small inshore current carrying about 15% of the transport, and the main current over the upper continental slope which carries the rest of the flow (Lazier and Wright, 1993). This inner branch eventually enters through the Strait of Belle Isle to the Gulf of St. Lawrence (Figure 2.1-8). The seawater characteristics in the Strait of Belle Isle have been derived from available temperature and salinity measurements gathered at locations shown in Figure 2.1-9.

The major oceanographic feature in of the Gulf of St. Lawrence is the outflow of fresh water from the St. Lawrence River into the estuary (Figure 2.1-8). The majority of the flow occurs along the North coast of the Gaspe Peninsula and is called the Gaspe Current (or Courant de Gaspé in Figure 2.1-8) which flows eastward. Once past the Gaspe Peninsula, the currents follow a general counter-clockwise flow in the Gulf of St. Lawrence with the majority of the water exiting the Gulf via the Cabot Strait along the Cape Breton coastline.

The tidal pulse from the Atlantic Ocean enters the Gulf of St. Lawrence from both the Cabot Strait and the Strait of Belle Isle. Tidal energies flow in a counter-clockwise direction around the Gulf increasing in height from 0.6 m at the Magdalen Islands to nearly 5 m at Quebec City (Farquaharson, 1970).

The water in the Gulf is highly stratified. In summer there is a three layer system; a warm (4 to 6 ^{o}C) salty (33 to 34.6 PSU[1]) bottom layer below 125 m; a cold (-1 to 2 ^{o}C) slightly fresher (31.5 to 33 PSU) intermediate layer between 80 and 100 m; and a warm (up to 20 ^{o}C) fresher (27 to 32 PSU) surface layer from 10 to 30 m (Drinkwater, 1993; Gratton et al., 1994; White and Johns, 1997). The cold bottom and intermediate water layers receive water from the Labrador Current which enters the Gulf from the Strait of Belle Isle (Bugden, 1991; Petrie et al., 1988; White and Johns, 1997).

[1] PSU: Practical Salinity Units, where the Practical Salinity Scale 1978 (PSS-78), adopted by the UNESCO/ICES/SCOR/IAPSO Joint Panel on Oceanographic Tables and Standards, is based on an equation relating salinity to the ratio of the electrical conductivity of seawater at 15°C to that of a standard potassium chloride solution. Practical salinity is dimensionless; however, the abbreviation PSU is used in this report to clarify that these are salinity values.

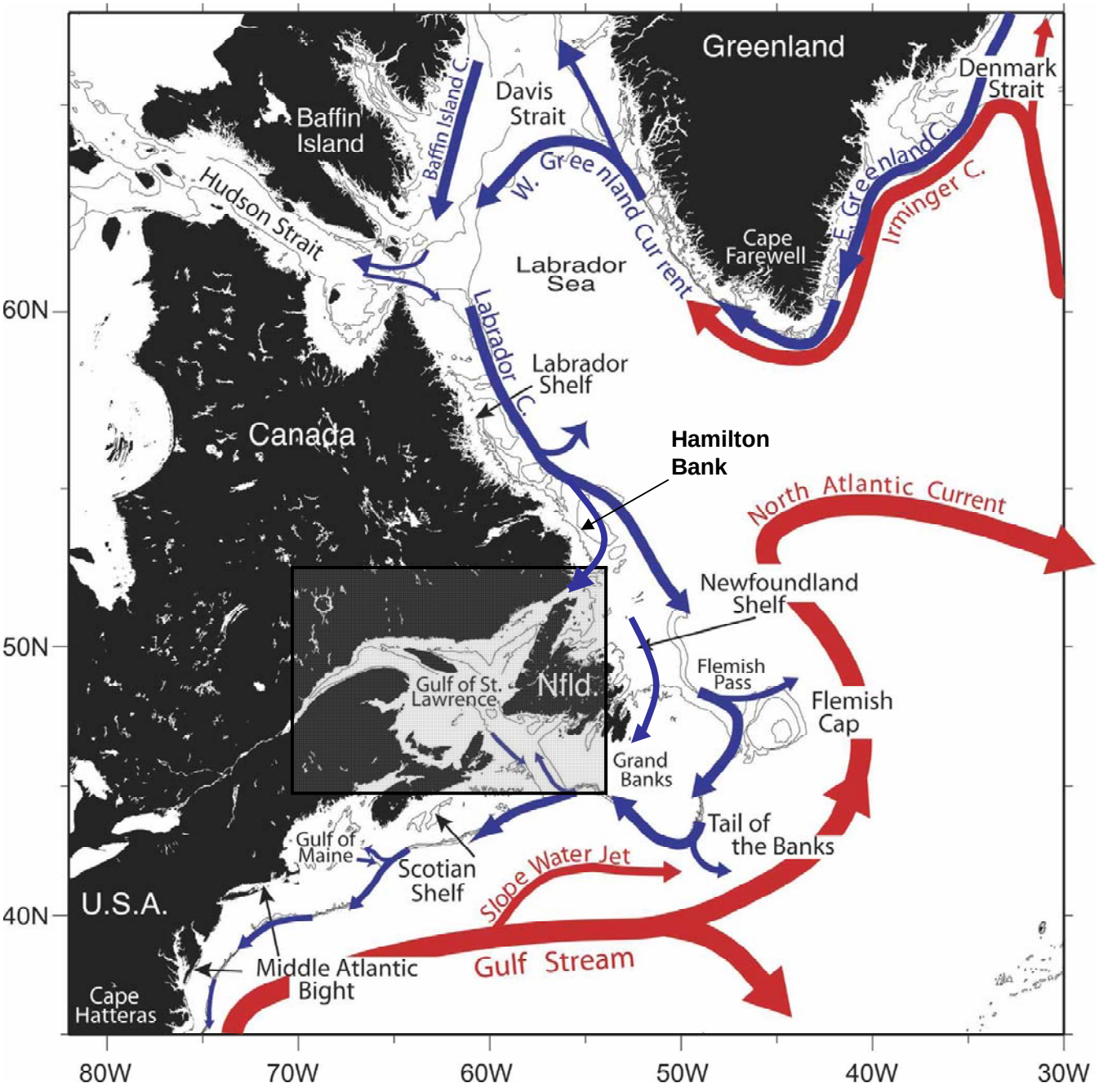

Figure 2.1-7: General Oceanographic Circulation of Eastern Canada, Modified from Lazier and Wright (1993).

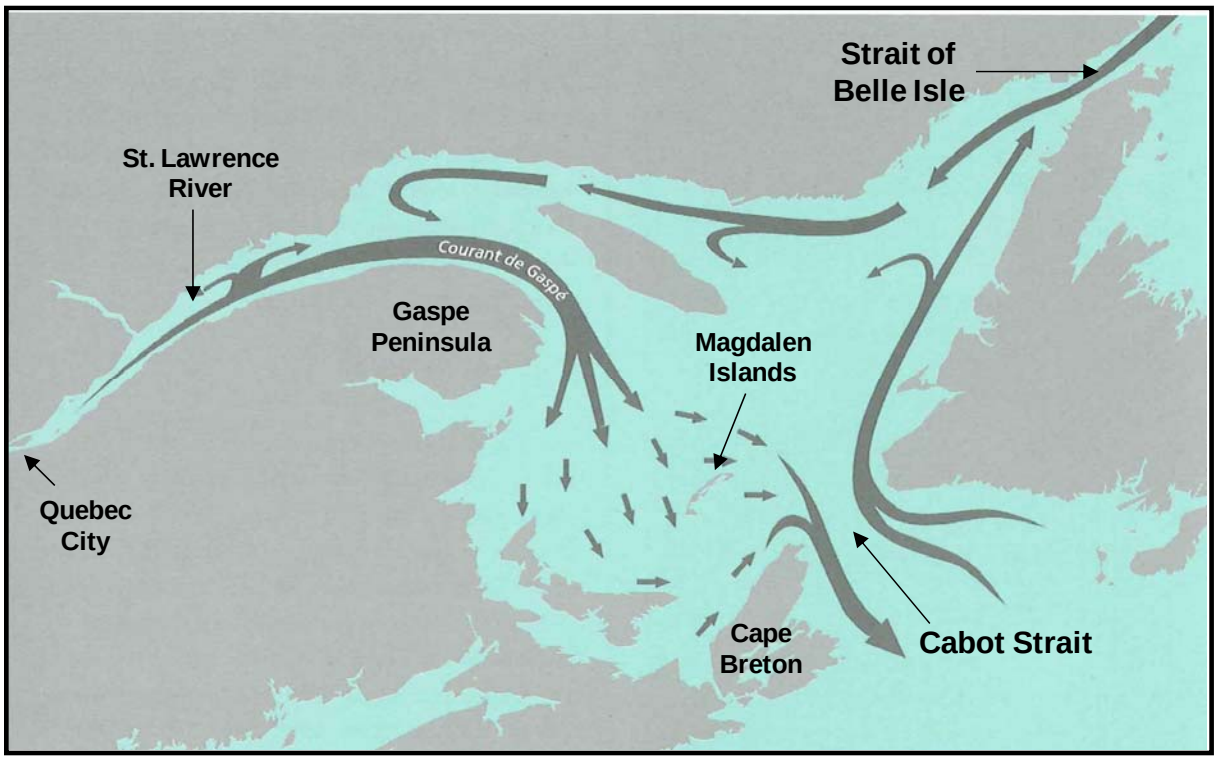

Figure 2.1-8: General Oceanographic Circulation in the Gulf of St. Lawrence, Modified from Smith et al. in White and Johns (1997).

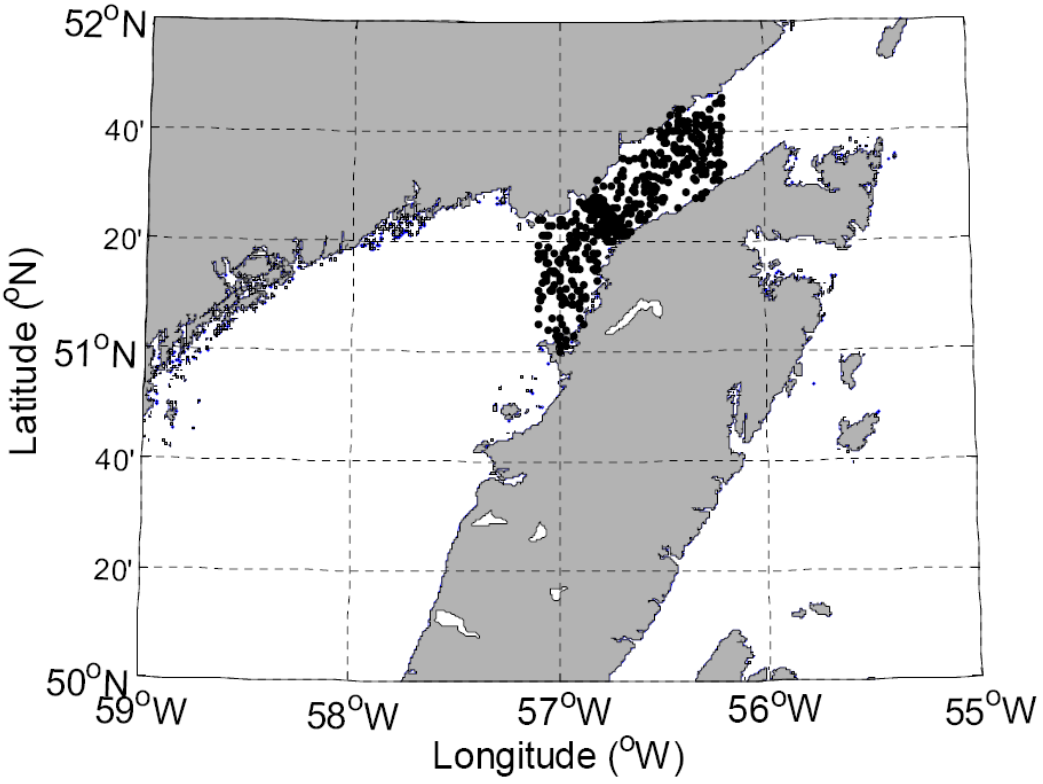

Figure 2.1-9: Temperature and Salinity Measurement Locations, from AMEC (2007).

2.1.2.2 Water Column Structure

Temperature and salinity statistics were derived from the DFO Hydrographic Climate database (see AMEC, 2007). The geographic limits used for this study were 51° N to 52° N, and 57.1° W to 56.2° W (Figure 2.1-9). Approximately 4944 measurements were available; these were averaged with depth bin size of 10 m for depths 0 to 100 m. The results are presented in Figure 2.1-10 and Figure 2.1-11.

The Strait of Belle Isle data show a similar pattern to the stratification in the Gulf although there is no bottom layer; it is a two layer system in summer and has one homogeneous layer in fall and winter. In summer the surface layer is down to a depth of 50 to 60 m with average temperatures reaching between 10 and 11 °C and average salinities between 30.5 and 32 PSU. In the bottom layer, below 60 m, average temperatures range between -0.4 and 3.5 °C and average salinities range between 31.5 and 32 PSU. The stratification changes in October to one homogeneous layer which is colder and saltier than the conditions in the summer. In fall and winter the average temperatures range from 2.73 °C in November to -1.8 °C in April, and the average salinities range from 31.6 PSU in November to 33.1 PSU in April (Figure 2.1-11).

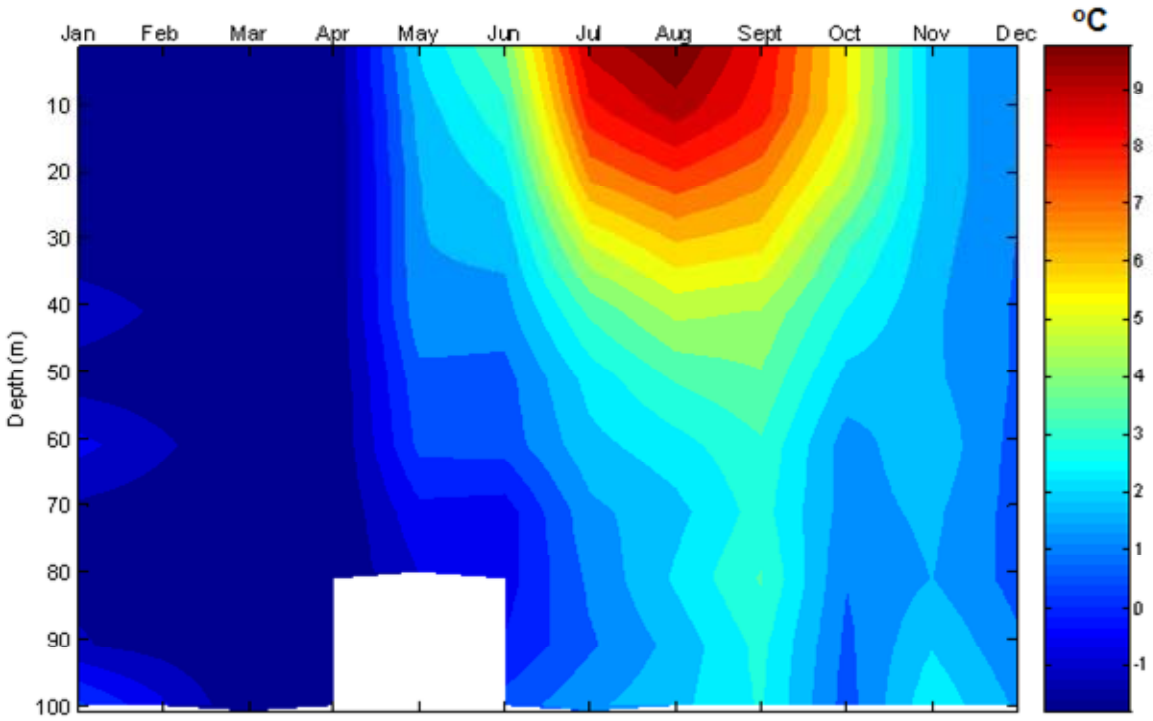

Figure 2.1-10: Strait of Belle Isle, Monthly Average Water Column Temperature.

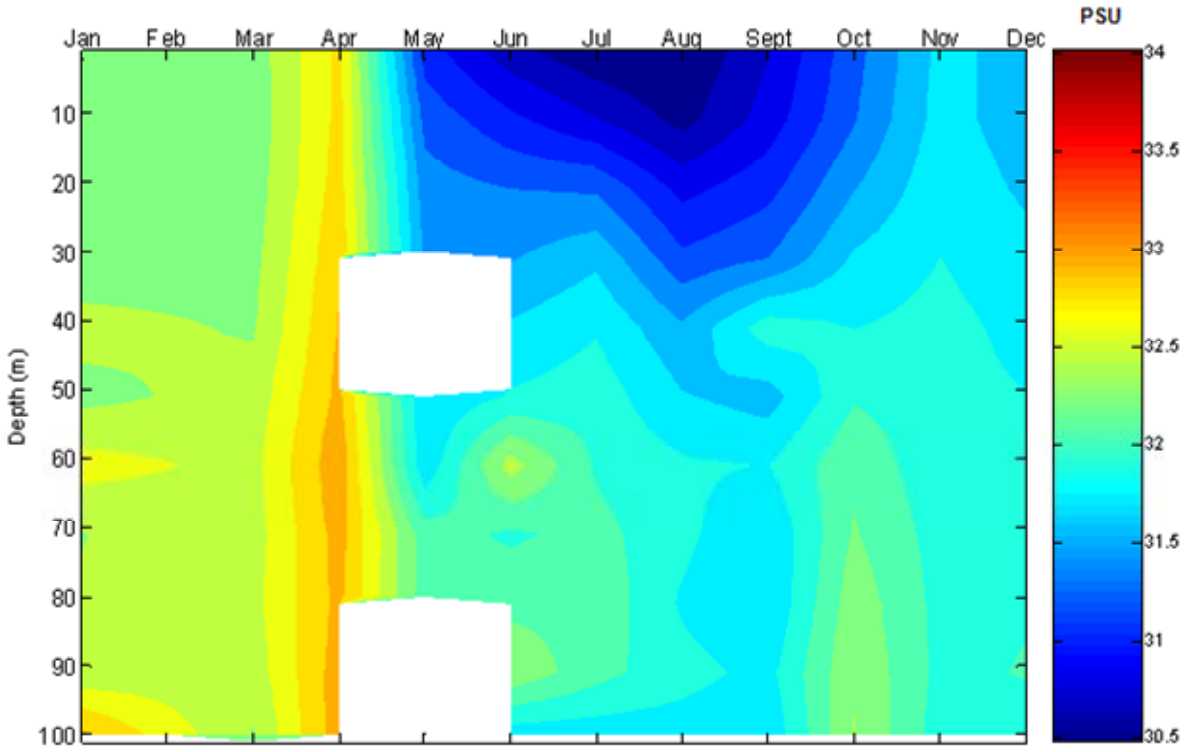

Figure 2.1-11: Strait of Belle Isle, Monthly Average Water Column Salinity.

2.1.2.3 Waves

Directional wave statistics were calculated using the MSC50 hindcast. The same node that was used for the wind (#18071) also represents the general conditions within the Strait, recognizing that significant variation may occur in this region due to local effects, i.e., bathymetry, and shoreline changes, especially near shorelines.

At this location, MSC50 #18071, the predominant wave direction is from the southwest (Figure 2.1-12), in the orientation of the Strait, which occurs about 35% of the time. Waves can reach up to 7 m significant wave height (Hs), but these occur very infrequently.

The strongest waves occur during the winter months (October to January, Figure 2.1-13), and the majority of waves are from the southwest and west directions, which is expected given the orientation of the Strait and the predominant wind directions.

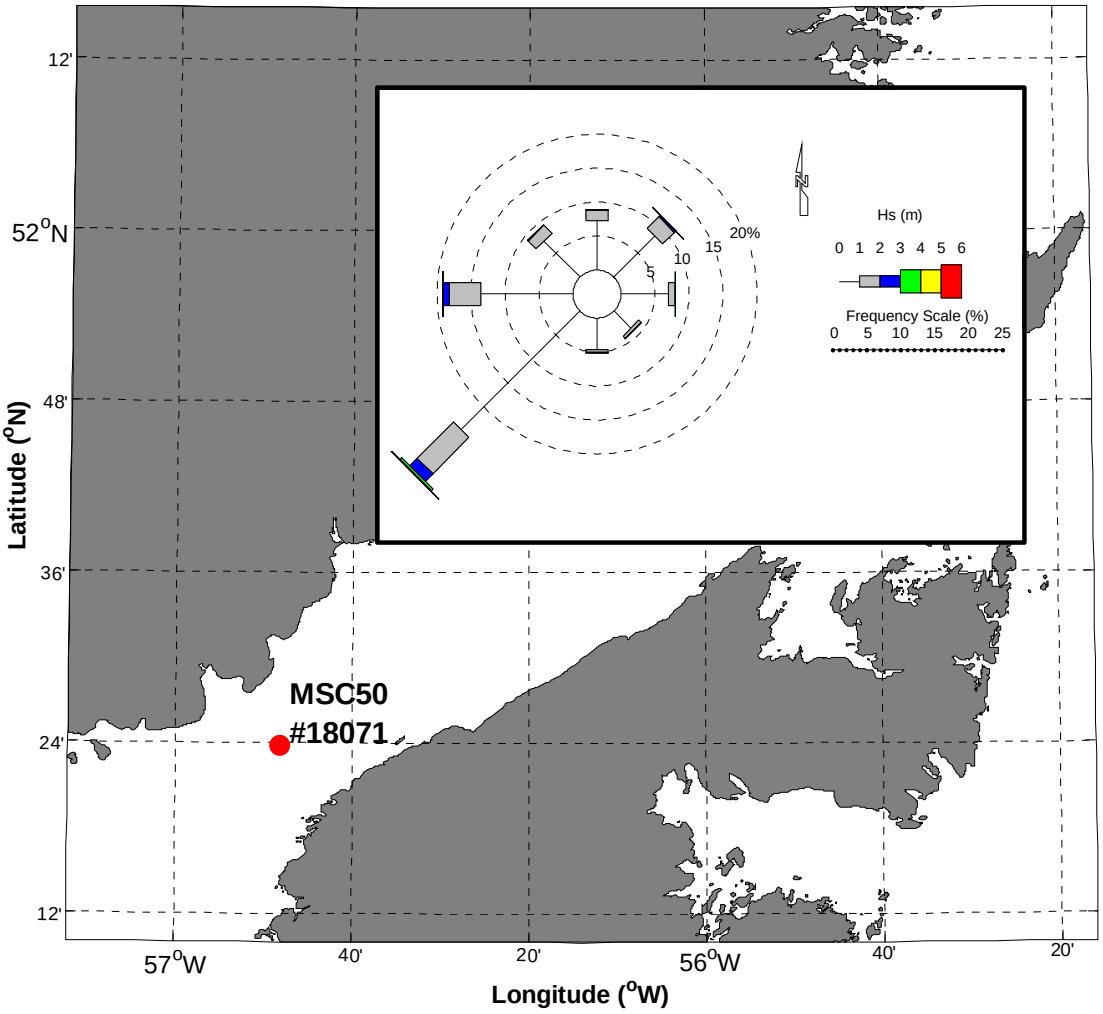

Figure 2.1-12: Strait of Belle Isle, MSC50 Node #18071, Location and Annual Wave Rose.

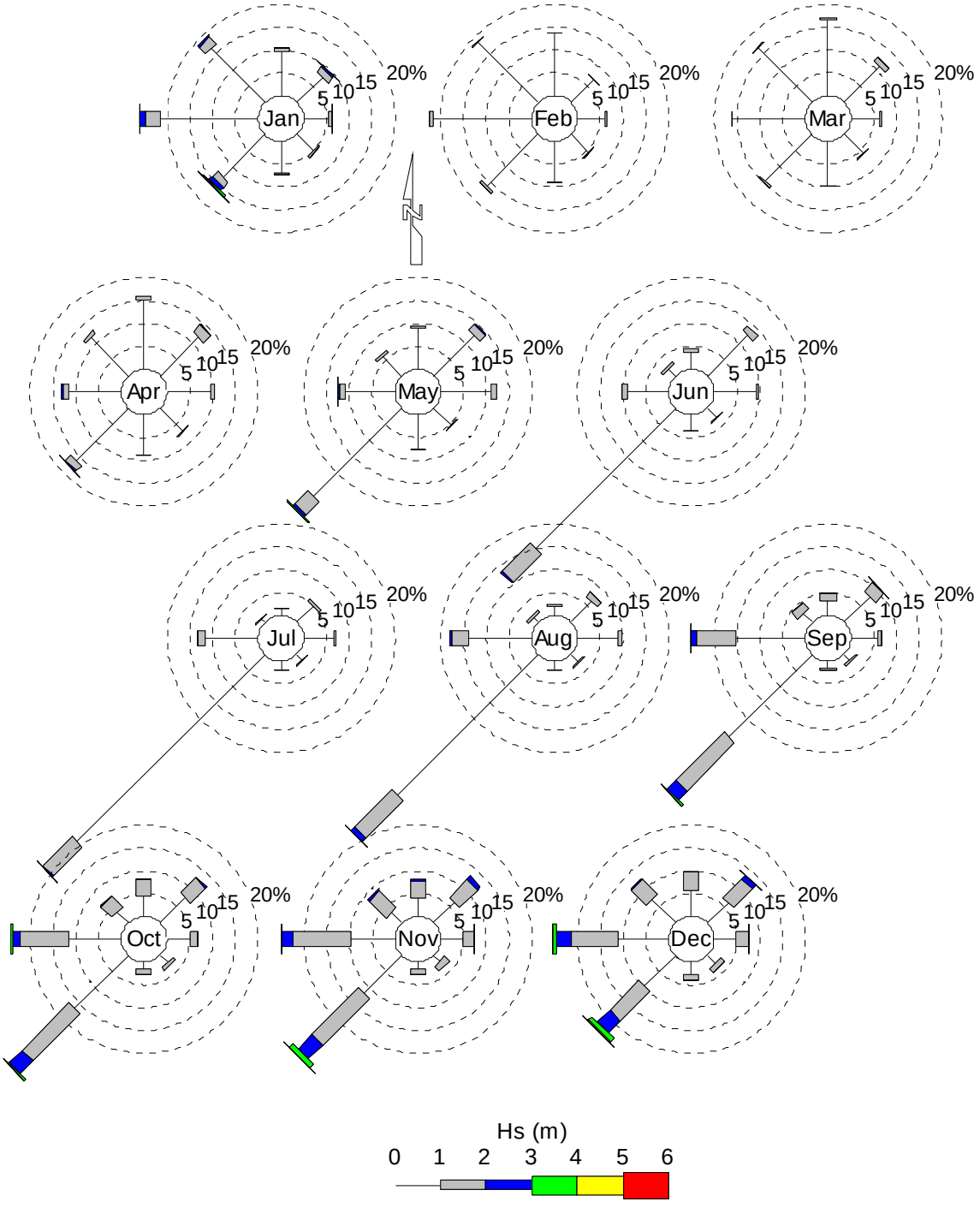

Figure 2.1-13: Strait of Belle Isle, MSC50 Node #18071, Monthly Wave Roses.

2.1.2.4 Tides

As described earlier, the tide propagating from the Gulf of St. Lawrence (counter-clockwise) combines with the tide from the Atlantic Ocean (Labrador Sea); but since the two do not have the same amplitude, a partial standing wave is formed. In the case of a true standing wave, a node is formed and there should be zero amplitude and a reversal of phase on either side. In the Strait of Belle Isle there is a degenerated node, exhibiting reduced amplitude and rapid spatial change in phase. This rapid change in phase translates into a rapid change of tide stage (i.e., high tide, low tide, etc.) over relatively short distances along the coast.

Tides in the Strait of Belle Isle can be considered mixed semi-diurnal, whereby two high and two low tides of different size occur every lunar day. An example of a typical cycle is presented in Figure 2.1-14 for Mistaken Cove, Newfoundland, located just north of Flower's Cove. This tidal prediction is representative of tides in the study area.

The amplitude of the tides recorded from the tidal gauges displayed for this study (see Section 2.2 for additional information), are on the order of 0.5 m for small (neap) tides and up to 1.5 m for large (spring) tides, generally increasing toward the Gulf (Figure 2.1-15). Tidal constituent M2 is the principal semi-diurnal lunar characteristic of the tide. Tidal constituent K1 is the luni-solar diurnal characteristic of the tide.

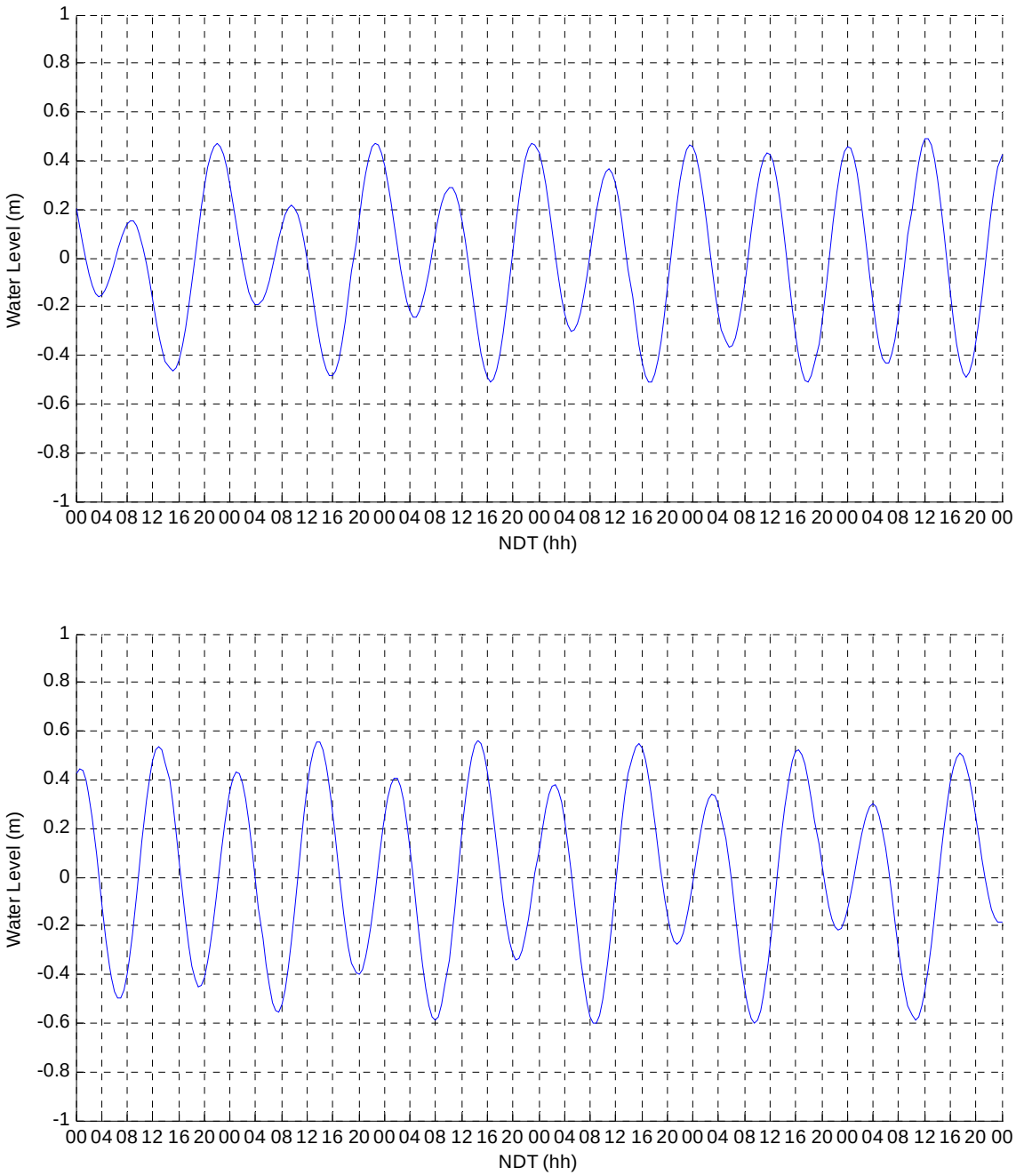

Figure 2.1-14: Tide Prediction (Water Level) at Mistaken Cove, Newfoundland during Neap to Spring Tides using DFO Webtide (Dupont et al., 2002). The top panel represents the period 31 August – 6 September 2009; the bottom panel represents the period 6-12 September 2009. Time in Newfoundland Daylight Time (NDT).

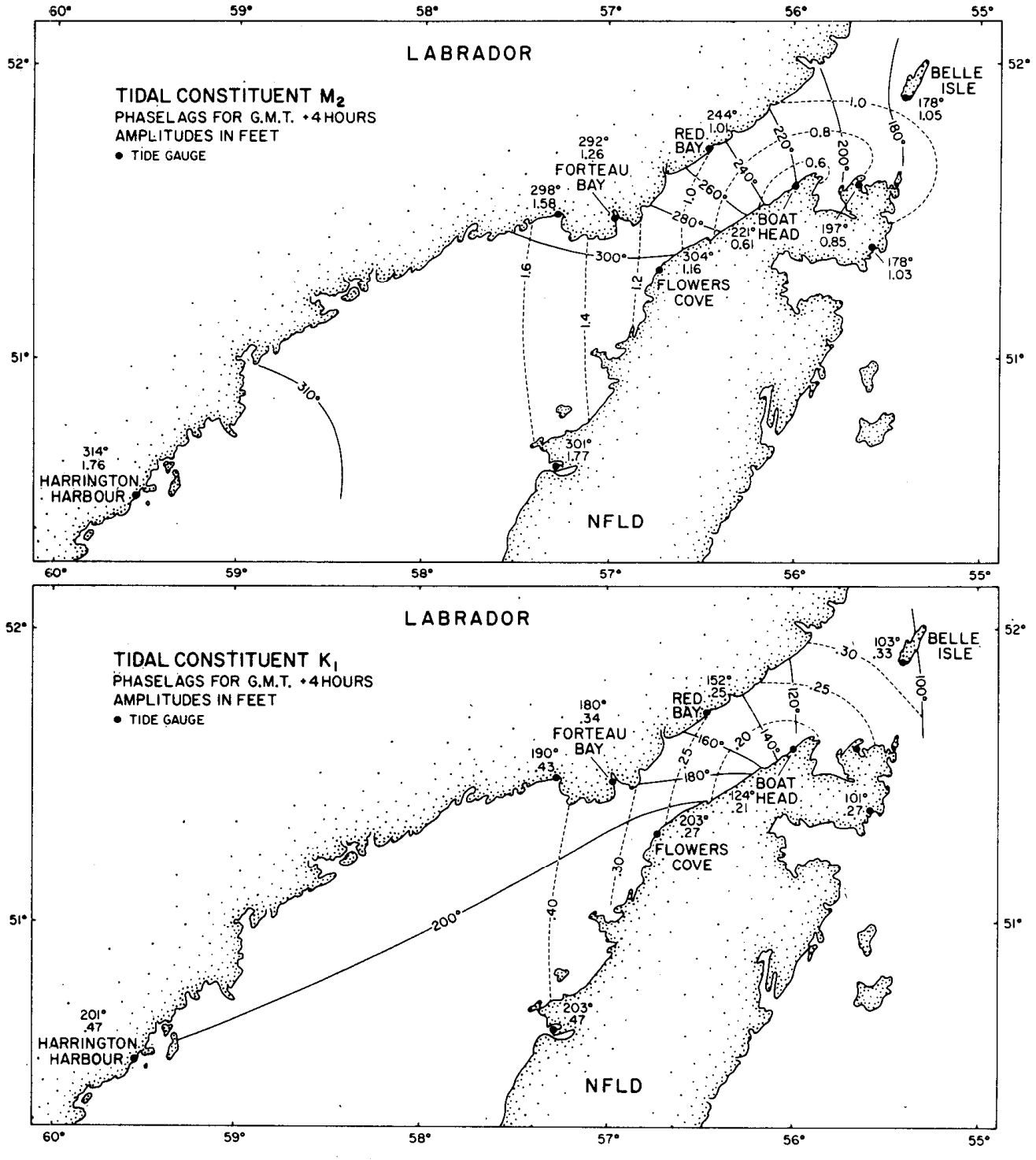

Figure 2.1-15: Cotidal and Coamplitude Charts for the Constituents M2 and K1 (Main Semidiurnal and Diurnal Constituents) for the Strait of Belle Isle (redrawn from Farquharson and Bailey, 1966, as in Garrett and Petrie, 1981).

2.1.2.5 Currents

Currents in the Strait of Belle Isle have been studied at various times over the past century, including Dawson's pioneering measurements in 1894 and 1906 (Dawson, 1907), and numerous research papers (Garrett and Petrie, 1981; Garrett and Toulany, 1981 and 1982; Toulany et al., 1987 Petrie et al., 1988; Galbraith, 2006) and engineering reports (NORDCO, 1978; SNC-Lavalin, 1982c), as well as a recent summary of seasonal current statistics by AMEC (2010b).

Overall, the currents in the Strait of Belle Isle are characterized by three main processes: 1) tides; 2) non-tidal processes acting on the order of several days associated with meteorological forcing; and 3) long-term (interannual) variability of the mean flow associated with the regional ocean circulation (described in Section 2.1.2.1).

Tidal Flows

Tidal flows in the Strait of Belle Isle are induced by the water elevation variation forcing on its two ends (Gulf of St. Lawrence and the Labrador Sea), described in Section 2.1.2.4. As the tidal wave propagates into the Strait, a reversing (going back and forward) current (or flow) occurs. The Strait has been characterized as having a partially standing tidal wave, where the tidal currents attain their maximum speed between the periods of high and low tide and have their minimum speed, near zero, at high and low tide. In the case of a perfectly standing wave, tidal currents are exactly zero at those periods, also called 'slack water', and have their maximum speed halfway between them.

Because of the Earth's rotation (and by means of the Coriolis Force), the tidal currents also rotate and trace the form of an ellipse. An example of the typical tidal currents ellipse in the Strait is presented in Figure 2.1-16 for a node located at the same position as the previously described MSC50 dataset (for wind and waves), and extracted from the DFO tide prediction model WebTide (Dupont et al., 2002). The shape of the ellipse varies within the Strait due to bathymetric and shoreline constraints.

The Webtide model results also indicate that the tidal ellipse tends to rotate counter clockwise in that area in accordance with the cotidal charts (phase increasing from northwest to southwest) of Farquharson and Bailey (1966). This also confirms that the tide propagates globally (as a partially standing wave) from the northeast to the southwest.

Overall, the tidal currents in the area are approximately 1 m/s (about 0.5 m/s on average, varying from 0 m/s to 1.5 m/s with 0.1 m/s standard deviation, AMEC, 2010b) and have been shown to be reduced by about 0 to 20% near the bottom (Toulany et al., 1987).

The tides represent the best understood process influencing the flow in the Strait and can be predicted with a high degree of certainty using harmonic analysis and numerical modelling.

Atmospheric Pressure Forcing Flow

The atmospheric forcing-induced flow in the Strait of Belle Isle was hypothesized as early as Dawson's first studies (Dawson, 1907) but was not well understood until the work of Garrett and Petrie (1981) and Garrett and Toulany (1981 and 1982).

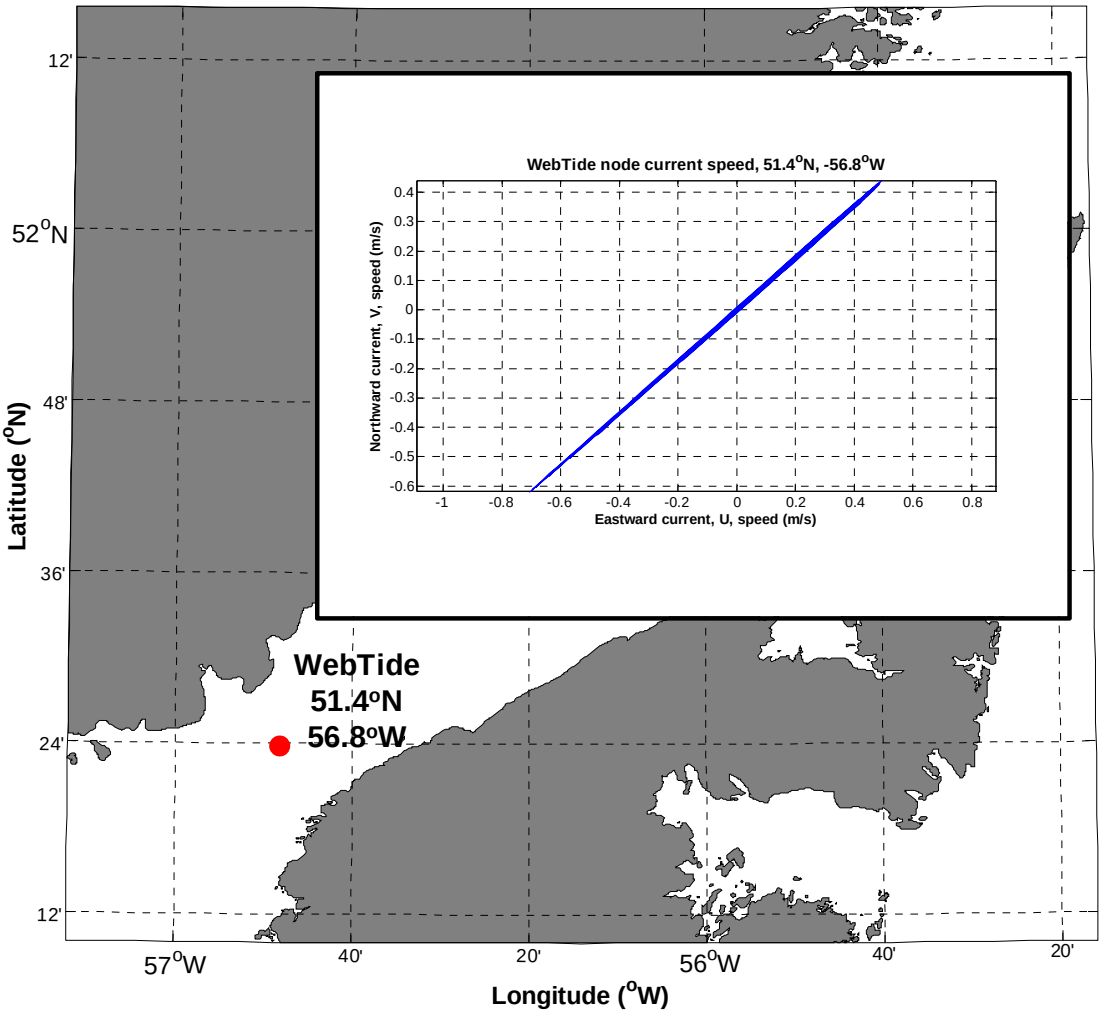

Figure 2.1-16: WebTide Node Current Prediction (Ellipse) at 51.4° N, 56.8° W, Representative of the Strait of Belle Isle Mid-channel, Average Tide Conditions.

Two mechanisms were hypothesized by Garrett and Petrie (1981) to produce flow along the Strait: 1) north-south atmospheric pressure gradients generating zonal north(east)-south(west) winds driving water into or out of the Gulf; and/or 2) zonal pressure gradients between the two ends of the Strait that would result in flows by redistribution of water to attain isostatic equilibrium. They concluded that the zonal wind forcing was the

dominant one, stating "large-scale winds roughly parallel to the Strait, result in a difference in sea level at the opposite ends of the Strait which drives the flow" (Garrett and Petrie, 1981, p. 386).

Garrett and Toulany (1981) found that an atmospheric pressure difference of 1 kPa (0.1 dbar) (Goose Bay minus Gander, see Table 2.1-1) is associated, at low temporal frequencies, with a sea level difference of approximately 0.1 m (from one end of the Strait to the other) and an associated surface current of 0.6 m/s at the narrowest point of the Strait.

Toulany et al. (1987) further indicated that the current amplitude near the seafloor of the Strait is generally reduced to 50 to 60% of the surface values at low frequencies (four to eight days), similar to those induced by the atmospheric forcing.

Additional analyses performed by AMEC incorporated available data to capture all recorded events of atmospheric forcing (AMEC, 2010b). It was found that the magnitude of the current contribution associated with atmospheric forcing was on the order of 1 m/s. The mean surface current was 0.2 m/s in winter, spring and fall, and 0.3 m/s in summer. The maximum surface current was 0.6 m/s in winter and 1.6 m/s in summer with an associated uncertainty[2] of 0.3 m/s.

Inter-annual Variability of the General Circulation

As described in Section 2.1.2, the general oceanic circulation of Eastern Canada induces a main inflow of the Labrador Current into the Strait of Belle Isle and another weaker outflow toward the Labrador Sea along the Newfoundland shore (Figure 2.1-7 and Figure 2.1-8).

As the Labrador Current is highly variable both seasonally and inter-annually (Lazier and Wright, 1993; Loder et al., 1998), the induced current also varies within the Strait.

The variability of this flow in the Strait was studied by Garrett and Petrie (1981) and Petrie et al. (1988) using sea level measurements from eight consecutive years (1970 to 1977) and assuming geostrophic balance within the Strait. In oceanographic terms, a flow is said to be in geostrophic balance when the pressure gradient is balanced by the Coriolis Force veering the flow to the right in the northern hemisphere. This propriety of the flow therefore allows direct correlation between the across-Strait sea-level difference and the mean along-Strait current speed.

Based on the mean and the variance of the seasonal current estimates presented in these two studies (Garrett and Petrie, 1981; and Petrie et al., 1988), the mean and maximum expected contribution due to inter-annual variability of the mean geostrophic flow was further re-calculated by AMEC (2010b). They found that the mean of this inter-annual flow contribution would be 0.5 m/s (0.67 m/s in winter, 0.34 m/s in the summer, with an associated uncertainty of 0.9 m/s) while the maximum value would be 1 m/s (1.5 m/s in spring, 1.2 m/s in winter and summer, with an associated standard deviation of 0.4 m/s). For surface currents Garrett and Petrie (1981) indicate that vertical density stratification typically observed in the Strait is associated with a reduction in mean geostrophic current speed, between the surface and the bottom, of a maximum of 0.25 m/s. The mean contributions to the flow were considered homogeneous for the entire water column.

[2] In AMEC (2010b), 'uncertainty' was estimated to be the maximum expected variability of the tidal, residual, and inter-annual components of the current

Another aspect to consider with the mean flow is that its structure was found to be fairly baroclinic, that is, not homogeneous for the entire water column across the Strait. The outflow (toward the Labrador Sea) is generally positioned above the inflow on the Newfoundland shore (Figure 2.1-17). There are different hypotheses to the nature and origin of this flow (Garrett and Petrie 1981); however, it has been noted that this structure is still relatively poorly understood. As the mean flow component represents only a fraction of the total observed flow (which includes tides and atmospheric forcing) in the Strait of Belle Isle it can be treated as barotropic and in geostrophic balance.

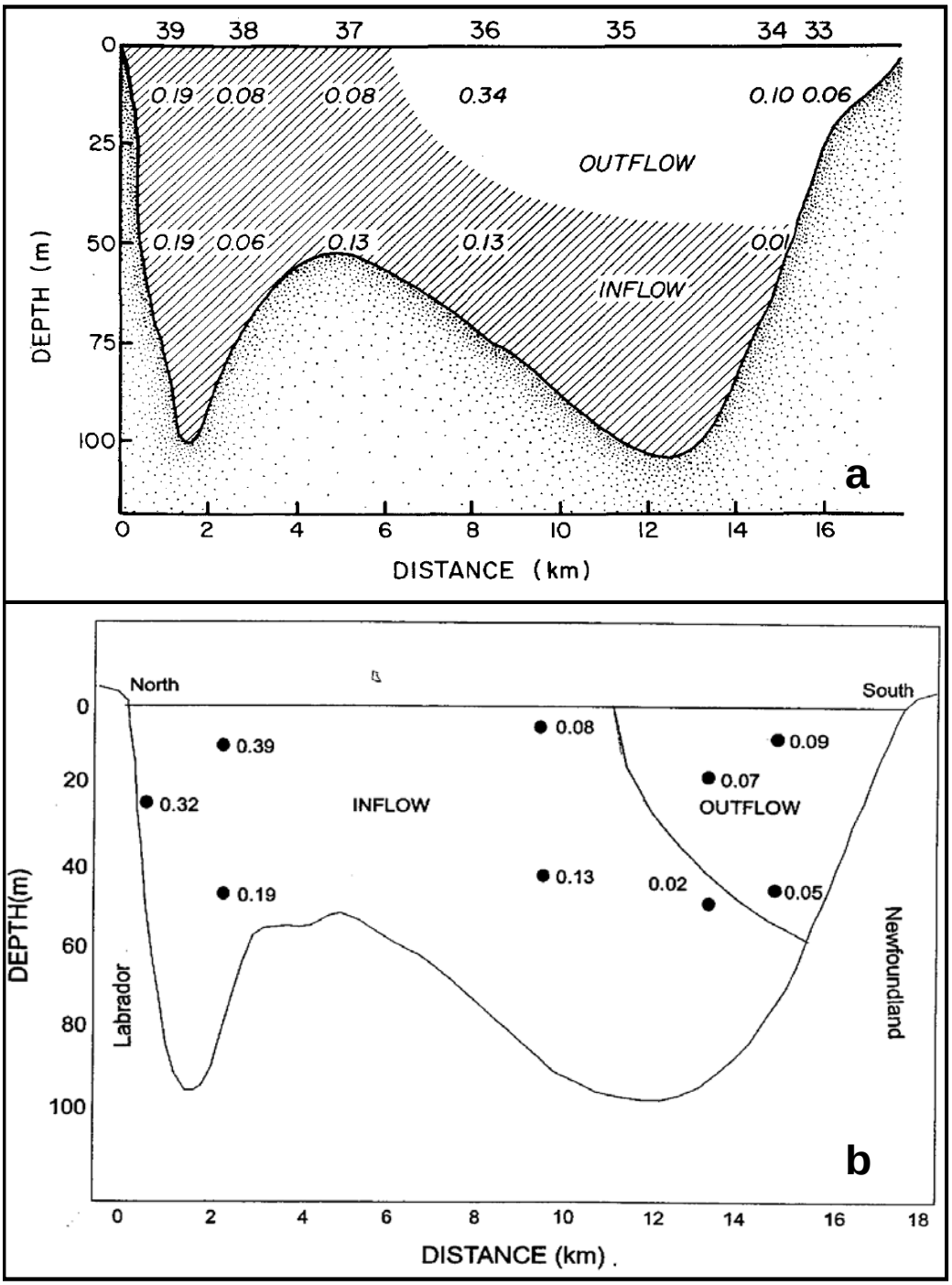

Figure 2.1-17: Mean Flow (m/s) through the Strait of Belle Isle from (a) the August to September 1963 Oceanographic Study (from Farquharson and Bailey 1966, as reported in Garrett and Petrie, 1981) and from (b) the July to October 1980 Oceanographic Study (Garrett and Petrie, 1981).

2.1.2.6 Bathymetry

Numerous surveys have been conducted in the Strait of Belle Isle by public agencies, e.g., Canadian Hydrographic Survey (CHS), and more recently, by the private sector (Fugro GEOS, 2007a; 2007b). The most detailed data available for the area were used to create a high resolution bathymetric grid (Figure 2.1-18). Details of the implementation of those data and the creation of the grid are presented in Section 2.2.2. The main geographical features are discussed in this section.

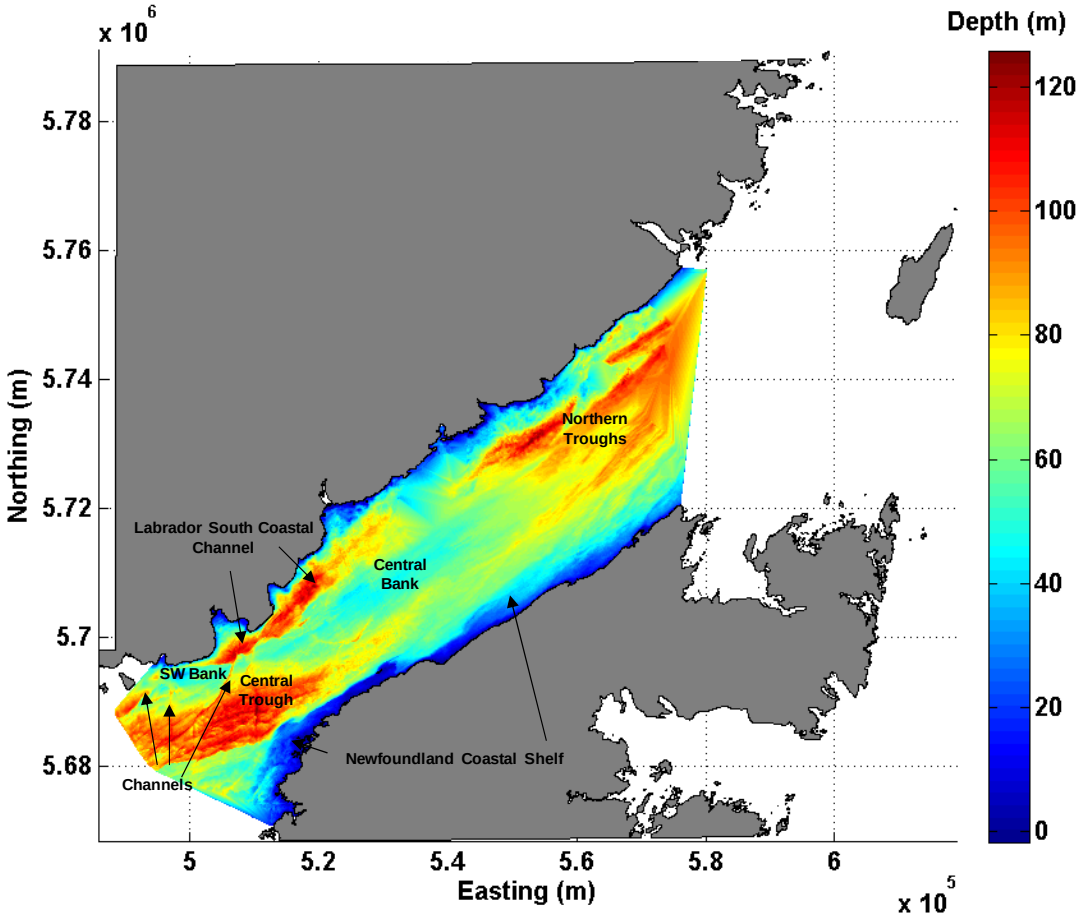

Figure 2.1-18: Bathymetry of the Strait of Belle Isle, noting Shelf, Bank, and Trough Features.

The Strait of Belle Isle is a relatively narrow (from about 17 km at its narrowest point to about 30 km at its northeast end) and shallow (about 70 m average depth) channel.

The Strait is characterized by banks and troughs as well as a few steep, narrow, and deep channels (Figure 2.1-18). The Labrador side is generally steeper than the Newfoundland side, which has a slightly wider shelf. The southern area (below Central Bank) is characterized by a deep (> 100 m), irregular channel on the Labrador side that is connected to the Central Trough by a deep and narrow channel (> 80 m) running between the shallow banks (central and southwest) and finally the Newfoundland coastal shelf at its widest (narrowing toward the north). The northern area is characterized by wider and on average a shallower series of irregular troughs.

2.1.2.7 Seafloor Sediment Characteristics

The seafloor within the study area (southern part) was investigated thoroughly over the past several decades and includes surveys conducted for the proposed Lower Churchill Development of the late 1970s and early 1980s, and more recently for the Labrador-Island Transmission Link. Data and summaries of these investigations have been presented by SNC-Lavalin (1982a, 1982b, 1982c), Woodworth-Lynas et al. (1992), Fugro GEOS (2007a, 2007b, 2008), FJGI (2010), and AMEC (2010b).

The most detailed data of the area were used to create a high resolution map of seafloor sediment types. Details on the implementation of those data and the creation of the grid are presented in Section 2.2.2, with only the main characteristics of the seafloor sediment discussed in this section.

Overall, these studies demonstrated a complex seafloor, both topographically and geologically. The topography, described in the previous section, revealed rapid changes of depths with channels, troughs and banks. The surficial geology consists mostly of a discontinuous veneer (typically < 5 m) of glacial and marine sediments overlying bedrock (Fugro GEOS, 2007a).

Across most of the Strait, the seabed is comprised of a coarse-grained armour of pebbles, cobbles and boulders overlying glacial till and localized glaciomarine deposits. Marine sands form a discontinuous surficial veneer in shallow water areas, and thicken locally to more than 10 m in some coastal embayments such as Forteau Bay. Bedrock is exposed on the seabed in places such as on the Newfoundland shore, near Flower's Cove). The bedrock consists of sandstone, dolomite and limestone, with some interbedded shale.

The following six general observations about seafloor conditions and processes were made by Fugro GEOS (2008):

"1. The seafloor throughout the survey region may be generally described as a gravelly to bouldery lag deposit, upon which northeast-southwest – oriented sand ribbons are superimposed;

2. In water depths greater than about 95 m the gravelly seafloor is dominated by numerous boulder and cobble-rich berms of relict iceberg scours, oriented approximately northeast-southwest;

3. A region of thick sandy sediments, 3 to 16 m thick, characterizes the L'Anse Amour (Forteau Bay) approach between 10 m and 58 m water depth;

4. From about 95 m water depth inshore to the Mistaken Cove (Flower's Cove) landing site on the Newfoundland side of the Strait, the seafloor is dominated by near-surface bedrock structure. In this region sediment overburden is generally < 1 m thick, and the seafloor is characterized by a sequence of thinly-mantled step-like bedrock scarps that are commonly 1 to 2 m in elevation, and exceptionally 6 to 7 m;

5. A north-northeast to south-southwest oriented bedrock channel dominates a portion of the Project Area in water depths between 82 m and 106 m. The channel is 5.75 km long, 20 to 30 m deep and partially filled with between 3 m and > 10 m of sediment;

6. In the Project cable corridors, modern iceberg scours, < 0.5 m deep were observed in water depths between 50 m and 58 m on the Newfoundland side and between 48 m and 77 m offshore from Forteau Point on the Labrador side, where they are < 0.75 m deep."

2.2 Model Setup and Implementation

2.2.1 Data Collection Program

In August 2009, Nalcor Energy installed four synchronized tidal gauges to monitor the water level at four locations in the Strait of Belle Isle over a period of about two months. The purpose of the monitoring program was to provide robust boundary conditions for the hydrodynamic numerical model (Section 2.2.3).

The four stations were selected at strategic locations within the Strait to be as close as possible to the model boundaries. The model used (HYDRO2D) is based on an orthogonal numerical grid, and the stations were selected to represent the outer corners of the study area to be used for the model (Figure 2.2-1).

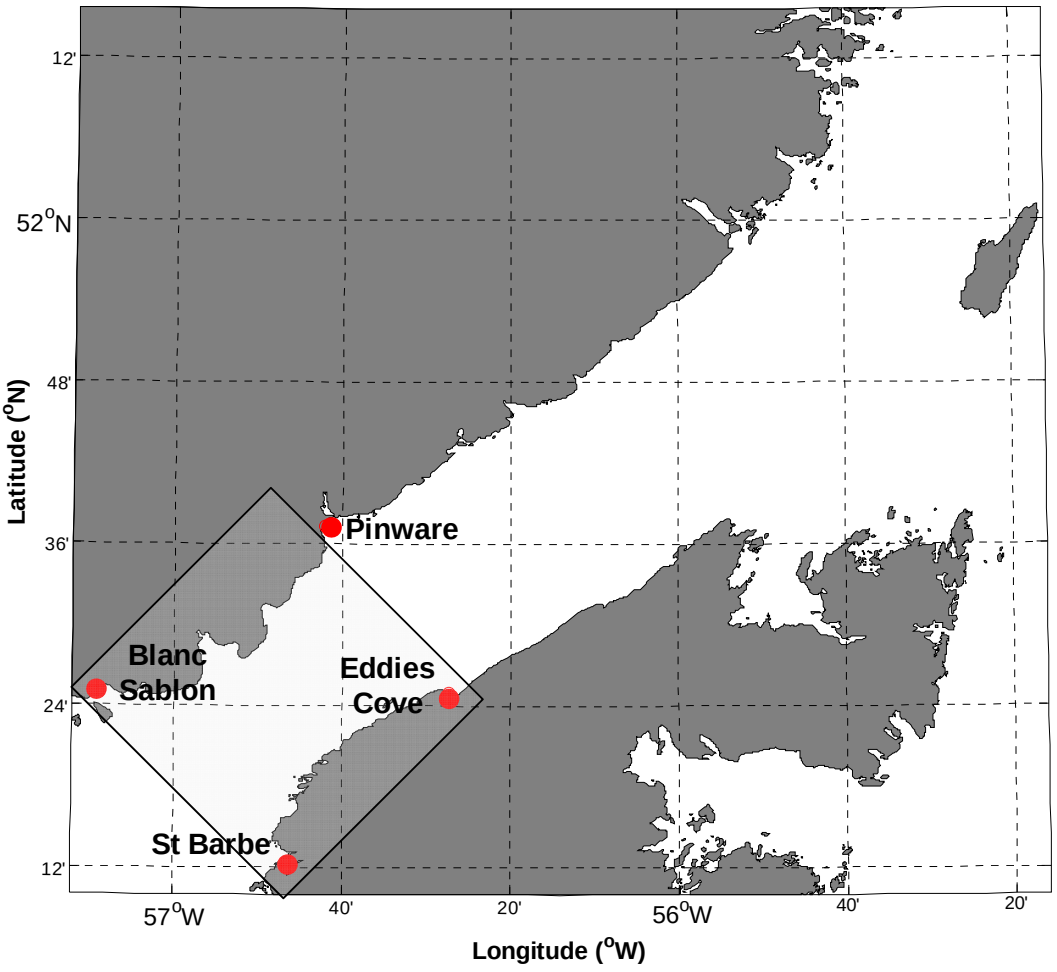

Figure 2.2-1: Nalcor Energy Tidal Gauge Stations (red dots) and Study/Numerical Model Study Area (box).

The instruments used for the monitoring program were RBR TWR-2050 high precision water level recorders (Figure 2.2-2). These pressure sensor-based instruments are capable of measuring over a range of 0-20 dBar (or up to a 20 m range) with an accuracy of ± 1 cm (manufacturer specifications). They were deployed on DFO Small Craft Harbour piers of the localities represented in Figure 2.2-1 (Blanc Sablon, Pinware, Eddies Cove, and St. Barbe) from August 18 to August 21, 2009 and retrieved from October 21 to October 23, 2009 (see an example in Figure 2.2-2). In total, 60 days of synchronized absolute pressure measurements were recorded.

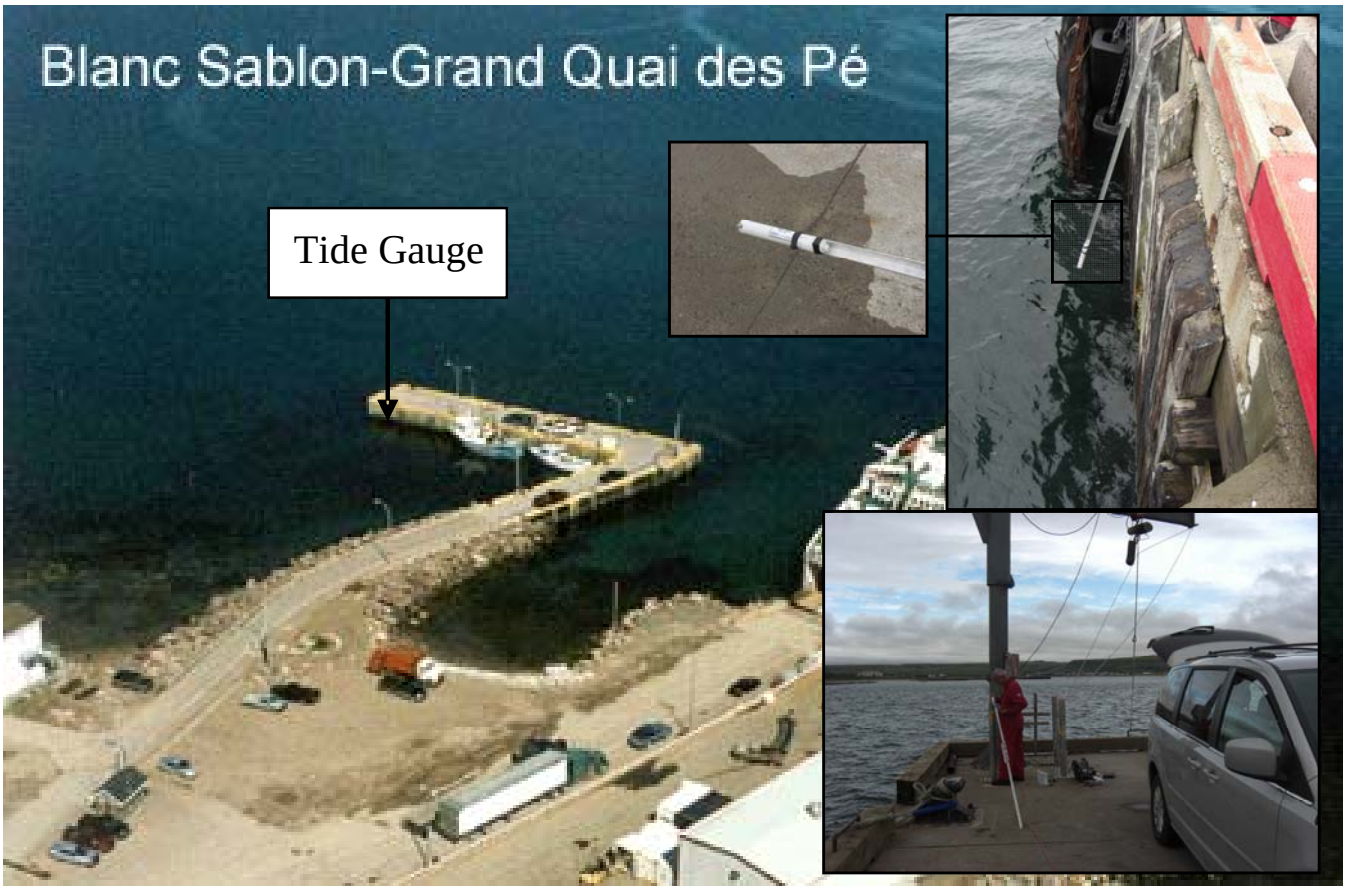

Figure 2.2-2: Installation and Retrieval of Nalcor Tidal Gauge at Blanc Sablon (background picture source: DFO List of Harbours and Harbour Authorities, 2009).

The absolute pressure data were extracted from those instruments and corrected for atmospheric pressure variation during the monitored period using the atmospheric pressure record from the Environment Canada Blanc Sablon airport station (Climate ID 7040813, Environment Canada, 2010c). The corrected pressure data were then converted to water depth from the mean sea level and analyzed for tide using the T_TIDE harmonic analysis package (Pawlowicz et al., 2002).

Figure 2.2-3 presents the atmospheric pressure corrected at sea level for Blanc Sablon. Figure 2.2-4 presents the tide gauge data corrected for atmospheric pressure variations including the tidal signal. The absolute pressure raw data were corrected for the atmospheric pressure variation and then converted to water level before being analyzed. A summary table of the tidal analysis for the four stations is presented in Table 2.2-1.

Overall, the tidal signal is clearly evident from the data (Figure 2.2-4) and was revealed by the analysis to represent 95.9%, 93.6%, 93.2% and 86.5% of the total observed variance for Blanc Sablon, Pinware, St. Barbe and Eddies Cove, respectively.

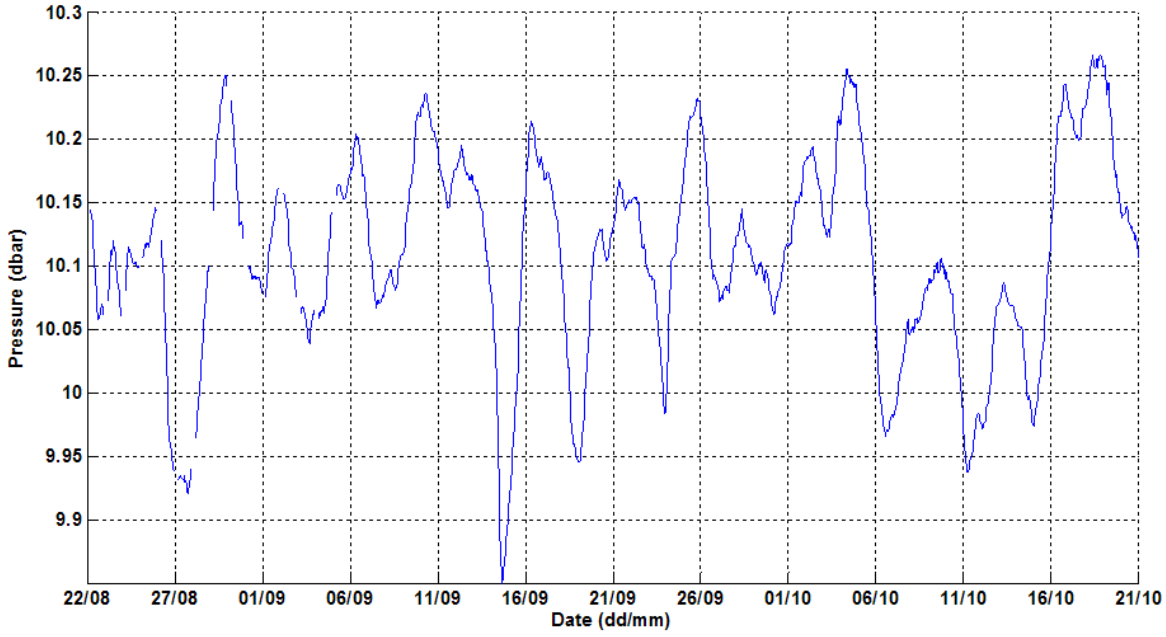

Figure 2.2-3: Blanc Sablon Environment Canada Airport Atmospheric Pressure (Corrected at Sea Level).

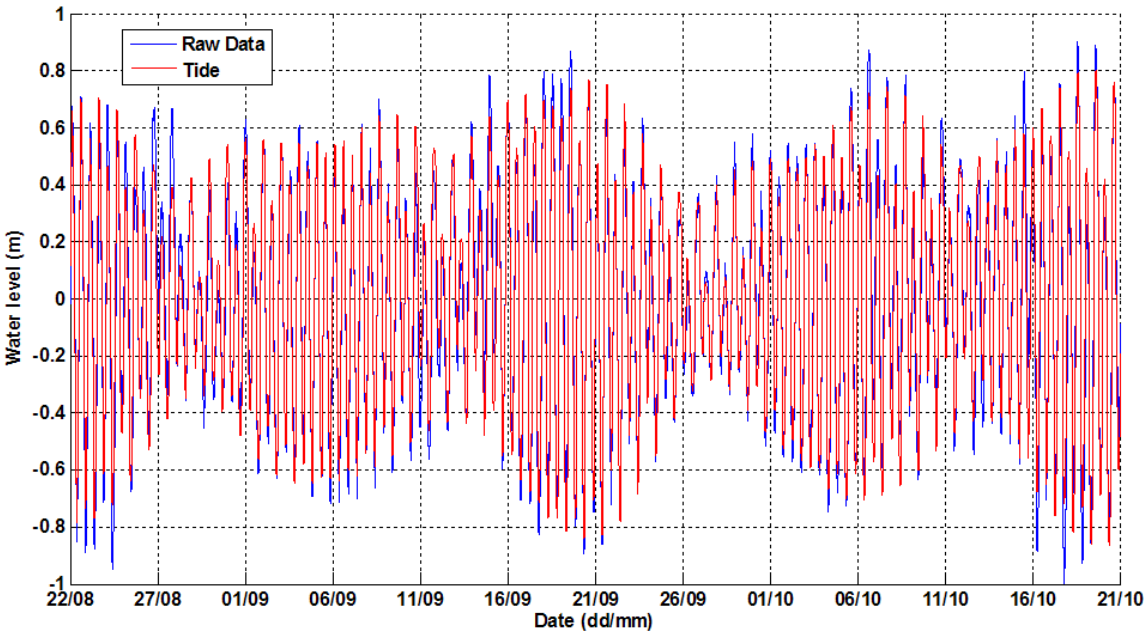

Figure 2.2-4: Nalcor Tide Gauge Data During Monitored Period (August to October 2009).

Table 2.2-1: Summary of Tidal Harmonic Analysis for the Four Main Constituents of the Monitored Sites.

Constituents	Site	Amplitude (m)	Phase (° from Greenwich)	Frequency (cycles/hr)
M2	St. Barbe	0.42	66 (4)	0.08051
	Eddies Cove	0.21	37 (2)	"
	Blanc Sablon	0.47	54 (3)	"
	Pinware	0.32	23 (1)	"
S2	St. Barbe	0.16	77 (4)	0.08333
	Eddies Cove	0.11	33 (2)	"
	Blanc Sablon	0.20	67 (3)	"
	Pinware	0.16	31 (1)	"
O1	St. Barbe	0.10	263 (4)	0.03873
	Eddies Cove	0.04	263 (3)	"
	Blanc Sablon	0.10	236 (2)	"
	Pinware	0.07	202(1)	"
K1	St. Barbe	0.07	257 (4)	0.04178
	Eddies Cove	0.05	223 (2)	"
	Blanc Sablon	0.09	238 (3)	"
	Pinware	0.08	209 (1)	"

As described in Section 2.1.2.4, the tide in the Strait is mainly semi-diurnal with semi-diurnal constituents M2 and S2 stronger than diurnal constituents O1 and K1 at all sites. Tidal constituent M2 is the principal semi-diurnal lunar characteristic of the tide. Tidal constituent S2 is the principal semi-diurnal solar characteristic of the tide. Tidal constituent O1 is the principal diurnal lunar characteristic of the tide, and tidal constituent K1 is

the luni-solar diurnal characteristic of the tide. Overall, the M2 tide amplitude is dominant. It is two to three times higher than the S2 component, four to five times higher than O1, and four to 10 times higher than K1. From the analysis, it can also be noted that the tidal waves propagate from northeast to southwest, reaching Pinware first, then Eddies Cove, Blanc Sablon and then St. Barbe as revealed by the phases of the constituents. The phases in Table 2.2-1 were calculated relative to Greenwich time. The phases presented in Figure 2.1-15 are relative to Greenwich + 4 hours so that approximately 120° and 60° must be added respectively to the M2 and K1 phases of Figure 2.1-15 for comparison with phases in Table 2.2-1 relative to Greenwich. Accounting for the 4 hour time difference supported by the tidal phases and amplitudes recorded during the fall of 2009 are historical records described in Figure 2.1-15.

Overall, the phase lags result in about a 30 minute tide phase difference between the monitored stations (Pinware is about 30 minutes earlier than Eddies Cove, which is about 30 minutes earlier than Blanc Sablon, which is about 30 minutes earlier than St. Barbe).

These phase lags also result in both “along shore” (Pinware to Blanc Sablon, or Eddies Cove to St. Barbe) and “cross shore” (Pinware to Eddies Cove, or Blanc Sablon to St. Barbe) water level difference fluctuations aimed to be reproduced by the numerical model.

For the model, only the tidal part of the signal from each of the four gauges (red line in Figure 2.2-4) was used to generate boundary conditions on the four corners of the grid as described in Section 2.2.3.

2.2.2 Development of the Bathymetric Grid

Several sources of data were used to produce the bathymetric grid for the hydrodynamic numerical model. The most up-to-date data available from the Strait were obtained from the latest survey work from Fugro (2007b). This survey; however, did not cover the entire study area for this modelling study (Figure 2.2-5), and thus, older field sheet data and digital charts from the Canadian Hydrographic Survey (CHS) were used to complete the coverage. All the data were available as x,y,z sounding ASCII files. The surveys were horizontally referenced to NAD83, and vertically referenced to LLWLT (Lower Low Water Large Tide, CHS, 2011)[3]. The horizontal resolution of Fugro’s survey was 10 m while the average resolution of the CHS surveys varied from 50 m to a few hundred metres.

To create the regular grid required for the numerical model, the data were first converted into UTM (Zone 21) horizontal coordinates and then interpolated over a regular mesh with a cell size of 100 m x 100 m (Figure 2.2-6 and Figure 2.2-7).

Depths from bathymetric surveys were acquired relative to Chart Datum (CD, LLWT), whereas the tide gauge data used to derive boundary conditions at the open boundaries of the model were referenced to Mean Sea Level (MSL). It was therefore necessary to adjust the bathymetric grid for comparison to the MSL instead of CD. This was calculated using tidal amplitudes from WebTide to determine MSL spatial variations over the grid domain.

[3] The ASCII files are text files consisting of x = x-coordinates, y = y-coordinates; z = z-coordinates (depth)

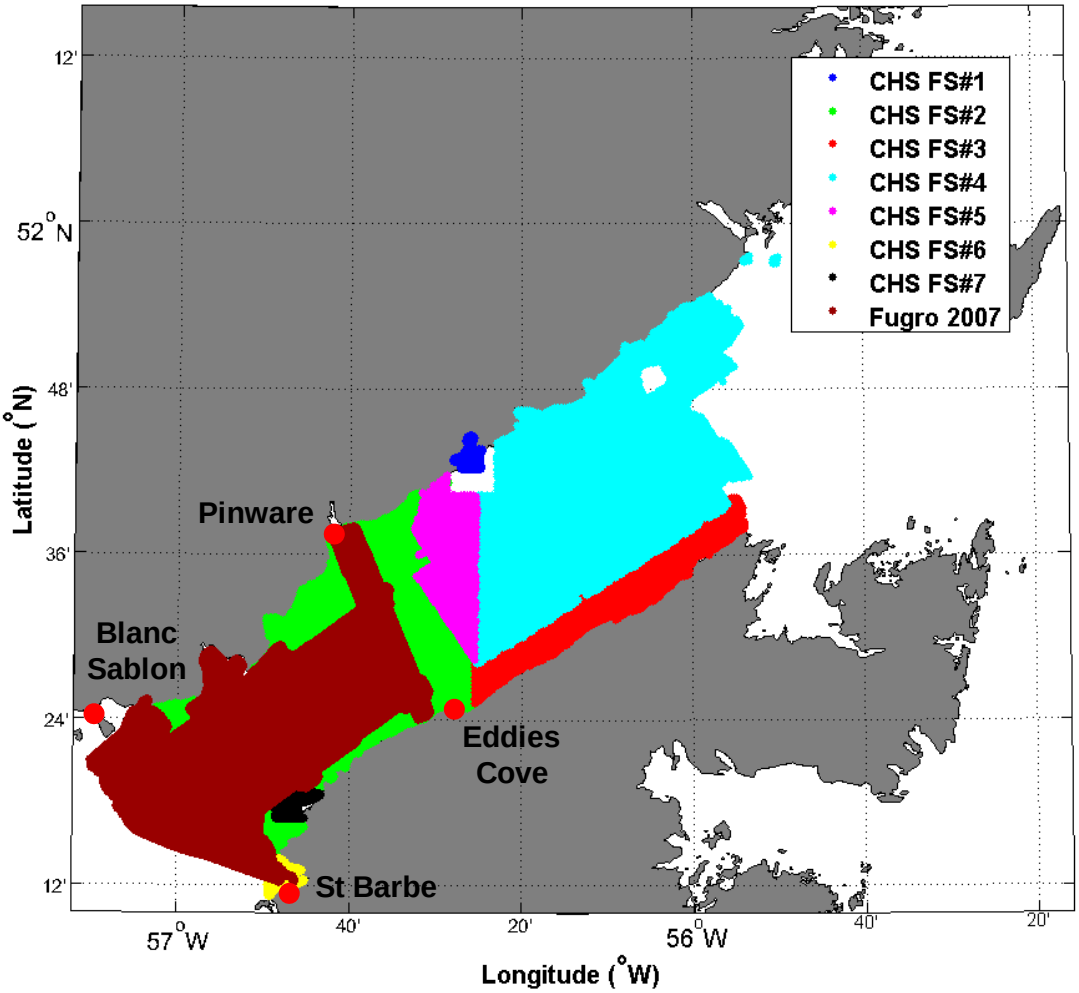

Figure 2.2-5: Bathymetry Data Sources (CHS and Fugro) and Coverage and Nalcor Tidal Gauge Stations (Red Dots).

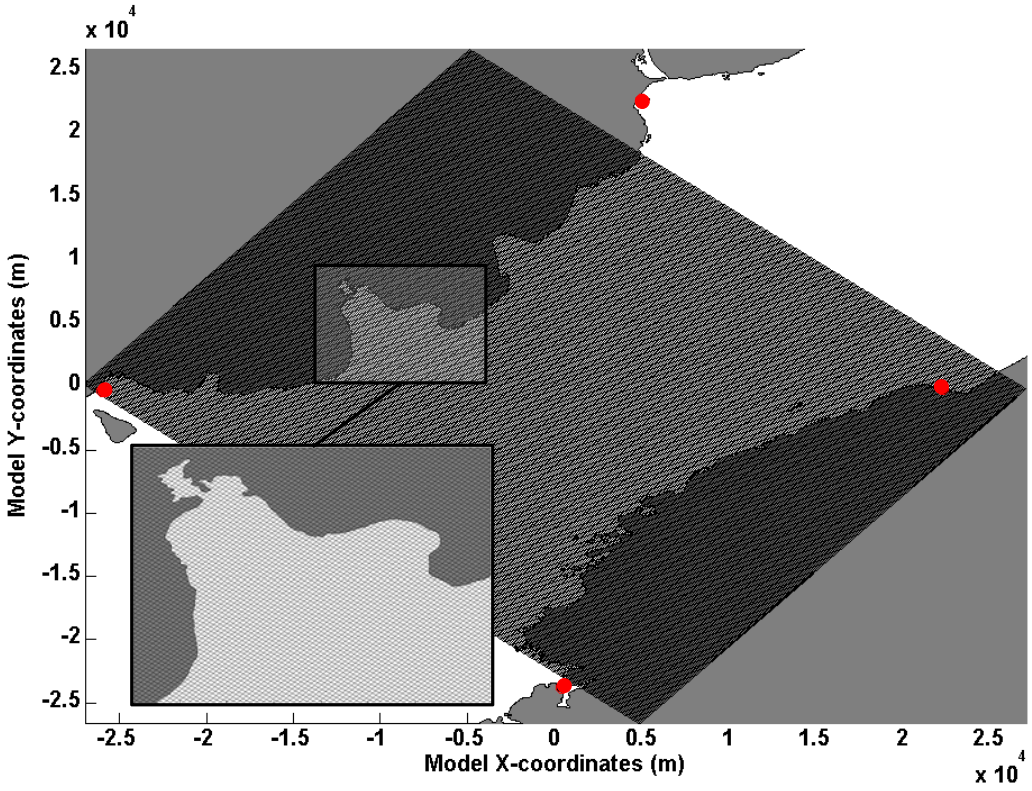

Figure 2.2-6: Numerical Model Grid Cells. Red Dots Represent Nalcor Tidal Gauge Positions Used for the Model Boundaries Input. The Inset for Forteau Bay Illustrates the Resolution of the Grid.

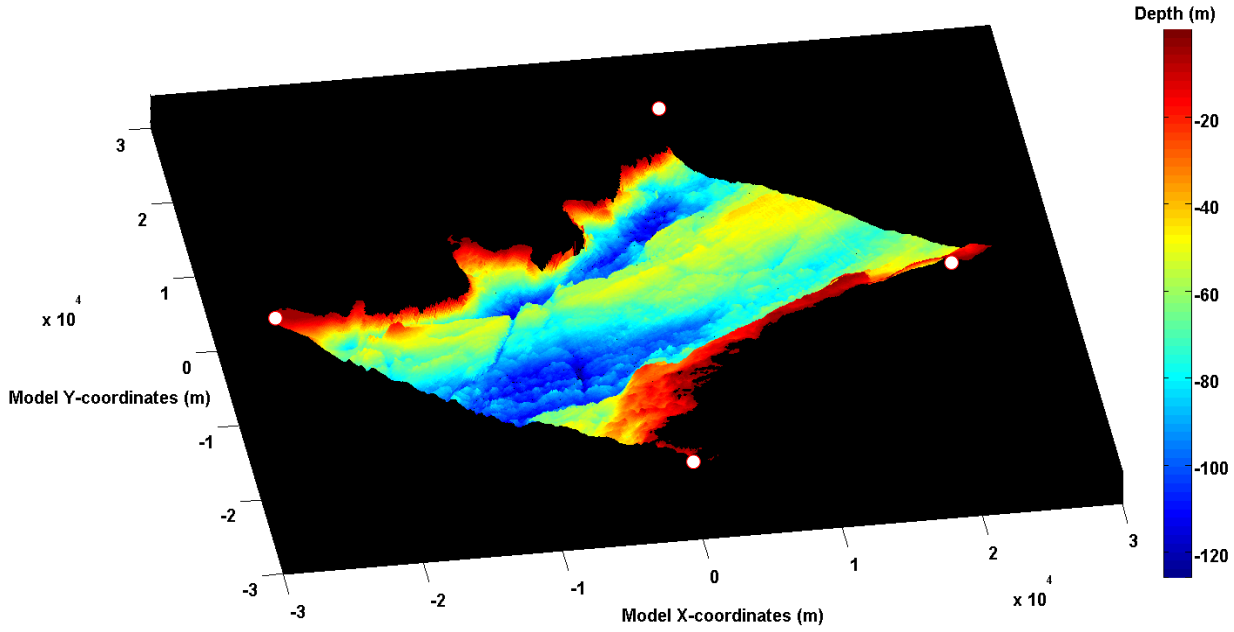

Figure 2.2-7: Numerical Model Bathymetry. White Dots Represent Nalcor Tidal Gauge Positions Used for the Model Boundaries Input.

2.2.3 HYDRO2D: Hydrodynamic Model

AMEC's fully non-linear hydrodynamic HYDRO2D was used to simulate currents within the Strait of Belle Isle study area. It was set up by incorporating the bathymetric grid described in Section 2.2.2 and forced using tidal water level variations recorded by the four tide gauges.

2.2.3.1 Model Description

HYDRO2D numerically solves, over a horizontal regular rectangular grid, the depth-averaged Shallow Water Equations (SWE) for an incompressible fluid with uniform density in a frame of reference rotating about a vertical axis with uniform angular velocity (projection of the earth planetary angular velocity vector on the local vertical axis of the modelled domain).

SWE are a simplified version of the Navier-Stokes equations that describe the behaviour of a fluid continuum (Newtonian fluid). SWE are well-fitted to represent motions affected by the earth's rotation that have a horizontal scale comparable to the water depth, but only if the projection on the local vertical axis of the earth angular velocity can be considered uniform over the domain (the "f-plane" approximation). This is the case for settings such as tidal or wind driven circulation in the coastal ocean environment or lakes. SWE consist of the continuity equation (that expresses the conservation of the mass of a material element as it moves), and the equation of motion (that expresses Newton's second law of motion: the rate of change of momentum of a material element is equal to the net force applied on it).

SWE implicitly contain the hydrostatic approximation which expresses the fact that because of the nearly horizontal character of the fluid trajectories, the vertical accelerations are so small that the pressure at any point in the fluid in motion is equal to the weight of the column of fluid above the point at that instant, as if the fluid were at rest. As a consequence of the validity of the hydrostatic approximation for large scale motions, the horizontal pressure gradients that produce the horizontal accelerations are independent of the depth. It follows the horizontal accelerations and therefore the velocities are also independent of the depth, so that the continuity and momentum equations can easily be integrated vertically to derive depth-averaged formulations.

2.2.3.2 Model Setup

The model was first set up on the bathymetric grid consisting of 347 rows by 419 columns of constant cell size of 100 m by 100 m, for an overall grid 34.7 km by 41.9 km and a total of 145,393 cells.

The two open boundaries defined by the 'lines' between Blanc Sablon and St. Barbe to the south and Pinware and Eddies Cove to the north were forced by the tidal elevation time-series obtained in Section 2.2.1 (Figure 2.2-8). Since the tide was only available for those four (corner) points, linear interpolation was performed between opposite sides (i.e., between Blanc Sablon water level and St. Barbe water level). The tide gauge stations did not exactly 'face' each other across the Strait, therefore to minimize the effects of the slight phase lags between stations and grid boundaries, the grid was built so that the boundaries were located exactly between opposite stations (that is, mid-distance between Pinware and Eddies Cove to the north (see Figure 2.2-6 and Figure 2.2-7).

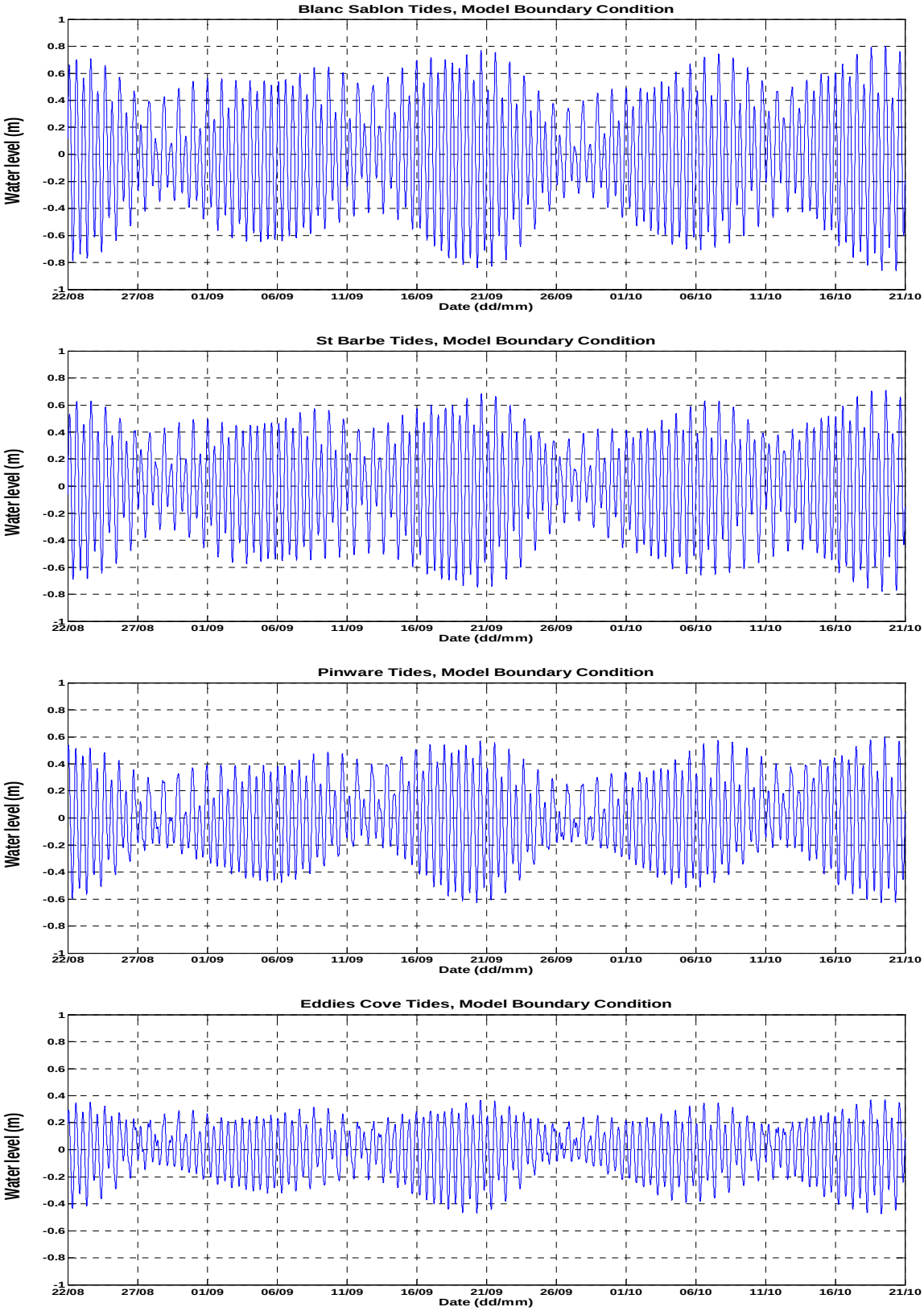

Figure 2.2-8: HYDRO2D Tide Time-Series Boundary Conditions.

The grid was quite large in terms of the number of cells with a high resolution (relative to the area being modelled) and required a small time step of 2 seconds to keep the numerical simulation stable.

The model was run over the period of 60 days monitored by the tidal gauges (August 22, 2009 to October 21, 2009) with output every 300 seconds (5 minutes), resulting in 17,280 output files.

In addition to this tidal circulation scenario, a second scenario was implemented to simulate the steady state circulation that results from atmospheric setup (difference in mean water level) between the south and north boundaries as described by Garrett and Toulany (1981) (Section 2.1.2).

2.2.3.3 Model Validation

The model was validated using historical tidal gauge data and moored current meters to test the ability of the model to simulate variations of the tidal elevations and tidal currents.

Tidal Elevations

No permanent stations are presently located in the Strait of Belle Isle and only historical data could be accessed. Data sets from five tidal gauges were available from the CHS website: West St. Modeste (#2595), Forteau Bay (#2590), Blanc Sablon (#2588), Anchor Point (#2637), and Savage Cove (#2633). Figure 2.2-9 indicates their location. A summary of the available data is presented in Table 2.2-2.

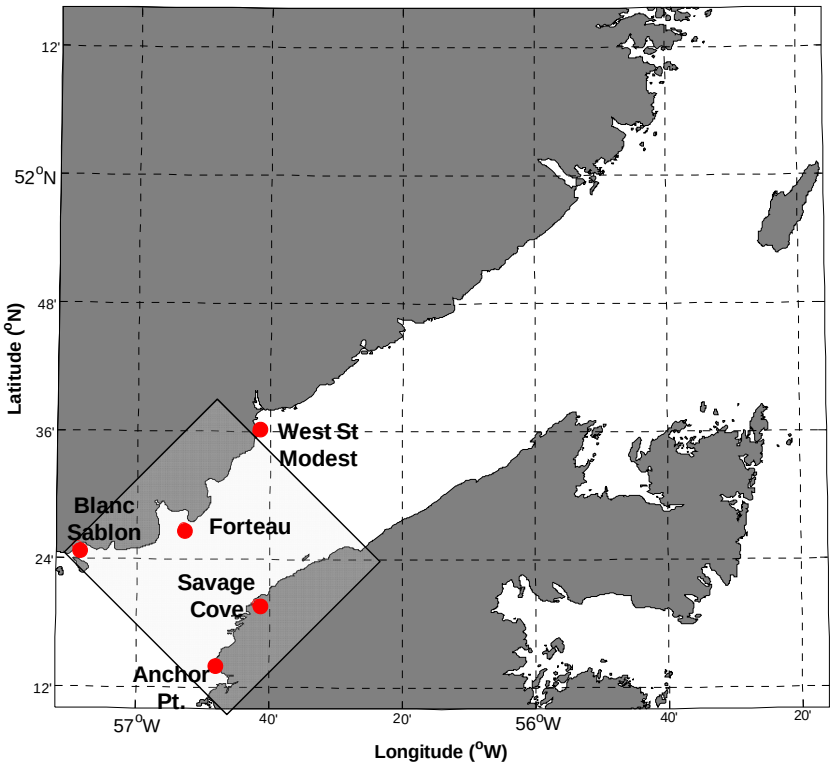

Figure 2.2-9: CHS Historical Tide Gauge Stations (Red Dots) and Study/Numerical Model Area (Box).

Table 2.2-2: Summary of CHS Tide Gauge Data.

Station Name and Number	Position	Monitored Period	Sampling Interval	Downloaded Data Period	Duration (days)	Missing Data
Anchor Point #2595	51.23°N 56.8°W	03-Oct-1969 to 15-Mar-2000	15 min	01-Jan-2000 To 01-Apr-2000	91	20 samples (<1%)
Blanc Sablon #2588	51.42°N 57.15°W	25-Sep-1985 to 15-Oct-1985	1 hour	25-Sep-1985 To 15-Oct-1985	19	0 samples (0%)
Savage Cove #2633	51.33°N 56.7°N	04-Oct-1969 to 10-Nov-1982	1 hour	19-Apr-1980 To 28-Jul-1980	101	0 samples (0%)
Forteau #2590	51.45°N 56.88°W	01-Sep-1898 to 31-Dec-1915	1 hour	02-Mar-1915 to 31-Dec-1915	304	175 samples (~2%)
West St. Modeste #2595	51.6°N 56.7°W	03-Oct-1969 To 15-Mar-2000	15 min	01-Jan-2000 To 15-Mar-2000	74	136 samples (~2%)

Data from a sixth station at Flower's Cove were inaccessible at the time of this study and the record from Blanc Sablon is too short to be used, as a minimum of 29 days is needed to resolve tidal semi-diurnal constituents. A minimum duration of 60 days would have been preferred to match that of Nalcor Energy's data collection.

Therefore, four stations were used for the validation, two positioned inside the study area (Savage Cove and Forteau) and two positioned on the two boundaries of the model (Anchor Point and West St. Modeste). Both boundaries and the interior of the model domain could then be validated.

The results of this validation exercise are presented in Figure 2.2-10 and Table 2.2-3 and illustrate agreement between the two data sources. For M2, the major constituent, the maximum error in amplitude is 3 cm (7%) and phase differences range from 1° to 12°.

S2 and the diurnal constituents O1 and K1 have smaller amplitudes and are relatively less resolved with a maximum amplitude difference of 4 cm and phase differences ranging from 2° to 40°.

Overall, Figure 2.2-10 shows an agreement between the modelled and measured time-series of the tidal water elevation variations at the four stations. Considering that the validation is somewhat indirect (i.e., historical data used through harmonic analysis) it is thought that the model performed well and reproduced the tide elevation accurately within the study area.

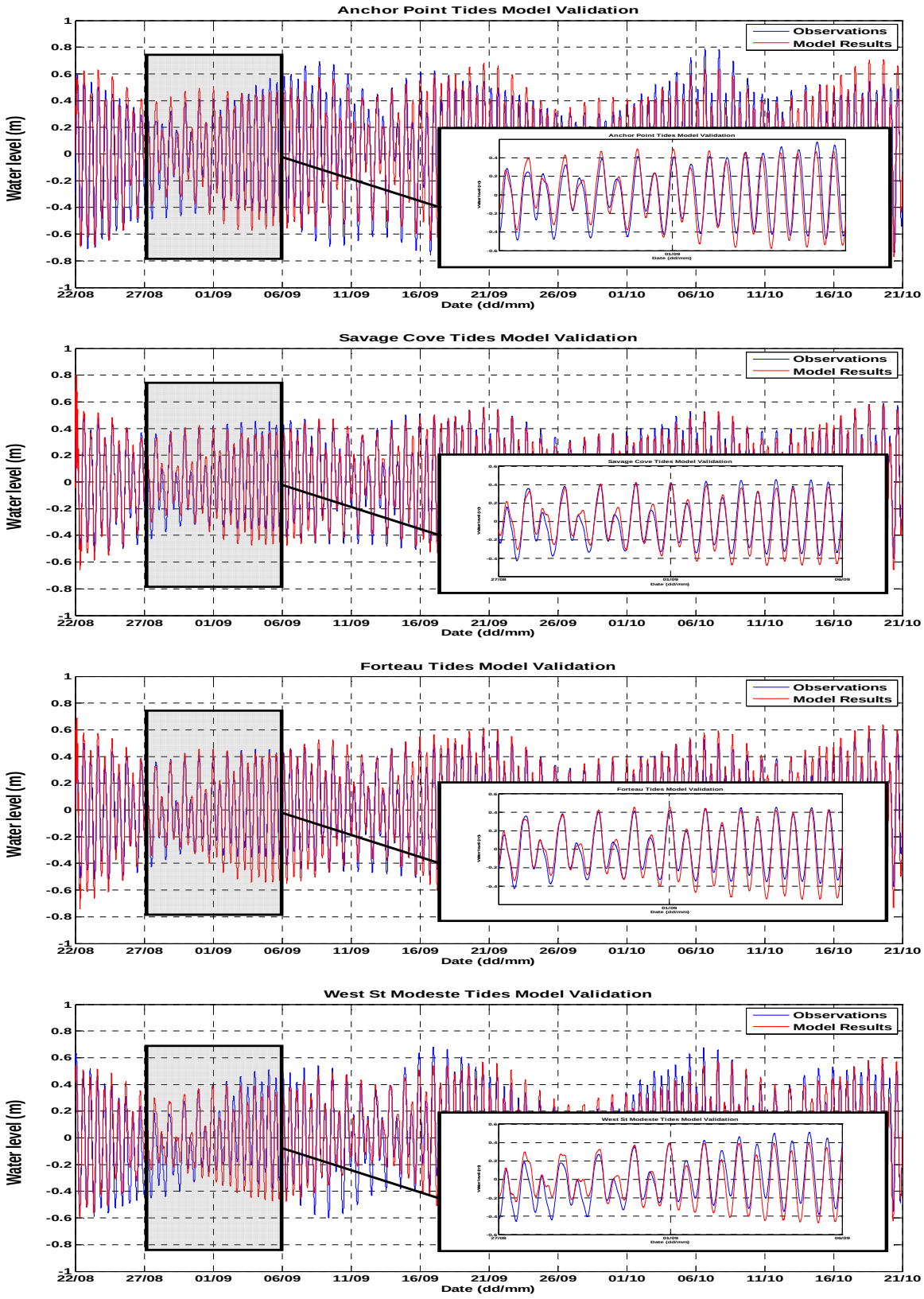

Figure 2.2-10: HYDRO2D Tidal Elevation Validation.

Table 2.2-3: HYDRO2D Model Tidal Elevation Validation.

Constituents	Site	Amplitude (m)		Phase (^{o} from Greenwich)	
		Gauge	Model	Gauge	Model
M2	Anchor Point	0.43	0.42	78	66
	Savage Cove	0.35	0.35	56	60
	Forteau	0.41	0.38	38	49
	West St. Modeste	0.34	0.32	22	23
S2	Anchor Point	0.15	0.17	116	76
	Savage Cove	0.10	0.14	68	66
	Forteau	0.14	0.17	56	58
	West St. Modeste	0.13	0.16	58	31
O1	Anchor Point	0.11	0.10	266	263
	Savage Cove	0.09	0.08	252	260
	Forteau	0.08	0.08	224	238
	West St. Modeste	0.07	0.07	206	202
K1	Anchor Point	0.10	0.07	295	257
	Savage Cove	0.09	0.06	253	250
	Forteau	0.11	0.08	237	234
	West St. Modeste	0.10	0.08	235	209

Tidal Currents

Time-series of four moored current meters were selected and extracted from DFO's Ocean Data Inventory (ODI) database. This database is an inventory of all of the oceanographic time-series data held by the Ocean Science Division at the Bedford Institute of Oceanography. The selection criteria were similar to those for CHS water level gauges, i.e., time-series sufficiently long enough to correctly resolve the semi-diurnal tidal constituent (29 days minimum, 60 days preferred) and a combination of locations that would best cover the study area.

The location of those moorings are presented in Figure 2.2-11 followed by a summary of the available data presented in Table 2.2-4. A summary of the results is presented in Figure 2.2-12 and Table 2.2-5.

The selected moorings spatially cover the study area in the Strait from northwest to southeast and are representative of the variation of the flow within the study area. Some of the data available however, were short with one record (MCM-02) which covered 33 days and another (MCM-01) 51 days. This still met the minimum required 29 days.

It should also be noted that the mooring data used in the previously mentioned Farquharson and Bailey (1966) and Garrett and Petrie (1981) studies (Section 2.1.2) are illustrated in Figure 2.1-17.

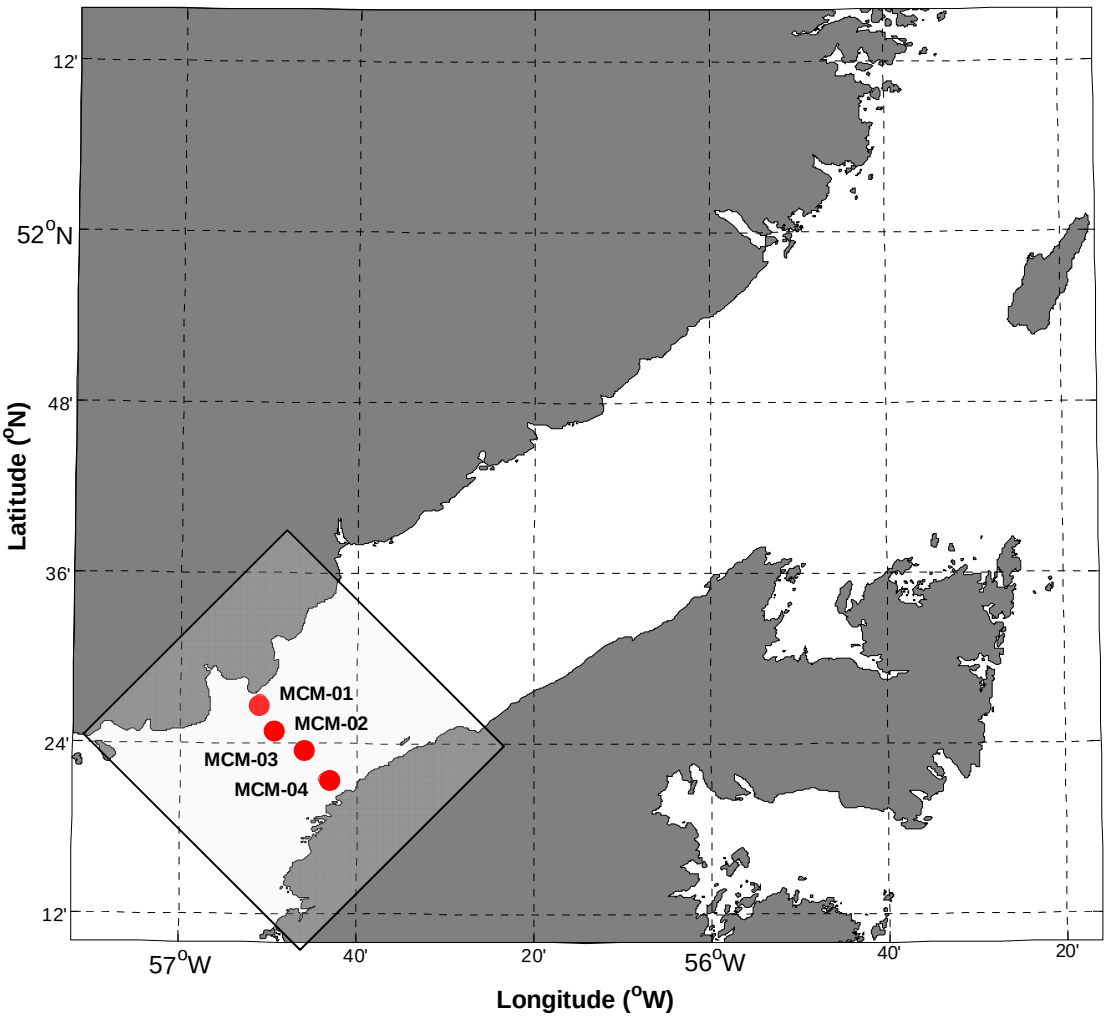

Figure 2.2-11: DFO Historical Moored Current Meter Stations (Red Dots) and Study/Numerical Model Area (Box).

Table 2.2-4: DFO Available Current Meter Data.

Mooring	Position	Monitored Period	Sampling Interval	Depth (m)	Downloaded Data Period	Duration (days)	Missing Data
MCM-01	51.45°N 56.85°W	01-Aug-1963 To 20-Sep-1963	5 min	50	01-Aug-1963 To 20-Sep-1963	51	0 samples (0%)
MCM-02	51.41°N 56.81°W	18-Aug-1963 To 20-Sep-1963	5 min	13	18-Aug-1963 To 20-Sep-1963	33	0 samples (0%)
MCM-03	51.4°N 56.77°W	26-Jul-1980 To 18-Oct-1980	30 min	43	26-Jul-1980 To 18-Oct-1980	84	0 samples (0%)
MCM-04	51.35°N 56.72°W	26-Jul-1980 To 18-Oct-1980	30 min	11	26-Jul-1980 To 18-Oct-1980	84	0 samples (0%)

M2 is the main component of the tidal current, with S2, O1 and K1 all comparable and at half, or less than half, the amplitude of M2 (Table 2.2-5).

For M2, differences between measured and modelled major tidal currents (i.e., the major semi-axis of the ellipse representing the flow as illustrated in Figure 2.1-16) range from 4 cm/s to 19 cm/s (8% to 28%). The values (measured and modelled) for the semi-minor axis are very small (a few centimetres per second or less) and the flow is mainly along the Strait. The phase differences range from 10° to 29°. The phase difference is significantly higher for the two northern sites (MCM-01 and MCM-02) than for the southern sites (MCM-03 and MCM-04, Table 2.2-5).

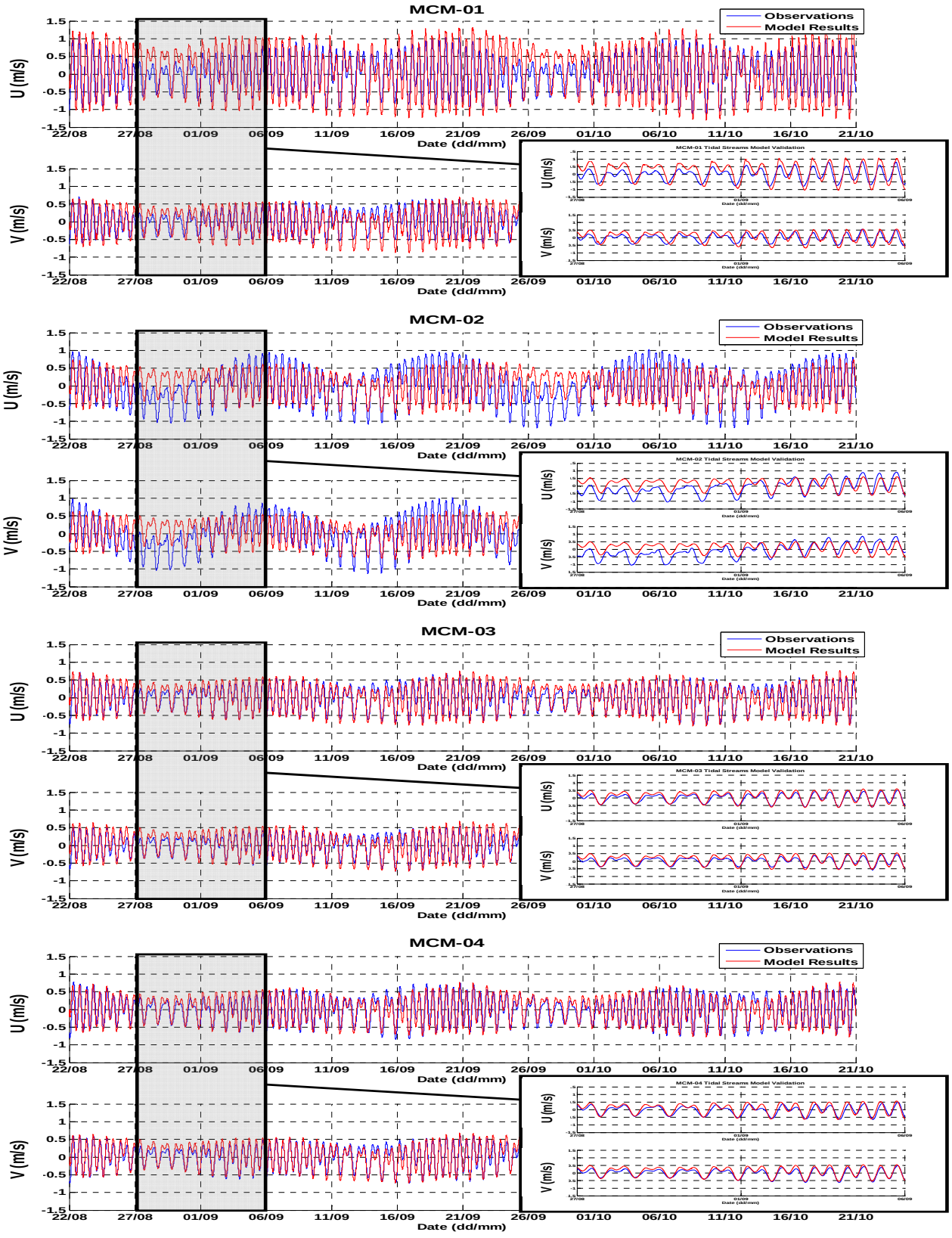

Figure 2.2-12: HYDRO2D Tidal Current Validation.

Table 2.2-5: HYDRO2D Model Tidal Current Validation.

Constituents	Site	Amplitude (m)				Phase (° from Greenwich)	
		Current meter		Model		Current meter	Model
		Major	Minor	Major	Minor		
M2	MCM-01	0.68	-0.01	0.87	0.03	138	167
	MCM-02	0.62	-0.05	0.55	-0.001	144	173
	MCM-03	0.47	-0.01	0.55	0.01	182	172
	MCM-04	0.51	-0.04	0.55	0.04	185	168
S2	MCM-01	0.26	-0.01	0.37	0.02	179	191
	MCM-02	0.27	-0.04	0.25	-0.003	180	201
	MCM-03	0.19	0.01	0.24	0.004	218	199
	MCM-04	0.23	-0.03	0.24	0.02	222	195
O1	MCM-01	0.23	0.004	0.32	0.04	318	327
	MCM-02	0.29	-0.01	0.25	0.01	331	342
	MCM-03	0.23	-0.02	0.24	0.02	335	340
	MCM-04	0.23	0.01	0.24	0.04	333	335
K1	MCM-01	0.21	0.01	0.24	0.03	2	2
	MCM-02	0.25	-0.04	0.18	0.01	21	13
	MCM-03	0.19	-0.001	0.18	0.01	31	11
	MCM-04	0.22	0.002	0.17	0.02	27	8

For the other three constituents, differences between measured and modelled semi-major axis range from 1 cm/s to 11 cm/s, and phase differences range from 0° to 27°.

As shown in Figure 2.2-12, the model reproduced the tidal currents within the study area reasonably well, and the model performance is similar to the DFO WebTide simulation of the Scotian Shelf (Dupont et al., 2002), and of the Gulf of St. Lawrence work from Lu et al. (2001).

The northern stations show somewhat less similarity than the southern stations, but still reproduce the patterns of the tidal current variations quite well. The most obvious difference is site MCM-02 which shows a low frequency, relatively large amplitude, oscillation (period of about 15 days) in the current meter record that is not reproduced by the model. Tidal analysis of the MCM-02 current data reveals that the low frequency tidal constituent MSF (period of 14.8 days) is very strong compared to the current meter records from the three other sites and the four tide gauge records used to force the model. Without a strong MSF constituent in its forcing, the model cannot produce a strong MSF tidal current. If the model were to produce a strong MSF tidal flow, it would most likely be for the entire domain and there would then be a large discrepancy with the current records at the three other sites which do not have a strong MSF constituent. Scrutiny of the results of tidal analysis on current meter records from the Strait other than the four retained for this validation show that, among the records long enough for the low frequency MSF signal to be resolved, some have a strong MSF constituent like MCM-02 and some have a weak MSF constituent like MCM-01, MCM03 and MCM-04. Further, there does not seem to be any correlation between the strength of the MSF signal and the location of the current meters in the Strait.

2.2.3.4 Atmospheric Forcing Scenario

In addition to the 60 day tidal current simulation, two model scenarios were completed to simulate the current field associated with adjustment of the Strait to typical atmospheric forcing in the region. One scenario simulated a southwest-northeast gradient and the other gradient in the opposite direction (northeast-southwest).

A sea level difference of 0.1 m between the two open boundaries of the model domain was assumed, following the estimates of Garrett and Toulany (1981), who found that a pressure gradient of that order would result in a current within the Strait of about 0.6 m/s (Section 2.1.2).

The model was run in 'steady-state' mode, (i.e., the water level at the boundaries were kept constant for the duration of the simulation (± 0.05 m at each end relative to mean water level). This scenario simulates a typical setup in the Strait resulting from atmospheric forcing.

Results of the simulation (water level elevation and current speed) at the same sites as for tidal forcing are presented in Figure 2.2-13 and demonstrate similar results expected from the analysis as those found by Garrett and Toulany (1981). After a period of less than a day of adjustment, the model reached an average current speed along the Strait of about 0.6 m/s.

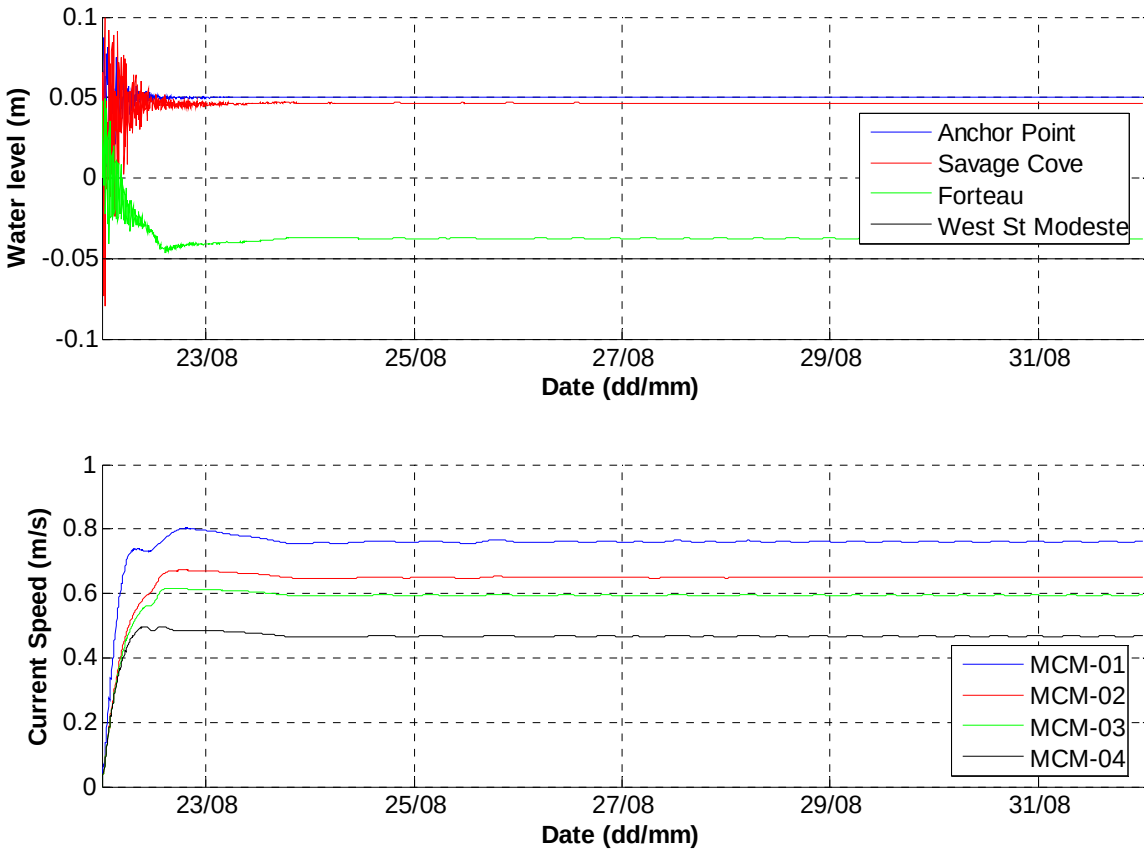

Figure 2.2-13: HYDRO2D Model Atmospheric Forcing Validation.

2.2.4 Benthic Boundary Layer Transport: Sediment Dispersion Model

The DFO sediment dispersion particle tracking BBLT (Benthic Boundary Layer Transport) model (Drozdowski et al., 2004, Drozdowski, 2009) was used to simulate the dispersion of sediment material (particles) within the Strait of Belle Isle study area. It was set up and forced using the hydrodynamic model (HYDRO2D) including the bathymetric grid, and a discharge scenario described below.

2.2.4.1 Model Description

BBLT is a particle tracking model, initially developed to simulate the fate of drilling mud in the ocean benthic boundary layer (Drozdowski, 2009). The model is based on these principles:

- an initial distribution of sediment on the bottom;
- the currents and associated bottom stress increase until a critical value of the stress is reached;
- all of the sediment becomes suspended and transported;
- the suspended sediment is sheared by the vertical structure of the horizontal currents and the suspended sediment is also (and mostly) smeared by the vertical mixing; and
- the currents weaken and the sediment settles back to the bottom with a broader distribution and a new centre of mass.

Since its early development in the mid-1990s (Hannah et al., 1995) the BBLT model has been developed significantly into a sophisticated tool which can be applied for a range of applications (Petrie et al., 2001; Tedford et al., 2003; Hannah and Drozdowski, 2005). It is currently able to be coupled with 3D current input data (Drozdowski, 2009). The version used for this application was the newly-released BBLT3D and was specifically customized to:

1) be coupled (forced) with the HYDRO2D current field data input; and
2) take into account temporally (time-series) and spatially variable discharge scenarios.

By default, BBLT assumes that the particles are always in suspension and transported as long as the currents are not null (the critical shear stress to move particles is set to zero). To represent a worst-case scenario of dispersion, this assumption was used for the present simulations. Also, since our hydrodynamic data input were two dimensional, a logarithmic profile was assumed and setup by BBLT to account for the vertical structure.

2.2.4.2 Model Setup and Discharge Scenario

The BBLT model requires a discharge scenario to be defined. The Project description indicates that horizontal directionally drilled (HDD) holes will be constructed for three cables to a nominal depth of about 80 m on each side of the Strait. Rock dumping would then provide protection for each of the three cables between the HDD holes (about 30 km long). These three cables will be located within the corridor (Figure 1.1-1).

Both drilling and rock placement are anticipated to result in a limited amount of sediment release in the environment.

Since drilling is to be conducted from shore, and underground, and not within the marine environment, this activity was not assessed in this study.

For the rock placement component, the following assumptions were made to represent possible release (or disturbance) of seabed sediment into the marine environment (water column).

Sediment release for the laying and protection activities (rock dumping) of a cable was assessed. The rock berm is assumed to be about 0.8 to 1.5 m high, and to have a slope ratio of 1:4 and 8 to 12 m wide at the base. The rocks to be used are estimated to be graded from about 50 to 200 mm in diameter. The placement rate is expected to be about 1000 tonnes/hr maximum, and about 200 to 300 tonnes/hr minimum, with an expected average of around 500 tonnes/hr.

From this information, the initial footprint (direct area of the seabed sediment disturbed) was assumed to be 10 m in width and 0.05 m (i.e., 5 cm) in depth, with a penetration of the first layer of rocks about a quarter of their largest diameter size. It was also assumed that the rate of progression along the corridor would be of 100 m per hour, roughly equivalent to 575 m^3 berm volume (considering a 1.15 m high triangular berm). Assuming 50% void and 2.65 tonnes/m^3 rock density, this would lead to an approximate rate of 762 tonnes/hr. This is in the higher end of the provided expected rate but is thought to provide a reasonable worst case scenario (more material released in less amount of time).

To simulate a release of sediment, the nature of the material released needed to be determined as well. As stated in Section 2.1.2, the surficial geology of the Strait was recently surveyed by Fugro GEOS (2007a, 2007b and 2008), FJGI (2010), and AMEC (2010a) and data from those studies were compiled to provide a high resolution sediment type coverage of the area (Figure 2.2-14). This dataset was originally compiled for the two corridors considered at the time of the surveys; however, the design of the corridors slightly changed over the course of the study, and a final corridor was introduced, covering most of the known sediment type area (Figure 2.2-14).

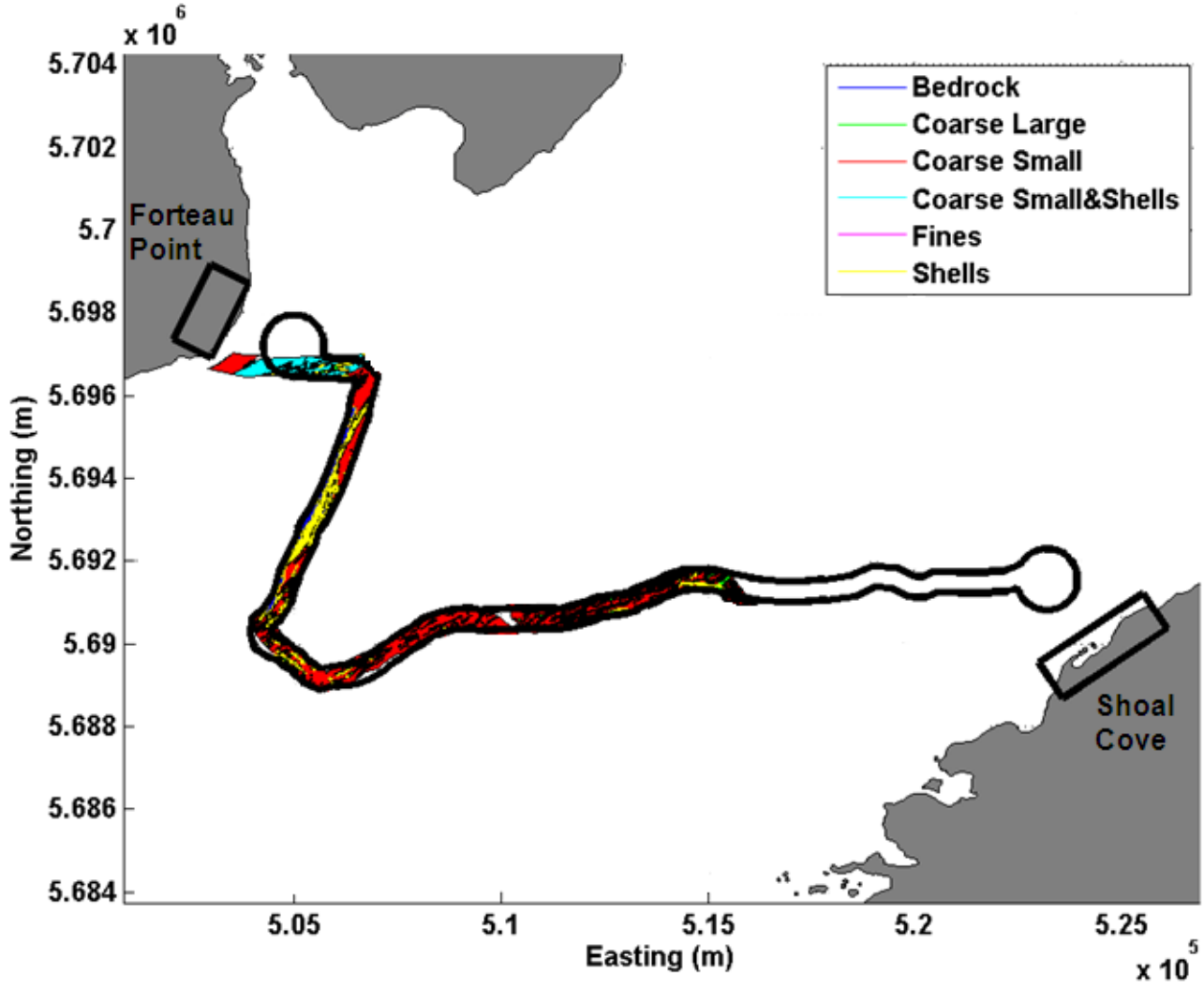

Figure 2.2-14: Seafloor Sediment Types Coverage and Cable Corridor.

Six categories of sediment type were defined in AMEC (2010a): Bedrock, Coarse Large, Coarse Small, Coarse Small and Shells (or with Shells), Fines, and Shells.

For each of those categories, a percentage of sand and silt were determined following the AMEC (2010a) findings. These two categories were chosen since they were the most likely particles to remain suspended for a significant amount of time; the other, coarser types of particles (such as gravel) are likely to settle within the vicinity of the berm, if they became suspended (which is unlikely).

The following percentages were used:

- Bedrock: 3.5% sand, 1% silt
- Coarse-Large: 1% sand, 1.5% silt

- Coarse-Small: 5% sand, 3% silt
- Coarse-Small and Shells: 30% sand, 10% silt
- Fines: 65% sand, 20% silt

To create an input file for the BBLT model, a centerline for the corridor was first created and then indexed to the bathymetric grid (also the base of the BBLT output grid) and the corridor was divided into 100 m by 100 m cells. The sediment categories were indexed using the same method and then compared with the centerline to extract a sediment type along the corridor cells. Each type was then assigned a percentage of sand and silt. These percentages of sediment type were converted into mass considering the volume of bottom material assumed to be released (or disturbed) from the rock placement activities (that is a 100 m long by 10 m wide by 0.05 m deep, 50 m^3, volume per cell) and assuming an arbitrary 2650 kg/m^3 average sediment density and 50% natural void. Typically less than 400 kg of sand and about 200 kg of silt were released per grid cell (Figure 2.2-15). For the portion of the corridor not covered by the sediment type survey, a default Coarse-Small category was assigned as being the most common type identified within the corridor (Figure 2.2-14 and Figure 2.2-15). In Figure 2.2-15 the x-axis is shown referenced to internal BBLT coordinates (in metres) and is from west (Forteau Point) to east (Shoal Cove). The peak represents the release of material in the area of Coarse-Small and Shells material which is represented in cyan in Figure 2.2-14, while the linear end (from about 3000 m to the end) represents the assumed Coarse-Small category.

The marine cable corridor centerline consisted of 290 cells, corresponding to a length of 29 km. Considering a progress rate of 100 m/hr (or 1 cell per hour) the BBLT model ran for a period of current field of 15 days. Hourly current fields from the hydrodynamic model results were imported from the model start date (i.e., 22-Aug-2009 00:00:00) and used as forcing. The same bathymetry file used for the hydrodynamics model was used as inputs into the model. Since the BBLT model can only perform outputs for one category of particles at a time (i.e., one settling velocity), two separate input release files were created and two separate runs were performed (one for sand, one for silt). The sand particles were assigned a settling velocity of 0.02 m/s (corresponding to a grain diameter of 0.2 mm, medium sand, and as defined in the Coastal Engineering Manual, 2002) and the silt particles were assigned a value of 0.0003 m/s (corresponding to a grain diameter of 0.02 mm, 20 microns, medium silt, Coastal Engineering Manual, 2002).

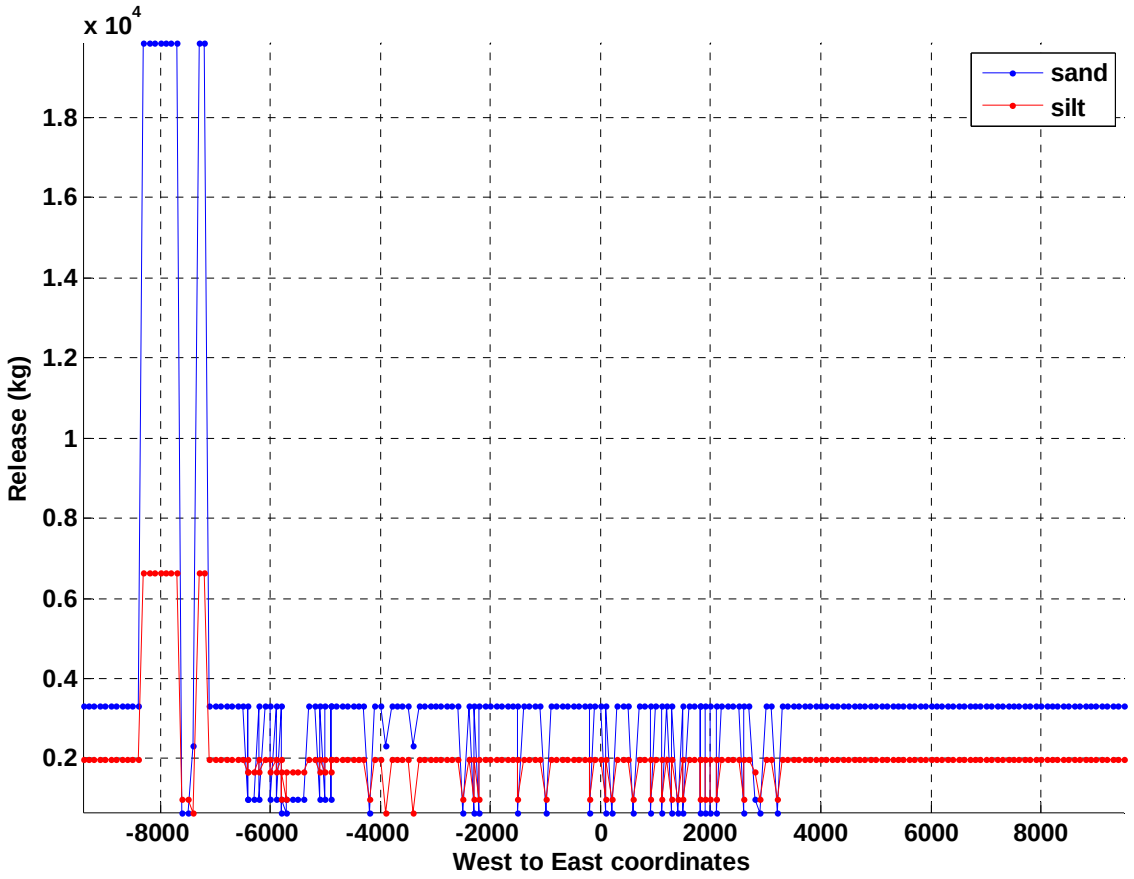

Figure 2.2-15: Sediment Release along the Proposed Strait of Belle Isle Cable Corridor Centreline.

3.0 RESULTS

The key results of the numerical model simulations are presented in this section, starting with the results from the hydrodynamic model (HYDRO2D), followed by those from the sediment dispersion model (BBLT).

3.1 Hydrodynamic Model (HYDRO2D)

The key results of the 60 days of tides hydrodynamic model are presented in Figure 3.1-1 to Figure 3.1-6 for two periods: a neap (small) and a spring (large). The conditions illustrated by these periods somewhat 'bracket' the overall (tidal) conditions that can occur within the study area.

The key observations can be summarized as follows:

- the tidal wave propagates from northeast to southwest and induces strong along-Strait currents of 1 m/s and greater;
- as a result, flood flows from northeast to southwest and ebb flows from southwest to northeast;
- the tide is asymmetric, particularly during neap periods, inducing asymmetric currents;
- cotidal lines are not perpendicular to the Strait but rather are curved;
- during neap tides, ebb and flood currents are of similar amplitude, the change of direction occurs about an hour after high or low water level, and strong currents occur during those periods. The tidal wave is therefore not standing and conserves many of the characteristics of a progressive wave;
- during neap tides, maximum current speed occur about 1 hr before low or high tides;
- from the model, during neap tides, lower high and low water levels occur consistently during an outflow to the northeast (ebb flow). This is presented in Figure 2.2-14 where MCM-01 and MCM-02 do not exhibit this characteristic, and is found in MCM-03 and MCM-04;
- the flow is generally stronger within the main channel of the Strait and weaker in the shallow areas, but present strong local acceleration within the Pt. Amour area. The cyclonic and anticyclonic gyre occurring regularly within Forteau Bay is also an interesting feature of the circulation; and
- during spring tides, the slack period (time of no current) occurs approximately between high tide and low tide and is maximum at high and low, very much like a progressive wave. The flood flow is also stronger than the ebb and reaches almost 1.5 m/s.

Figure 3.1-7 presents the result of the atmospheric forcing steady state situation and illustrates the influence of the geostrophy that veers the gradient to the right.

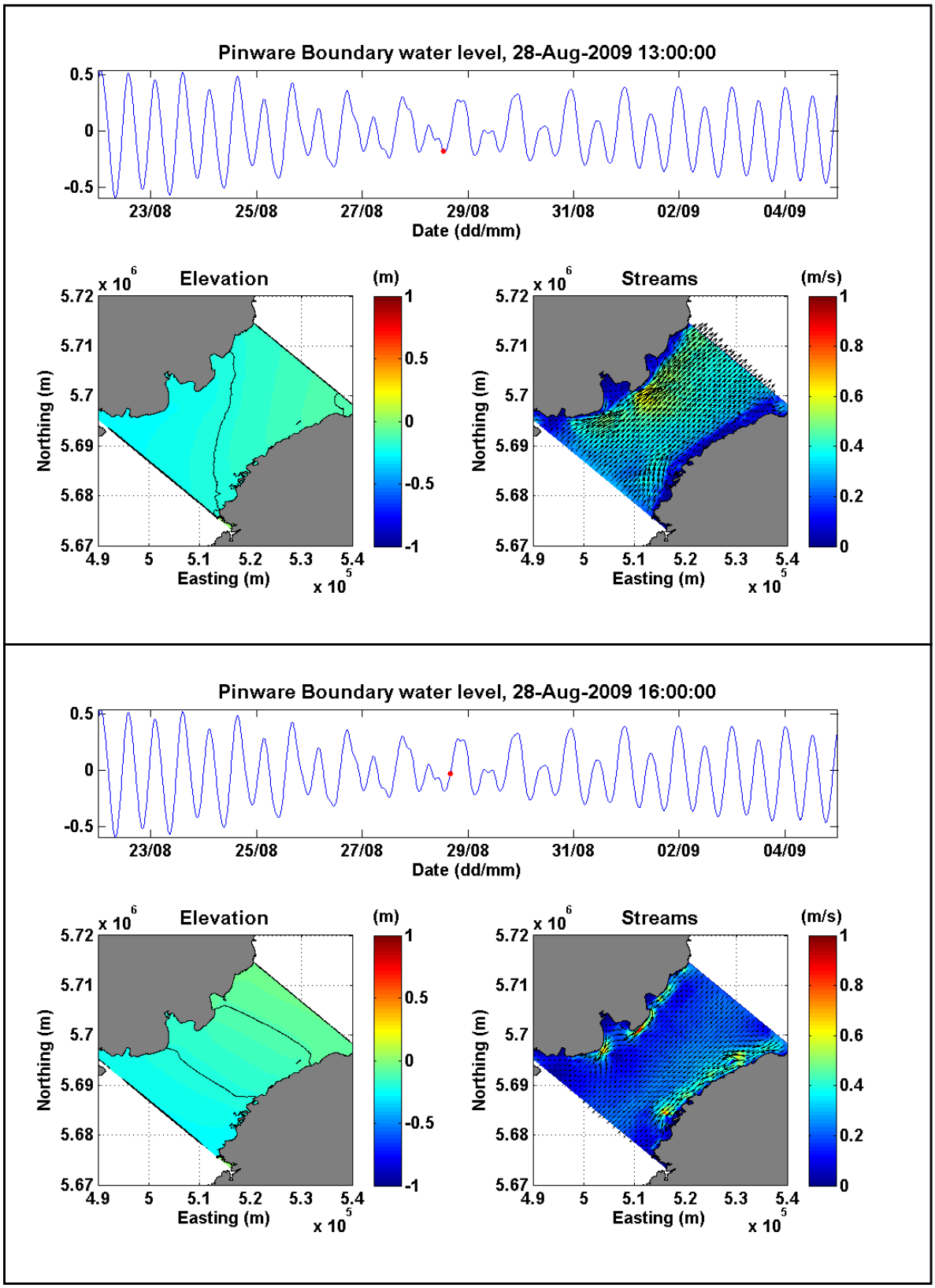

Figure 3.1-1: Flooding Tides during Neap Tide Conditions.

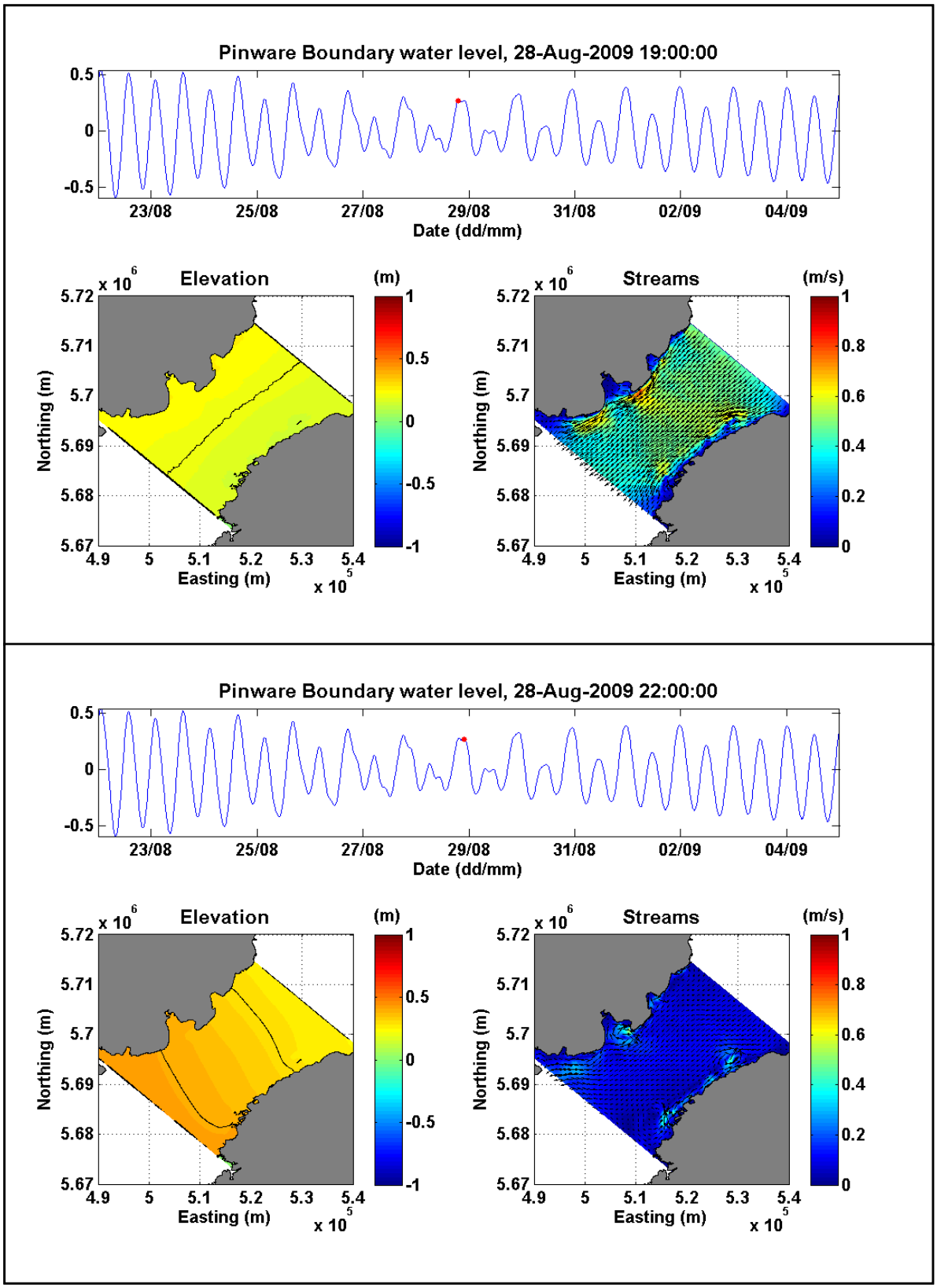

Figure 3.1-2: High Tides during Neap Tide Conditions.

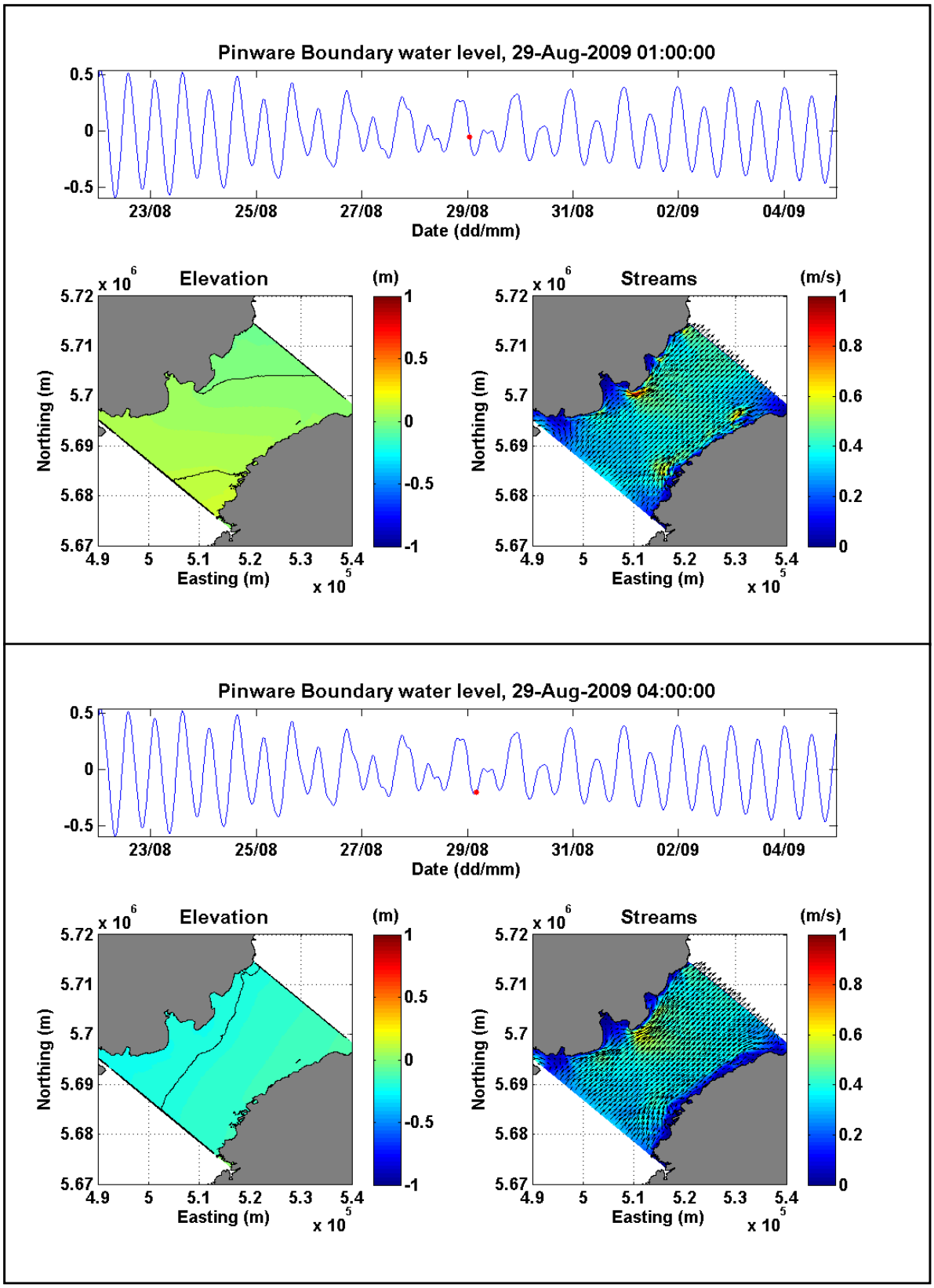

Figure 3.1-3: Ebbing Tides during Neap Tide Conditions.

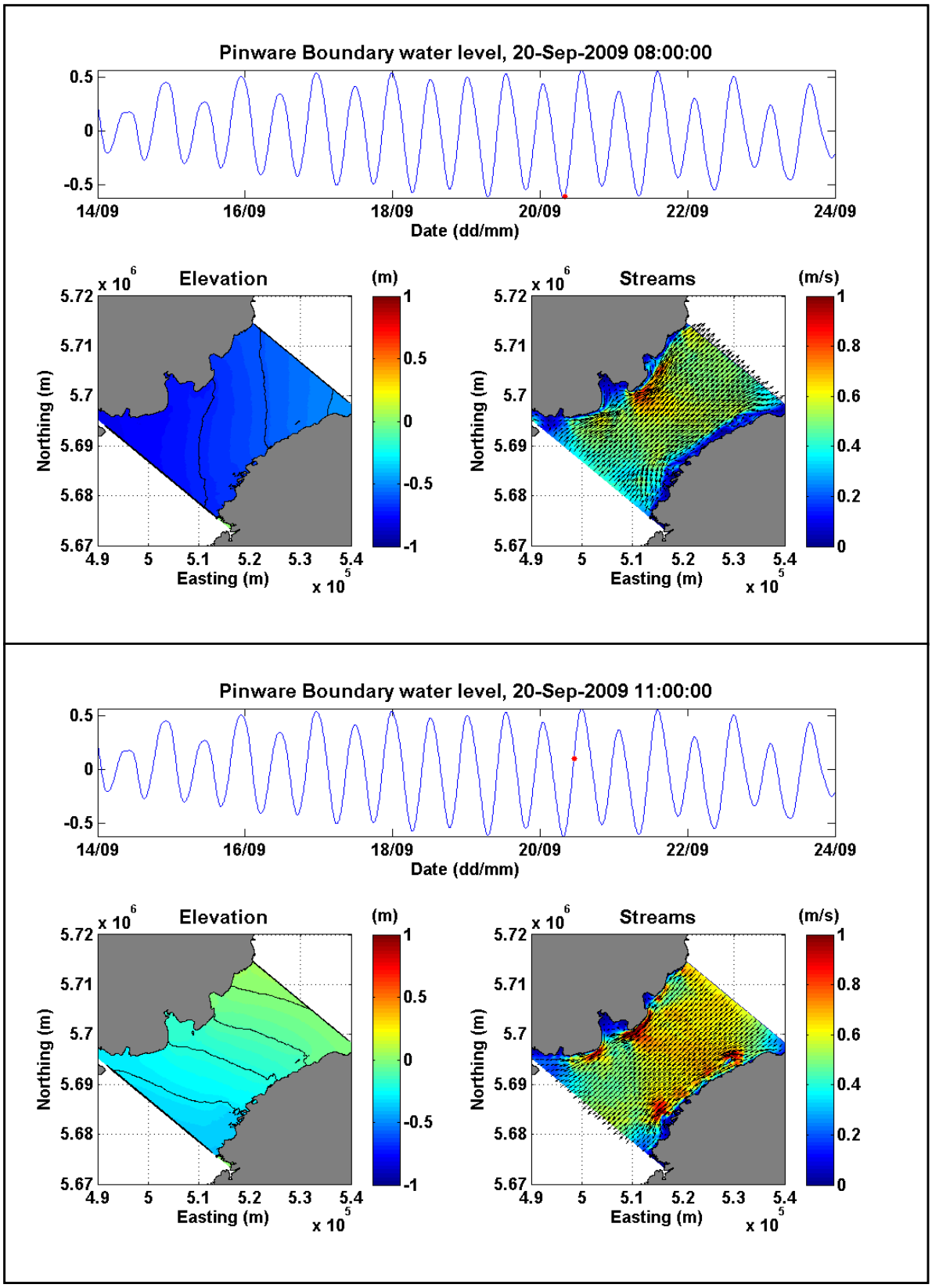

Figure 3.1-4: Flooding Tides during (High) Spring Tide Conditions.

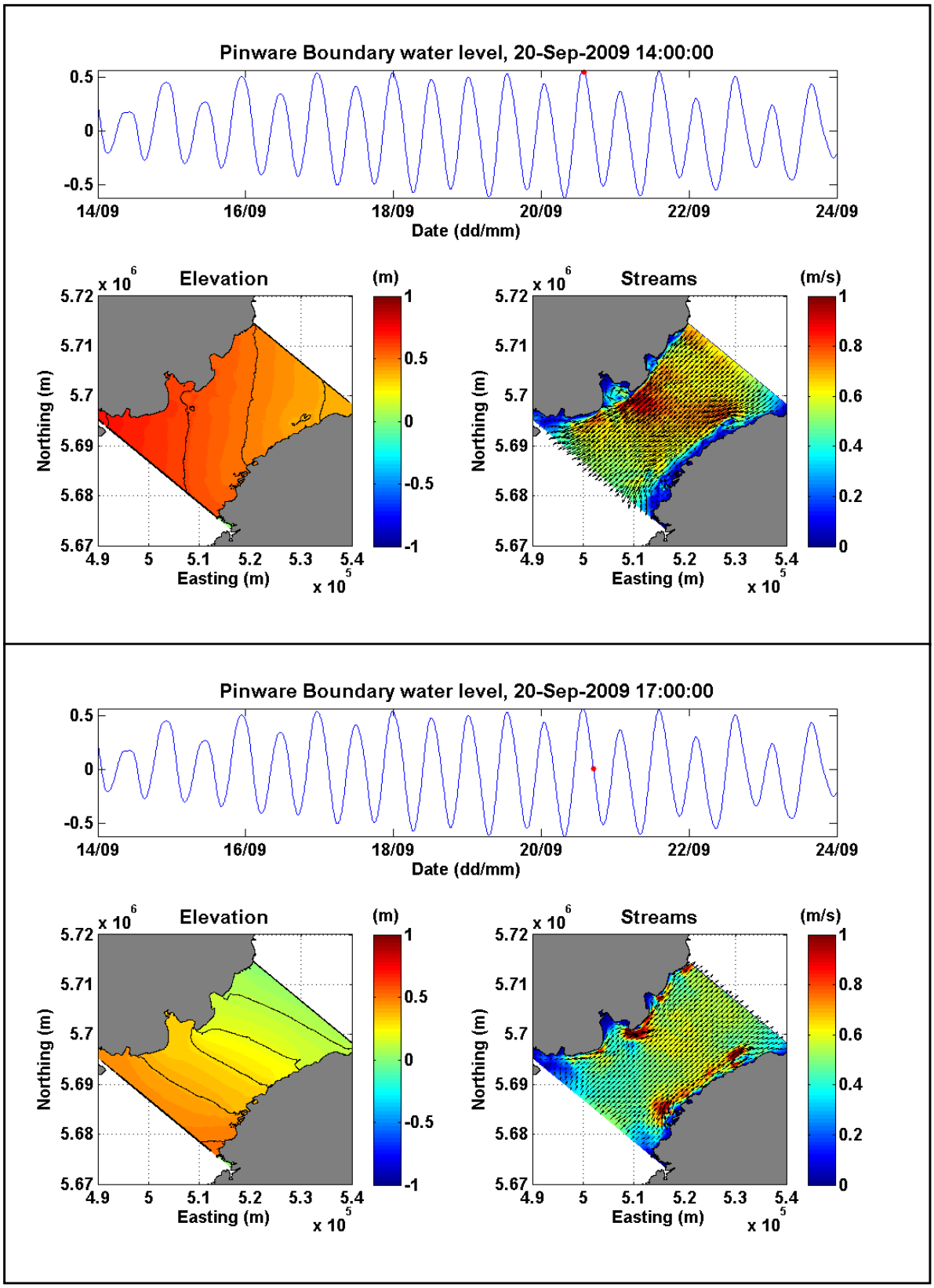

Figure 3.1-5: Ebbing Tides during (High) Spring Tide Conditions.

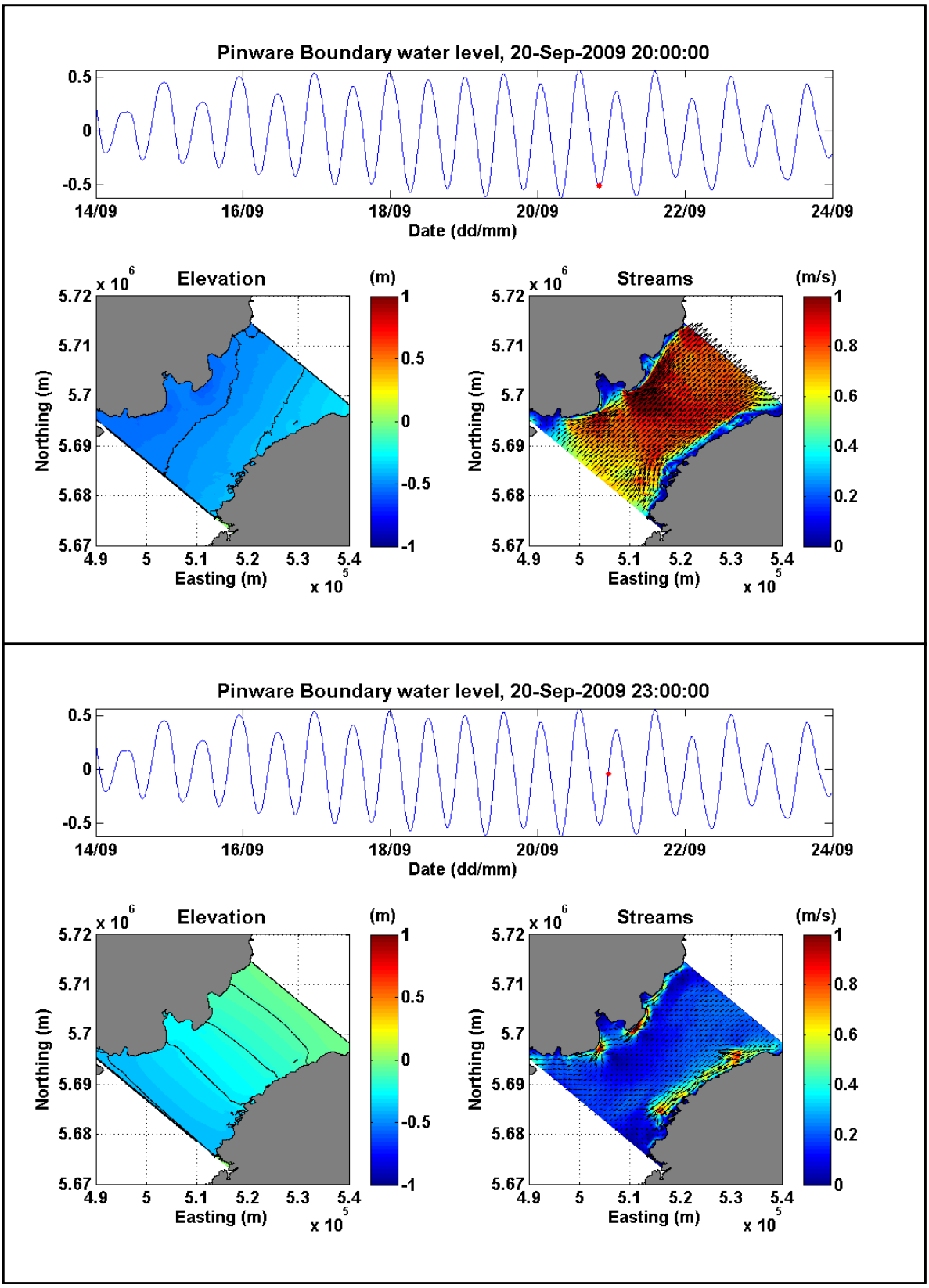

Figure 3.1-6: Flooding Tides during (Low) Spring Tide Conditions.

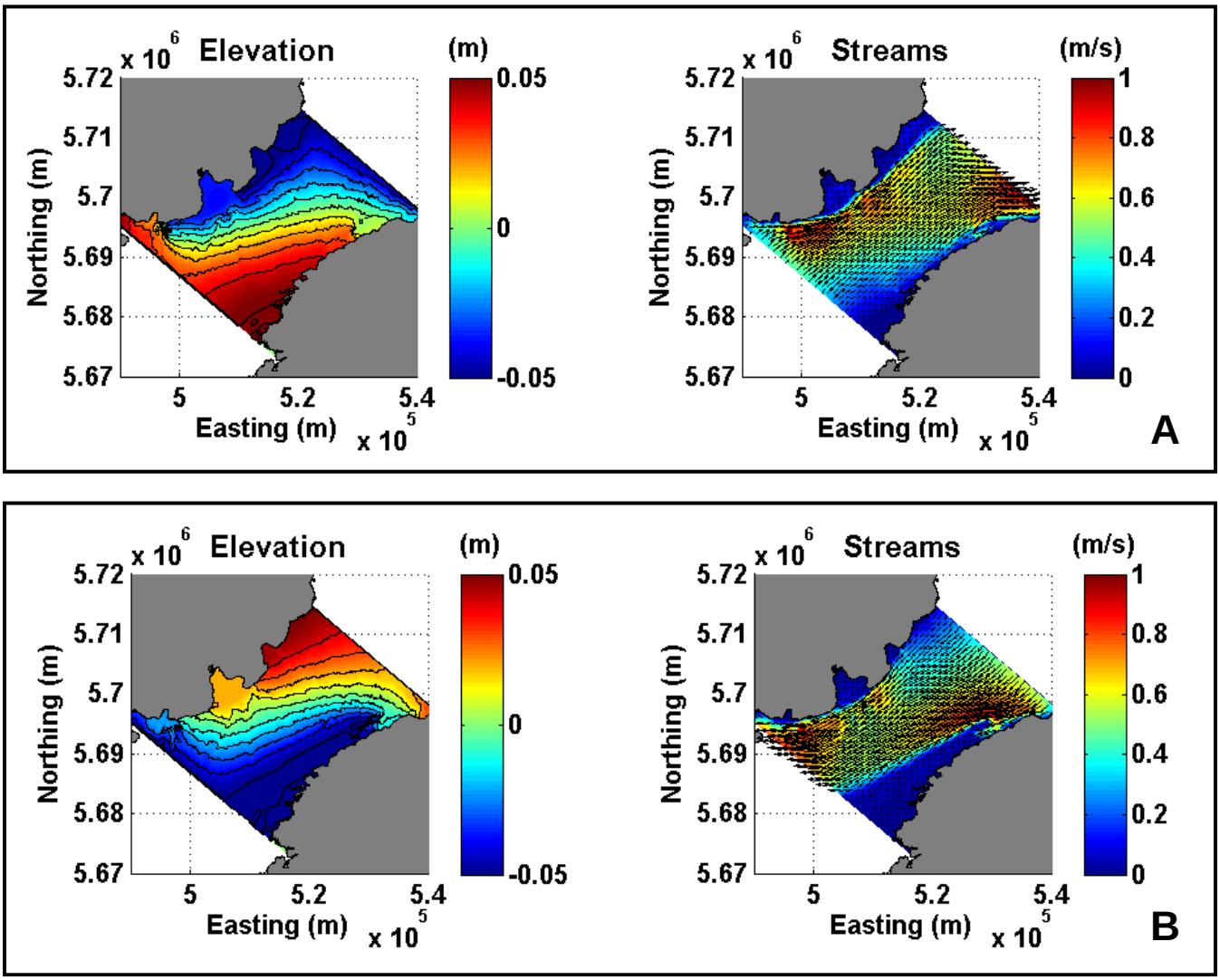

Figure 3.1-7: Atmospheric Forcing Scenarios, (A) Southwest to Northeast Pressure Gradient, and (B) Northeast to Southwest Pressure Gradient.

3.2 Sediments Dispersion (Benthic Boundary Layer Transport)

As mentioned in Section 2.2.4, the BBLT model was run over a period of 15 days with tide-only forcing currents, for separate release of sand and silt material (Figure 2.2-15).

The model was set up to output an hourly suspended solid concentration map (grid based on bathymetry) of the first metre of water above the sea floor, in mg/L. The output of the two scenarios were first combined to yield a total concentration of material (as opposed to concentration of sand or silt only) and then analyzed to create:

- a composite of maximum concentration, i.e., a map representing the maximum encountered concentration over the 15 days of simulation at a given cell (Figure 3.2-1)

- a composite of maximum thickness; i.e., a map representing the maximum thickness the mobilized material would create if they were to settle on a given cell. This composite is basically derived from the maximum concentration map, taking the maximum deposit from the maximum concentration of sediment in the water column and assuming total settling from that point. The sediment was also assumed to be a density of 2650 kg/m^3 and have a 50% void ratio once deposited (Figure 3.2-2)
- three composites of maximum duration concentration over the thresholds (100 mg/L, 10 mg/L and 1 mg/L) were created to represent the maximum duration a given concentration of released sediment could be over a 15 day period of dumping activities(Figure 3.2-3, Figure 3.2-4 and Figure 3.2-5)

Overall, the noticeable sediment resuspension footprint (greater than 100 mg/L concentration) of the rock placement activities was determined to be relatively limited to the vicinity (a few hundred metres) of the activity.

The maximum thickness of material potentially deposited was found to be very small with values ranging from about 0.1 to a maximum of 1.5 mm.

The duration of elevated suspended sediment concentration (over 100 mg/L) was found to range from 1 hour for various locations along and near the corridor with total area 10.9 km^2, to 100 hours or more for fewer locations totaling 1.3 km^2 in area.

Table 3.2-1 presents a summary highlighting the main results of these simulations.

Table 3.2-1: Sediment Dispersion Modelling Summary.

	Maximum Concentration			**Maximum Thickness**			**Maximum Duration***		
	>100 mg/L	>10 mg/L	>1 mg/L	>1 cm	>0.5 cm	>0.1 cm	>100 hrs	>10 hrs	> 1hr
Area (km^2)	11.7	25.5	180	0	0	0.07	1.3 19.8 34.7	7.7 38.1 379.7	10.9 103.5 572.0
* the maximum duration area results are presented for scenarios of > 100 mg/L, > 10 mg/L and > 1 mg/L respectively (from top line to bottom line)									

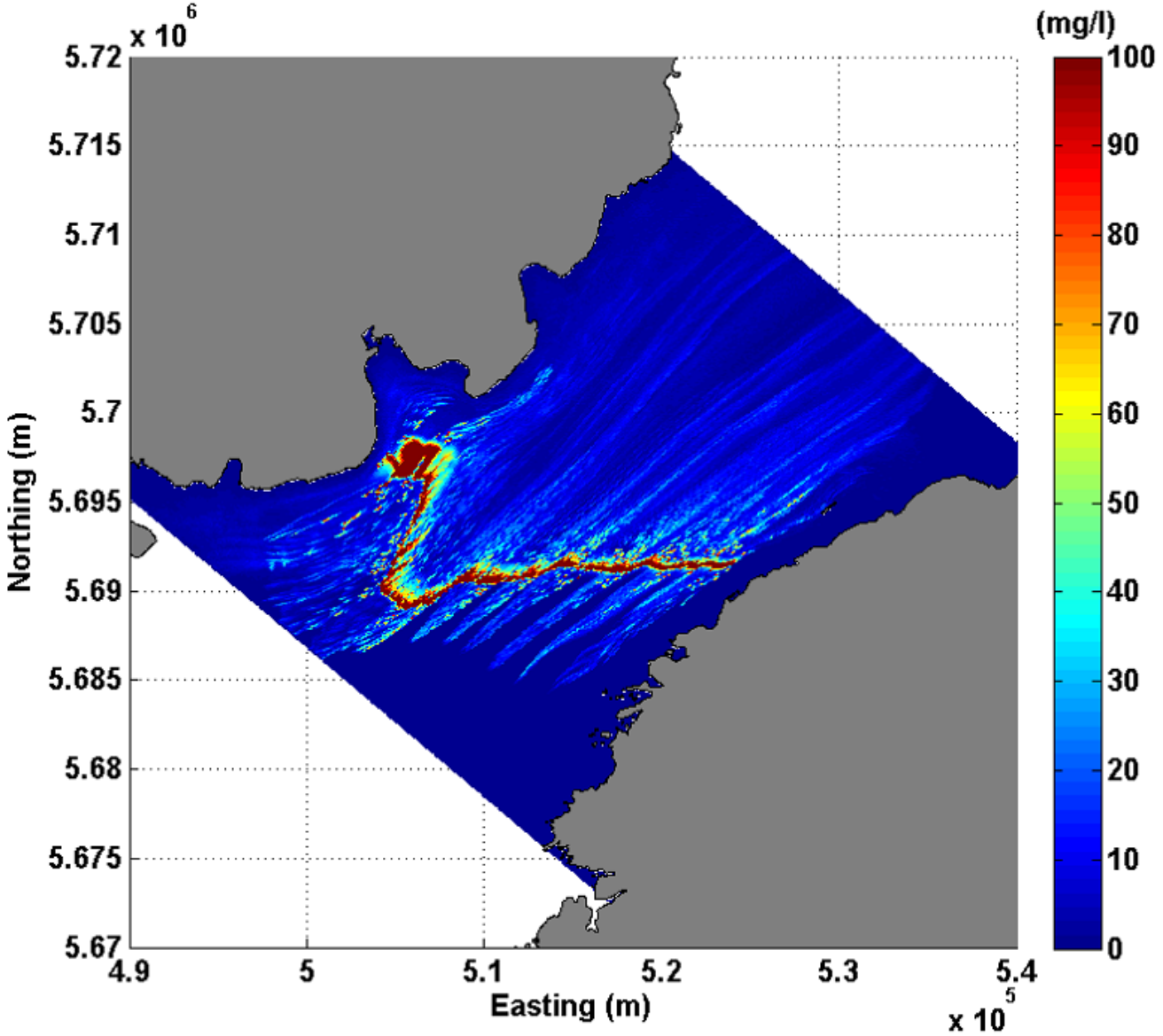

Figure 3.2-1: Maximum Concentration of Rock Dumping Release Material Composite in the Strait of Belle Isle.

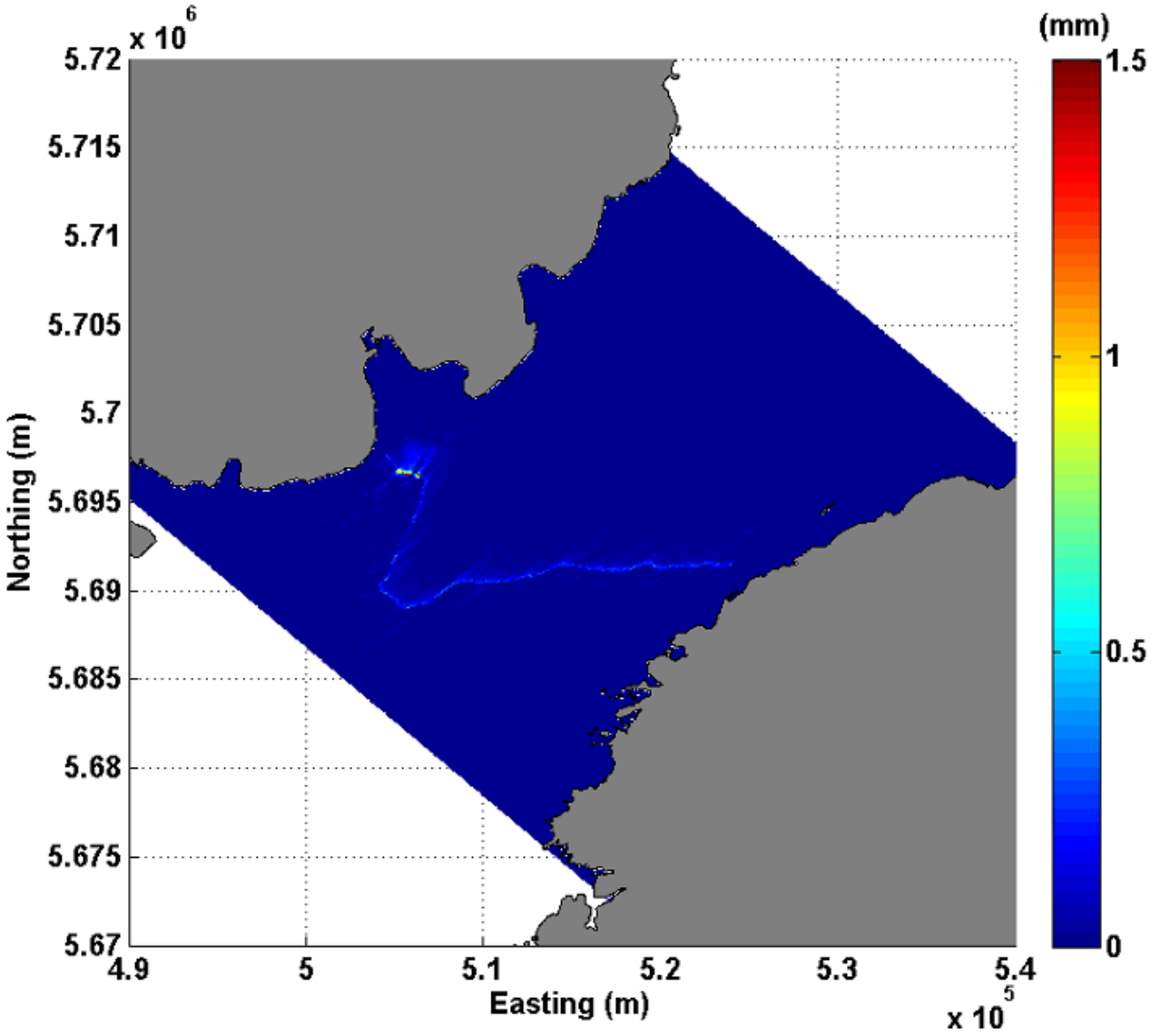

Figure 3.2-2: Maximum Thickness Deposit of Material Composite from Rock Placement Activities.

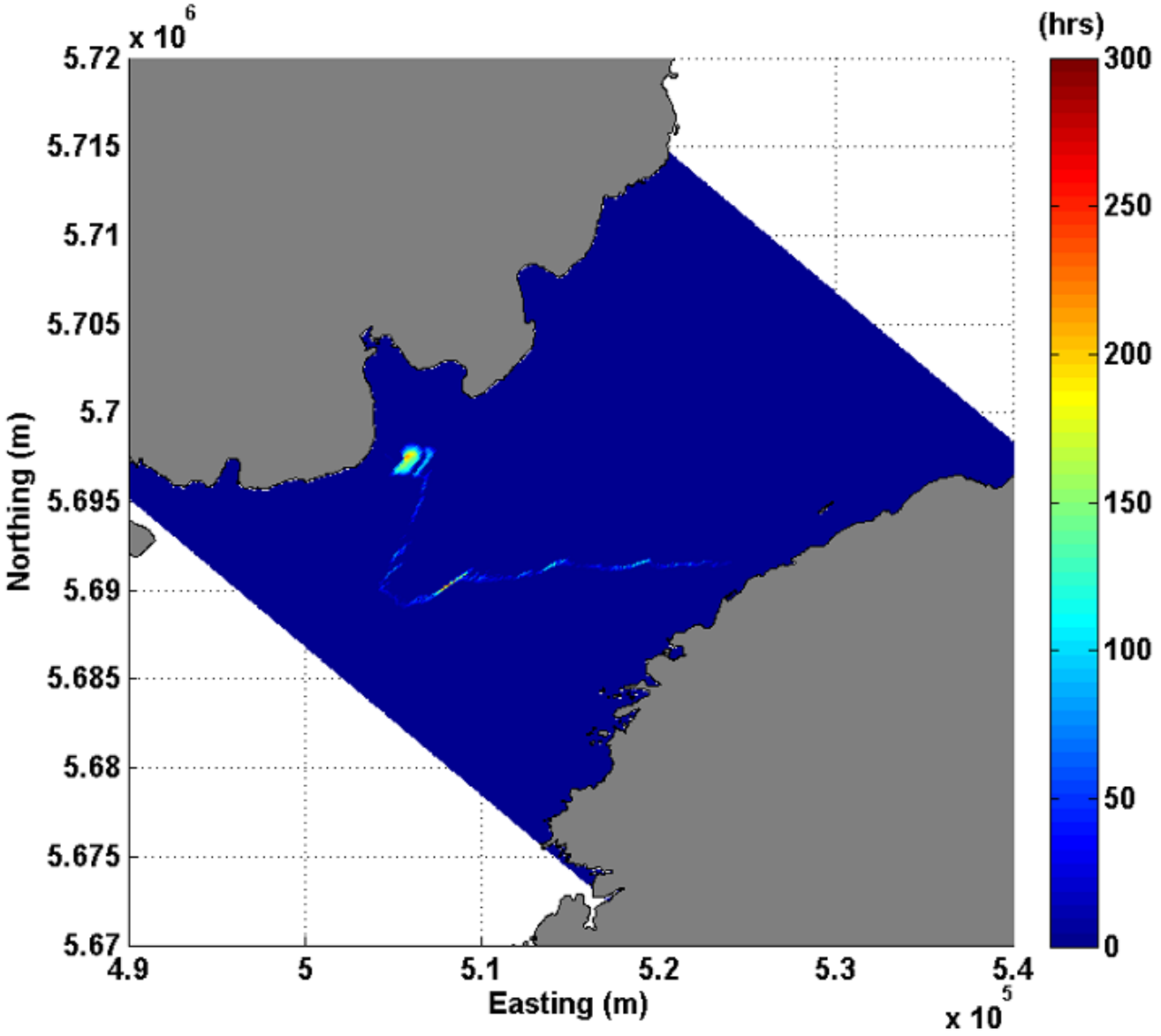

Figure 3.2-3: Maximum Duration Composite for Concentrations greater than 100 mg/L.

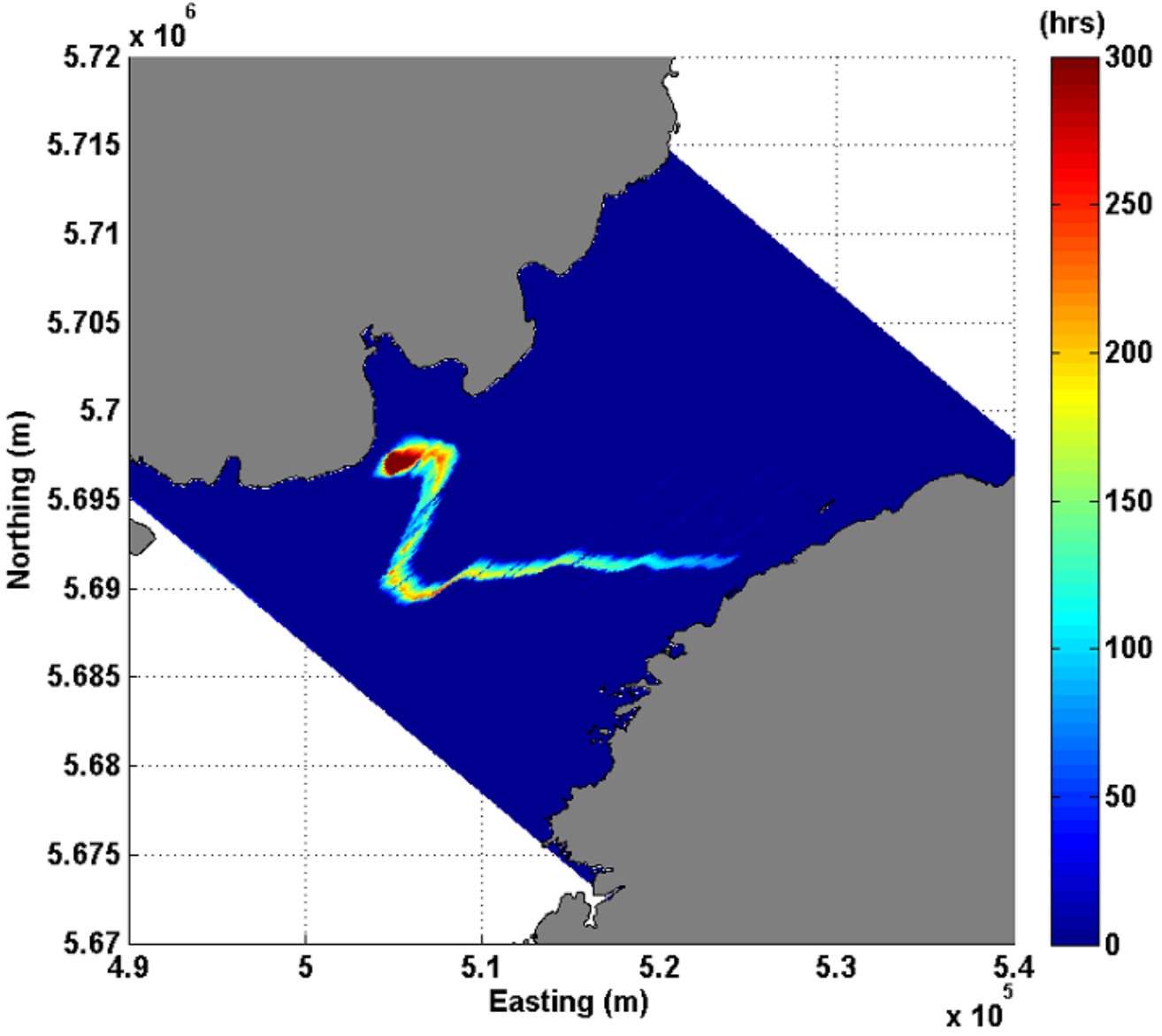

Figure 3.2-4: Maximum Duration Composite for Concentrations greater than 10 mg/L.

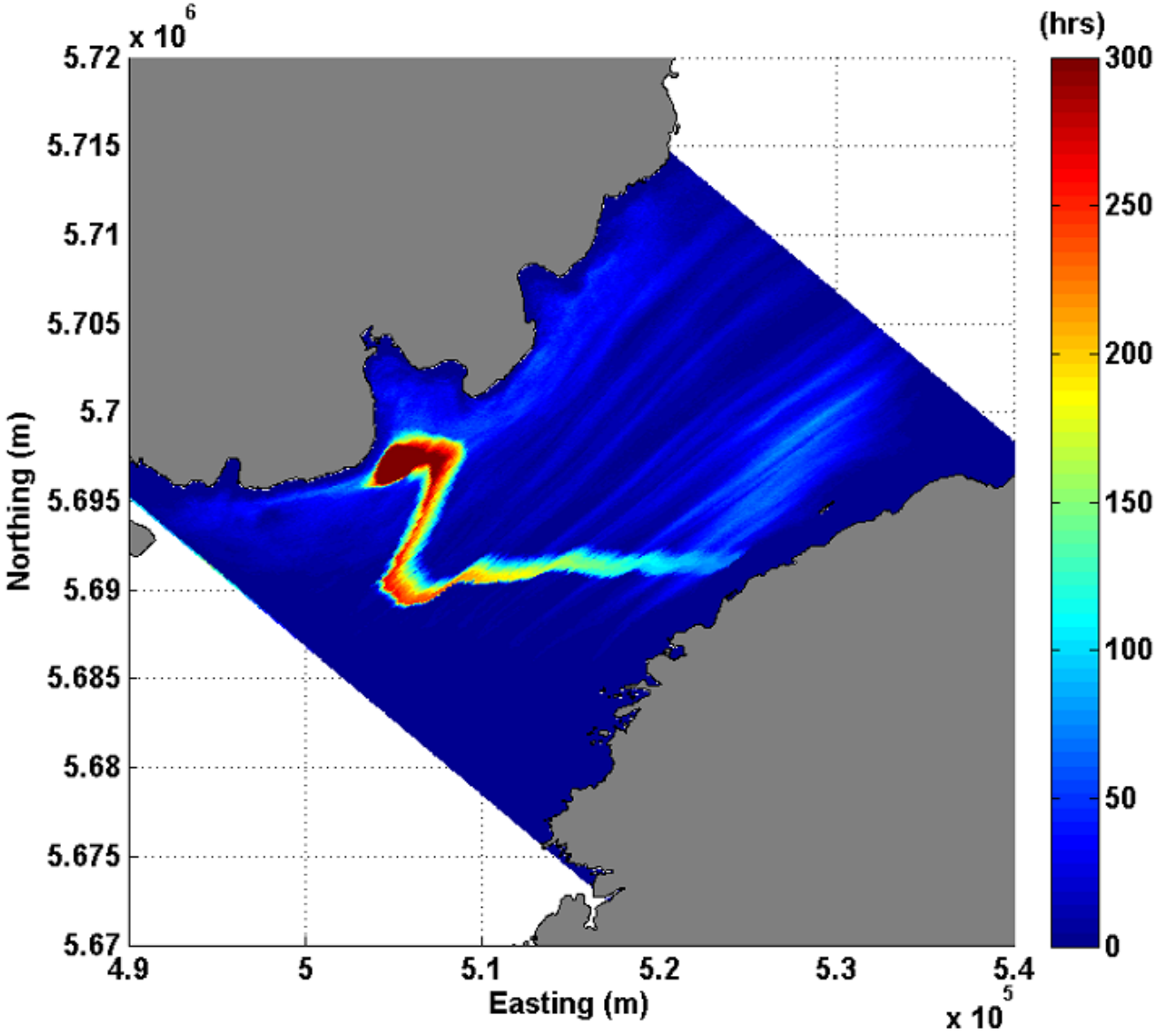

Figure 3.2-5: Maximum Duration Composite for Concentrations greater than 1 mg/L.

4.0 SUMMARY AND CONCLUSIONS

The submarine cable crossing component of the proposed Labrador – Island Transmission Link will likely entail the installation of three cables across the Strait of Belle Isle. Cable installation will initially involve the development of three HDD holes, extending from identified on-land cable landings on the Labrador side (potentially Forteau Point) and Newfoundland side (potentially Shoal Cove) of the Strait of Belle Isle. These HDD holes will each extend for a distance of approximately 1.5 to 2.5 km underground, and to a water depth of approximately 80 m before piercing the seabed. On the seabed, the individual cables will each be protected by a dedicated rock berm, approximately 30 to 35 km long (depending on their specific routings). The three rock berms will each be approximately 0.8 to 1.5 m high and 8 to 12 m wide at the base, and be comprised of approximately 1 million tonnes of rock in total, placed by a fall pipe vessel. The current rock size has been specified to be 2 to 8" graded.

In preparation for and support of the EA of the Project, this Study was completed in order to model and describe key aspects of the oceanographic environment in the Strait, as well as the likely characteristics of sedimentation that may occur as a result of marine construction activities associated with the Strait of Belle Isle submarine cable crossings.

The modelling involved a two step process. The first step involved the creation of a hydrodynamic model to simulate the current fields and other hydrodynamic processes for the Strait of Belle Isle. The second step involved the use of a BBLT sediment transport model that used the current fields output from the hydrodynamic model to simulate the dispersion of the sediment material being released by potential construction activities.

The hydrodynamic model was created using bathymetric data previously acquired by Nalcor Energy and forced by tidal water level variations obtained from tidal gauges specifically installed for this study. Due to the tide being the strongest and most replicable forcing parameter in this area, tide-only simulation was performed initially and validated against historical data. An additional run was conducted with the aim to simulate currents associated with atmospheric forcing in the Strait, as described in the scientific literature. Overall, the output and validation process was successful and demonstrated the ability of the model to reproduce water level and current fluctuations associated with tides and atmospheric forcing.

The surficial sea-bottom survey results previously acquired by Nalcor Energy and the output of the hydrodynamic tidal simulation were used as inputs for the sediment dispersal model. Available information regarding the proposed construction activities (rock placement) in the marine environment was also compiled to provide a hypothetical scenario of bottom sediment release.

The key results of the sediment dispersion model demonstrated:

- the most noticeable effect (i.e., that of suspended sediment concentrations greater than 100 mg/L, following the rock placement activities) was found to be relatively limited to within a few hundred metres of the activity location;
- the maximum thickness of material potentially deposited was found to be very small with values ranging from about 0.1 mm to a maximum of 1.5 mm; and

- the duration of elevated suspended sediment concentration (greater than 100 mg/L) was found to range from 1 hour for various locations along and near the corridor with total area 10.9 km^2, to 100 hours or more for fewer locations totaling 1.3 km^2 in area.

5.0 REFERENCES

AMEC, 2007. Physical Environmental Description for the Cable Crossing at the Strait of Belle Isle. August 2007. Internal report prepared for Fugro Jacques Geosurveys Inc. as part of a desktop review of the oceanographic environment in the Strait of Belle Isle for Newfoundland and Labrador Hydro.

AMEC, 2010a. Labrador – Island Transmission Link, Marine Flora, Fauna and Habitat Survey – Strait of Belle Isle Subsea Cable Crossing Corridors 2008 and 2009. February, 2010.

AMEC, 2010b. Summary of Ocean Current Statistics for the Cable Crossing at the Strait of Belle Isle. August, 2010. Internal Report prepared for Nalcor Energy, Document number: ILK-AM-CD-0000-EN-RP-0001-01.

Bugden G.L., 1991. Changes in the temperature and salinity characteristics of the deeper water of the Gulf of the St. Lawrence over the past several decades. In J.C. Therriault (ed.). The Gulf of the St. Lawrence: Small Ocean or Big Estuary? Canada Special Publication of Fisheries and Aquatic Sciences, No. 113 pp. 139-147.

Canadian Hydrographic Survey, 2011. Tides, Currents and Water Levels Glossary.
http://www.waterlevels.gc.ca/english/glossary/L.shtml

Coastal Engineering Manual (CEM), 2002. Coastal Sediment Properties; Chapter 1, part III. EM 1110-2-1100.

Dawson W.B., 1907. The currents in Belle Isle Strait. Department of Marine and Fisheries, Ottawa, Canada.

Department of Fisheries and Oceans (DFO), 2009. List of Harbours and Harbour Authorities.
http://www.dfo-mpo.gc.ca/sch-ppb/list-liste-eng.htm

Department of Fisheries and Oceans (DFO), 2010. Hydrographic Database and Ocean Data Inventory Database.
http://www2.mar.dfo-mpo.gc.ca/science/ocean/database/doc2006/clim2006app.html

Drinkwater K.F., 1993. Overview of environmental conditions in the Northwest Atlantic in 1992. DFO Atlantic Fisheries Research Document, 93/1.

Drozdowski A., Hannah C., Tedford T., 2004. bblt Version 7.0 User's Manual. Canadian Technical Report of Hydrography and Ocean Sciences 240. Ocean Sciences Division Maritimes Region, Fisheries and Oceans Canada. Bedford Institute of Oceanography, P.O. Box 1006. Dartmouth, N.S., Canada B2Y 4A2.

Drozdowski A., 2009. BBLT3D, the 3D Generalized Bottom Boundary Layer Transport Model: Formulation and Preliminary Applications. Canadian Technical Report of Hydrography and Ocean Sciences 263. Ocean Sciences Division Maritimes Region, Fisheries and Oceans Canada. Bedford Institute of Oceanography, P.O. Box 1006. Dartmouth, N.S., Canada B2Y 4A2.

Dupont F., Hannah C.G., Greenberg D.A., Cherniawsky J.Y. and Naimie C.E., 2002. Modelling System for Tides. Can. Tech. Rep. Hydrogr. Ocean Sci. 221: vii + 72p.

Environment Canada, 2010a. Canadian Climate Normals or Averages 1971-2000.
http://climate.weatheroffice.gc.ca/climate_normals/index_e.html

Environment Canada, 2010b. Canadian Climate Normals or Averages 1961-1990.
http://climate.weatheroffice.gc.ca/climate_normals/index_1961_1990_e.html

Environment Canada, 2010c. National Climate Data and Information Archive. http://www.climate.weatheroffice.gc.ca/climateData/canada_e.html

Farquharson W.I., and Bailey W.B., 1966. Oceanographic study of Belle-Isle Strait 1963, Rep. 66-9, Bedford Inst. Oceanogr. Dartmouth, N.S., 78p.

Farquharson W.I., 1970. Tides, Tidal streams and currents in the Gulf of St. Lawrence, Second Edition – Part 1- TIDES AND TIDAL STREAMS – AOL report 1970-5, Atlantic Oceanographic Laboratory, Bedford Institute, Dartmouth, Nova Scotia.

Forrester W.D., 1983. Canadian Tidal Manual. Department of Fisheries and Oceans, Ottawa.

Fugro GEOS, 2007a. Lower Churchill Hydro Development Proposed Subsea HVDC Cable Route, Strait of Belle Isle, Newfoundland and Labrador, Data Compilation Desk Study. Report Document No. 7045SGN-DC1132-DKSD-001.

Fugro GEOS, 2007b. Lower Churchill Hydro Development Proposed Subsea HVDC Cable Route, Strait of Belle Isle Crossing and Southwest Newfoundland Landfall (Cabot Strait), Newfoundland and Labrador, Regional/Reconnaissance Multibeam Survey. Report Document No. 7045SGN-DC1133-RPT-001.

Fugro GEOS, 2008. Lower Churchill Hydro Development Proposed Subsea HVDC Cable Route, Strait of Belle Isle, Newfoundland and Labrador, Volume I – Survey Results. Report Document No. 7045SGN-DC1131-RPT-001.

FJGI (Fugro Jacques Geosurveys, Inc.), 2010. Labrador - Island Transmission Link - Marine Habitats in the Strait of Belle Isle: Interpretation of 2007 Geophysical (Sonar) Survey Information for the Submarine Cable Crossing Corridors. January, 2010. Prepared for Nalcor Energy. Contract #LC-EV-012.

Galbraith P.S., 2006. Winter water masses in the Gulf of St. Lawrence. Journal of Geophysical Research, 111, C0602, doi:10.1029/2005JC003159.

Garrett C. and Petrie B., 1981. Dynamical Aspect of the Flow Through the Strait of Belle Isle. Journal of Physical Oceanography. Vol. 11, pp. 376-393.

Garrett C. and Toulany B., 1981. Variability of the Flow through the Strait of Belle Isle. Journal of Marine Research, vol. 39, pp 376-393.

Garrett C. and Toulany B., 1982. Sea Level Variability due to Meteorological Forcing in the Northeast Gulf of St. Lawrence. Journal of Geophysical Research, Vol. 87, C3, pp. 1968-1978.

Gratton Y.B., Pettigrew B., Pelchat D., Gilbert D., Couture M. and Laundry J., 1994. Overview of environmental conditions in the Gulf of the St. Lawrence in 1993. DFO Atlantic Fisheries Research Document, 94/55.

Hannah, C.G., Y. Shen, J.W. Loder and D.K. Muschenheim. 1995. bblt: Formulation and Exploratory Applications of a Benthic Boundary Layer Transport Model. Can. Tech. Rep. Hydrogr. Ocean Sci. 166 vi +52 p.

Hannah C.G. and Drozdowski A., 2005. Characterizing the near-bottom dispersion of drilling mud on three Canadian offshore banks. Marine Pollution Bulletin, vol. 50, issue 11, pp 1433-1443.

Lazier L. R. N. and Wright D. G., 1993. Annual Velocity Variations in the Labrador Current. Journal of Physical Oceanography, Vol. 23, No. 4.

Loder J.W., Petrie B., Gawarkiewicz G., 1998. The Coastal Ocean Off Northeastern North America: A Large-Scale View, Coastal Segment (1,W). John Wiley & Son, The Sea, Volume 11.

Lu Y., Thompson K. and Wright D., 2001. Tidal currents and mixing in the Gulf of St. Lawrence: an application of the incremental approach to data assimilation. Canadian Journal of Fisheries and Aquatic Science, 58: pp. 723-735.

NORDCO Ltd., 1978. Current Metering Program, 1978, Strait od Belle Isle. Report to Newfoundland and Labrador Hydro.

Pawlowicz R., Beardsley B. and Lentz S., 2002. Classical Tidal Harmonic Analysis Including Error Estimates in MATLAB using T_TIDE, Computers and Geosciences, 28 (2002), pp. 929-937.

Petrie B., Toulany B. and Garrett C., 1988. The transport of water, heat and salt through the Strait of Belle Isle. Atmosphere-Ocean 26, pp234-251.

SNC-Lavalin, 1982a. Strait of Belle Isle Crossing: Submarine Cable Scheme, Vol. I – Engineering Report – Cost Estimate and Project Schedule, Contract Report for Lower Churchill Development Corporation.

SNC-Lavalin, 1982b. Strait of Belle Isle Crossing: Submarine Cable Scheme, Vol. II – 1981 Field Program, Contract Report for Lower Churchill Development Corporation.

SNC-Lavalin, 1982c. Strait of Belle Isle Crossing: Submarine Cable Scheme, Vol. III – Environmental Field Data Observations, Contract Report for Lower Churchill Development Corporation.

Smith E.H., Soule F.M. and Mosby O., 1937. The Marion and General Green expeditions to Davis Strait and Labrador Sea. Bull. U.S. Coast Guard, 19, 259p

Swail, V.R., V.J. Cardone, M. Ferguson, D.J. Gummer, E.L. Harris, E.A. Orelup and A.T. Cox, 2006. The MSC50 Wind and Wave Reanalysis. 9th International Wind and Wave Workshop, September 25-29, 2006, Victoria, B.C.

Toulany B., Petrie B. and Garrett C., 1987. The frequency-dependent structure and dynamics of flow through the Strait of Belle Isle. Journal of Physical Oceanography, Vol. 17, pp. 185-196.

White L. and Johns F., 1997. Evaluation du milieu marin de l'estuaire et du golfe du St Laurent. DFO, Dartmouth, NS

Woodworth-Lynas C.M.T., Guigne J.Y. and King E.L., 1992. Surfacial and Bedrock Geology Beneath the Strait of Belle Isle in the Vicinity of a Proposed Power Cable Crossing.

Labrador – Island Transmission Link

Sound Modelling: Proposed Strait of Belle Isle Cable Installation Activities

Prepared for:

Nalcor Energy
Hydro Place, 500 Columbus Drive, PO Box 12800
St. John's, Newfoundland and Labrador
Canada A1B 0C9

Contract # LC-EV-039

Prepared by:

JASCO Applied Sciences
202 – 32 Troop Avenue
Dartmouth, Nova Scotia
Canada B3B 1Z1

Project # P001107-002

June 7, 2011

EXECUTIVE SUMMARY

Nalcor Energy is proposing to develop the Labrador – Island Transmission Link (the Project), a high voltage direct current (HVdc) transmission system extending from Central Labrador to the Island of Newfoundland's Avalon Peninsula which will include the installation of submarine cables across the Strait of Belle Isle (SOBI).

In support of the Project's EA this *Sound Modelling: Proposed Strait of Belle Isle Cable Installation Activities* study was undertaken to estimate and describe potential sound levels resulting from the proposed construction activities associated with underwater cable installation in the Strait. Acoustic propagation from five activities were considered: (1) horizontal directional drilling (from on-land at Forteau Point, Labrador and Shoal Cove, Newfoundland and out under the Strait), (2) transit of cable-laying vessel, (3) operations of cable-laying vessel in dynamic positioning (DP) mode, (4) transit of rock-placement vessel, and (5) operations of rock-placement vessel in DP mode. Vessel transit and operations were modelled at four locations along the proposed cable crossing corridor. The acoustic footprint and maximum distance (range) to underwater sound pressure level isopleths between 200 to 120 dB re 1µPa root mean square (RMS) were determined for each activity.

Rock-placement operations with the vessel in DP mode are expected to produce the largest ensonified area and longest range radius to an isopleth level at 120 dB re 1µPa RMS of 11,615 m. Cable laying operations with the vessel in DP mode are similar with the maximum radius to 120 dB re 1µPa RMS of 8,900 m. Vessel transit maximum radii to 120 dB re 1µPa RMS for the cable-laying vessel and the rock- placement vessel are approximately 1,500 m and 5,000 m respectively, with the maximum occurring when the vessel is near the center of the SOBI. The maximum radius to 120 dB re 1µPa RMS for horizontal directional drilling at either location is < 2000 m. The actual placement of the rocks themselves is not expected to be a significant source of noise in the marine environment.

Different operations have different dominant frequencies at which the maximum noise levels are produced. Drilling activities produce the lowest dominant frequencies of 1.3 to 1.6 Hz. The dominant frequencies for a transiting vessel range from 40 to 80 Hz, and vessels operating in DP mode produce maximal noise between 400 and 800 Hz. The range to 120 dB re 1µPa RMS can be corrected for the hearing ability of different animal groups (M-weighted). When M-weighting is applied, the range to 120 dB re 1µPa RMS for drilling operations decrease from 1,870 m to 269 m (85% reduction) for the low-frequency cetaceans. Drilling operations should not be detectable in the water column by mid-frequency and high-frequency cetaceans, nor pinnipeds. For vessel transit, M-weighting has no effect on the radii for the low-frequency cetaceans, but results in a 35% reduction for pinnipeds, a 55% reduction for mid-frequency cetaceans, and 62% reduction for high-frequency cetaceans. M-weighting has little effect on maximum range radii during rock- placement and cable laying operation while the vessels are in DP mode.

The predicted sound levels were compared with the ambient noise level values measured as part of *Strait of Belle Isle: Ambient Noise and Marine Mammal Survey* (JASCO Applied Sciences, 2011). The loudest source per modelling site was considered for comparison. The quietest, 95th percentile ambient noise spectrum, was selected as the baseline. The maximum increase over the natural noise level is estimated to be no more than 110 dB and only in the immediate vicinity, i.e., less than 10 m, from the source. Broad band noise levels as high as 50 dB above ambient are expected to be detected as far as 14 km from the source.

TABLE OF CONTENTS

LIST OF FIGURES

LIST OF TABLES

1.0 INTRODUCTION

Nalcor Energy is proposing to develop the *Labrador – Island Transmission Link* (the Project), a High Voltage Direct Current (HVdc) transmission system extending from Central Labrador to the Island of Newfoundland's Avalon Peninsula.

The environmental assessment (EA) process for the Project was initiated in January 2009 and is in progress. An Environmental Impact Statement (EIS) is being prepared by Nalcor Energy, which will be submitted for review by governments, Aboriginal and stakeholder groups and the public.

In preparation for and support of the EA of the Project, this *Sound Modelling: Proposed Strait of Belle Isle Cable Installation Activities* study was undertaken to estimate and describe potential sound levels resulting from the proposed construction activities associated with underwater cable installation in the Strait.

1.1 Project Overview

The proposed Project involves the construction and operation of transmission infrastructure within and between Labrador and the Island of Newfoundland. Nalcor Energy is proposing to establish an HVdc transmission system extending from Central Labrador to Soldiers Pond on the Island's Avalon Peninsula.

The proposed transmission system, as currently planned, will include the following key components:

- an ac-dc converter station in Central Labrador, on the lower Churchill River adjacent to the Lower Churchill Hydroelectric Generation Project;
- an HVdc transmission line extending from Central Labrador across southeastern Labrador to the Strait of Belle Isle (SOBI). This overhead transmission line will be approximately 400 km in length with a cleared right-of-way averaging approximately 60 m wide, and will consist of single galvanized steel lattice towers;
- cable crossings of the SOBI with associated infrastructure, including cables placed across the Strait through various means to provide the required cable protection;
- an HVdc transmission line (similar to that described above) extending from the Strait of Belle Isle across the Island of Newfoundland to the Avalon Peninsula, for a distance of approximately 700 km;
- a dc-ac converter station at Soldiers Pond on the Island of Newfoundland's Avalon Peninsula; and
- electrodes at each end of the HVdc transmission line in Labrador and on the Island, with overhead lines connecting them to their respective converter stations.

Project planning and design are currently at a stage of having identified a 2 km wide corridor for the on-land portions of the proposed HVdc transmission line and a 500 m wide corridor for the proposed SOBI cable crossing. Potential (alternative) on-land corridors and study areas have also been identified for the proposed electrodes, although the nature, type and location of these electrodes are the subject of ongoing analysis and engineering.

It is these proposed transmission corridors and components that were the subject of Nalcor Energy's environmental study program. Project planning is in progress, and it is anticipated that the Project description will continue to evolve as engineering and design work continue. The EA of the Project will also identify and evaluate alternative means of carrying out the Project that are technically and economically feasible. In conjunction and concurrent with the EA process, Nalcor Energy will be continuing with its technical and environmental analyses of the corridors, in order to identify and select a specific routing for the Project. The eventual transmission route and location will be selected with consideration of technical, environmental and socioeconomic factors.

1.2 Study Purpose and Focus

The purpose of this study by JASCO Applied Sciences (JASCO) was to provide estimates of sound pressure levels, which may result from construction activities associated with the proposed underwater cable installation components of the Project.

Three submarine cables are proposed to be installed across the SOBI between Forteau Point (Labrador) and Shoal Cove (Newfoundland). The installation of the cables will use several techniques. At the on-land cable landing sites, the cables will be installed using horizontal directional drilling (HDD) and pulled through boreholes. The plan is for the boreholes to extend out under the seabed to approximately the 80 m isobath, up to several kilometres from the shore. Between these two seabed piercing points, these cables will be laid on the sea bottom and each covered with a rock berm.

The following equipment is expected to be used during the cable installation activities:

- Borehole drilling equipment
- Cable laying vessel
- Rock placement vessels, and
- Various supply and support vessels

The objective of this study was to estimate acoustic footprints and maximum distances to underwater sound pressure levels from 200 to 120 dB re µPa root mean square (RMS) that will be generated during the above described cable construction and installation activities.

For the purposes of this acoustic modelling study, six locations were chosen along the proposed submarine cable corridor (Figure 1.1). At two locations, which correspond to the approximate exits of the cable from the boreholes onto the sea bottom, modelling of the sound field from the drilling activity was performed. Modelling was also conducted of sound propagation from typical cable installation and rock-placement vessels at four locations along the cable corridor (Figure 1.1).

The cable installation and rock placement processes will require precise positioning of construction and installation vessels. Therefore vessels equipped with dynamic positioning (DP) systems will be required. Currents in the Strait have been documented to be as high as 7 knots (Ingram, 1982). The DP systems may be required to be operated close to maximal power output levels. Overall, the sound source levels from vessels in transit mode and in DP mode are expected to differ.

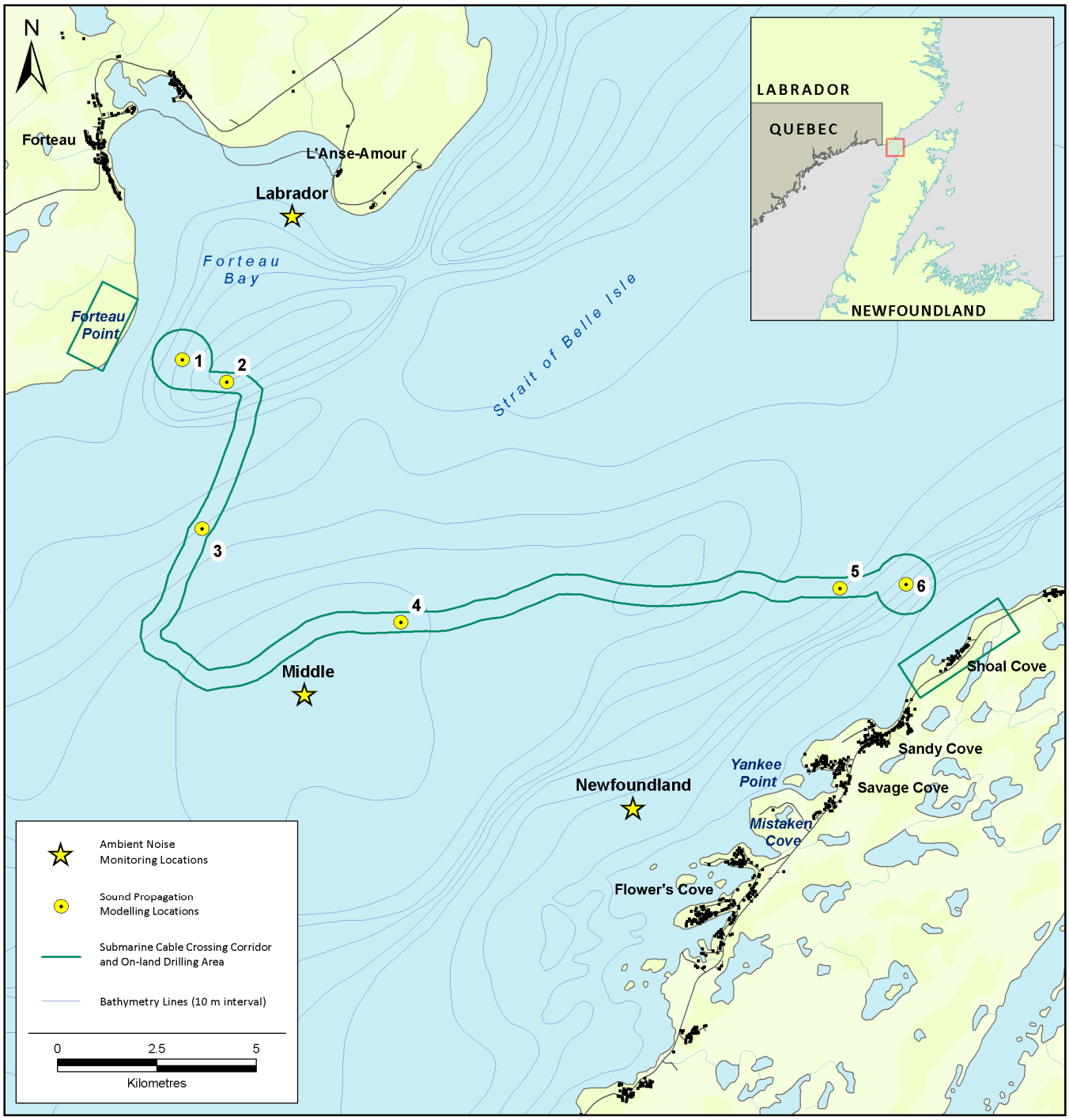

Figure 1.1 Sound Modelling Locations in the Strait of Belle Isle

The source levels for drilling activity and vessel operation in DP mode were derived from recorded data of similar sound sources. The source levels due to vessels in transit were estimated using an empirical formula with input data such as vessel length and transit velocity. The geoacoustic properties of the seabed and sound velocity profiles were estimated for each modelling location using data provided by Nalcor Energy. In addition, bottom topography estimates were based on multi-beam bathymetry data also provided by Nalcor Energy.

The objectives of this modelling study were therefore as follows:

- Determine the sound source levels for drilling activity and for the two vessels (cable laying vessel and rock placement vessel) in two operational modes (transit and DP mode);
- Model the sound field from the three source types at six different locations;
- Estimate the maximum range from sound source to isopleths of sound pressure level from 200 to 120 dB re µPa (RMS) in 10 dB increments;
- Estimate the potential for interaction between the calculated sound fields and various marine mammal groups by applying M-weighting filters; and
- Estimate the increase in the noise levels due to construction activities using the results of ambient noise level study as the baseline.

2.0 APPROACH AND METHODS

The following sections describe the key inputs to the modelling exercise and the approach and methods used.

2.1 Sound Source Levels

As described previously, SOBI cable installation will be completed in two phases. The first phase involves HDD of bore holes from onshore extending out and under the seafloor for a distance of approximately several kilometres from shore. Drilling equipment and operations will be based on land at Forteau Point (Labrador) and Shoal Cove (Newfoundland). The second phase involves the laying of cables on the sea bottom across the SOBI, and the construction of a protective rock berm on top of each of the cables using rock placement vessels.. In this report, vessels involved in cable installation activities, e.g., cable laying and rock placement, are referred together as cable installation vessels (CIV).

2.1.1 **Horizontal Directional Drilling**

Boreholes will be drilled using HDD to install the cable from land and underground to the seabed piercing zones (the larger circle-shaped ends of the corridor as shown in Figure 1.1). All drilling equipment will be positioned on land approximately a hundred metres or more from shore. Boreholes are proposed to be drilled out and under the seabed at depths between 10 to 30 m. Once the drilling head approaches the exit location, the drill bit will be directed towards the sea bottom and the drilling will continue until the bit pierces the seafloor.

HDD activities consist of two main sources of sound: noise generated by the machinery at the mouth of the borehole, and propagated substrate vibrations due to the drilling head. The drill rigs and machinery will be installed on shore, and therefore are not expected to be a significant contributor to underwater noise. The drill head, however, produces vibrations during the drilling process. The vibrations and the corresponding acoustic energy (sound) is similar in frequency to the rotary motion of the drill rig turntable. The rotational speed of the drill bit depends on the substrate. Typical for a soft substrate are 150–250 revolutions per minute (rpm) and 50–100 rpm for hard substrate (0.8–1.7 Hz) (Nguyen, 1996). The substrate vibrations resulting from the drilling head may propagate sound energy into the water column.

The source levels of drilling activity can be estimated using measurements of similar activity in Condemn Bay, Alaskan Beaufort Sea (Hall and Francine, 1991). Their measurements were obtained during drilling activity with a rig installed on a concrete island at a water depth of 10 to 15 m. Monitoring hydrophones were placed 259 m from the rig. The frequency range for the reported data was between 1 and 100 Hz.

To estimate source levels from the drill head, a back propagation technique was used. Transmission loss modelling was performed for the central frequencies of each third-octave band in the 1 to 100 Hz range, then source levels were estimated for each band using the following equation:

$$SL = RL + TL\,, \tag{1}$$

where SL is the source level, RL is the reported received level in the band, and TL is the estimated transmission loss for the specified frequency. Transmission loss modelling was conducted using appropriate environmental parameters specific to the area where the monitoring occurred.

The recovered source levels in the frequency range from 1 Hz to 100 Hz are presented in Figure 2.1.

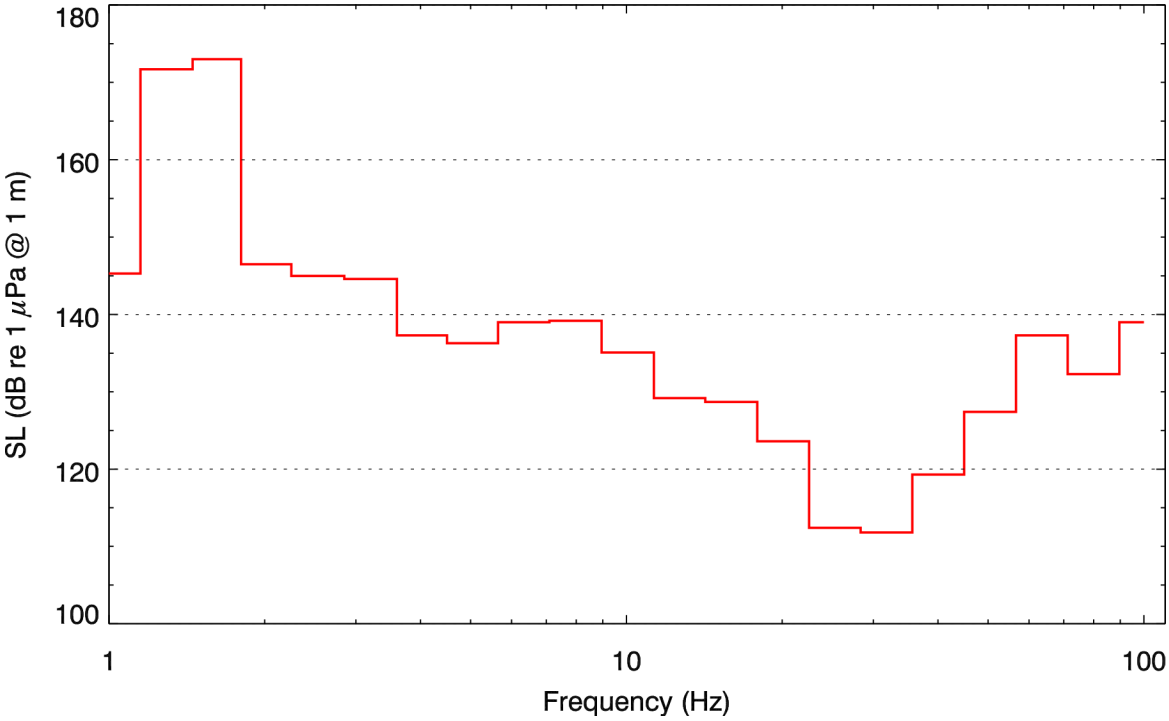

Figure 2.1 Acoustic Source Levels Near a Drill Head (based on Hall and Francine, 1991)

Sound spectra indicate that the highest levels of acoustic energy occur within a low-frequency band (i.e., below 10 Hz). And, within the low-frequency band, strong tonals are present at 1.3 and 1.6 Hz. These tonals correspond to the rotation frequency of the drill rig turntable. Source levels from the Condemn Bay study were used as input for sound propagation in the present modelling.

2.1.2 Cables Installation and Rock Placement

While in transit, ships emit sound underwater from their various components, including onboard machinery and propellers. The anticipated high level of vessel traffic during cable installation will be a key contributor of sound energy. CIV will also be involved in cable-laying and rock-placement activities. During these marine activities, sound could also be produced by material entering the water and material hitting the seafloor. Although little information is available on sound levels produced during these activities, it is reasonable to expect that this low-frequency noise will be dependent on the size of the material, the water depth, and the type of seabed at the landing zone. As in air, the laying of cables may also produce sound, but this will be at lower source levels than rock placement.

Acoustic source levels will also depend on the method employed for cable laying and rock placement. Underwater release of material is expected to produce lower sound levels than that of in-air release, reducing the noise from the underwater implosion of air bubbles formed behind the rocks entering the water. In addition, the use of fall-pipes vessels (i.e., rock-placement vessels) may also introduce noise through the interaction between the rock material and the pipe itself.

During the cable laying and rock placement activities, the CIV will be required to maintain position. Maintaining position in the SOBI will require the use of dynamic positioning (DP) systems. The DP mode produces significant sound levels from machinery and propellers as a result of the largely variable power demand. As a comparison, sound produced during dredging operations, from the vessel`s machinery and propulsion generally is the dominant sound (Hannay et al., 2007).

Project engineering is currently ongoing, and therefore at this stage of the EA the exact CIV and their specifications are unknown. For modelling purposes, Nalcor Energy provided data on various cable laying vessels that have been involved in the installation of marine cables elsewhere, and represent these typically used for such activities in similar environments. Rock placement vessels range in size, and the specifications provided represent an average size that will be used and has been utilized for such activities in similar environments.

The specifications for these vessels are presented in Table 2.1 along with the specifications from another, which was used in estimating DP mode source levels (Section 2.1.4). Again, at this stage of the engineering, these vessels were selected based on typical industry standards and averages.

Table 2.1 Vessels Specifications

	Typical Cable-laying Vessel	Typical Rock-placement Vessel	Vessel Used for DP Sound Recording
Dead Weight Tonnage	7150 t	19000 t (maximum capacity)	N/A
Overall Length	112.25 m	162.00 m	107 m
Draft	5.4 m	8.34 m	6.6 m
Transit Speed	10 knots	12 knots	N/A
Propulsion (including DP systems)	- 3 x stern thrusters - 2 x bow thrusters	- 2 x main propellers - 4 x azimuth thrusters - 1 x bow thruster	- 3 x bow thrusters - 3 x stern thrusters - 2 × engines each driving a single variable pitch propeller
Propeller Diameter	2 m (estimated)	N/A	- main propellers: 4 m - thrusters: 2 – 2.5 m
Total Horsepower (including DP systems)	10,415 BHP	15,020 BHP	11,732 BHP
Dynamic Positioning	Class II	Class II	Class II

2.1.3 Vessels in Transit

Noise spectra from large vessels are generally dominated by propeller cavitation noise. Ross (1976) has shown that the intensity of propeller cavitation noise can be related to the vessel's speed and dead weight tonnage (DWT). Based on multiple recordings of large merchant ships, Ross (1976) developed an equation to estimate the overall (broadband and omnidirectional) sound level of ships over 100 m in length operating in calm open waters:

$$L = 112 + 50\log(u/10) + 15\log(DWT), \quad (2)$$

where *L* is the broadband source level and *u* is the vessel's speed (knots). This equation was shown to produce source levels that are in agreement with the measured average ship spectrum (Hallet, 2004).

The Ross (1976) "Post-WWII" reference spectrum was adjusted to provide the broadband level as calculated with Equation (2) using specified transit speed and DWT for the typical vessels described in Table 2.1. The assumed spectra for the two modelled vessels in transit mode are presented in Figure 2.2. The estimated broadband level for each spectrum is also presented in Figure 2.2.

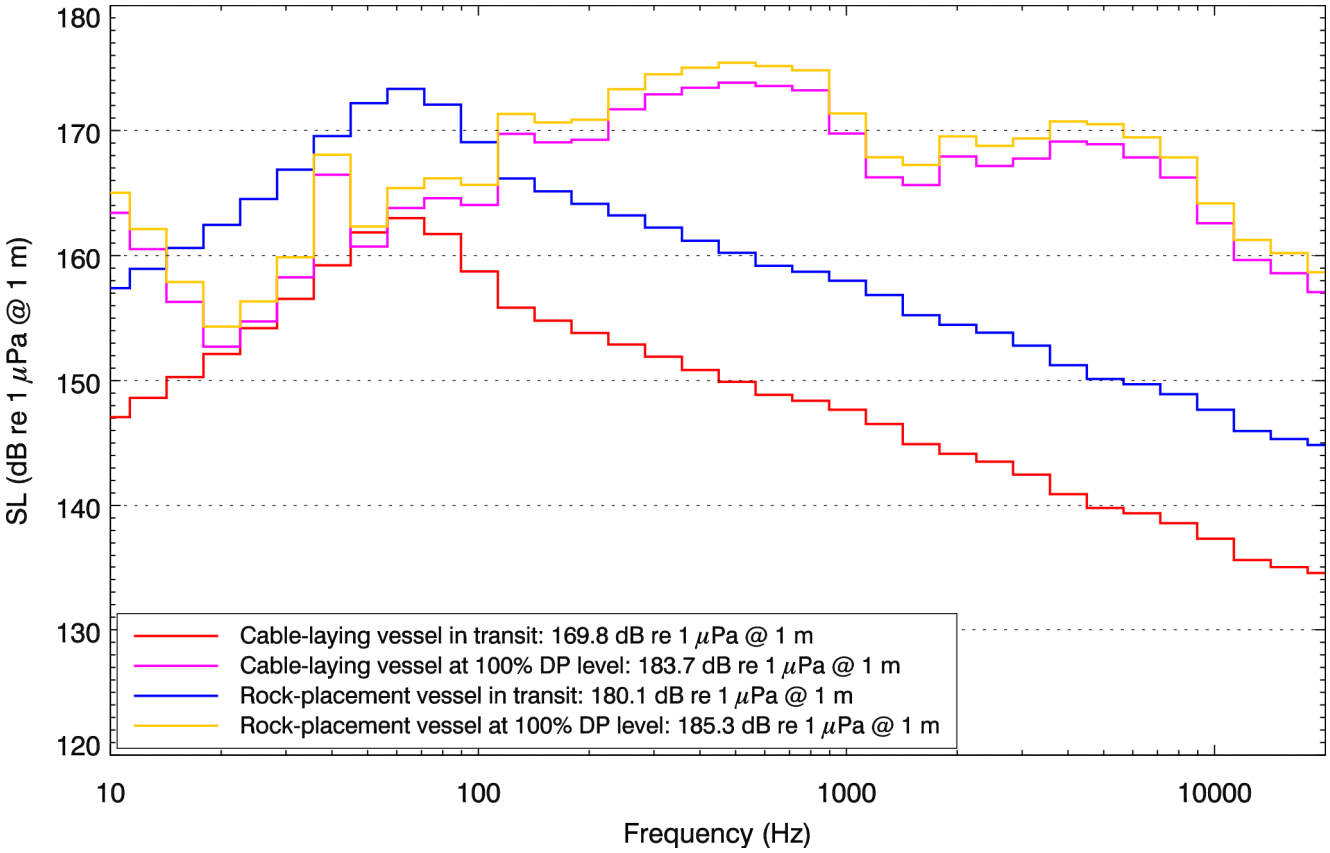

Figure 2.2 Assumed Third-octave Band Source Levels for the Typical Vessels in Transit and in DP Mode

2.1.4 Vessels in Dynamic Positioning (DP) Mode

DP systems allow for the automatic control of the vessels propellers and/or thrusters to maintain the vessel's position and heading during various marine activities. In DP mode, the propulsion system may vary signficantly in power to counter external forces such as currents and wind. Consequently, the broadband source level from a vessel in DP mode may be higher than for transiting at constant speed.

The dive support vessel *DSV Fu Lai* was recorded by JASCO while operating in DP mode, with DP levels of 25%, i.e., at approximately 3000 HP (MacGillivray, 2006). The calculated source levels from these recordings were used to estimate the source levels for vessels in DP mode during the proposed construction activities for the SOBI submarine cables.

Strong surface currents in the SOBI have been reported up to 3.6 m/s (7.2 knots) (Ingram, 1982). The modelled vessels were therefore assumed to operate at 100% DP levels. The final spectra were adjusted for the difference in total horsepower between the *DSV Fu Lai* (a typical dive support vessel) and the typical cable laying vessel (-0.5 dB), and between the *DSV Fu Lai* and the typical rock placement vessel (Table 2.1) (+1.1 dB) using the following equation:

$$SL = SL_{FuLai} + 10\log(HP / HP_{ref}), \quad (3)$$

where HP_{ref} is the level of reference, i.e., 3000 HP. These spectra were then plotted againts the assumed sprecta for vessels in transit that were presented in Figure 2.2.

2.2 Modelling Methodology

The Marine Operations Noise Model (MONM), described in Section 2.2.1, estimates the acoustic field at any range from the source. The sound propagation modelling uses acoustic parameters specific to the geographic region of interest, including water column sound speed profile, bathymetry, and bottom geoacoustic properties, to produce site-specific estimates of the radiated noise field as a function of range and depth. MONM is used to predict the directional transmission loss footprint from source locations. The received level (RL) at any 3-dimensional location away from the source is calculated by combining the source level (SL) and transmission loss (TL), both of which are direction dependent:

$$RL = SL - TL \tag{4}$$

Acoustic transmission loss and received sound level depend on depth, range, bearing, and environmental properties. The received levels estimated by MONM, like the source levels from which they are computed, are equivalent to the sound exposure level (SEL) over the duration of a single acoustic pulse, or RMS sound pressure level (SPL) for continuous sound signals. SEL is expressed in units of dB re 1 $\mu Pa^2 \cdot s$, while RMS SPL is expressed in units of dB re 1 µPa.

The safety and disturbance criteria currently applied to marine seismic surveys by the U.S. National Marine Fisheries Service (NMFS) are based on the RMS SPL metric as adapted for impulsive sound sources.

2.2.1 **Sound Propagation Model – In-water Source**

JASCO's MONM was used to estimate acoustic fields at frequencies below 5 kHz. MONM computes received SEL for impulsive sources if SEL source levels are input. For a continuous source, such as a vessel, dredge or drill rig, MONM outputs RMS SPL.

MONM treats sound propagation in range-varying acoustic environments through a wide-angled parabolic equation (PE) solution to the acoustic wave equation. The parabolic equation code used by MONM is based on a version of the US Naval Research Laboratory's Range-dependent Acoustic Model (RAM), which has been modified to account for an elastic seabed. The PE method has been extensively benchmarked and is widely employed in the underwater acoustics community (Collins et al., 1996).

MONM computes acoustic fields in three dimensions by modelling transmission loss along evenly spaced 2-Dimensional (2-D) radial traverses covering a 360° swath from the source, an approach commonly referred to as N×2-D. The model fully accounts for depth and/or range dependence of several environmental parameters including bathymetry and sound speed profiles in the water column and the sub-bottom. It also accounts for the additional reflection loss at the seabed that is due to partial conversion of incident compressional waves to shear waves at the seabed and sub-bottom interfaces. It includes wave attenuations in all layers, and the acoustic environment is sampled at a fixed range step along radial traverses.

MONM treats frequency dependence by computing acoustic transmission loss at the center frequencies of third-octave bands, from 10 to 5000 Hz for the current Project. This frequency range includes the important

bandwidth of noise emissions for the vessels and drilling activities. Third-octave band received levels are computed by subtracting band transmission loss values from the corresponding directional source levels. Broadband received levels are then computed by summing the received band levels. MONM's sound level predictions have been validated against experimental data (Hannay and Racca, 2005). The computed source levels were input to MONM to determine the predicted received levels in the environment surrounding the vessels or drill location.

Processing of the output data from the modelling code involved gridding all the data points in each horizontal plane separately (i.e., at each modelled depth). The resulting stack of grids was collapsed into a single grid using a maximum-over-depth rule, meaning that the sound level at each planar point was taken to be the maximum value that occurred over all modelled depths for that point.

2.2.2 Sound Propagation Model – In-ground Source

An in-ground source sound propagation model requires a slightly different modelling approach. Elastic media, such as sediments, support propagation of shear waves. With the source being in the ground, the contribution of the shear wave propagation in the sediments plays a noticeable role in the estimation of the sound field in the water. JASCO uses RAM-S code for sound propagation in special cases when shear wave handling is required.

The RAM-S code (Collins, 1993) was the result of the extension of RAM to include the capability to handle propagation of S-waves. The code takes five geoacoustic properties for the sediment layer: P-wave velocity and attenuation, S-wave-velocity and attenuation, and density. All five properties can be defined as a vertical profile, i.e., variation of a specific property is allowed with depth. RAM-S is a range dependent model, i.e., the properties of the waveguide can also vary with distance from the source. The variation allows for the water depth, the sound velocity profile in the water and the geoacoustic properties. The output from the RAM-S modelling code has been tested against the data acquired during a controlled acoustic propagation experiment in a laboratory setting (Collis, 2007). The results obtained in that study for the range-dependent sloped case provide support for the validity of the parabolic equation derivation in its elastic formulation.

2.2.3 M-Weighting

The potential for marine construction activity noise to affect marine species depends on the species' ability to hear the sounds produced (Ireland et al., 2007). Noises are less likely to disturb animals if they are at frequencies that the animal cannot hear well. An exception is when the sound pressure is so high that it can cause physical injury. For non-injurious sound levels, frequency weighting curves based on audiograms may be applied to weight the importance of sound levels at particular frequencies in a manner reflective of the receiver's sensitivity to those frequencies (Nedwell and Turnpenny, 1998).

An NMFS-sponsored Noise Criteria Committee has proposed standard frequency weighting curves — referred to as M-weighting filters — for use with marine mammal species (Gentry et al., 2004). M-weighting filters are band-pass filter networks that are designed to reduce the importance of inaudible or less-audible frequencies for four marine mammal functional hearing groups:

1. Low-frequency cetaceans,
2. Mid-frequency cetaceans,

3. High-frequency cetaceans, and
4. Pinnipeds.

The amount of discount applied by M-weighting filters for less-audible frequencies is not as great as would be indicated by the corresponding audiograms for these groups of species. The rationale for applying a smaller discount than would be suggested by the audiogram is in part due to an observed characteristic of mammalian hearing that perceived equal loudness curves increasingly have less rapid roll-off outside the most sensitive hearing frequency range as sound levels increase. This is the reason that C-weighting curves for humans, used for assessing very loud sounds such as blasts, are flatter than A-weighting curves used for quiet to mid-level sounds. Additionally, out-of-band frequencies, though less audible, can still cause physical injury if pressure levels are very high. The M-weighting filters therefore are primarily intended to be applied at high sound levels where effects such as temporary or permanent hearing threshold shifts may occur. The use of M-weighting should be considered precautionary (in the sense of overestimating the potential for an effect) when applied to lower level effects such as onset of behavioral response. Figure 2.3 shows the decibel frequency weighting of the four standard underwater M-weighting filters.

The M-weighting filters have unity gain (0 dB) through the pass band, and their high and low frequency roll offs are approximately –12 dB per octave. The amplitude response in the frequency domain of the M-weighting filters is defined by:

$$G(f) = -20\log_{10}\left[\left(1+\frac{f_{lo}^2}{f^2}\right)\left(1+\frac{f^2}{f_{hi}^2}\right)\right] \quad (5)$$

The roll off and pass band of these filters are defined by the parameters f_{lo} and f_{hi}. The parameter values of the standard M-weighing curves are presented in Table 2.2.

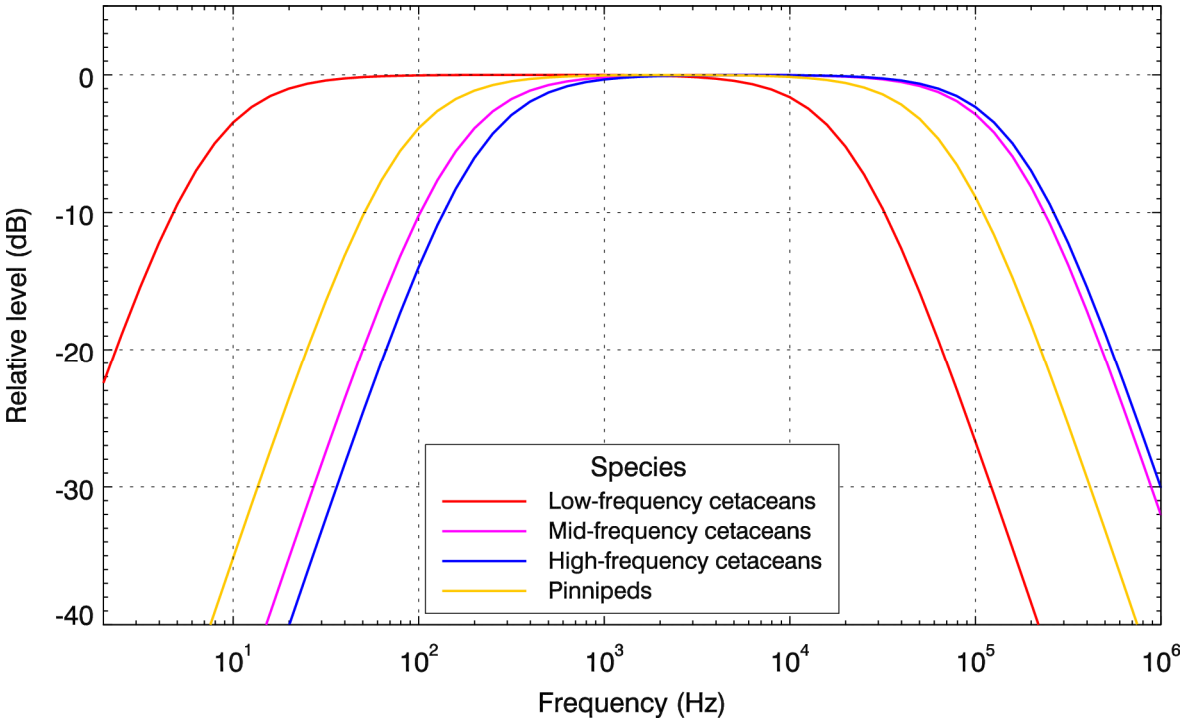

Figure 2.3 Standard M-weighting Curves for Low-, Mid-, and High-frequency Cetaceans, and Pinnipeds Underwater

Table 2.2 Low Frequency (f_{lo}) and High Frequency (f_{hi}) Cutoff Parameters for Standard Marine Mammal M-weighting Curves

M-weighting filter	f_{lo} (Hz)	f_{hi} (Hz)
Low frequency cetaceans	7	22 000
Mid-frequency cetaceans	150	160 000
High-frequency cetaceans	200	180 000
Pinnipeds underwater	75	75 000

2.2.4 Modelling Parameters

Locations

Six locations along the proposed SOBI seabed crossing were selected to provide a representative analysis of underwater acoustic propagation due to the proposed construction activities in the SOBI (see Figure 1.1 and Table 2.3). Drilling activities were modelled at Locations 1 (offshore Forteau Point) and 6 (offshore Shoal Cove), which represent the approximate planned marine exit locations for the HDD boreholes. Sound fields resulting from CIVs were modelled at Locations 2 through 5. In total, 4 drilling scenarios and 16 vessel scenarios were modelled.

Table 2.3 Sound Modelling Locations in the Strait of Belle Isle

Location	Description	Latitude/Longitude	Northing/Easting (UTM21)	Water Depth
1	Exit location for the HDD holes; offshore Forteau Point (Labrador)	51° 25' 33.76" N / 56° 55' 41.20" W	504998 / 5697204	88 m
2	Forteau Point - offshore	51° 25' 15.63" N / 56° 54' 43.97" W	506104 / 5696648	111 m
3	Shallow trench near the middle of SOBI	51° 23' 15.72" N / 56° 55' 15.97" W	505490 / 5692943	89 m
4	Middle of SOBI	51° 21' 59.72" N / 56° 50' 57.38" W	510493 / 5690603	112 m
5	Shoal Cove - offshore	51° 22' 26.02" N / 56° 41' 26.03" W	521538 / 5691450	87 m
6	Exit location for the HDD holes; offshore Shoal Cove (Newfoundland)	51° 22' 28.98" N / 56° 39' 59.87" W	523204 / 5691549	68 m

Geoacoustics

Seabed properties are important inputs for acoustic modelling, especially in the shallow environment. The description of the bottom and shallow sub-bottom geology for the area was provided by Nalcor Energy. The seabed geoacoustic parameters were estimated using Buckingham's sediment grain-shearing model (Buckingham, 2005), which computes the acoustic properties of the sediments from porosity and grain-size measurements. The geoacoustic parameters predicted by the grain-shearing model included: density (ρ), compressional speed (V_p), compressional attenuation coefficient in decibels per wavelength (α_p), shear wave speed (V_s), and shear wave attenuation coefficient (α_s). The input parameters for the geoacoustic model were the bottom type (grain size) from the geological description and sediment porosity. Sediment porosity values were estimated using generalized porosity/density curves (Einsele, 2000) in accordance with the sediment grain size. The geoacoustic properties for limestone were estimated based on the average values for this type of rock (Barton, 2006). Three geoacoustic models were constructed based on the data.

Offshore Forteau Point

In the region offshore of Forteau Point, the seabed consists of thin sediment underlain by limestone. At a water depth of 10 m a wedge of sediment builds out seaward, and has maximum thickness of 16 m. Fine sediment with ripples is found along the 14 m isobath, and fine sediment with smooth surface, made either of sorted clasts or organic material, is found along the 30 m isobath (Fugro-Jacques Geosurveys Inc., 2010).The constructed geoacoustic model for this region consists of a limestone bedrock 15 m below the seafloor that is overlaid by fine sand sediments. This geoacoustic model is presented in Table 2.4.

Table 2.4 Geoacoustic Model for Sound Propagation Modelling at Sites Offshore Forteau Point

Depth (m)	ρ (g/cm^3)	V_P (m/s)	α_P (dB/λ)	V_S (m/s)	α_S (dB/λ)
0–5	1.52–1.57	1580–1670	0.5–0.8	150	0.1
5–10	1.57–1.59	1670–1730	0.8–1.0		
10–15	1.59–1.61	1730–1775	1.0–1.1		
>15	2.7	3000	0.05		

Strait of Belle Isle

The sediment thickness in the Strait of Belle Isle varies between from 1 to 3 m. At depths greater than 50 m, the seabed is characterized by a surface related to the reworking of underlying glacial sediment where areas of bedrock outcrops, surficial sand ribbons, and boulders occur locally (Fugro-Jacques Geosurveys Inc., 2010). The calculated geoacoustic profile for modelling at locations within the Strait of Belle Isle (Locations 3 and 4) consist of a limestone bedrock at 3 m below the seafloor, overlaid by sand of medium grain size. This geoacoustic model is presented in Table 2.5.

Table 2.5 Geoacoustic Model for Sound Propagation Modelling at Sites in the Strait of Belle Isle

Depth (m)	ρ (g/cm^3)	V_P (m/s)	α_P (dB/λ)	V_S (m/s)	α_S (dB/λ)
0–3	1.52–1.54	1650–1740	0.8–1.1	200	0.2
>3	2.7	3000	0.05		

Offshore Shoal Cove

Offshore of Shoal Cove the seabed is characterized by the heavy presence of dolomitic limestone (dolostone), and a surficial layer of sandy gravel with occasional boulders and bedrock outcrops in shallower water (Fugro-Jacques Geosurveys Inc., 2010). The calculated geoacoustic profile for the region consists of the limestone bedrock at 1 m below the seafloor, overlaid by sandy gravel. The geoacoustic model for the location is presented in Table 2.6.

Table 2.6 Geoacoustic Model for Sound Propagation Modelling at Sites Offshore Shoal Cove

Depth (m)	ρ (g/cm^3)	V_P (m/s)	α_P (dB/λ)	V_S (m/s)	α_S (dB/λ)
0–1	1.61	1870	0.5–0.8	250	0.4
>1	2.7	3000	0.05		

2.2.5 **Bathymetry**

The accuracy of the sound propagation prediction depends on the quality of bathymetry data used. For the purpose of this modelling study, a bathymetrical grid was created with the cell size of 50 m x 50 m. The grid covers the area of approximately 100 km x 100 km around the proposed submarine cable corridor. It incorporated three bathymetry datasets. One of the datasets included very-high resolution multibeam survey data provided by Nalcor Energy.

In 2007, Fugro-Jacques Geosurveys Inc. conducted a detailed bathymetric survey of the Strait of Belle Isle on behalf of Nalcor Energy to verify the seabed conditions and aid in the eventual planning and selection of the

submarine cable corridor(s). Detailed sub-sea sonar surveys of the general crossing area were undertaken, including side-scan sonar, multi-beam and sub-bottom profile surveys. These sonar surveys provided detailed information on the proposed 500 m wide submarine cable corridor. A total of 840 km of geophysical survey lines were surveyed. The multibeam survey provided very high resolution (approximately 10 m x 10 m) sea-bottom topography extending approximately 20 km either side of the corridor.

In the near-shore areas, which were not covered by the multibeam survey, digitized isobaths from Map 90-05 Bedrock Geology of the Strait of Belle Isle (1:50,000 scale) were used. Bathymetry data from the SRTM30+ data base (Becker et al., 2008) were used outside the main area covered by multibeam survey. The irregular spaced depth data points were gridded using a minimum curvature gridding method.

2.2.6 Sound Speed Profile

Water column sound speed profiles (SSPs) for each of the three regions (Offshore Forteau Point, SOBI, and Offshore Shoal Cove) were constructed based on the sound velocity measurements conducted in the Strait of Belle Isle in August to September of 2007 (Figure 2.4). More than 30 sound velocity profiles were available from various locations in the Strait (data provided by Nalcor Energy).

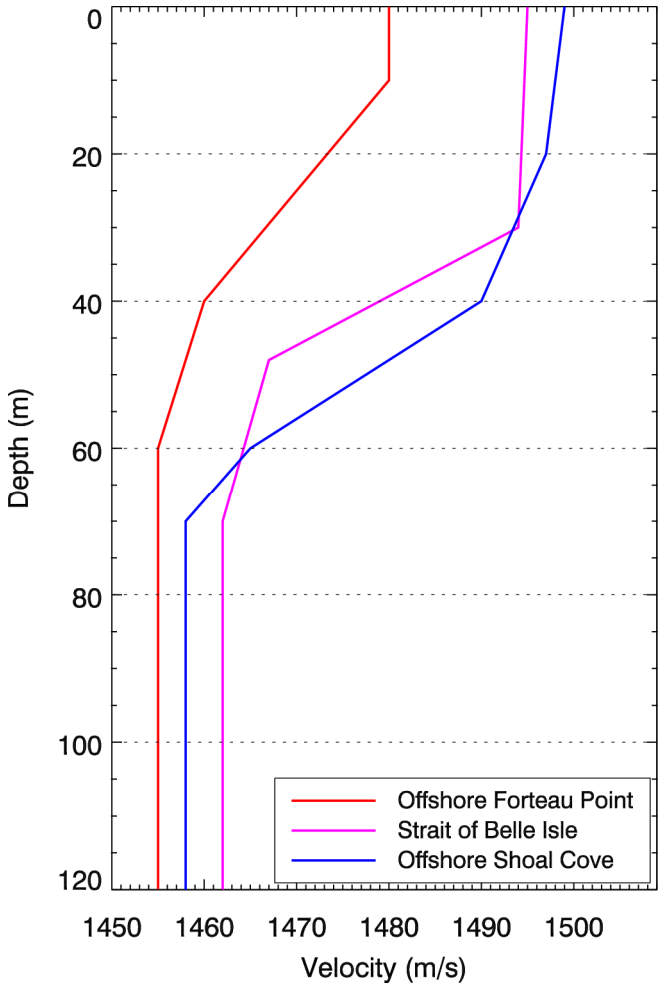

Figure 2.4 Sound Velocity Profiles in the Water Column for the Strait of Belle Isle

2.3 Study Team

The study team for the modelling project consisted of highly skilled and knowledgeable staff with JASCO. The key contributors were: Mikhail Zykov, Marie-Noël Matthews, and David Zeddies.

Mikhail Zykov

Mikhail Zykov, Senior Project Scientist, was the lead for this modelling study and also performed the duties of project manager. He was responsible for designing the modelling approach, modelling of the sound field from drilling operation, data quality control, report writing, and overall management of the project.

Mikhail Zykov obtained his PhD degree at the University of Victoria, BC in geophysics, and he also holds a Masters Certificate in Project Management. He joined JASCO in 2006 and since then has been involved in multiple modelling projects as well as field work. Mikhail's responsibilities mainly include developing specific scientific approaches to different projects, defining the source levels for various sources, modelling of the sound field propagation, report writing, and overall management of projects.

Marie-Noël Matthews

Marie-Noël Matthews, Project Scientist, was responsible for defining the source levels for the noise sources, modelling of the sound field propagation, post-processing of the modelling output data, and report writing.

Marie-Noël Matthews obtained her Master of Science in oceanography at Dalhousie University. Her thesis work involved the use of underwater acoustic propagation models and inversion algorithms to determine the geoacoustic properties of gassy sediments. Prior to joining JASCO, Marie-Noël was employed as Defense Scientist at Defense Research & Development Canada – Atlantic while serving as a Maritime Surface and Sub-surface (MAR SS) Officer in the Canadian Forces. Since she joined JASCO in February 2010, her primary duties include underwater sound propagation modelling, data analysis, and software development.

David Zeddies

David Zeddies, Senior Project Scientist, assisted with the modeling study and report writing as well as scientific editing.

David Zeddies obtained a PhD at Northwestern University in Evanston, IL from the Department of Neurobiology and Physiology. He is also trained as an engineer with a BSME from University of Illinois in Champaign-Urbana. He has studied acoustics, neural processing of acoustic information, and the impacts of sounds on hearing for over fifteen years and published numerous papers. He joined JASCO in 2011.

3.0 RESULTS

Estimates of the sound field around specific cable laying activities were modelled by combining the transmission loss modelling with the respective sound source levels. The values of transmission loss were calculated at different depths in the water column because the sound field is not homogeneous in the vertical direction.

Processing of the output data from the modelling code involved gridding of all the data points in each horizontal plane separately (i.e., at each modelling depth). The resulting stack of grids was collapsed into a single grid using a maximum-over-depth rule; that is, the sound level at each point was taken to be the maximum value that occurred over all modelled depths for that point.

Calculations of maximum distances to the specific ensonification levels were performed based on the grids of the modelled sound field. For each level, two distances were reported: 1) R_{max} – the maximum distance at which the specific sound level was registered in the modelled field; 2) $R_{95\%}$ – the maximum distance to a grid point at which the specific sound level was registered after exclusion of 5% furthest points. Distances were calculated based on unweighted sound field, as well as with M-weighting filters applied.

3.1 Horizontal Directional Drilling

In the modelling exercise, the acoustic source for the HDD activity was "placed" at the proposed exit points for the boreholes. Two modelling scenarios with source depths of 1 m and 10 m below the sea bottom were created. It is expected that during the drilling operation the drill head will be at 10 m below the sea bottom or lower most of the time. The shallower position of the drill bit is expected to occur only at the final stage of the operation, while it is piercing the bottom into the water at the exit point.

Sound propagation modelling was performed using RAM-S propagation code (see Section 2.2.2). The modelling frequency range was from 1 Hz to 100 Hz (for twenty one third-octave bands), as the drilling emits acoustic energy with low frequencies. The resolution of the computational grid was set to 10 m in the horizontal direction, and transmission loss values were obtained for the circular area with a radius of 5 km around the acoustic source at location 1 and for the area with radius of 10 km at location 6. The selected size of the modelling area fully enclosed the 120 dB contour. In the vertical direction, the ensonification values were obtained at 15 different constant depths ranging from 1 m to 100 m below the sea surface and at the surface parallel to the sea bottom with 2 m upward offset.

The resultant ensonification fields from the HDD activity are presented in Figures 3.1–3.4. The distances to specific ensonification levels are presented in Tables 3.1–3.4.

The sound field for at Location 6 reveals significant variation in the sound propagation in different directions. The contours on the shore side from the source are compressed, since the sound energy attenuates faster as it enters shallow waters of the near shore areas.

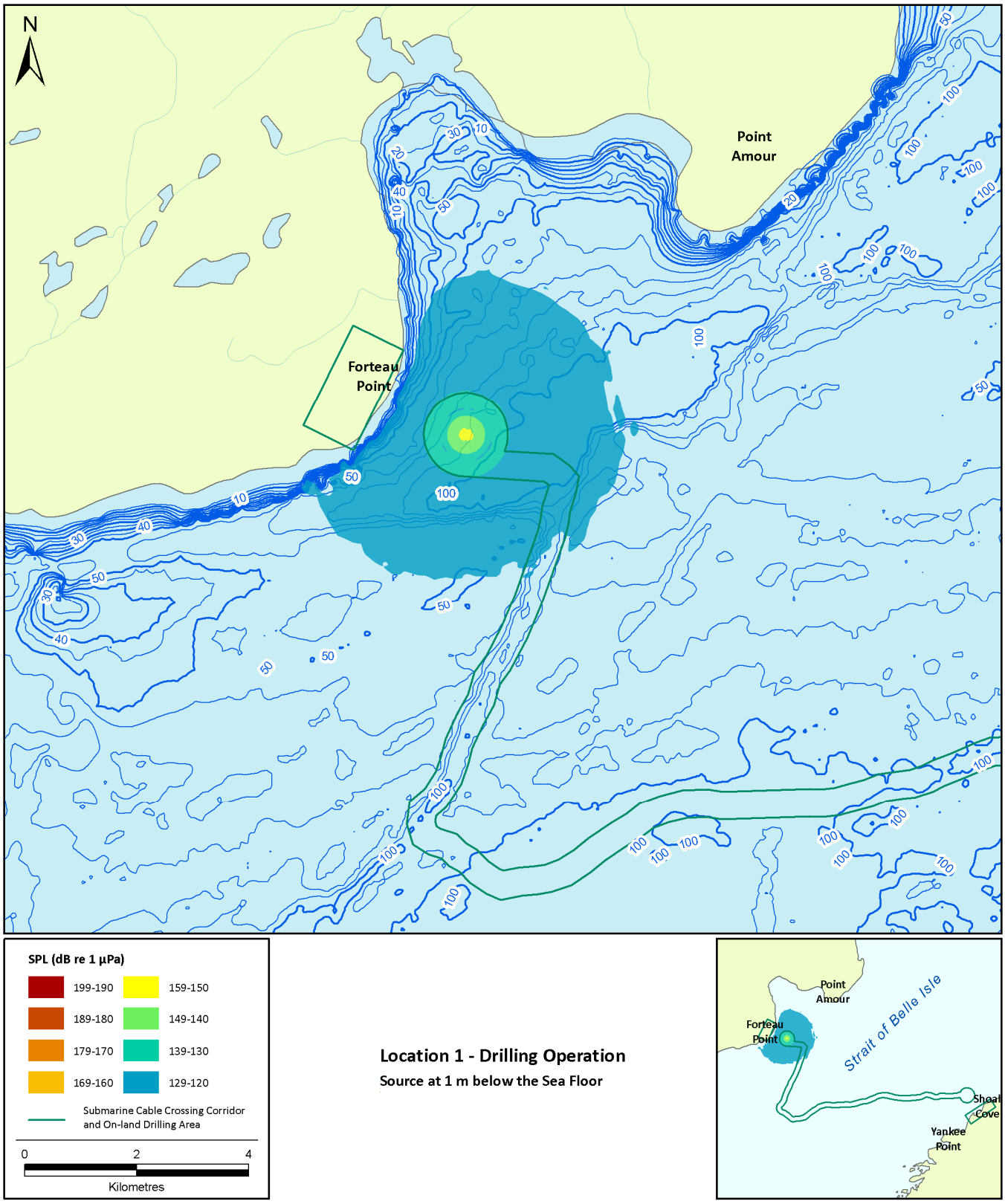

Figure 3.1 Predicted Sound Pressure Levels for the Drilling Operation at Location 1 – Offshore Forteau Point. Source is at 1 m below the Sea Floor

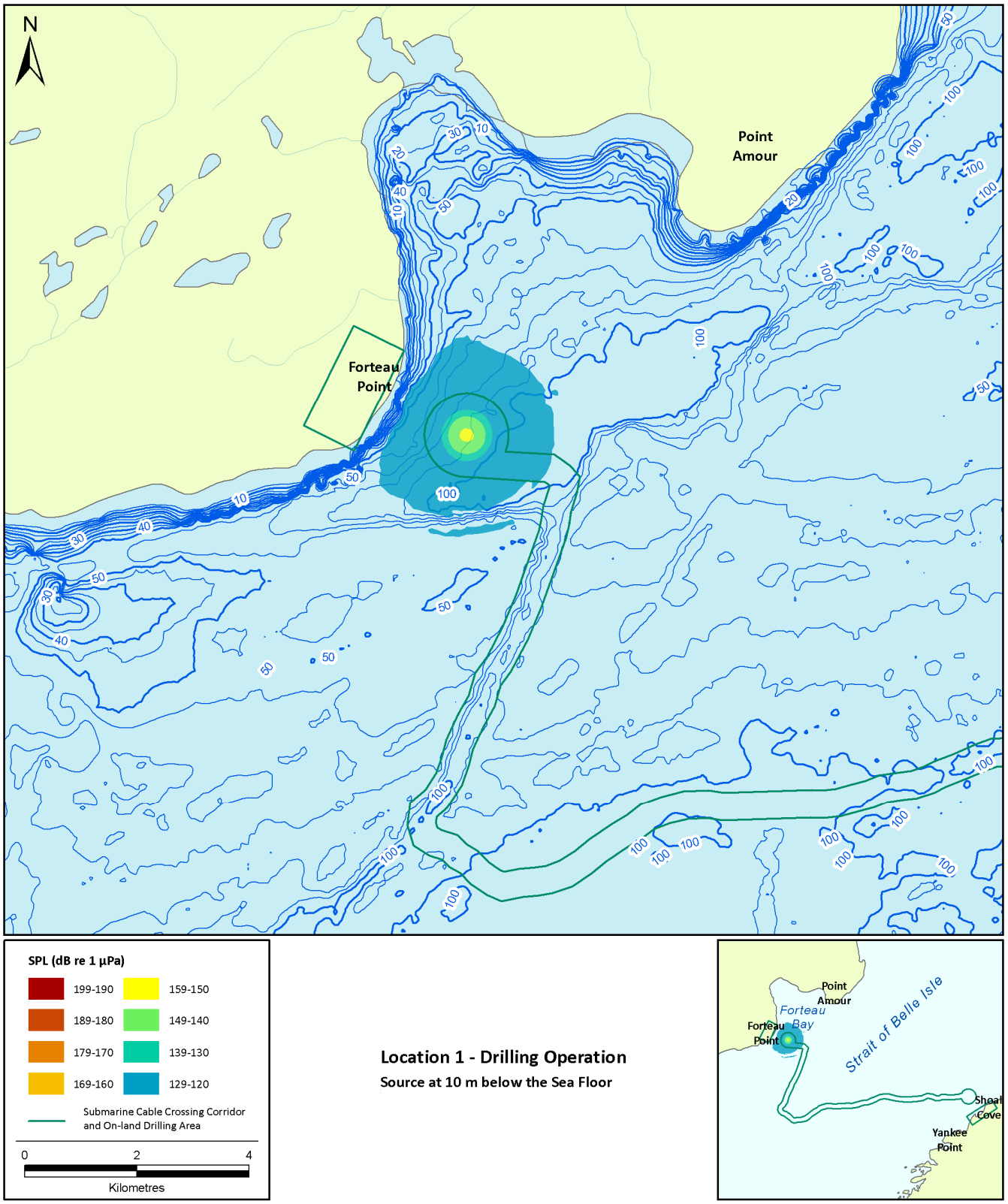

Figure 3.2 Predicted Sound Pressure Levels for the Drilling Operation at Location 1 – Offshore Forteau Point. Source is at 10 m below the Sea Floor

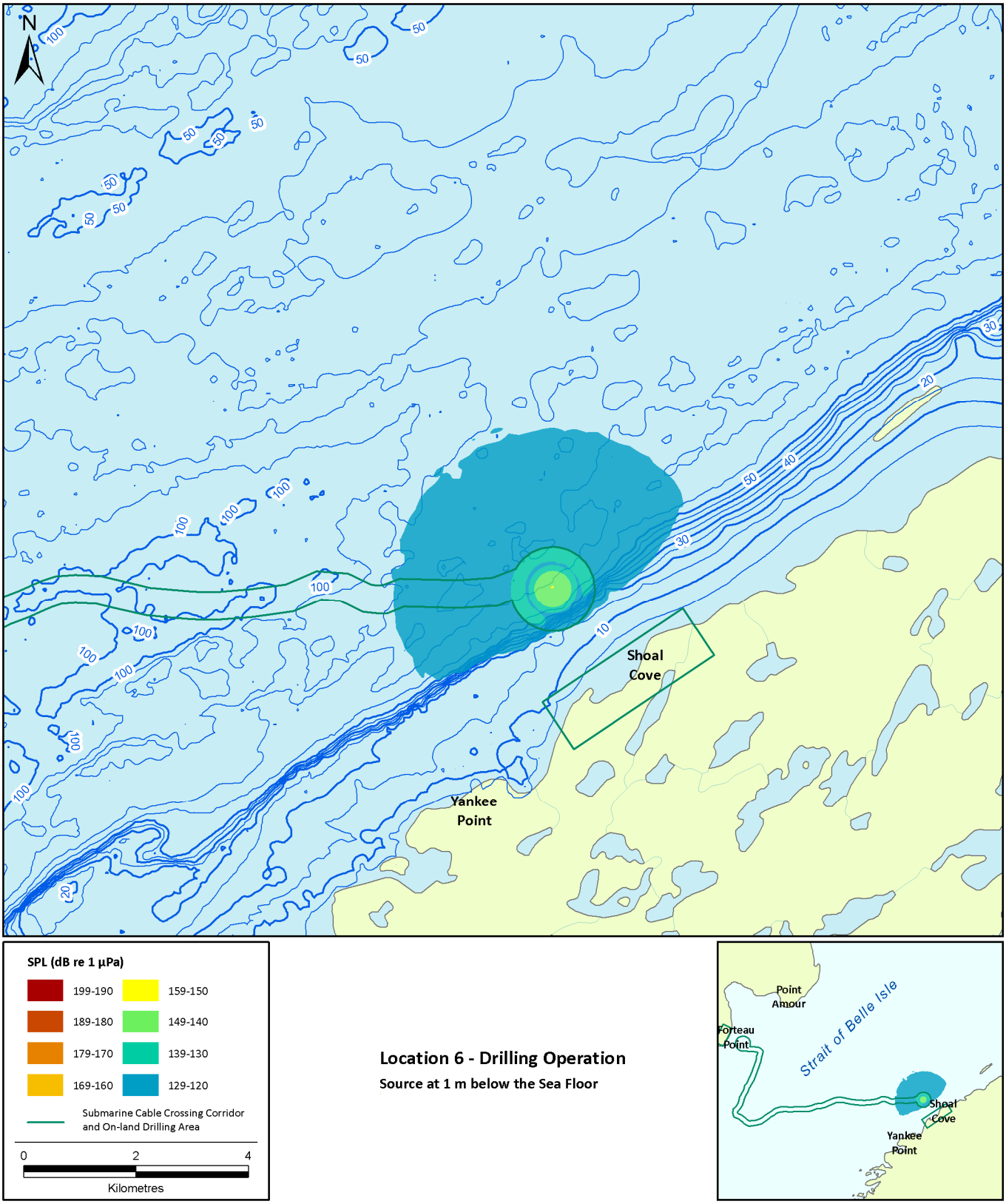

Figure 3.3 Predicted Sound Pressure Levels for the Drilling Operation at Location 6 – Offshore Shoal Cove. Source is at 1 m below the Sea Floor

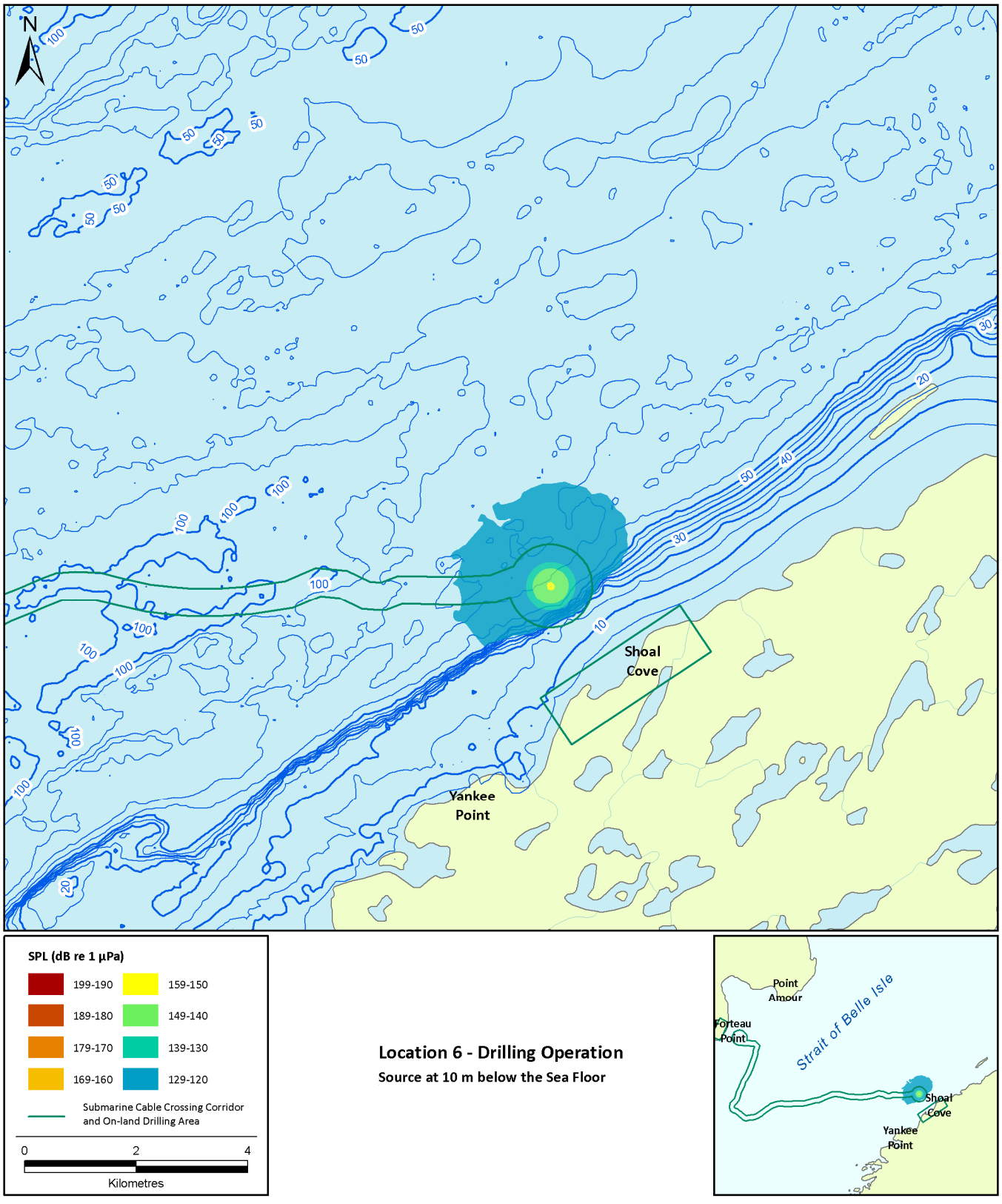

Figure 3.4 Predicted Sound Pressure Levels for the Drilling Operation at Location 6 – Offshore Shoal Cove. Source is at 10 m below the Sea Floor

Table 3.1 Threshold Distances for the Drilling Operation at Location 1 – Offshore Forteau Point. Source is at 1 m below the Sea Floor

RMS SPL (dB re 1 µPa)	Threshold distances (m)									
	No weighting applied		Cetaceans						Pinnipeds	
			Low-frequency		Mid-frequency		High-frequency			
	R_{max}	$R_{95\%}$	R_{max}	$R_{95\%}$	R_{max}	$R_{95\%}$	R_{max}	$R_{95\%}$	R_{max}	$R_{95\%}$
160	< 5	< 5								
150	140	125								
140	345	330	< 5	< 5						
130	800	750	45	41	< 5	< 5			< 5	< 5
120	3150	2750	300	280	16	16	< 5	< 5	46	43
110	8000	6150	3950	2100	95	85	38	36	820	410
100	> 10 000	> 10 000	> 10 000	> 10 000	1730	1075	520	400	4025	2475
90					> 10 000	> 10 000	> 10 000	> 10 000	> 10 000	> 10 000

Table 3.2 Threshold Distances for the Drilling Operation at Location 1 – Offshore Forteau Point. Source is at 10 m below the Sea Floor

RMS SPL (dB re 1 µPa)	Threshold distances (m)									
	No weighting applied		Cetaceans						Pinnipeds	
			Low-frequency		Mid-frequency		High-frequency			
	R_{max}	$R_{95\%}$	R_{max}	$R_{95\%}$	R_{max}	$R_{95\%}$	R_{max}	$R_{95\%}$	R_{max}	$R_{95\%}$
160	< 5	< 5								
150	129	122								
140	340	325	< 5	< 5						
130	470	445	51	47					< 5	< 5
120	1870	1600	275	260	< 5	< 5	< 5	< 5	22	21
110	7900	4600	200	1175	53	50	20	18	165	155
100	> 10 000	> 10 000	> 10 000	> 10 000	460	380	135	120	5850	2850
90					> 10 000	> 10 000	4600	2350	> 10 000	> 10 000
80							> 10 000	> 10 000		

Table 3.3 Threshold Distances for the Drilling Operation at Location 6 – Offshore Shoal Cove. Source is at 1 m below the Sea Floor

RMS SPL (dB re 1 µPa)	Threshold distances (m)									
	No weighting applied		Cetaceans						Pinnipeds	
			Low-frequency		Mid-frequency		High-frequency			
	R_{max}	$R_{95\%}$	R_{max}	$R_{95\%}$	R_{max}	$R_{95\%}$	R_{max}	$R_{95\%}$	R_{max}	$R_{95\%}$
160	< 5	< 5								
150	62	70								
140	333	320	< 5	< 5						
130	950	750	43	38					< 5	< 5
120	3150	2800	315	285	< 5	< 5	< 5	< 5	51	47
110	> 10 000	> 10 000	3350	2000	71	67	41	39	415	290
100			> 10 000	> 10 000	890	670	300	250	> 10 000	> 10 000
90					> 10 000	> 10 000	> 10 000	> 10 000		

Table 3.4 Threshold Distances for the Drilling Operation at Location 6 – Offshore Shoal Cove. Source is at 10 m below the Sea Floor

RMS SPL (dB re 1 µPa)	Threshold distances (m)									
	No weighting applied		Cetaceans						Pinnipeds	
			Low-frequency		Mid-frequency		High-frequency			
	R_{max}	$R_{95\%}$	R_{max}	$R_{95\%}$	R_{max}	$R_{95\%}$	R_{max}	$R_{95\%}$	R_{max}	$R_{95\%}$
160	< 5	< 5								
150	77	70								
140	325	310	< 5	< 5						
130	450	425	48	46					< 5	< 5
120	1900	1725	280	250	< 5	< 5	< 5	< 5	30	29
110	6050	5250	1800	1350	55	51	28	26	175	152
100	> 10 000	> 10 000	> 10 000	> 10 000	435	315	140	119	3050	1700
90					> 10 000	> 10 000	3050	1350	> 10 000	> 10 000
80							> 10 000	> 10 000		

3.2 Vessels in Transit

Through the model, the acoustic sources for vessels in transit were "placed" at 4 locations along the proposed cable crossing corridor. The depth for the sources was chosen to be 5 m below the sea surface, based on the likely position of the vessels' main propulsion systems.

The sound propagation modelling was performed using MONM propagation code (see Section 2.2.1) for frequencies between 10 and 2000 Hz. The resolution of the computational grid was 5 m in the horizontal direction, and transmission loss values were obtained for the circular area with a radius of 30 km around the acoustic sources at locations 2, 3, 4, and 5. In the vertical direction, the ensonification values were obtained at 11 different constant depths ranging from 1 m to 125 m below the sea surface.

The distances to specific ensonification levels from the typical cable laying and rock placement vessels (described earlier) in transit at speeds 10 knots and 12 knots respectively are presented in Tables 3.5 –3.12. The resultant ensonification fields are presented in Figures 3.5 –3.12.

3.2.1 Location 2 – Offshore Forteau Point

Table 3.5 Threshold Distances for the Typical Cable Laying Vessel in Transit (10 Knots) at Location 2 – Offshore Forteau Point

RMS SPL (dB re 1 µPa)	Threshold distances (m)									
	No weighting applied		Cetaceans						Pinnipeds	
			Low-frequency		Mid-frequency		High-frequency			
	R_{max}	$R_{95\%}$	R_{max}	$R_{95\%}$	R_{max}	$R_{95\%}$	R_{max}	$R_{95\%}$	R_{max}	$R_{95\%}$
160	< 5	< 5	< 5	< 5					< 5	< 5
150	10	10	10	10	< 5	< 5	< 5	< 5	10	10
140	35	35	35	35	15	15	10	10	20	20
130	255	135	220	130	50	50	40	40	65	65
120	1050	745	1050	740	310	295	245	135	525	400

Table 3.6 Threshold Distances for the Typical Rock Placement Vessel in Transit (12 Knots) at Location 2 – Offshore Forteau Point

RMS SPL (dB re 1 µPa)	Threshold distances (m)									
	No weighting applied		Cetaceans						Pinnipeds	
			Low-frequency		Mid-frequency		High-frequency			
	R_{max}	$R_{95\%}$	R_{max}	$R_{95\%}$	R_{max}	$R_{95\%}$	R_{max}	$R_{95\%}$	R_{max}	$R_{95\%}$
170	< 5	< 5	< 5	< 5					< 5	< 5
160	10	10	10	10	< 5	< 5	< 5	< 5	10	10
150	35	35	35	35	15	15	10	10	20	20
140	275	250	265	215	50	50	40	40	75	70
130	1085	800	1085	785	315	300	275	145	525	425
120	3225	2375	3225	2360	2050	1375	1825	1240	2700	1700

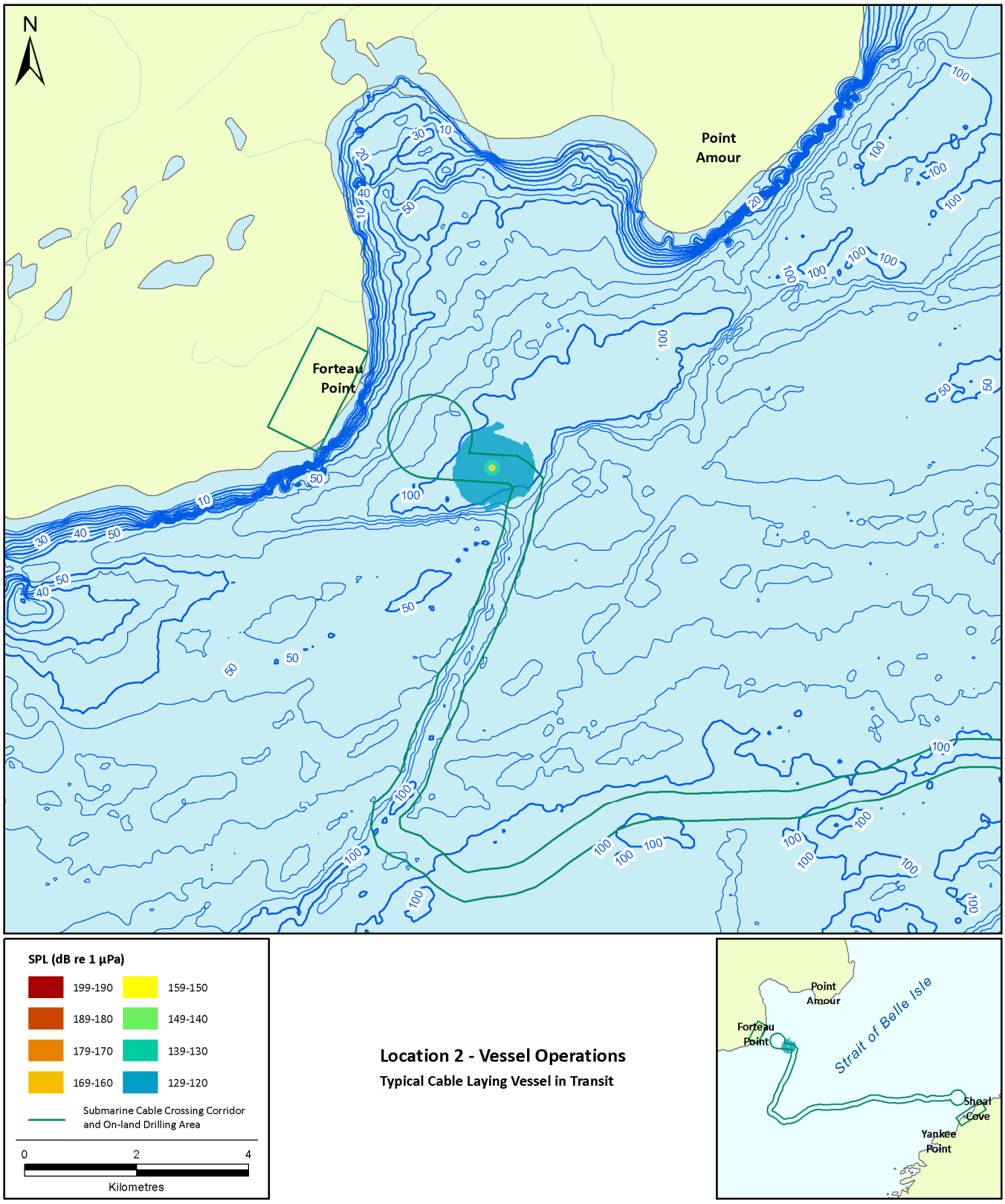

Figure 3.5 Predicted Sound Pressure Levels for the Typical Cable Laying Vessel in Transit (10 Knots) at Location 2 – Offshore Forteau Point

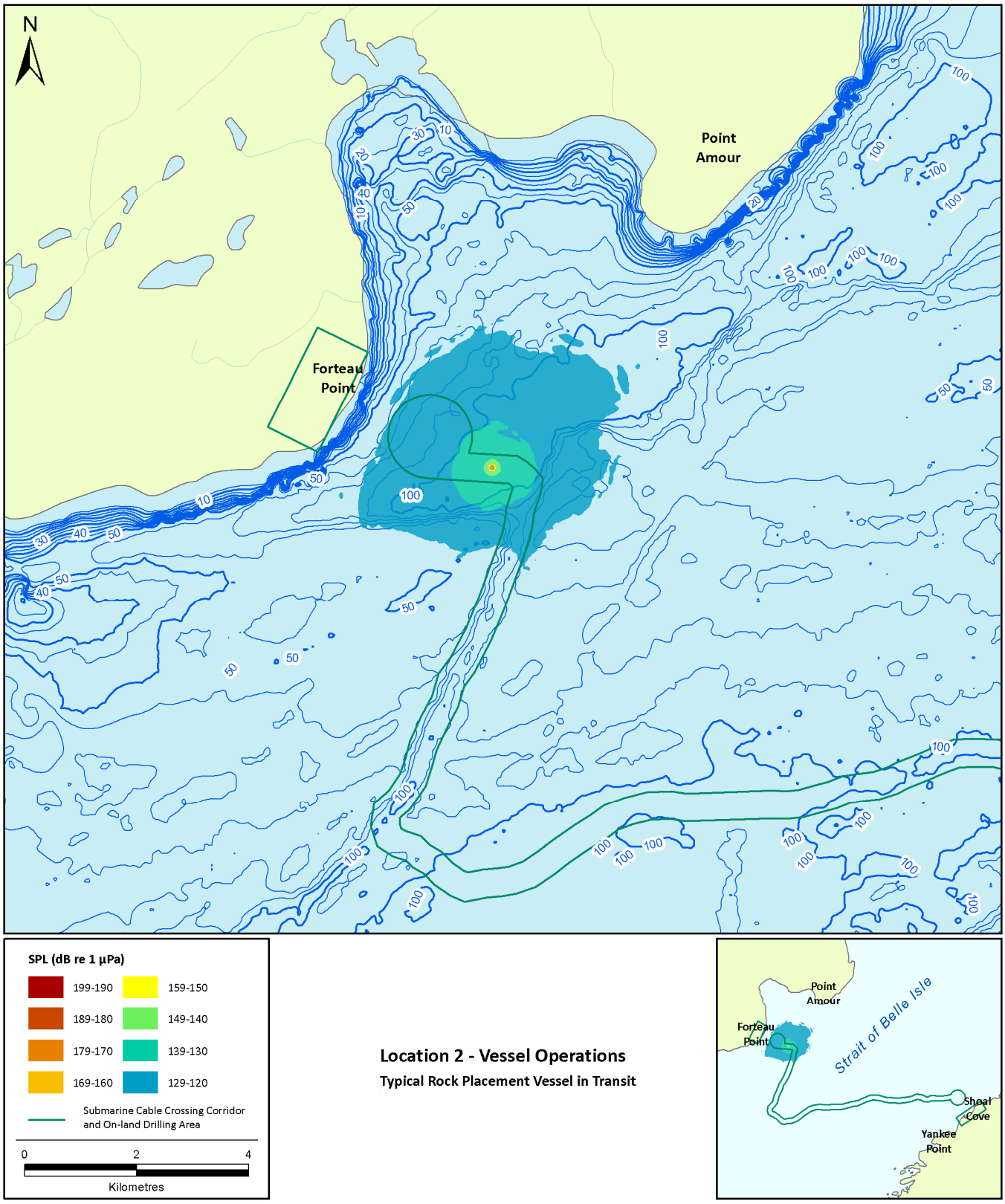

Figure 3.6 Predicted Sound Pressure Levels for the Typical Rock Placement Vessel in Transit (12 Knots) at Location 2 – Offshore Forteau Point

3.2.2 Location 3 – Shallow Trench near the Middle of Strait of Belle Isle

Table 3.7. Threshold Distances for the Typical Cable Laying Vessel in Transit (10 Knots) at Location 3 – Shallow Trench near the Middle of Strait of Belle Isle

RMS SPL (dB re 1 µPa)	Threshold distances (m)									
	No weighting applied		Cetaceans						Pinnipeds	
			Low-frequency		Mid-frequency		High-frequency			
	R_{max}	$R_{95\%}$	R_{max}	$R_{95\%}$	R_{max}	$R_{95\%}$	R_{max}	$R_{95\%}$	R_{max}	$R_{95\%}$
160	< 5	< 5	< 5	< 5						
150	10	10	10	10	< 5	< 5	< 5	< 5	< 5	< 5
140	35	35	35	35	15	15	10	10	20	20
130	240	200	235	200	45	45	40	40	70	65
120	1435	1030	1430	1015	330	280	275	245	725	525

Table 3.8. Threshold Distances for the Typical Rock Placement Vessel in Transit (12 Knots) at Location 3 – Shallow Trench near the Middle of Strait of Belle Isle

RMS SPL (dB re 1 µPa)	Threshold distances (m)									
	No weighting applied		Cetaceans						Pinnipeds	
			Low-frequency		Mid-frequency		High-frequency			
	R_{max}	$R_{95\%}$	R_{max}	$R_{95\%}$	R_{max}	$R_{95\%}$	R_{max}	$R_{95\%}$	R_{max}	$R_{95\%}$
170	< 5	< 5	< 5	< 5					< 5	< 5
160	10	10	10	10	< 5	< 5	< 5	< 5	10	10
150	35	35	35	35	15	15	10	10	25	20
140	245	215	245	215	50	50	45	40	75	50
130	1630	1085	1435	1065	425	290	285	250	760	575
120	4120	3125	4120	3085	1985	1425	1635	1230	2080	2055

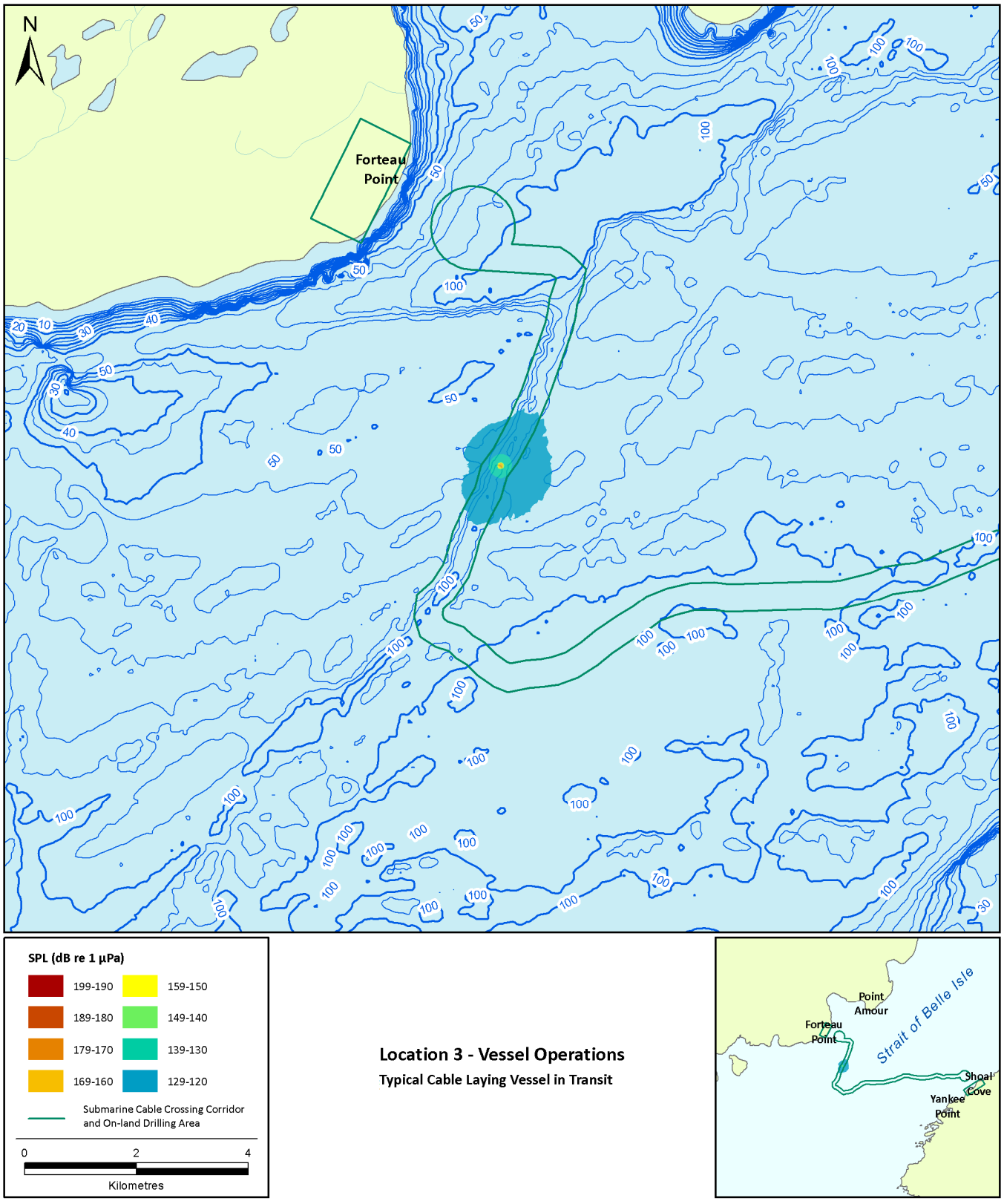

Figure 3.7 Predicted Sound Pressure Levels for the Typical Cable Laying Vessel in Transit (10 Knots) at Location 3 – Shallow Trench near the Middle of Strait of Belle Isle

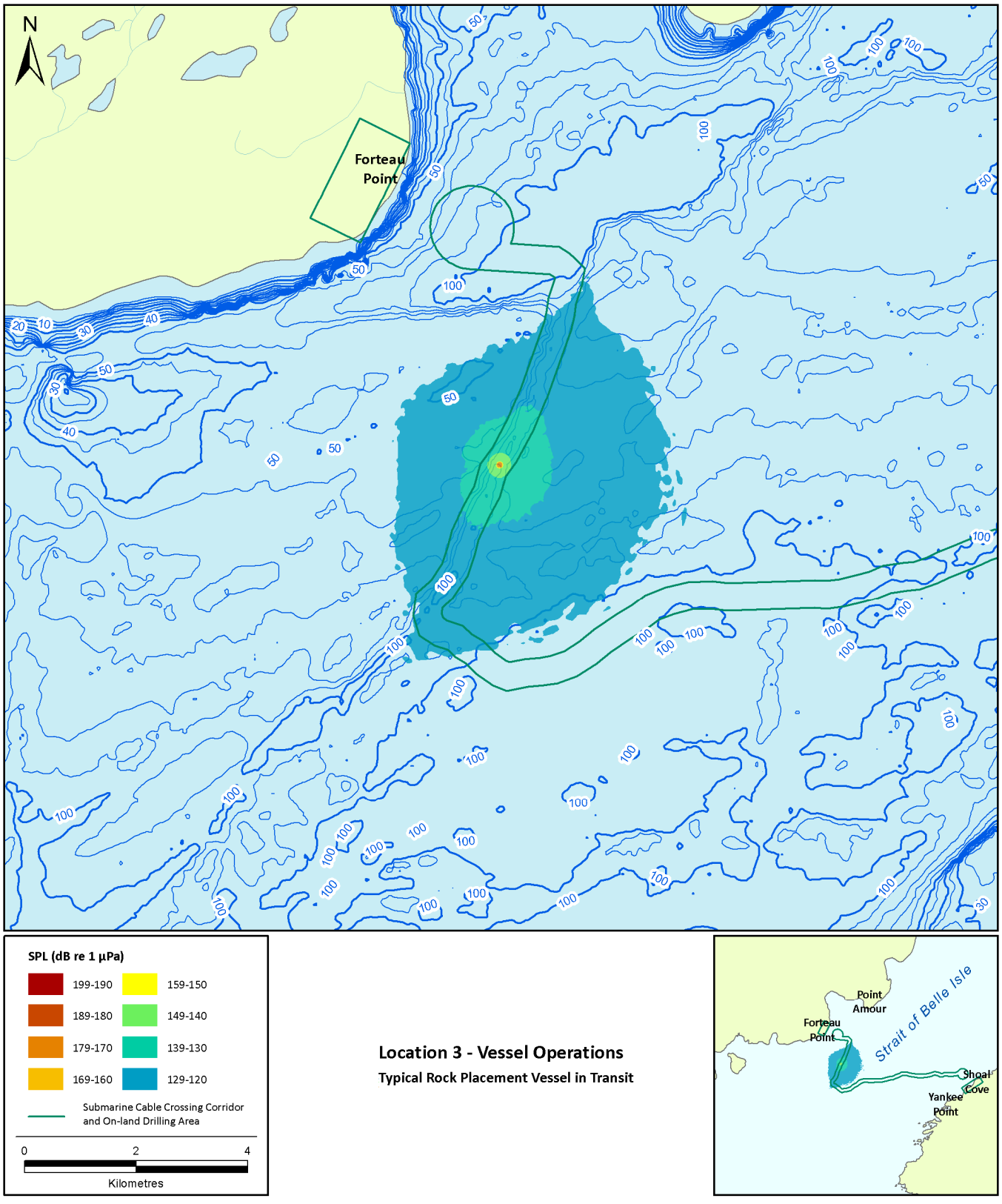

Figure 3.8 Predicted Sound Pressure Levels for the Typical Rock Placement Vessel in Transit (12 Knots) at Location 3 – Shallow Trench near the Middle of Strait of Belle Isle

3.2.3 Location 4 – Middle of Strait of Belle Isle

Table 3.9 Threshold Distances for the Typical Cable Laying Vessel in Transit (10 Knots) at Location 4 – Middle of Strait of Belle Isle

RMS SPL (dB re 1 µPa)	Threshold distances (m)									
	No weighting applied		Cetaceans						Pinnipeds	
			Low-frequency		Mid-frequency		High-frequency			
	R_{max}	$R_{95\%}$	R_{max}	$R_{95\%}$	R_{max}	$R_{95\%}$	R_{max}	$R_{95\%}$	R_{max}	$R_{95\%}$
160	< 5	< 5	< 5	< 5					< 5	< 5
150	10	10	10	10	< 5	< 5	< 5	< 5	10	10
140	35	35	35	35	15	15	10	10	20	20
130	225	215	225	215	45	45	40	40	70	65
120	1380	1090	1375	1075	330	290	290	235	840	515

Table 3.10 Threshold Distances for the Typical Rock Placement Vessel in Transit (12 Knots) at Location 4 – Middle of Strait of Belle Isle

RMS SPL (dB re 1 µPa)	Threshold distances (m)									
	No weighting applied		Cetaceans						Pinnipeds	
			Low-frequency		Mid-frequency		High-frequency			
	R_{max}	$R_{95\%}$	R_{max}	$R_{95\%}$	R_{max}	$R_{95\%}$	R_{max}	$R_{95\%}$	R_{max}	$R_{95\%}$
170	< 5	< 5	< 5	< 5					< 5	< 5
160	10	10	10	10	< 5	< 5	< 5	< 5	10	10
150	35	35	35	35	15	15	10	10	20	20
140	230	220	225	215	50	50	45	45	75	70
130	1420	1135	1400	1115	345	300	300	240	850	555
120	4900	3475	4900	3440	2200	1575	1870	1265	3200	2280

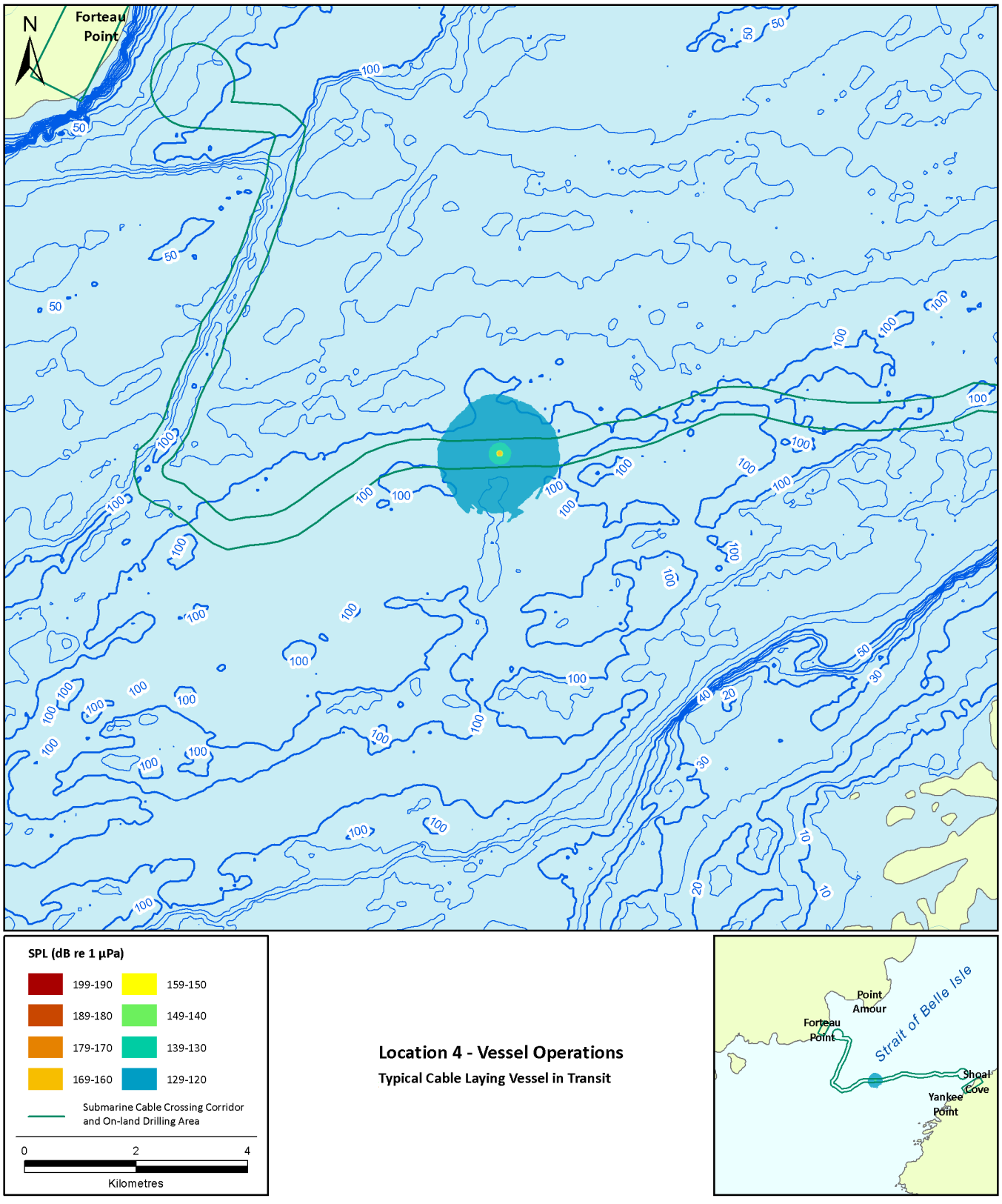

Figure 3.9 Predicted Sound Pressure Levels for the Typical Cable Laying Vessel in Transit (10 Knots) at Location 4 – Middle of Strait of Belle Isle

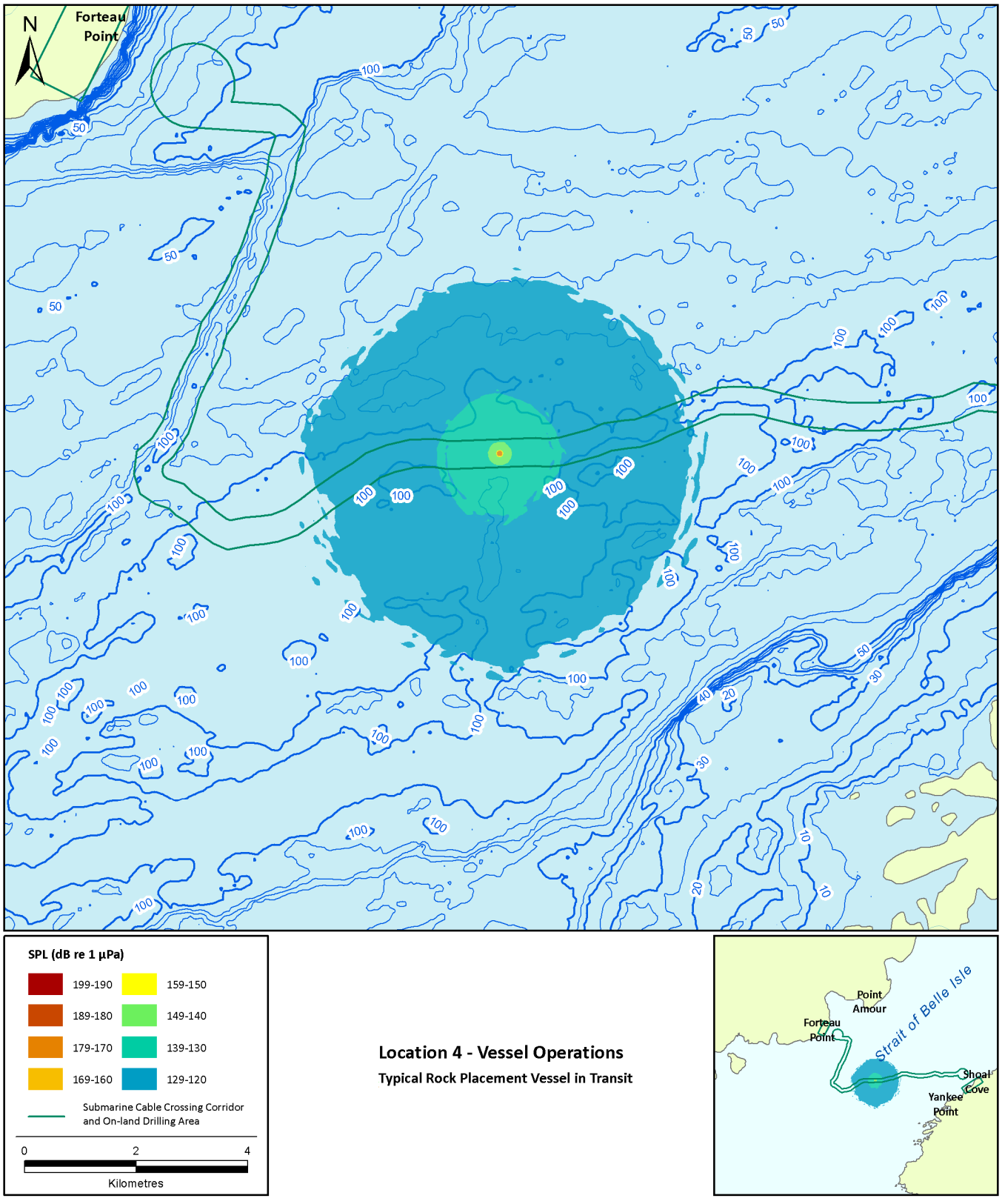

Figure 3.10 Predicted Sound Pressure Levels for the Typical Rock Placement Vessel in Transit (12 Knots) at Location 4 – Middle of Strait of Belle Isle

3.2.4 Location 5 – Offshore Shoal Cove

Table 3.11 Threshold Distances for the Typical Cable Laying Vessel in Transit (10 Knots) at Location 5 – Offshore Shoal Cove

RMS SPL (dB re 1 µPa)	Threshold distances (m)									
	No weighting applied		Cetaceans						Pinnipeds	
			Low-frequency		Mid-frequency		High-frequency			
	R_{max}	$R_{95\%}$	R_{max}	$R_{95\%}$	R_{max}	$R_{95\%}$	R_{max}	$R_{95\%}$	R_{max}	$R_{95\%}$
160	< 5	< 5	< 5	< 5						
150	10	10	10	10	< 5	< 5	< 5	< 5	< 5	< 5
140	40	35	35	35	15	15	10	10	20	20
130	315	230	315	230	50	45	40	40	120	110
120	1585	1160	1585	1140	415	310	285	245	780	645

Table 3.12 Threshold Distances for the Typical Rock Placement Vessel in Transit (12 Knots) at Location 5 – Offshore Shoal Cove

RMS SPL (dB re 1 µPa)	Threshold distances (m)									
	No weighting applied		Cetaceans						Pinnipeds	
			Low-frequency		Mid-frequency		High-frequency			
	R_{max}	$R_{95\%}$	R_{max}	$R_{95\%}$	R_{max}	$R_{95\%}$	R_{max}	$R_{95\%}$	R_{max}	$R_{95\%}$
170	< 5	< 5	< 5	< 5						
160	10	10	10	10	< 5	< 5	< 5	< 5	< 5	< 5
150	40	35	30	35	15	15	10	10	20	20
140	325	280	320	245	50	45	45	40	125	120
130	1715	1245	1715	1225	440	330	325	255	900	660
120	4540	3570	4455	3525	2225	1715	2050	1440	3115	2340

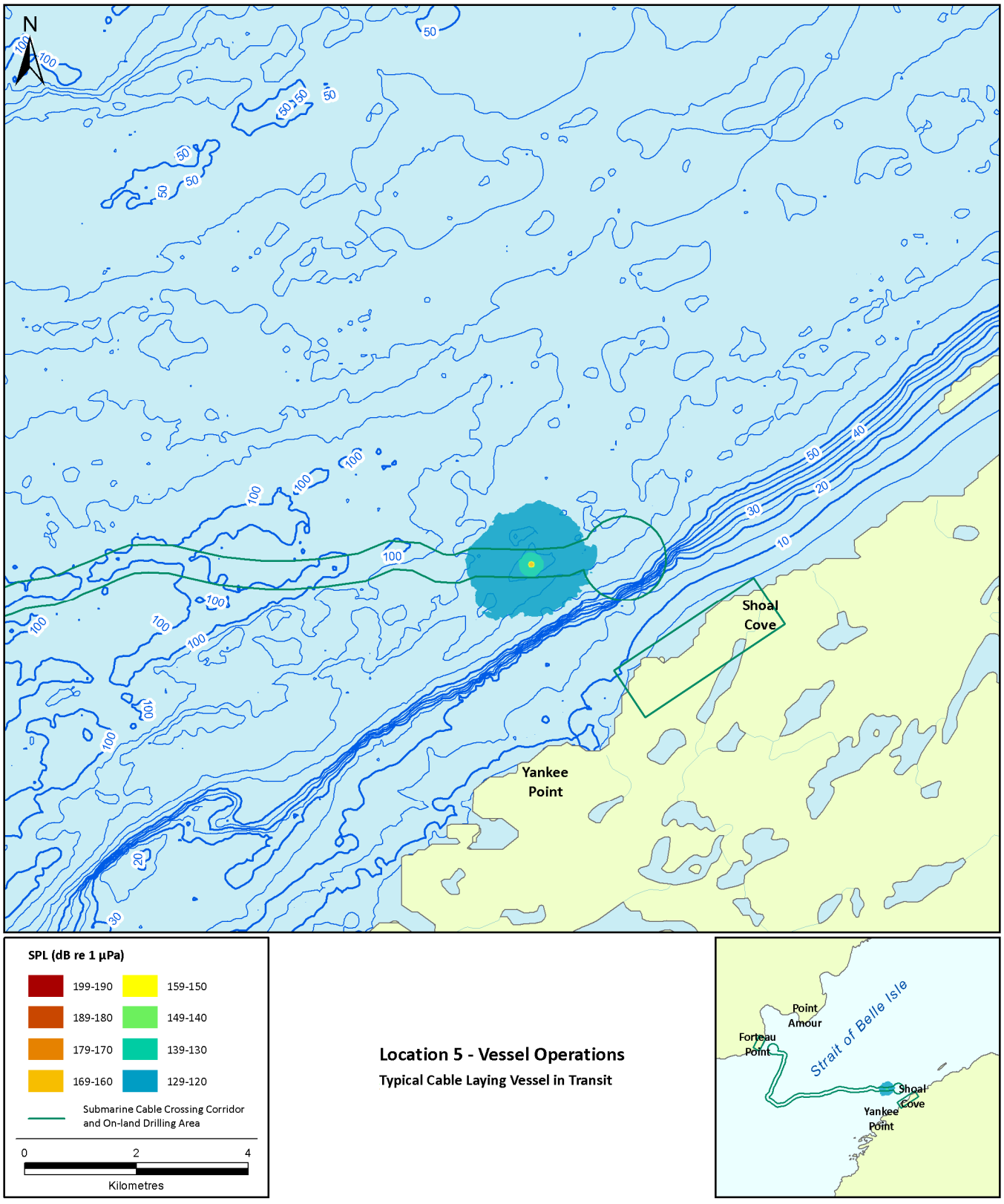

Figure 3.11 Predicted Sound Pressure Levels for the Typical Cable Laying Vessel in Transit (10 Knots) at Location 5 – Offshore Shoal Cove

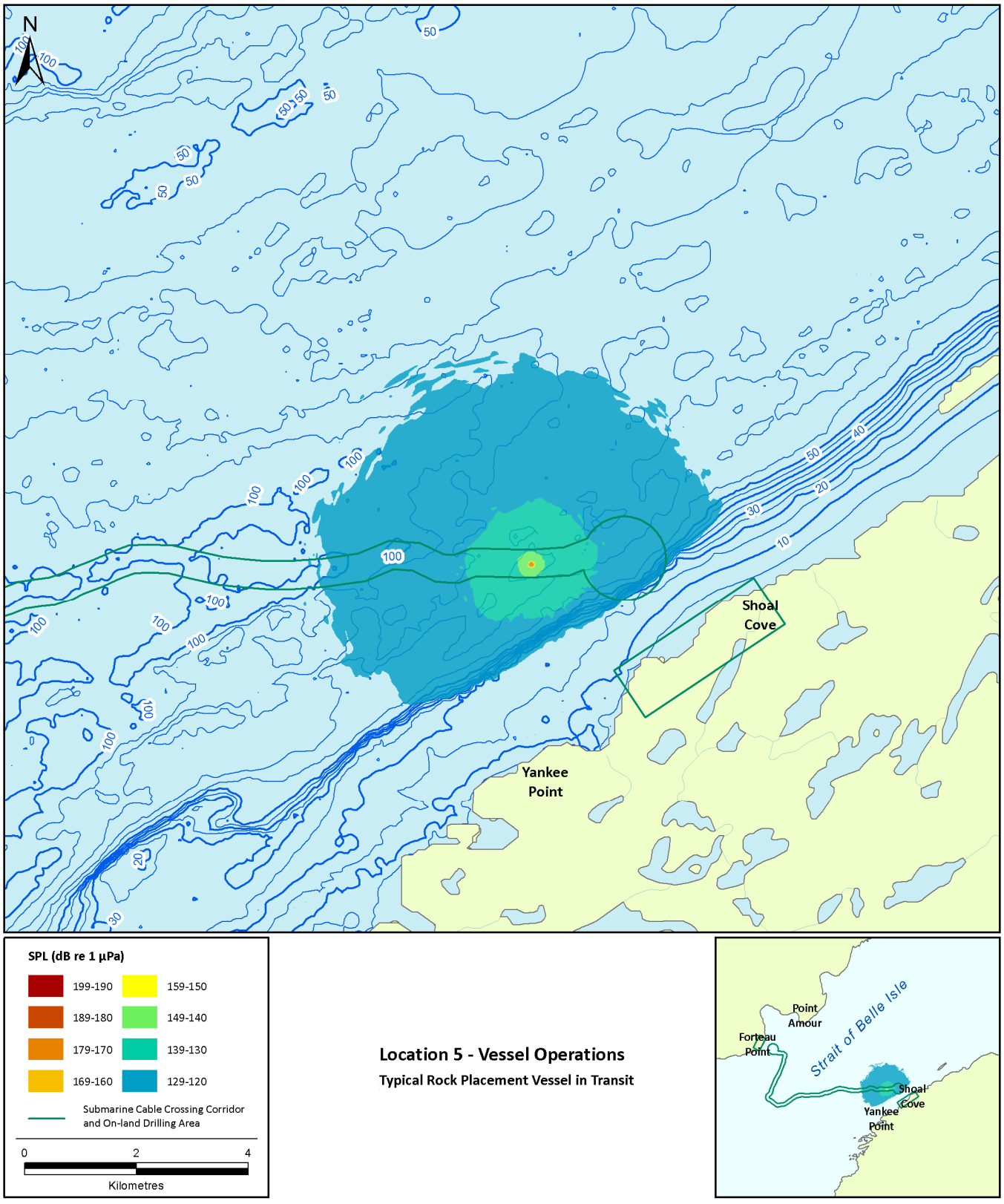

Figure 3.12 Predicted Sound Pressure Levels for the Typical Rock Placement Vessel in Transit (12 Knots) at Location 5 – Offshore Shoal Cove

3.3 Vessels in Dynamic Positioning Mode

The acoustic sources for vessels in DP mode were modelled at the same four locations along the proposed seabed crossing corridor as the vessels in transit. The configuration of the propulsion system of the vessels in the DP mode is different from the transit mode. First of all, greater number of propellers is engaged. Secondly, some propellers are lowered as much as 2 m from their positions for transit mode. For the purpose of modelling the sound field around vessels working in the DP mode the source was placed at depth of 7 m below the sea surface.

The sound propagation modelling was performed using MONM propagation code (see Section 2.2.1) for frequencies between 10 and 5000 Hz. The resolution of the computational grid was 5 m in the horizontal direction. The transmission loss values were obtained for the circular area with a radius of 30 km around the acoustic sources at locations 2, 3, 4, and 5. In the vertical direction, the ensonification values were obtained at 11 different constant depths ranging from 1 m to 125 m below the sea surface.

In the Strait, the factor that influences the sound propagation the most is the water depth. The low frequencies do not propagate well in shallow environments (first tens of metres of water) and attenuate faster compared to the mid-depth environment (about 100 m water depth). The effect of the shallow water environment on the sound propagation can be observed in the modeling results for Location 6 (Figures 3.3 and 3.4), where the sound attenuates significantly faster towards the shore compared to the directions towards the middle of the Strait or along the shore line.

The distances to specific ensonification levels from the typical cable laying and rock placement vessels (described earlier) in DP mode are presented in Tables 3.13–3.20. The resultant ensonification fields are presented in Figures 3.13–3.20.

3.3.1 Location 2 – Offshore Forteau Point

Table 3.13 Threshold Distances for the Typical Cable Laying Vessel in DP Mode at Location 2 – Offshore Forteau Point

RMS SPL (dB re 1 µPa)	Threshold distances (m)									
	No weighting applied		Cetaceans						Pinnipeds	
			Low-frequency		Mid-frequency		High-frequency			
	R_{max}	$R_{95\%}$	R_{max}	$R_{95\%}$	R_{max}	$R_{95\%}$	R_{max}	$R_{95\%}$	R_{max}	$R_{95\%}$
170	< 5	< 5	< 5	< 5	< 5	< 5	< 5	< 5	< 5	< 5
160	20	20	20	20	20	20	15	15	20	20
150	70	65	70	65	65	60	60	55	70	65
140	440	385	430	385	335	320	325	300	400	360
130	3000	1975	2985	1965	2785	1710	2360	1600	2825	1875
120	8900	5425	8900	5400	7450	5020	6800	4875	7465	5255

Table 3.14 Threshold Distances for the Typical Rock Placement Vessel in DP Mode at Location 2 – Offshore Forteau Point

RMS SPL (dB re 1 µPa)	Threshold distances (m)									
	No weighting applied		Cetaceans						Pinnipeds	
			Low-frequency		Mid-frequency		High-frequency			
	R_{max}	$R_{95\%}$	R_{max}	$R_{95\%}$	R_{max}	$R_{95\%}$	R_{max}	$R_{95\%}$	R_{max}	$R_{95\%}$
170	< 5	< 5	< 5	< 5	< 5	< 5	< 5	< 5	< 5	< 5
160	25	25	25	25	25	25	20	20	25	25
150	85	80	85	80	80	75	75	70	85	80
140	960	460	960	460	600	390	425	375	960	440
130	3980	2400	3980	2400	3220	2135	3125	1985	3675	2285
120	9050	6155	9050	6135	8920	5670	8915	5455	8935	5965

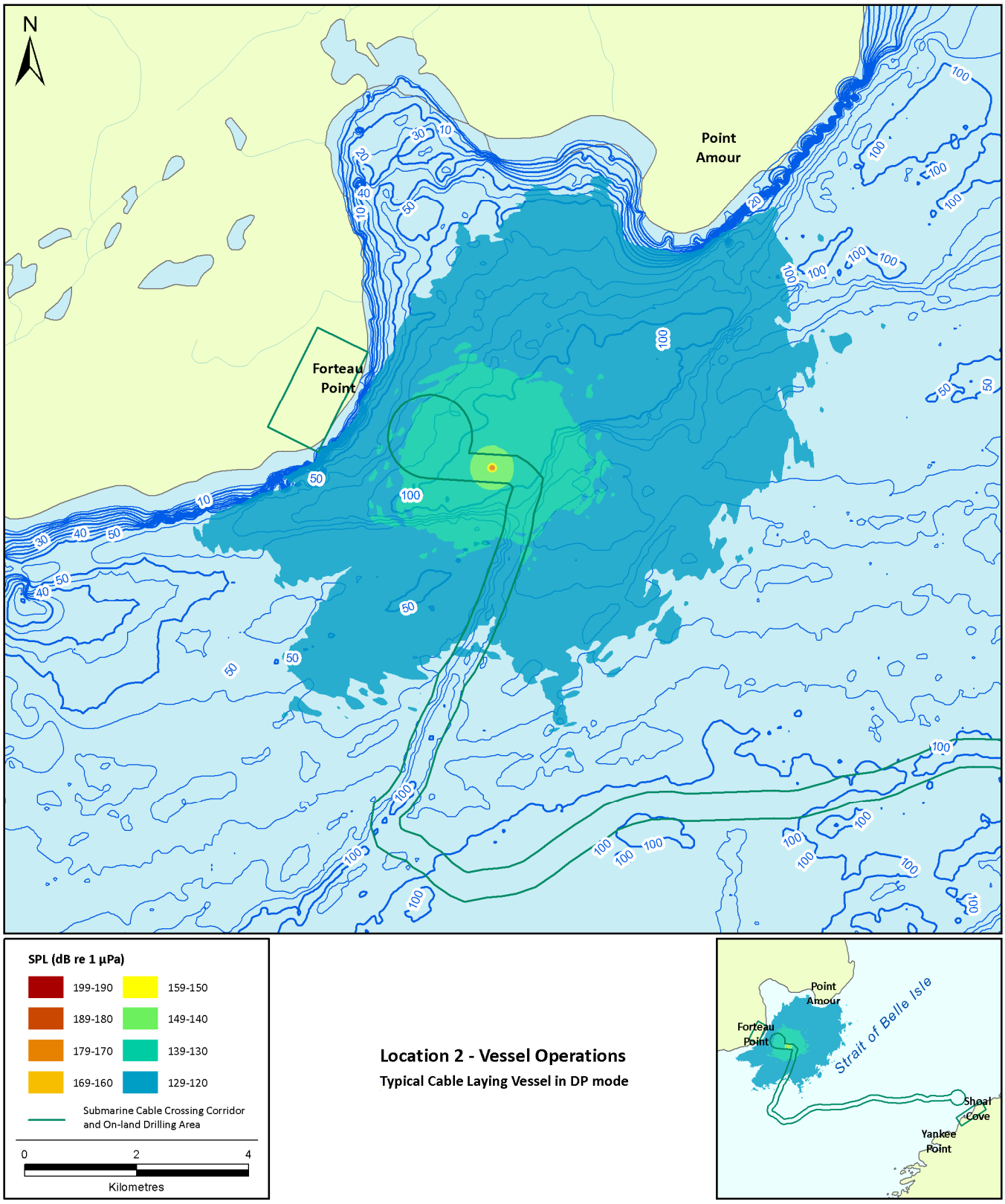

Figure 3.13 Predicted Sound Pressure Levels for the Typical Cable Laying Vessel in DP Mode at Location 2 – Offshore Forteau Point

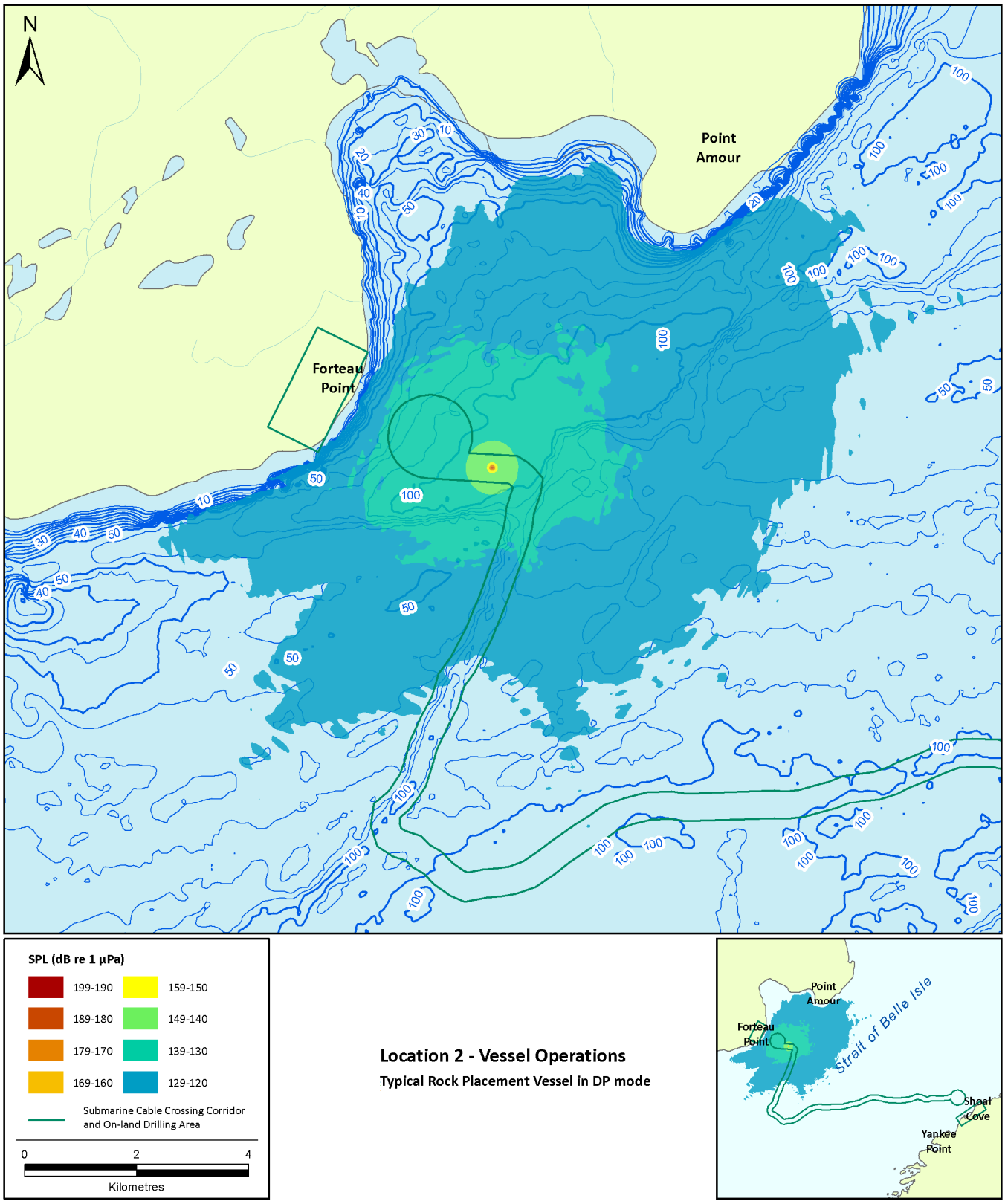

Figure 3.14 Predicted Sound Pressure Levels for the Typical Rock Placement Vessel in DP Mode at Location 2 – Offshore Forteau Point

3.3.2 Location 3 – Shallow Trench near the Middle of Strait of Belle Isle

Table 3.15 Threshold Distances for the Typical Cable Laying Vessel in DP Mode at Location 3 – Shallow Trench near the Middle of Strait of Belle Isle

RMS SPL (dB re 1 µPa)	Threshold distances (m)									
	No weighting applied		Cetaceans						Pinnipeds	
			Low-frequency		Mid-frequency		High-frequency			
	R_{max}	$R_{95\%}$	R_{max}	$R_{95\%}$	R_{max}	$R_{95\%}$	R_{max}	$R_{95\%}$	R_{max}	$R_{95\%}$
170	< 5	< 5	< 5	< 5	< 5	< 5	< 5	< 5	< 5	< 5
160	20	20	20	20	20	20	15	15	20	20
150	75	70	75	70	70	65	65	60	75	70
140	685	400	685	400	425	315	350	300	490	355
130	2680	1960	2680	1950	2410	1655	2220	1535	2520	1835
120	8620	6150	8620	6120	7875	5365	7500	5055	8160	5850

Table 3.16 Threshold Distances for the Typical Rock Placement Vessel in DP Mode at Location 3 – Shallow Trench near the Middle of Strait of Belle Isle

RMS SPL (dB re 1 µPa)	Threshold distances (m)									
	No weighting applied		Cetaceans						Pinnipeds	
			Low-frequency		Mid-frequency		High-frequency			
	R_{max}	$R_{95\%}$	R_{max}	$R_{95\%}$	R_{max}	$R_{95\%}$	R_{max}	$R_{95\%}$	R_{max}	$R_{95\%}$
170	< 5	< 5	< 5	< 5	< 5	< 5	< 5	< 5	< 5	< 5
160	25	25	25	25	25	25	20	20	25	25
150	100	90	100	90	85	75	75	75	90	85
140	825	560	835	555	685	400	490	365	700	485
130	3175	2340	3175	2330	2680	2015	2550	1900	3170	2200
120	11,615	7385	11,615	7350	11,415	6455	8620	6100	11,570	7050

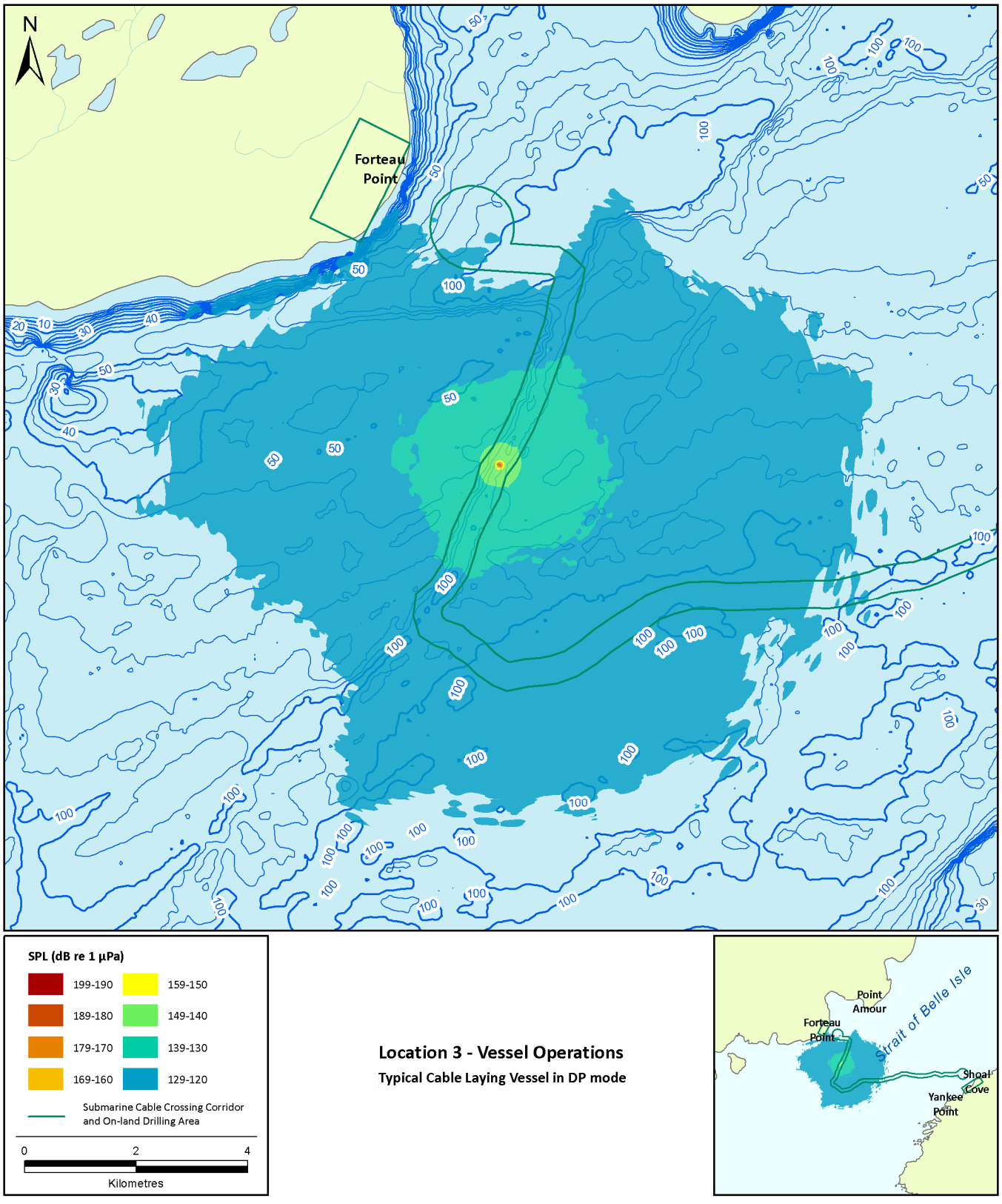

Figure 3.15 Predicted Sound Pressure Levels for the Typical Cable Laying Vessel in DP Mode at Location 3 – Shallow Trench near the Middle of Strait of Belle Isle

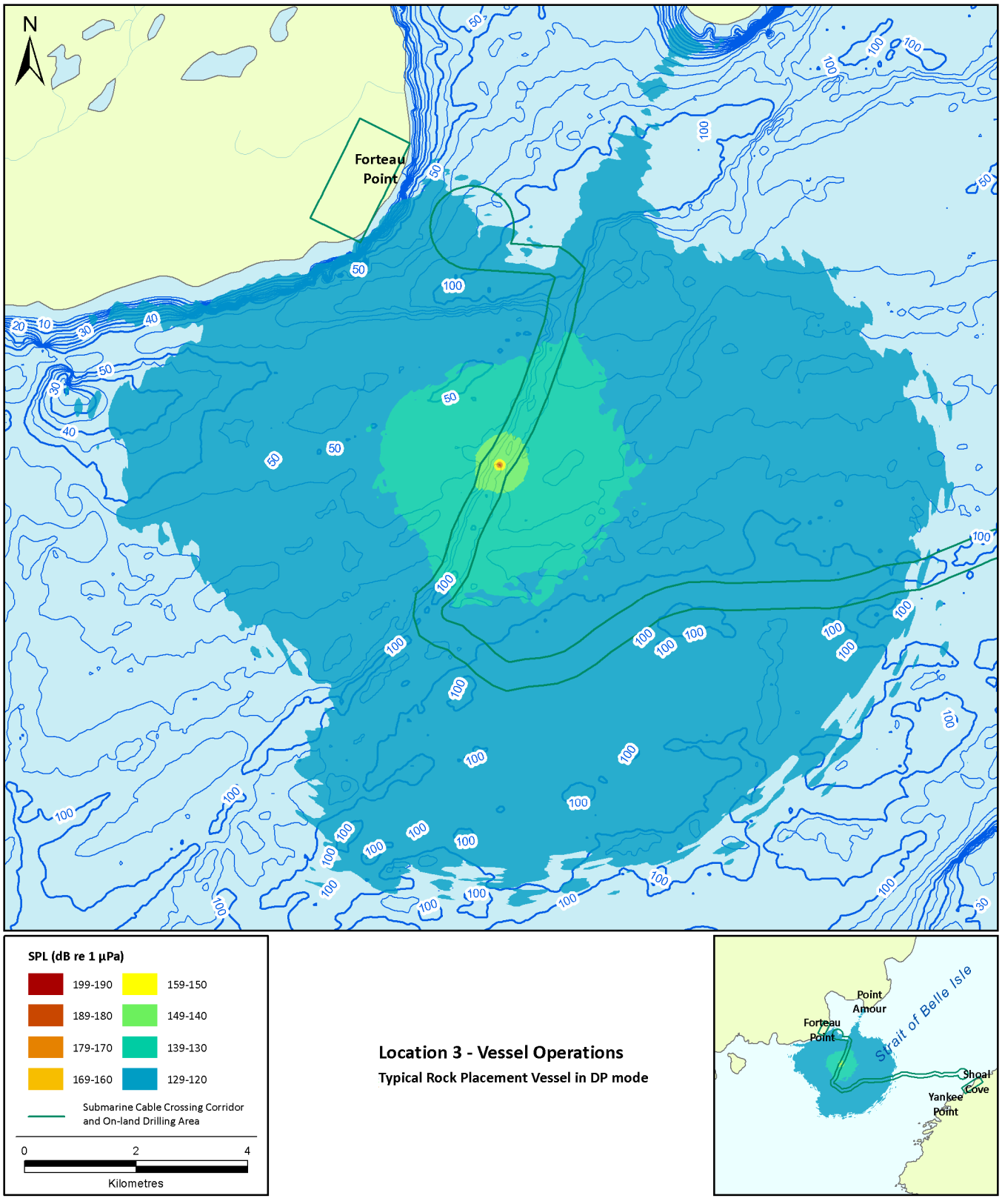

Figure 3.16 Predicted Sound Pressure Levels for the Typical Rock Placement Vessel in DP Mode at Location 3 – Shallow Trench near the Middle of Strait of Belle Isle

3.3.3 Location 4 – Middle of Strait of Belle Isle

Table 3.17 Threshold Distances for the Typical Cable Laying Vessel in DP Mode at Location 4 – Middle of Strait of Belle Isle

RMS SPL (dB re 1 µPa)	Threshold distances (m)									
	No weighting applied		Cetaceans						Pinnipeds	
			Low-frequency		Mid-frequency		High-frequency			
	R_{max}	$R_{95\%}$	R_{max}	$R_{95\%}$	R_{max}	$R_{95\%}$	R_{max}	$R_{95\%}$	R_{max}	$R_{95\%}$
170	< 5	< 5	< 5	< 5	< 5	< 5	< 5	< 5	< 5	< 5
160	20	20	20	20	20	20	15	15	20	20
150	75	70	75	70	65	60	60	60	75	65
140	475	400	475	400	375	325	335	310	425	355
130	3265	2200	3185	2180	3000	1865	2860	1700	3125	2060
120	8185	6220	8185	6200	7925	5515	7685	5260	8155	5920

Table 3.18 Threshold Distances for the Typical Rock Placement Vessel in DP Mode at Location 4 – Middle of Strait of Belle Isle

RMS SPL (dB re 1 µPa)	Threshold distances (m)									
	No weighting applied		Cetaceans						Pinnipeds	
			Low-frequency		Mid-frequency		High-frequency			
	R_{max}	$R_{95\%}$	R_{max}	$R_{95\%}$	R_{max}	$R_{95\%}$	R_{max}	$R_{95\%}$	R_{max}	$R_{95\%}$
170	< 5	< 5	< 5	< 5	< 5	< 5	< 5	< 5	< 5	< 5
160	25	25	25	25	25	25	20	20	25	25
150	90	85	90	85	80	75	80	75	85	80
140	1020	500	1020	500	600	400	465	365	835	445
130	3820	2760	3815	2750	3435	2285	3430	2130	3700	2540
120	9045	7200	9045	7180	8640	6400	8450	6060	8960	6885

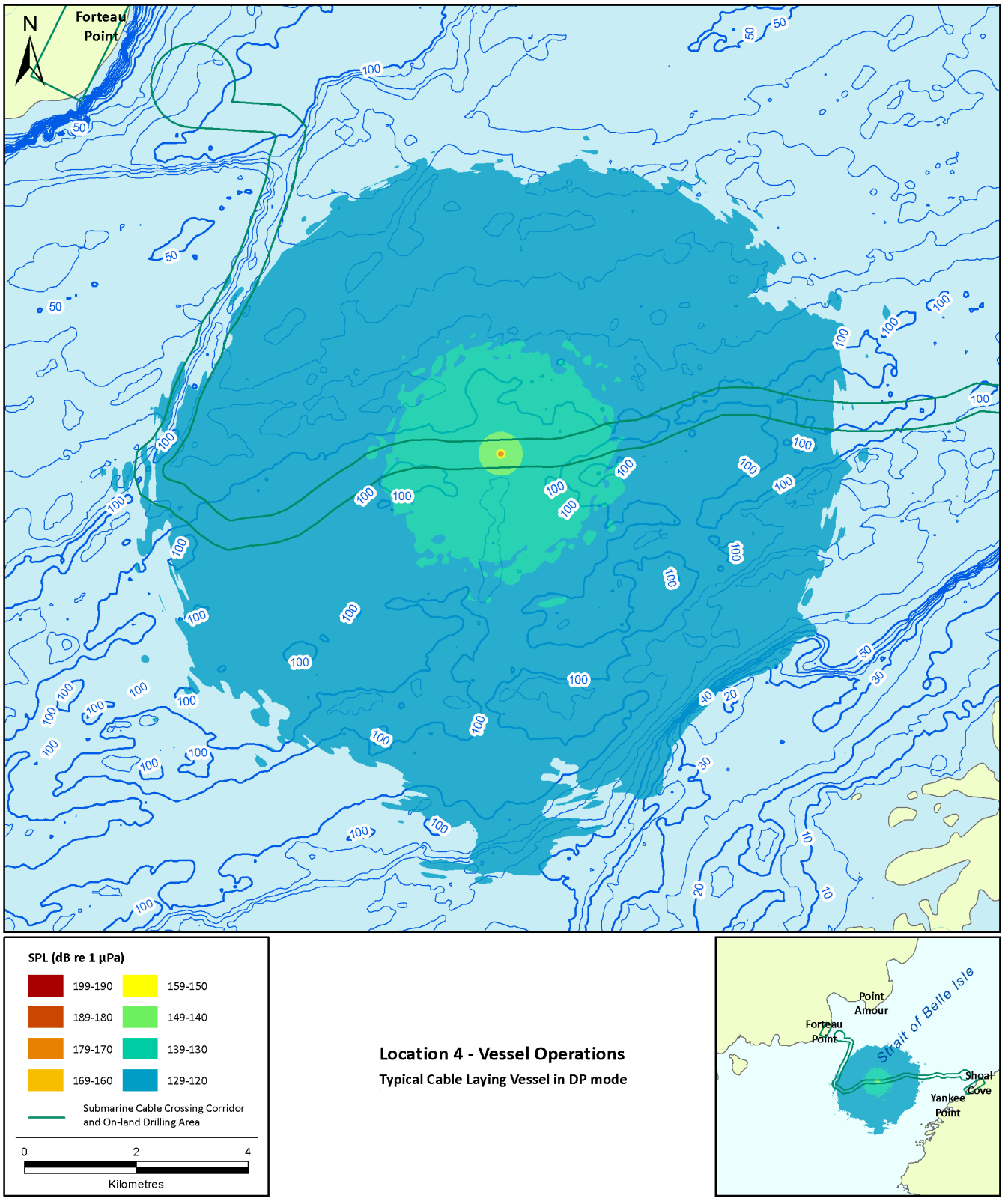

Figure 3.17 Predicted Sound Pressure Levels for the Typical Cable Laying Vessel in DP Mode at Location 4 – Middle of Strait of Belle Isle

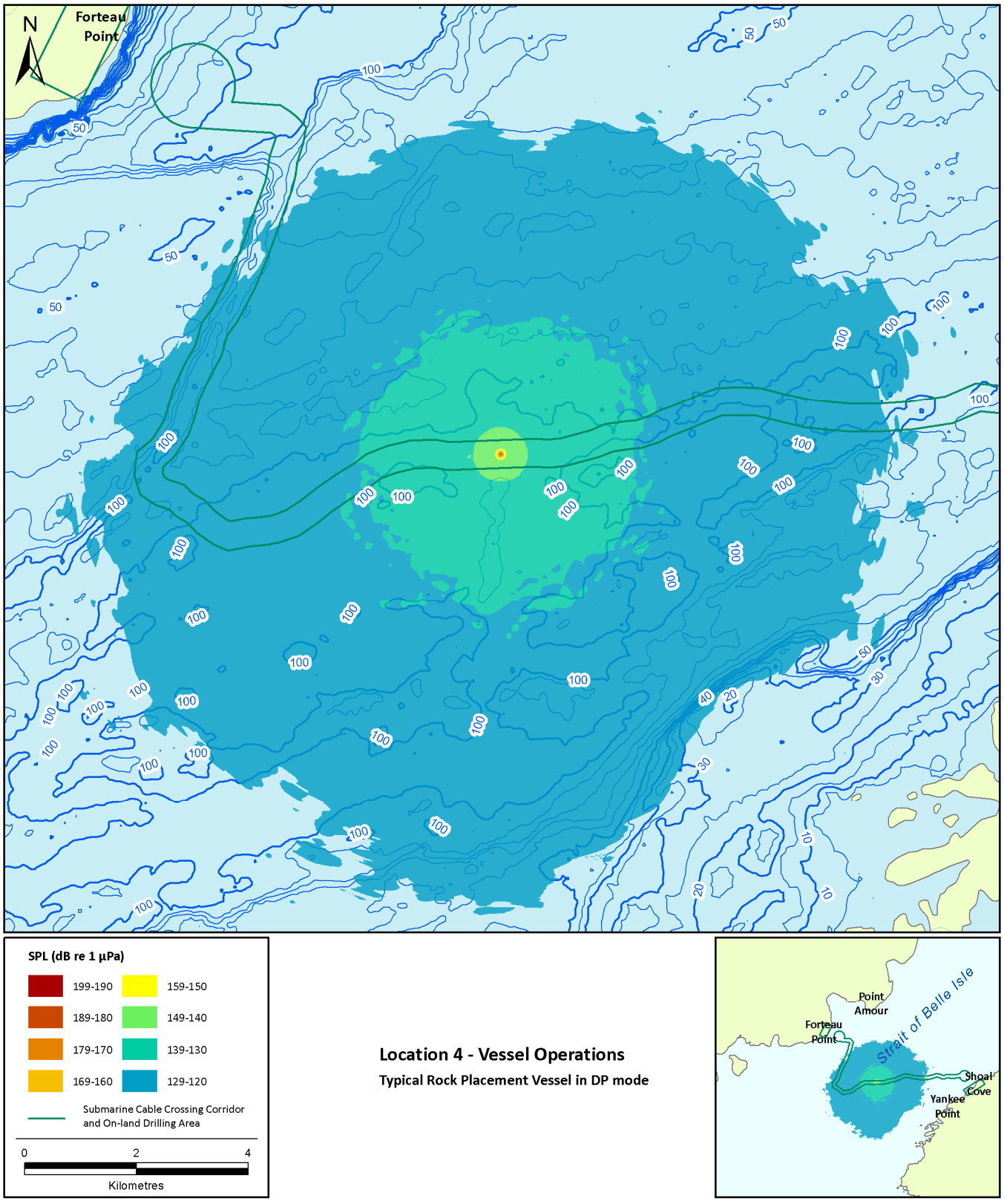

Figure 3.18 Predicted Sound Pressure Levels for the Typical Rock Placement Vessel in DP Mode at Location 4 – Middle of Strait of Belle Isle

3.3.4 Location 5 – Offshore Shoal Cove

Table 3.19 Threshold Distances for the Typical Cable Laying Vessel in DP Mode at Location 5 – Offshore Shoal Cove

RMS SPL (dB re 1 µPa)	Threshold distances (m)									
	No weighting applied		Cetaceans						Pinnipeds	
			Low-frequency		Mid-frequency		High-frequency			
	R_{max}	$R_{95\%}$	R_{max}	$R_{95\%}$	R_{max}	$R_{95\%}$	R_{max}	$R_{95\%}$	R_{max}	$R_{95\%}$
170	< 5	< 5	< 5	< 5	< 5	< 5	< 5	< 5	< 5	< 5
160	20	20	20	20	20	20	15	15	20	20
150	80	75	80	75	65	65	65	60	75	70
140	790	555	790	545	600	400	550	355	700	470
130	3160	2325	3160	2315	3040	1960	2885	1835	3050	2170
120	9730	6950	9725	6920	8085	6245	8085	5930	8970	6670

Table 3.20 Threshold Distances for the Typical Rock Placement Vessel in DP Mode at Location 5 – Offshore Shoal Cove

RMS SPL (dB re 1 µPa)	Threshold distances (m)									
	No weighting applied		Cetaceans						Pinnipeds	
			Low-frequency		Mid-frequency		High-frequency			
	R_{max}	$R_{95\%}$	R_{max}	$R_{95\%}$	R_{max}	$R_{95\%}$	R_{max}	$R_{95\%}$	R_{max}	$R_{95\%}$
170	< 5	< 5	< 5	< 5	< 5	< 5	< 5	< 5	< 5	< 5
160	25	25	25	25	25	20	20	20	25	25
150	120	115	120	115	90	80	85	75	115	85
140	1325	700	1325	700	1325	565	775	500	1325	655
130	3940	2735	3940	2725	3400	2400	3235	2550	3475	2600
120	10,400	7975	10,340	7940	9735	7215	9725	6900	10,330	7660

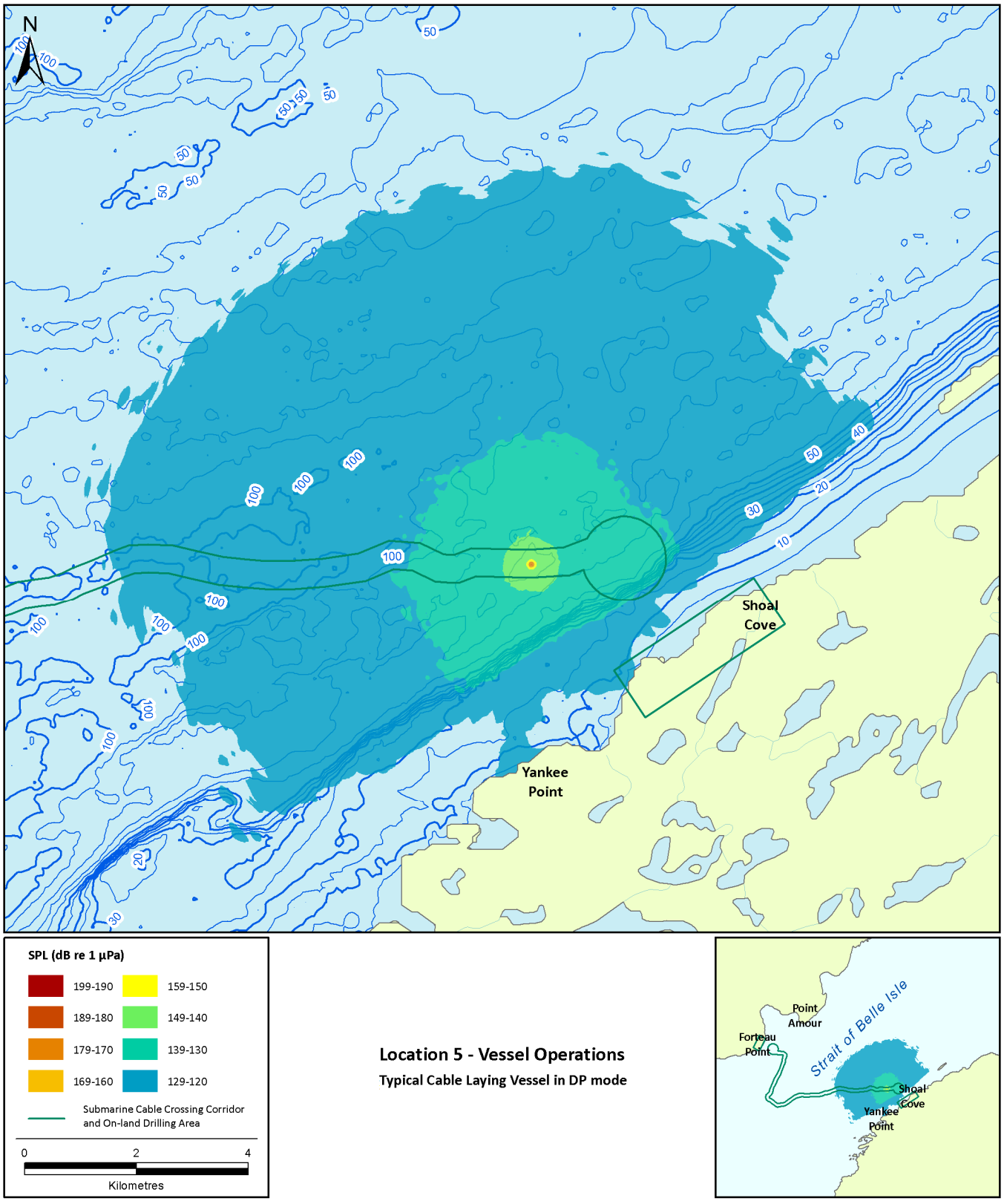

Figure 3.19 Predicted Sound Pressure Levels for the Typical Cable Laying Vessel in DP Mode at Location 5 – Offshore Shoal Cove

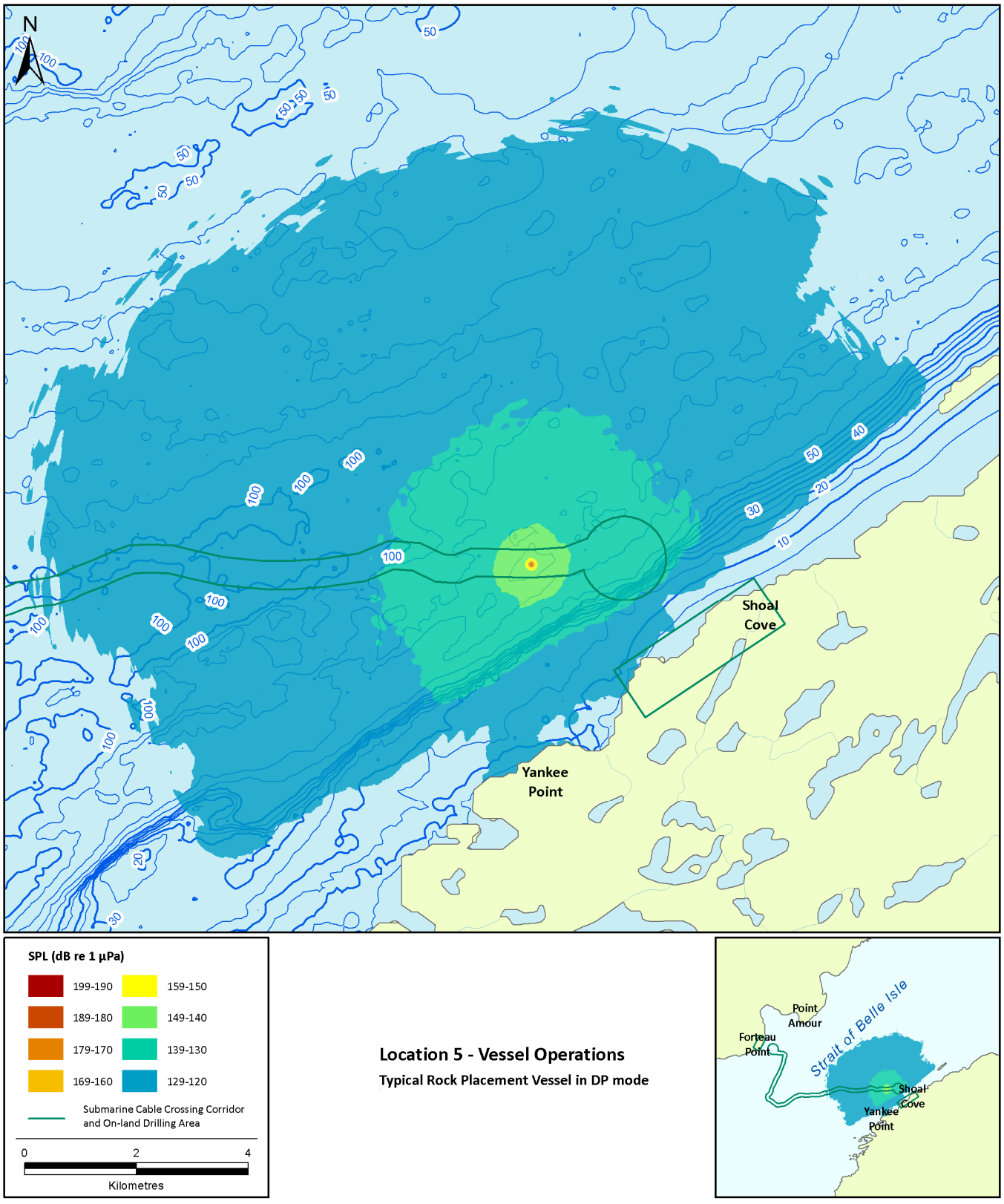

Figure 3.20 Predicted Sound Pressure Levels for the Typical Rock Placement Vessel in DP Mode at Location 5 – Offshore Shoal Cove

3.4 Noise Levels above Ambient

In order to assess the noise impact of the construction operation the modelled sound levels were compared with ambient noise levels. The ambient noise levels were measured as a part of the *Strait of Belle Isle: Ambient Noise and Marine Mammal Survey* conducted by JASCO for Nalcor Energy in the SOBI (JASCO, 2011). The measurements were conducted at three locations: Labrador side of the Strait, middle of the Strait, and Newfoundland side (Figure 1.1).

The comparison of the modelling results with ambient levels was performed at each of the six modelling sites (Figure 1.1). Only the loudest source at each site was chosen for the comparison. For each modelling site the ambient levels were taken from the nearest ambient noise monitoring station. For comparison, the quietest — 95^{th} percentile — ambient levels were selected. Table 3.21 provides the list of sources used for the comparison with ambient noise levels at each modelling location along with the ambient noise monitoring station the data were compared with.

Modelling results of SPL provided previously in Sections 3.1, 3.2, and 3.3 are presented in dB re 1 µPa, as those values are calculated relative to 1 µPa pressure level. Since the predicted SPL above ambient are calculated relative to the ambient levels, the units for the SPL above ambient are presented in dB.

During the comparison, the ambient noise levels were subtracted from the modelled noise levels in each third-octave band separately and then summed up to produce broad band levels (Table 3.22). Since the maximum ambient level in an individual band is about 70 dB re 1 µPa, 120 dB re 1 µPa roughly corresponds to 50 dB above ambient. The 50 dB above ambient level was selected as the minimal level to display on the figures.

Table 3.21 List of Sources Used for Comparison with Ambient Levels at each Location

Modelling Location	Source	Ambient Levels Data Used
1	Drilling, source at 1 m	Labrador station
2	Typical rock dumping vessel, DP mode	Labrador station
3	Typical rock dumping vessel, DP mode	Middle station
4	Typical rock dumping vessel, DP mode	Middle station
5	Typical rock dumping vessel, DP mode	Newfoundland station
6	Drilling, source at 1 m	Newfoundland station

Table 3.22 Summary Table of Threshold Distances to the Sound Levels above Ambient

Level Above Ambient (dB)	Location 1		Location 2		Location 3		Location 4		Location 5		Location 6	
	R_{max}	$R_{95\%}$	R_{max}	$R_{95\%}$	R_{max}	$R_{95\%}$	R_{max}	$R_{95\%}$	R_{max}	$R_{95\%}$	R_{max}	$R_{95\%}$
110			< 5	< 5	< 5	< 5	< 5	< 5	< 5	< 5		
100			9	9	9	9	9	9	9	9		
90	< 5	< 5	35	34	34	33	34	33	36	35		
80	21	21	210	115	255	210	220	200	270	220	< 5	< 5
70	275	260	1850	1000	1350	975	1350	1100	1850	1280	56	47
60	420	400	5900	3300	4250	3200	4900	3650	5400	4100	330	310
50	3950	2500	11,750	7600	14,000	9750	11,300	8600	13,500	10,150	2800	1880

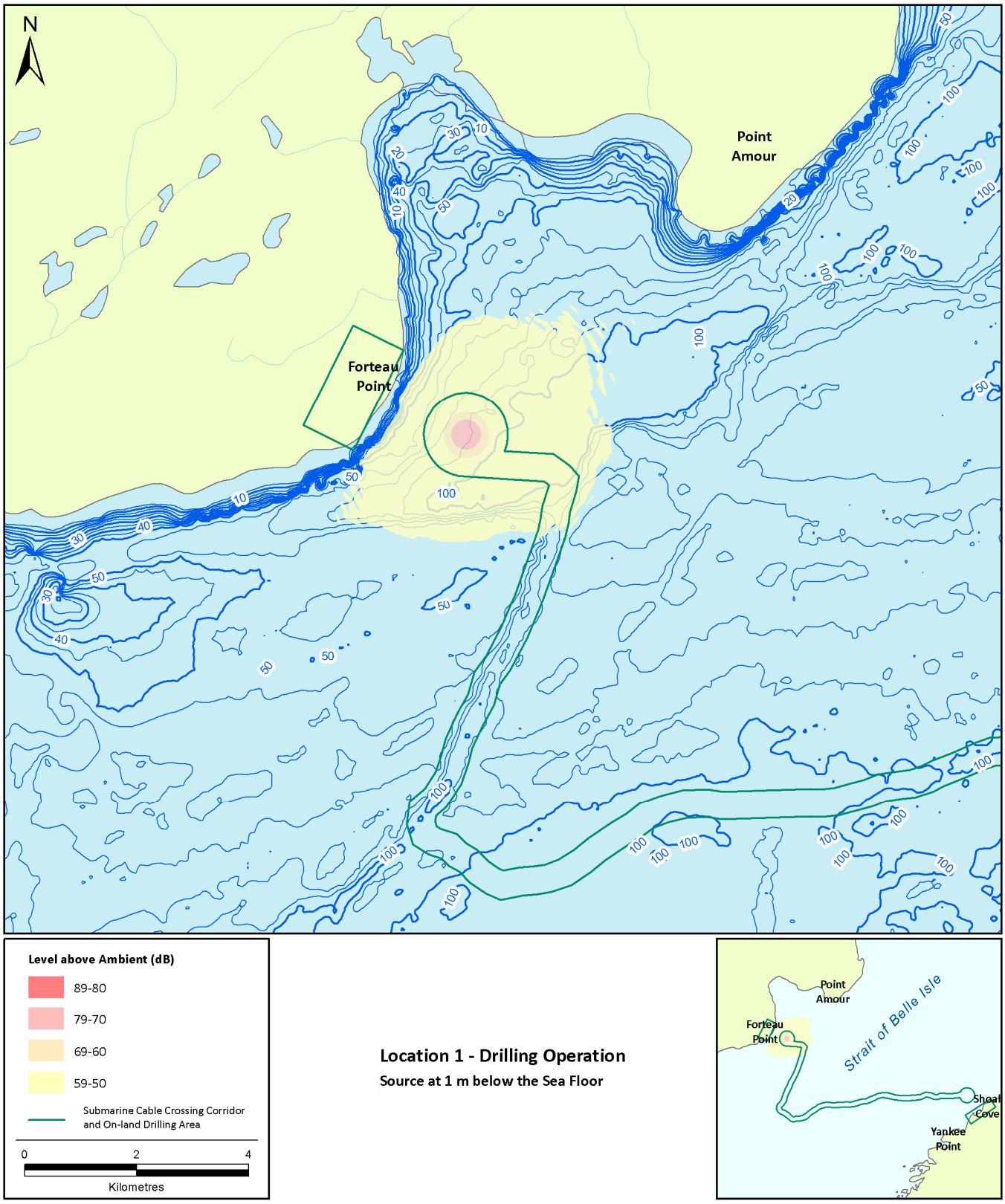

Figure 3.21 Predicted Sound Pressure Levels above Ambient Levels for the Drilling Operation at Location 1 – Offshore Forteau Point. Source is at 1 m below the Sea Floor

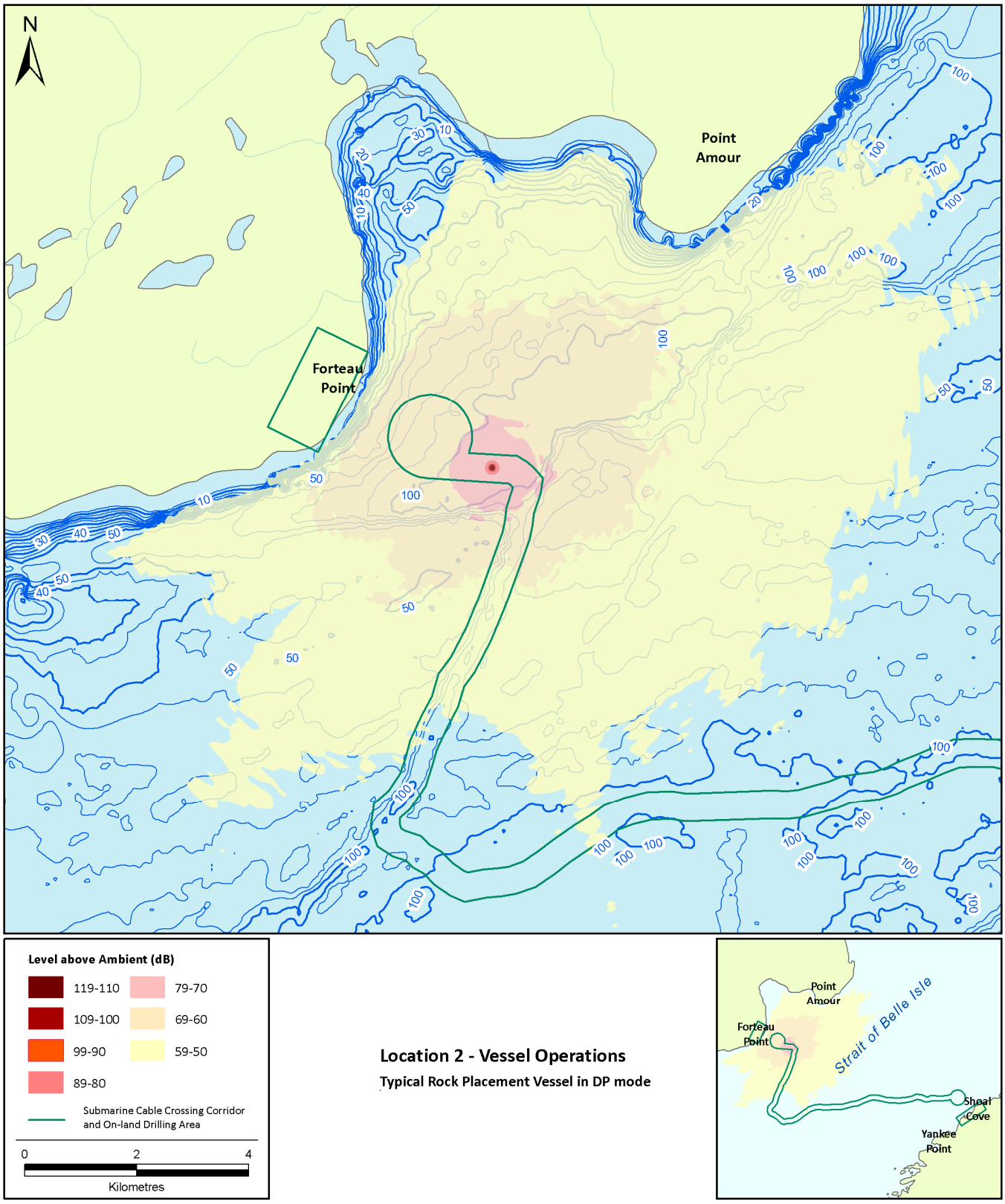

Figure 3.22 Predicted Sound Pressure Levels above Ambient Levels for the Typical Rock Placement Vessel in DP Mode at Location 2 – Offshore Forteau Point

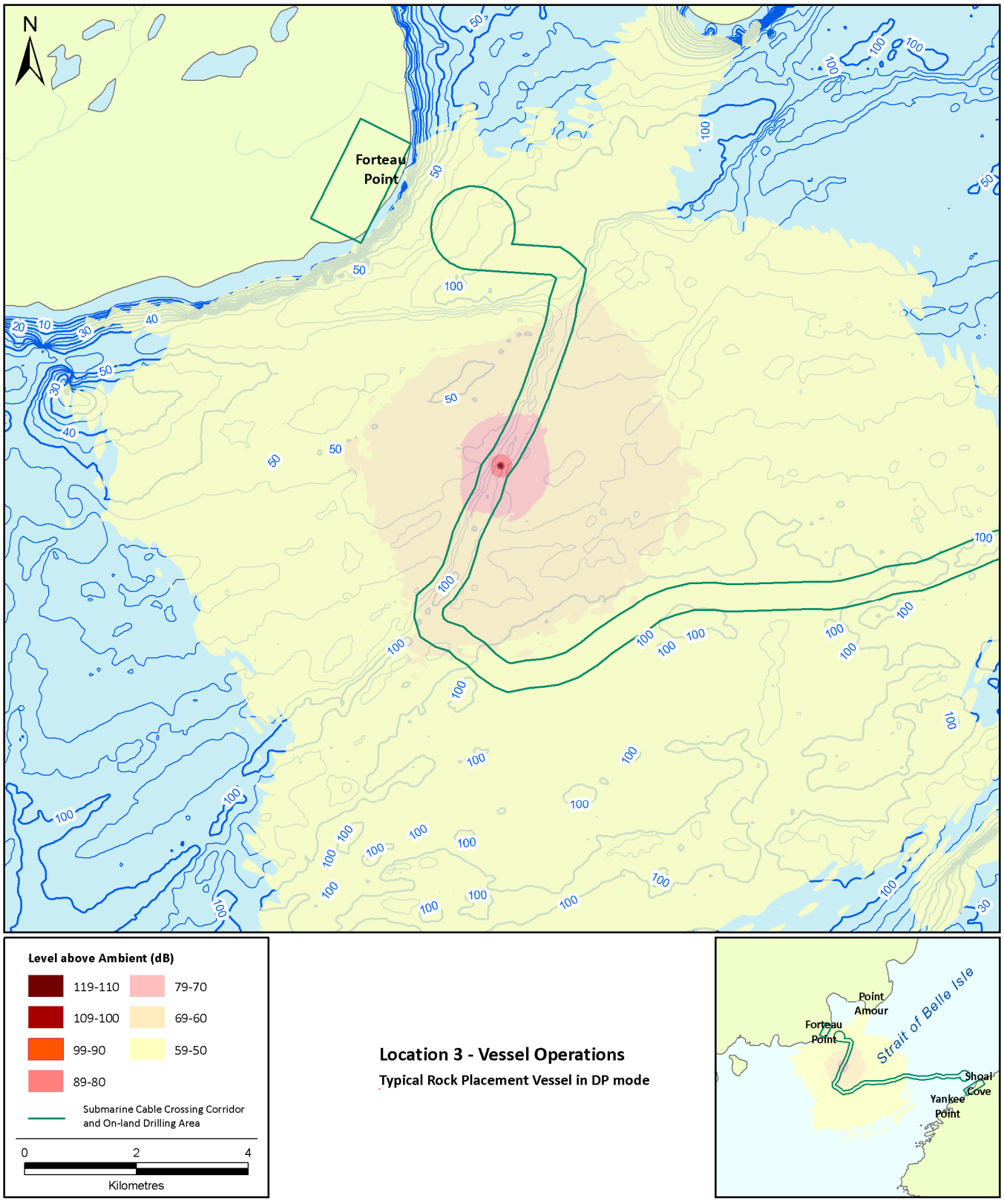

Figure 3.23 Predicted Sound Pressure Levels above Ambient Levels for the Typical Rock Placement Vessel in DP Mode at Location 3 – Shallow Trench near the Middle of Strait of Belle Isle

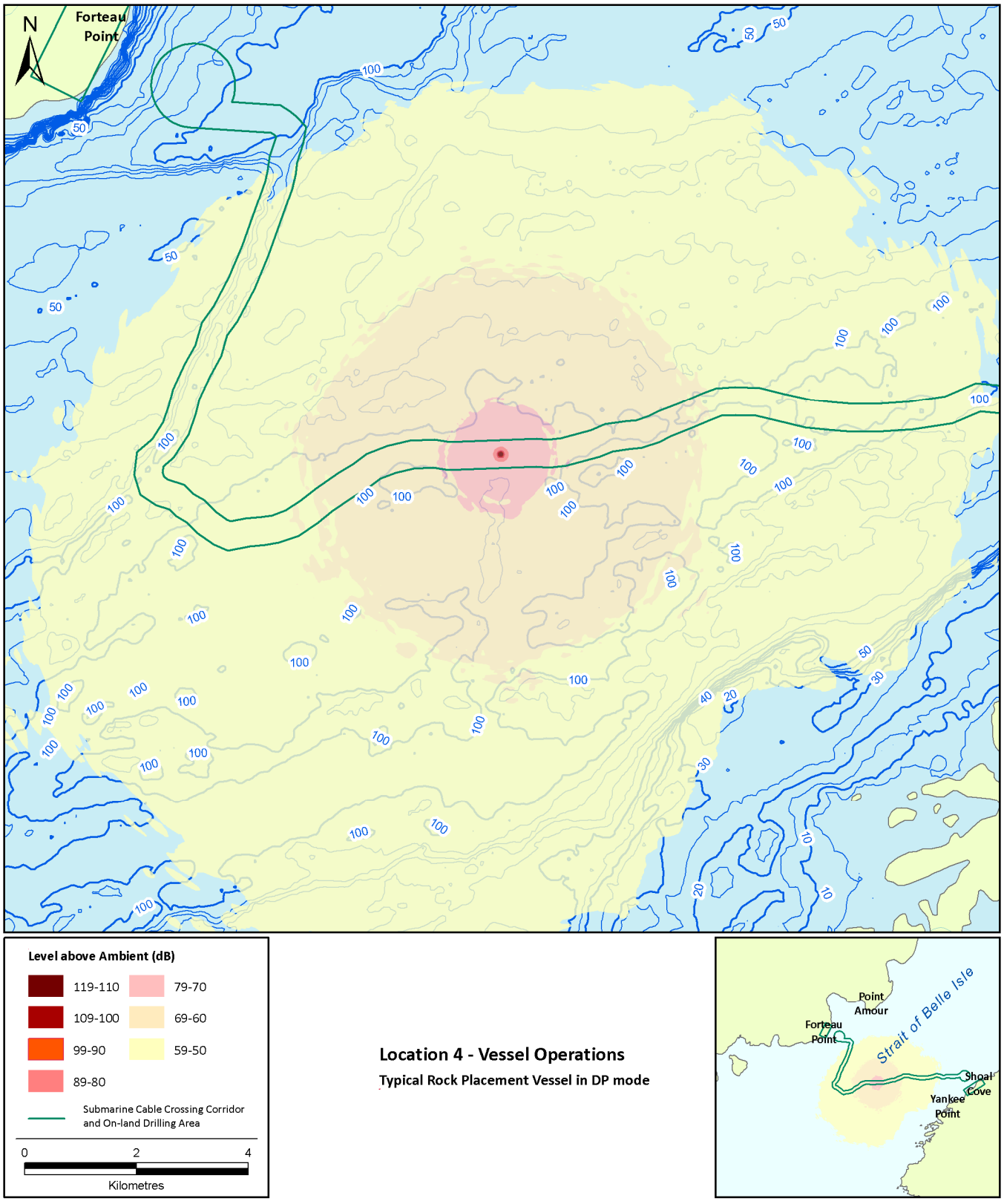

Figure 3.24 Predicted Sound Pressure Levels above Ambient Levels for the Typical Rock Placement Vessel in DP Mode at Location 4 – Middle of Strait of Belle Isle

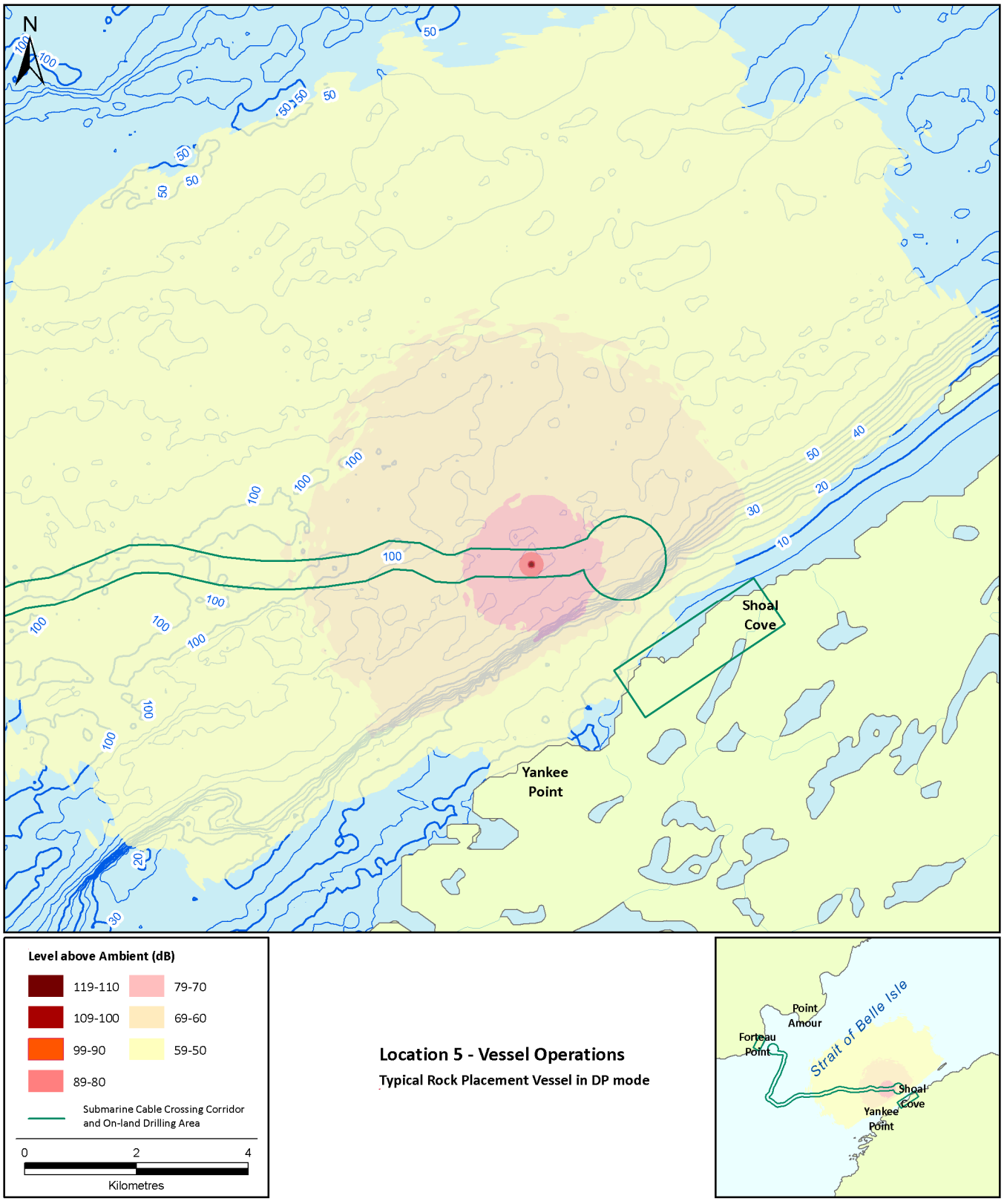

Figure 3.25 Predicted Sound Pressure Levels above Ambient Levels for the Typical Rock Placement Vessel in DP Mode at Location 5 – Offshore Shoal Cove

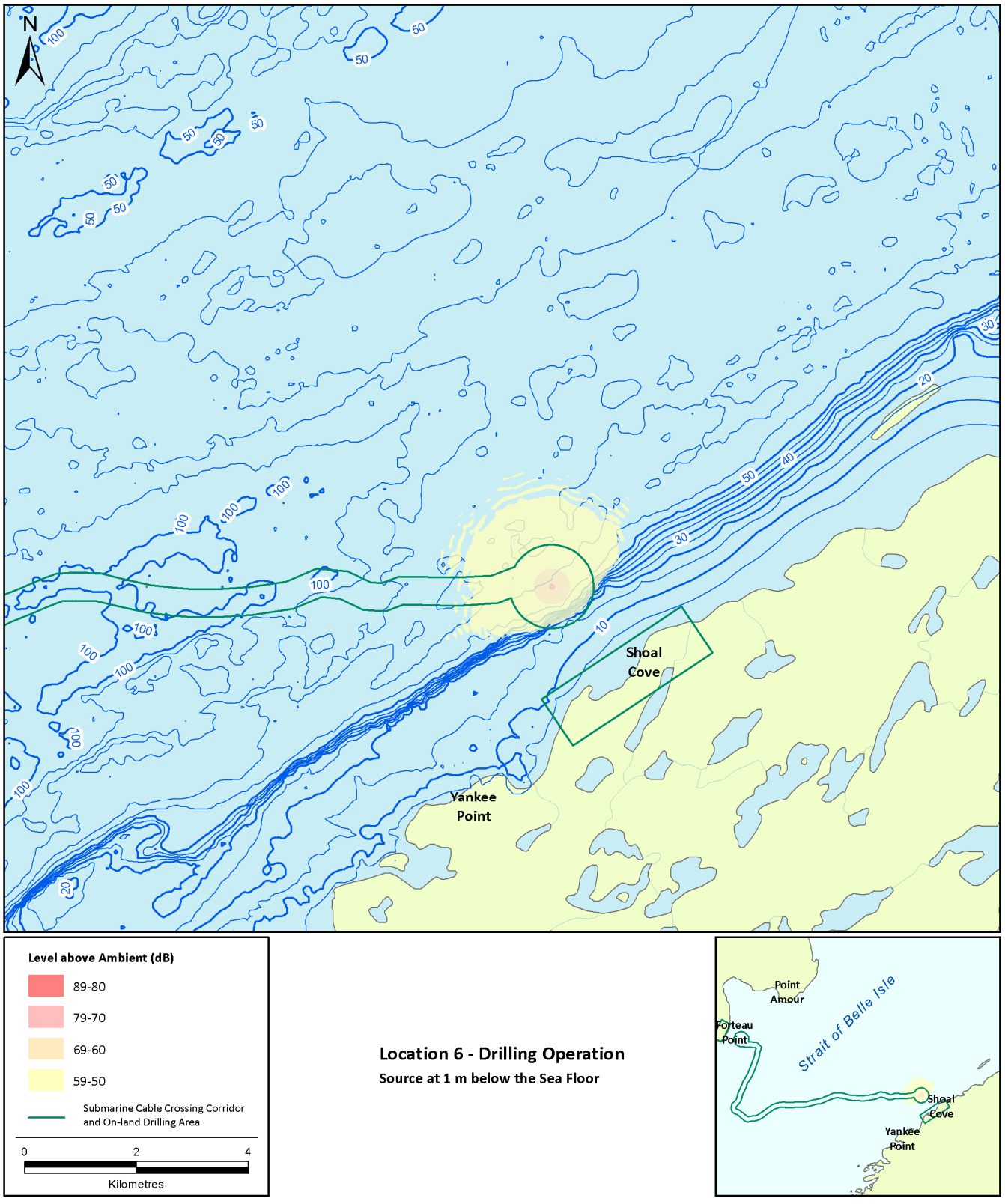

Figure 3.26 Predicted Sound Pressure Levels above Ambient Levels for the Drilling Operation at Location 6 – Offshore Shoal Cove. Source is at 1 m below the Sea Floor

3.4.1 Combined Effect from Two Sources Operating Simultaneously

If two identical vessels operate at the same location the combined sound field increases by 3 dB – this is the maximum increase from a combination of two sources. In case of different loudness of the sources or different distances from the sources, the higher acoustic energy will dominate. For example, if two acoustic signals arrive to the same point and one is 10 dB lower, the combined acoustic signal level from the two will be just 0.5 dB more than the higher acoustic signal. In general, the increase of the sound levels due to multiple identical sources operating together can be calculated using the following formula:

$$\Delta SPL = 10\log(N), \tag{6}$$

where N is the number of source.

4.0 SUMMARY

Nalcor Energy is proposing to develop the Labrador – Island Transmission Link, an HVdc transmission system extending from Central Labrador to the Island of Newfoundland's Avalon Peninsula which will include the installation of submarine cables across the SOBI. In support of the Project's EA this S*ound Modelling: Proposed Strait of Belle Isle Cable Installation Activities* study was undertaken to model potential sound resulting from the proposed construction activities associated with underwater cable installation in the SOBI.

This report presents acoustic propagation modelling results for various proposed construction-related activities that are associated with the HVdc submarine cable installation across the Strait of Belle Isle. The specific noise sources modelled were:

1. Horizontal directional drilling at Forteau Point (Labrador) and Shoal Cove (Newfoundland)
2. Typical cable laying vessel in transit
3. Typical cable laying vessel in DP mode
4. Typical rock placement vessel in transit
5. Typical rock placement vessel in DP mode

Vessel transit and operations were modelled at four locations, each along the proposed cable corridor. The acoustic footprint and maximum distance (range) to underwater sound pressure level isopleths between 200 to 120 dB re 1µPa root mean square (RMS) were determined for each activity.

Of the various noise source models, rock-placement operations with the vessel in DP mode are expected to produce the largest ensonified area and longest range radius to an isopleth level at 120 dB re 1µPa RMS of 11,615 m was produced at Location 4.

The actual placement of rocks is not expected to be a significant source of noise, as the sound field from the rock placement activity in the marine environment (excluding the noise from the vessel operating in DP mode) is considered to be very low. Neither the rocks falling into the water, nor the rocks falling onto the seabed are expected to be a significant sound source. Dispersion of rock material will be done through a fall pipe and the terminal velocity of the rocks is low due to water resistance. Similar construction activity was monitored during channel maintenance in Cook Inlet, Alaska (Dickerson et al., 2001). The activity, for which the noise levels were recorded, was a split-haul barge dumping sediment into the water. The sediment was coarse sand and gravel. Measured broadband received level at 316 m from the barge was about 120 dB re µPa (after Dickerson et al., 2001). The levels from the dumping vessels, which will be operating in DP mode during the activity, at the same distance would reach 146–141 dB re µPa, i.e. 21–26 dB greater. It should also be noted that split-haul barges dump significantly larger volumes of sediments at one time.

Cable laying operations with the vessel in DP mode are similar to that produced by the rock placement vessel in DP with the maximum radius to 120 dB re 1µPa RMS of 8900 m. Vessel transit maximum radii to 120 dB re 1µPa RMS for the cable-laying vessel and the rock-placement vessel are approximately 1500 and 5000 m respectively, with the maximum occurring when the vessel is near the center of the SOBI. The maximum radius to 120 dB re 1µPa RMS for horizontal drilling at either location is < 2000 m.

Different operations have different dominant frequencies at which the maximum noise levels are produced. Drilling activities produce the lowest dominant frequencies of 1.3 to 1.6 Hz. The dominant frequencies for a transiting vessels range from 40 to 80 Hz, and vessels operating in DP mode produce maximal noise between 400 and 800 Hz. The range to 120 dB re 1µPa RMS can be corrected for the hearing ability of different animal groups (M-weighted). When M-weighting is applied, the range to 120 dB re 1µPa RMS for drilling operations decreases from 1870 m to 269 m (85% reduction) for the low-frequency cetaceans. Drilling operations should not be detectable in the water column by mid-frequency and high-frequency cetaceans, nor pinnipeds. For vessel transit, M-weighting has no effect on the radii for the low-frequency cetaceans, but results in a 35% reduction for pinnipeds, a 55% reduction for mid-frequency cetaceans, and 62% reduction for high-frequency cetaceans. M-weighting has little effect on maximum range radii during rock-placement and cable laying operation while the vessels are in DP mode. And, any reduction in the threshold radius occurs only for high-frequency cetaceans.

A summary of the maximum range (R_{max}) to received level isopleths is shown in Table 4.1.

Table 4.1 Summary of Maximum Extent (R_{max}) of the Specific Threshold Distances for the Unweighted Field

RMS SPL (dB re 1 µPa)	Threshold distances (m)																	
	HDD		Typical Cable Laying Vessel								Typical Rock Placement Vessel							
			In Transit				DP Mode				In Transit				DP Mode			
	L 1	L 6	L 2	L 3	L 4	L 5	L 2	L 3	L 4	L 5	L 2	L 3	L 4	L 5	L 2	L 3	L 4	L 5
170							< 5	< 5	< 5	< 5	< 5	< 5	< 5	< 5	< 5	< 5	< 5	< 5
160	< 5	< 5	< 5	< 5	< 5	< 5	20	20	20	20	10	10	10	10	25	25	25	25
150	140	62	10	10	10	10	70	75	75	80	35	35	35	40	85	100	90	120
140	345	333	35	35	35	40	440	685	475	790	275	245	230	325	960	825	1020	1325
130	800	950	255	240	225	315	3000	2680	3265	3160	1085	1630	1420	1715	3980	3175	3820	3940
120	3150	3150	1050	1435	1380	1585	8900	8620	8185	9730	3225	4120	4900	4540	9050	11,615	9045	10,400

At each modelling site the loudest noise source was compared with the ambient noise levels as detected by the nearest monitoring station (JASCO, 2011). The quietest, 95th percentile, ambient noise spectrum levels were selected as the baseline. The maximum increase over the natural noise level is estimated to be no more than 110 dB and only in the immediate vicinity, i.e., less than 10 m, from the source (Table 3.22). Broad band noise levels as high as 50 dB above ambient are expected to be detected as far as 14 km from the source.

5.0 REFERENCES

Barton, N. (2006). Rock Quality, Seismic Velocity, Attenuation and Anisotropy. Taylor & Francis.

Becker, J. J., Sandwell, D. T., Smith, W. H., Braud, J., Binder, B., Depner, J., et al. (2008, October 8). Global Bathymetry and Elevation Data at 30 Arc Seconds Resolution: SRTM30_PLUS, submitted to Marine Geodesy.

Buckingham, M. J. (2005). Compressional and shear wave properties of marine sediments: Comparison between theory and data. J. Acoust. Soc. Am. , 117 (1), 137-152

Collins, M. D. (1993). An energy-conserving parabolic equation for elastic media. *J. Acoust. Soc. Am.* 94, pp. 975-982.

Collins, M. D., R. J. Cederberg, D.B. King, and S.A. Chin-Bing. (1996). Comparison of algorithms for solving parabolic wave equations. *Journal of the Acoustical Society of America* 100:178–182.

Collis, J. M., Siegmann, W. L., Collins, M. D., Simpson, H. J., and Soukup, R. J. (2007). Comparison of simulations and data from a seismo-acoustic tank experiment. *J. Acoust. Soc. Am.* 122, pp. 1987-1993.

Dawson, W. B. (1920). *The Currents in Belle Isle Strait, the Northern Entrance to the Gulf of St. Lawrence*. The Bulletin of the Geographical Society of Philadelphia, No. 1-2, January-April, 1920. Philadelphia: The Society.

Dickerson, C., Reine, K. J., and Clarke, D. G. (2001). Characterization of underwater sounds produced by bucket dredging operations. *DOER Technical Notes Collection* (ERDC TN-DOER-E14), U.S. Army Engineer Research and Development Center, Vicksburg, MS. *www.wes.army.mil/el/dots/doer*

Einsele, G. (2000). Sedimentary basins; evolution, facies, and sediment budget (2 ed.). Springer.

Fugro-Jacques Geosurveys Inc. (2010) Marine habitat in the Strait of Belle Isle: Interpretation of 2007 geophysical (sonar) survey information for the submarine cable crossing corridors. Report prepared for Nalcor Energy.

Gentry, R., Bowles, A., Ellison, W., Finneran, J., Greene, C., Kastak, D., et al. (2004). Noise exposure criteria. *Presentation to U.S. Mar. Mamm. Commis. Advis. Commit*.

Hall, J. D., and Francine, J. (1991). Measurements of underwater sound from a concrete island drilling structure located in the Alaskan sector of the Beaufort Sea. *J. Acoust. Soc. Am.* 90 (3), pp. 1665-1667.

Hallet, M. A. (2004). Characteristics of merchant ship acoustic signatures during port entry/exit. *In Proceedings of Acoustics*, 3–5 November 2004, Gold Coast, Australia, 577–580

Hannay, D. E., MacGillivray, A., Laurinolli, M., and Racca, R. (2007). *Source level measurements from 2004 acoustics program*, JASCO Report presented to Sakhalin Energy (extended version for JASCO use).

Hannay, D. E. and Racca, R. (2005). *Acoustic Model Validation*. Technical report for Sakhalin Energy Investment Company by JASCO Research Ltd.

Ingram, R. G. (1982). Proposed Strait of Belle Isle Submarine Cable Installation – Oceanographic Aspects.

Ireland, D., D. Hannay, R. Rodrigues, H. Patterson, B. Haley, A. Hunter, et al. (2007). *Marine mammal monitoring and mitigation during open water seismic exploration by GX Technology in the Chukchi Sea, October—November 2006: 90-day report. LGL Draft Rep. P891-1. Rep.* Silver Spring, MD: LGL Alaska Research

Associates Inc., Anchorage, AK, LGL Ltd., King City, Ont., and JASCO Research, Ltd., Victoria, B.C., Can. for GX Technology, Houston, TX, and Nat. Mar. Fish. Serv.

JASCO Applied Sciences. (2011). *Strait of Belle Isle: Ambient Noise and Marine Mammal Survey.* Report for Nalcor Energy by JASCO Applied Sciences Ltd.

MacGillivray, A. (2006). Underwater acoustic source level measurements of Castoro Otto and Fu Lai. Internal Report by JASCO Applied Sciences.

Nedwell, J. R. and A. W. H. Turnpenny (1998). The use of a generic frequency weighting scale in estimating environmental effect. *Proc. Workshop on Seismics and Marine Mammals*. June 1998, London, UK.

Nguyen, J.-P. (1996). Drilling, Oil and Gas Field Development Techniques. Editions Technip, Paris.

Ross, D. (1976). *Mechanics of Underwater Noise*, Pergamon, New York, Chapter 8.

Labrador – Island Transmission Link

Environmental Modelling: Proposed Shore Electrodes

Prepared for:

Nalcor Energy
Hydro Place, 500 Columbus Drive, PO Box 12800
St. John's, Newfoundland and Labrador
Canada A1B 0C9

Contract #15074-OB

Prepared by:

Hatch Ltd.
500 Portage Avenue, 6th Floor
Winnipeg, Manitoba
Canada R3C 3Y8

Hatch Project H335672
H335672-TBR0110-70-124-0002, Rev. 1

August 25, 2011

EXECUTIVE SUMMARY

Nalcor Energy is proposing to develop the Labrador – Island Transmission Link (the Project), a 900 MW High Voltage Direct Current (HVdc) transmission system extending from Central Labrador to the Island of Newfoundland's Avalon Peninsula. In preparation for and in support of the Project's environmental assessment (EA), this *Electrode Modelling: Proposed Shore Electrodes* study has been completed with the objective to model the types of emissions associated with electrode operations.

The Project has been designed as a bipolar system with a converter station at each end of the transmission link; a two-conductor transmission line connecting the two converter stations; and a shoreline pond electrode connected to each converter station via an electrode line, providing a ground return path. The shoreline electrodes will be constructed and installed at two locations: L'Anse au Diable (LAD) North, Labrador (connected to the Muskrat Falls converter station) and Dowden's Point, Newfoundland (connected to the Soldiers Pond converter station).

During normal balanced bipolar operation, the two conductors (one positive and one negative with respect to ground) provide a path for the dc current, and small amounts of electrical current will flow through the electrode (i.e., less than 1% of the electrode's total capacity). If both poles are in service, the system can operate at its full rated capacity.

If a transmission conductor failure or a pole fault were to occur, the electrodes can provide a temporary ground return path for the current for the duration of the fault. The electrodes may be used during a pole outage if metallic return is not available. This is expected to occur for a duration of less than 40 hours per year; the ground return duration will be shorter than 40 hours if metallic return is used for some of the outages. The use of the electrodes to provide a long term return path for the full current is expected to occur only under specific circumstances, such as two submarine cables or an overhead conductor failure.

At the time of this study, the definition of the HVdc scheme operating parameters had not been finalized; therefore, two HVdc system voltage levels, 320 kV and 400 kV, were used in the modelling.

The key objectives of the study were to estimate the emissions associated with monopolar and bipolar operations of the electrode for the 320 kV and 400 kV systems, and to review the effect of the electrodes' operation on surrounding infrastructure. One shoreline pond electrode design at LAD North and two shoreline pond options (extended breakwater into the sea and recessed breakwater at the shoreline) at Dowden's Point were reviewed. In total, six design scenarios were analyzed in this report to provide inputs for the EA of the Project, which included the following:

- Review the electrode duties and develop high level designs of the shoreline electrode installations;
- Model the ground potential rise (GPR) which determines the electric field produced to evaluate the possible effect on infrastructure and marine life;
- Model the magnetic field at 1 m above sea level to estimate the effect on ship navigation (i.e., compass deviations);
- Model the magnetic field at sea level to estimate the magnetic field in the marine environment; and

- Model and estimate the chemical and physical emissions associated with electrode operations. For chemical emissions, each scenario was studied for cathodic and anodic operations for the primary reactions (chlorine at the anode and hydrogen at the cathode).

For the L'Anse au Diable North electrode, the key design data, modelling results and effects include:

- The number of high silicon chromium chill cast iron electrode elements required is 60 for the 320 kV scenario and 48 for the 400 kV scenario.
- The proposed breakwater is approximately 205 m along the centerline and is sized to meet the safety limits for marine life and humans. The permeable zone of the breakwater will consist of stones in the range of 0.5 m to 1.0 m in diameter. The pond water exchange rate is estimated to be 401 L/s due to tidal flushing.
- The calculated dc stray currents through the transformer windings of the distribution circuit near LAD North associated with monopolar operation of the electrode are lower than the permissible limits. The calculated dc stray currents through the pole grounding rods of this distribution network are higher than the permissible level for a few pole grounding rods near the shoreline pond electrode. Corrosion of the grounding rods is not a major concern because the rods can be inspected and replaced as required. The dc stray currents associated with the bipolar operation are insignificant and will not affect the infrastructure.
- The zone extending into the sea in which the magnetic compass deviation exceeds 0.5° as a result of maximum continuous electrode operation is limited to 500 m from the electrode for the 320 kV and 400 kV scenarios; the induced horizontal magnetic field interacts with earth horizontal magnetic field (13.6 A/m at LAD N location) and the resultant horizontal magnetic field deviates from the true magnetic north which is the cause of compass deviation. During normal bipolar operation, the compass deviation is estimated to be less than 0.1° at a distance of 100 m from the electrode.
- The estimated difference between the resultant absolute value of magnetic field at the surface of the sea and that of the earth's natural magnetic field (53.6 μT near LAD North) is less than 0.8 μT and 0.6 μT at a distance of 500 m from the electrode for the continuous maximum currents of the 320 kV and 400 kV scenarios, respectively. During normal bipolar operation, the estimated difference is less than 0.2 μT and 0.1 μT at a distance of 50 m from the electrode for the 320 kV and 400 kV scenarios, respectively.
- When operating at maximum continuous duty as an anode, the estimated chlorine produced per day is 6.89×10^{-4} g/L for the 320 kV scenario and 5.51×10^{-4} g/L for the 400 kV scenario, assuming the worst case chlorine selectivity of 30%. For operation as a cathode, the estimated hydrogen produced per day is 2.62×10^{-4} g/L for the 320 kV scenario and 2.09×10^{-4} g/L for the 400 kV scenario, assuming 100% hydrogen selectivity. It is important to note these values do not consider gas exchange with the air or through the breakwater.
- When operating as an anode during normal bipolar operation and assuming a current imbalance of 1% of the nominal electrode duty, the estimated chlorine produced per day is 4.59×10^{-6} g/L for the 320 kV scenario, and 3.67×10^{-6} g/L for the 400 kV scenario, assuming the worst case chlorine selectivity of 30%. For operation as a cathode during normal bipolar operation, the estimated hydrogen produced per day is 1.74×10^{-6} g/L for the 320 kV scenario and 1.40×10^{-6} g/L for the 400 kV scenario, assuming 100% hydrogen selectivity. These values do not consider gas exchange with the air or through the breakwater.

- Tidal flushing continuously reduces the emission concentrations in the pond. The expected maximum chlorine concentration from a day of electrode operation as anode is 3.15 x 10^{-4} g/L for 320 kV scenario and 2.52 x 10^{-4} g/L for 400 kV scenario. During the bipolar operation, the expected chlorine concentration is 2.10 x 10^{-6} g/L and 1.68 x 10^{-6} for the 320 kV and 400 kV scenarios respectively. The values do not consider gas exchange with the air or exchange with the sea water due to concentration differential.

- At the maximum continuous electrode current duties, the heat emissions from the electrode for the 320 kV scenario will be less than 4.0 W/m^3 in the water in contact with the breakwater on the sea and the pond side, and 30.8 W/m^3 in the breakwater. The corresponding temperature rise in the pond will be less than 0.5°C. The corresponding dissipation levels for the 400 kV scenario are expected to be approximately 64% of the 320 kV scenario levels. During normal bipolar operation, assuming a current imbalance of 1% of the nominal electrode duty, the heat emissions are expected to be 0.01% of the values stated above.

For the Dowden's Point electrode, the key design data, modelling results and effects include:

- The number of high silicon chromium chill cast iron elements required is 60 for the 320 kV scenario and 48 for the 400 kV scenario.

- Option 1: The size of the extended breakwater option is selected to meet the safety criteria and the length of the breakwater along the centerline is approximately 385 m. The land side toe of the breakwater is approximately 79 m from the shoreline and the sea side toe is approximately 129 m from the shoreline. The stone size of the permeable zone will be in the range of 0.5 m to 1.0 m in diameter and the pond water exchange rate due to tidal flushing is estimated to be 587 L/s.

- Option 2: The length of the recessed breakwater measures 90 m for the 320 kV scenario and 75 m for the 400 kV scenario. In this option, the seabed needs to be excavated to a depth of 4 m in the pond and on the sea side of the breakwater to meet the electrical and safety requirements. The permeable zone stone size will be 0.5 m to 1.0 m in diameter and the pond water exchange rate is estimated to be 55 L/s for the 320 kV scenario and 46 L/s for the 400 kV scenario.

- The calculated dc stray currents associated with the electrode operation through the transmission infrastructure equipment and structures adjacent to the electrode locations or connected via transmission lines are less than the published permissible values for both options. The dc stray currents associated with the bipolar operation are insignificant and will not affect the infrastructure.

- The zone extending into the sea in which the magnetic compass deviation exceeds 0.5° as a result of maximum continuous electrode operation is limited to 500 m from the electrode for the 320 kV and 400 kV scenarios. During normal bipolar operation, the compass deviation is estimated to be less than 0.1° at a distance of 100 m from the electrode.

- The estimated difference between the resultant magnetic field at the surface of the sea and that of the earth's natural magnetic field (51.4 µT near Dowden's Point) is less than 2.2 µT and 1.9 µT at a distance of 500 m from the electrode for the continuous maximum currents of the 320 kV and 400 kV scenarios, respectively. During normal bipolar operation, the estimated difference is less than 0.3 µT and 0.2 µT at a distance of 100 m from the electrode for 320 kV and 400 kV scenarios, respectively.

- When operating at maximum continuous duty as an anode, the estimated chlorine produced in the extended pond option (Option 1) per day is 8.97 x 10^{-4} g/L for the 320 kV scenario and 7.18 x 10^{-4} g/L for

the 400 kV scenario, assuming the worst case chlorine selectivity of 30%. For operation as a cathode, the estimated hydrogen produced per day is 3.41×10^{-4} g/L for the 320 kV scenario and 2.73×10^{-4} g/L for the 400 kV scenario, assuming 100% hydrogen selectivity. These values do not consider the gas exchange with the air or through the breakwater.

- When operating at maximum continuous duty as an anode, the estimated chlorine produced in the recessed pond option (Option 2) per day is 7.44×10^{-3} g/L for the 320 kV scenario and 7.14×10^{-3} g/L for the 400 kV scenario, assuming the worst case chlorine selectivity of 30%. When operating at maximum continuous duty as a cathode, the estimated hydrogen produced per day is 2.83×10^{-3} g/L for the 320 kV scenario and 2.71×10^{-3} g/L for the 400 kV scenario, assuming 100% hydrogen selectivity. It is important to note these values do not consider gas exchange with the air or through the breakwater.

- When operating as an anode during normal bipolar operation, the estimated chlorine produced in the extended pond option (Option 1) per day is 5.98×10^{-6} g/L for the 320 kV scenario and 4.78×10^{-6} g/L for the 400 kV scenario, assuming the worst case chlorine selectivity of 30%. For operation as a cathode, the estimated hydrogen produced per day is 2.27×10^{-6} g/L for the 320 kV scenario and 1.82×10^{-6} g/L for the 400 kV scenario, assuming 100% hydrogen selectivity. These values do not consider gas exchange with the air or through the breakwater.

- When operating as an anode during normal bipolar operation, the estimated chlorine produced in the recessed pond option (Option 2) per day is 4.96×10^{-5} g/L for the 320 kV scenario and 4.76×10^{-5} g/L for the 400 kV scenario, assuming the worst case chlorine selectivity of 30%. When operating as a cathode, the estimated hydrogen produced in the recessed pond option per day is 1.88×10^{-5} g/L for the 320 kV scenario and 1.81×10^{-5} g/L for the 400 kV scenario, assuming 100% hydrogen selectivity. These values do not consider gas exchange with the air or through the breakwater or account for tidal flushing.

- Tidal flushing continuously reduces the gas concentration in the pond. For the extended breakwater option (Option 1) when operating at maximum continuous duty as an anode, the expected maximum chlorine concentration in one day is 2.75×10^{-4} g/L for 320 kV scenario and 2.20×10^{-4} g/L for 400 kV scenario. For the recessed breakwater option (Option 2) the expected maximum chlorine concentration in one day is 2.70×10^{-3} g/L for 320 kV scenario and 2.58×10^{-3} g/L for 400 kV scenario. The values do not consider gas exchange with the air or exchange with the sea water due to concentration differential.

- For the extended breakwater option (Option 1) during normal bipolar operation as an anode, the expected maximum chlorine concentration in one day considering the tidal flushing is 1.83×10^{-6} g/L for 320 kV scenario and 1.47×10^{-6} g/L for 400 kV scenario. For the recessed breakwater option (Option 2), the expected maximum chlorine concentration in one day is 1.80×10^{-5} g/L for 320 kV scenario and 1.72×10^{-5} g/L for 400 kV scenario. The values do not consider gas exchange with the air or exchange with the sea water due to concentration differential.

- At the maximum continuous electrode current duties, the heat emissions from the recessed electrode for the 320 kV scenario will be less than 4.1 W/m^3 in the water in contact with the breakwater on the sea and the pond side, and at most 32.5 W/m^3 in the breakwater for 320 kV and 400 KV scenarios. The heat loss for the extended breakwater option will be lower than the values for the recessed breakwater because of larger breakwater area in contact with the sea. The corresponding temperature rise from electrode operation only in the pond will not exceed 0.5°C for the extended breakwater option, and will not exceed 3.5°C for the recessed breakwater option. During normal bipolar operation, assuming a current imbalance of 1% of the nominal electrode duty, the heat emissions from the electrode is expected to be 0.01% of the values stated above.

Table of Contents

List of Figures

List of Tables

1.0 INTRODUCTION

Nalcor Energy is proposing to develop the Labrador – Island Transmission Link, a High Voltage Direct Current (HVdc) transmission system extending from Central Labrador to the Island of Newfoundland's Avalon Peninsula.

The environmental assessment (EA) process for the Project was initiated in January 2009 and is in progress. An Environmental Impact Statement (EIS) is being prepared by Nalcor, which will be submitted for review by governments, Aboriginal and stakeholder groups, and the public.

This study provides the results of a modelling exercise that was undertaken to provide information on the design characteristics, possible emissions, ground potential rise and induced magnetic fields that may be associated with the operation of the proposed shore electrode components of the Project, for use in the environmental effects analyses being completed for the Project's EIS.

1.1 Project Overview

The proposed Labrador – Island Transmission Link (the Project) involves the construction and operation of transmission infrastructure within and between Labrador and the Island of Newfoundland.

The proposed transmission system, as currently planned, will include the following key components:

- an ac-dc converter station near the lower Churchill River in Central Labrador, adjacent to the switchyard for the Lower Churchill Hydroelectric Generation Project;
- a HVdc transmission line extending across Southeastern Labrador to the Strait of Belle Isle. This overhead transmission line will be approximately 400 km in length with a cleared right-of-way averaging approximately 60 m wide, and will consist of single galvanized steel lattice towers;
- cable crossings of the Strait of Belle Isle with associated infrastructure, including cables placed across the Strait and under the seafloor through various means to provide the required cable protection;
- a HVdc transmission line (similar to that described above) extending from the Strait of Belle Isle across the Island of Newfoundland to the Avalon Peninsula, for a distance of approximately 700 km;
- a dc-ac converter station at Soldiers Pond on the Island of Newfoundland's Avalon Peninsula; and
- electrodes at each end of the HVdc transmission line in Labrador and on the Island, with overhead lines connecting them to their respective converter stations.

Of particular relevance to this study, the proposed HVdc transmission system will include the installation of electrodes, or high capacity grounding systems, in the vicinity of marine environments of Labrador and Newfoundland. The current Project concept would see the development of two "shoreline pond electrodes" - one at a location on the Labrador side of the Strait of Belle Isle (L'Anse au Diable North) and one in Conception Bay, Newfoundland (Dowden's Point).

1.2 Study Purpose and Objectives

In preparation for and in support of the EA of the Project, this study was completed to assess the likely effects of electrode operation on various components of the environment. This report describes the shoreline pond electrode installations, models the ground potential rise and induced magnetic fields, and estimates the chemical and physical emissions, associated with electrode operations. At the time of this study, the definition of operating parameters and main equipment ratings for the HVdc scheme were not finalized; therefore, two HVdc system voltage levels of 320 kV and 400 kV were considered to establish "book-end" results for inputs into the EIS.

The two voltage scenarios are considered at each of the electrode sites, L'Anse au Diable (LAD) North and Dowden's Point, with two shoreline pond options considered at Dowden's Point (extended breakwater into the sea and recessed breakwater at the shoreline). In total, six design scenarios are analyzed in this report to provide inputs for the EA of the Project. Additionally, for chemical emissions, each scenario is studied for cathodic and anodic operation.

Previous studies conducted by Nalcor Energy identified shoreline pond electrodes at LAD North on the north shore of the Strait of Belle Isle and at Dowden's Point in Conception Bay as viable options for the Labrador and Island converter stations, respectively. The scope of this current study is to model the environmental effects of the electrodes with a focus on the specific information requirements for the Project's EIS.

Specifically, the scope of the review included the six modelling scenarios listed above and included the following key tasks:

Electrode Description and Design

- Review and define the electrode duties including bipolar imbalance for the analysis.
- Review the sea and soil model and define the safe step potential limits.
- Review the electrode duties and establish the electrical design parameters of the shoreline pond electrode including type, number and arrangement of electrode elements; and pond and breakwater sizes.
- Define civil/structural design including layouts and sections; selection of rock size required for the key breakwater sections; and the expected turnover/residency rate of water in the pond.

Modelling of Ground Potential Rise (GPR)

- Describe the GPR resulting from electrode operation, the resultant electric fields and the effects on infrastructure in the vicinity.
- Model the electrode, estimate the GPR and GPR gradients, and compare the calculated GPR gradients against the prescribed safe values.
- Review previous studies conducted on corrosion effect assessment models and acceptable limits, including identification of the cases to be reviewed, and perform electrical interference and corrosion effects assessment, and identify mitigation measures if required for specific circumstances.

Modelling of Magnetic Field

- Describe the magnetic field associated with the shoreline electrode operations.

- Model and calculate magnetic field at 1 m above sea level to estimate the resultant compass deviations.
- Model and calculate magnetic field strength at sea level to estimate the resultant magnetic flux density in the marine environment.

Modelling of Chemical and Physical Emissions

- List and describe the chemical and physical emissions associated with the anodic and cathodic operation of an electrode for the selected element types. The chemical emissions include the primary, secondary and tertiary reactions which may occur as a result of electrode operation.
- Review and estimate the chemical emissions including sensitivity of the chemical reactions to electrode element current densities, pH variations, electrode element types, and temperature.
- Estimate the emission rates of chlorine and hydrogen during bipolar and monopolar operations for the 320 kV and 400 kV systems.
- Using the chemical emission estimates for chlorine, calculate the concentration expected with and without tidal flushing.
- Review and estimate the physical emissions (e.g., heat) and associated design considerations.

2.0 APPROACH AND METHODS

In preparation for and in support of the EA of the Project, modelling the emissions associated with electrode operations is required. Previous studies conducted by Nalcor Energy [1] [2] assessed the effects of the electrodes on surrounding infrastructure in detail, and carried out a high-level review of the possible environmental effects. However, the HVdc transmission system parameters used in previous studies are not the same as those currently being considered for the Project. Thus, this *Environmental Modelling: Proposed Shore Electrodes* study was conducted.

2.1 Site Descriptions

2.1.1 **Labrador Site**

A cove on the North shore of the Strait of Belle Isle near L'Anse-au-Diable (LAD) was identified as a suitable site for the Labrador shoreline electrode; the electrode site is referred to as LAD North. This site is in a south facing cove with somewhat rectangular dimensions of 130 m to 150 m wide and approximately 150 m long. The majority of the shoreline is exposed granite gneiss bedrock. A pancake shoal that is exposed at low tide exists at the east side of the entrance to the cove. A bedrock ridge that is probably awash at high tide exists near the west of centre of the cove that extends south for approximately two thirds of the length of the cove. Sand has accumulated within the inner reaches of the cove and the shoreline north of the cove. Several raised beach strand lines are visible, extending about 100 m north of the beach. The bottom of the cove comprises a mix of exposed rock, sand and boulders. The depth at the southwest, outside end of the cove is approximately 5 m at low tide. The area north of the beach area is generally wet with developed bog land containing small ponds. A small intermittent stream flows south to enter the beach area at about the centre of the cove. The effect on the performance of the electrode from this stream is not expected to be significant. A developed quarry exists in the hillside about 200 m north of the cove. The rock in the vicinity of the cove in the lower elevations is near very close-jointed granite gneiss. Figure 2-1 is the northeast view of the cove.

Figure 2-1: View of LAD North Looking Northeast

There are four quarries and a borrow pit located within 1 km of the site. Three of the quarries are in granite gneiss rock and show signs of recent activity while the fourth one is in limestone/shale and is overgrown with a thick growth of brush. A distribution line runs along Trans-Labrador Highway (Hwy 510). A marine service centre exists at a distance of 600 m to the west of the site. The HVdc submarine cable north end terminal may be potentially located approximately 13 km from the site. Figure 2-2 shows the overall map of the area; however, the HVdc cable landing is not in the view.

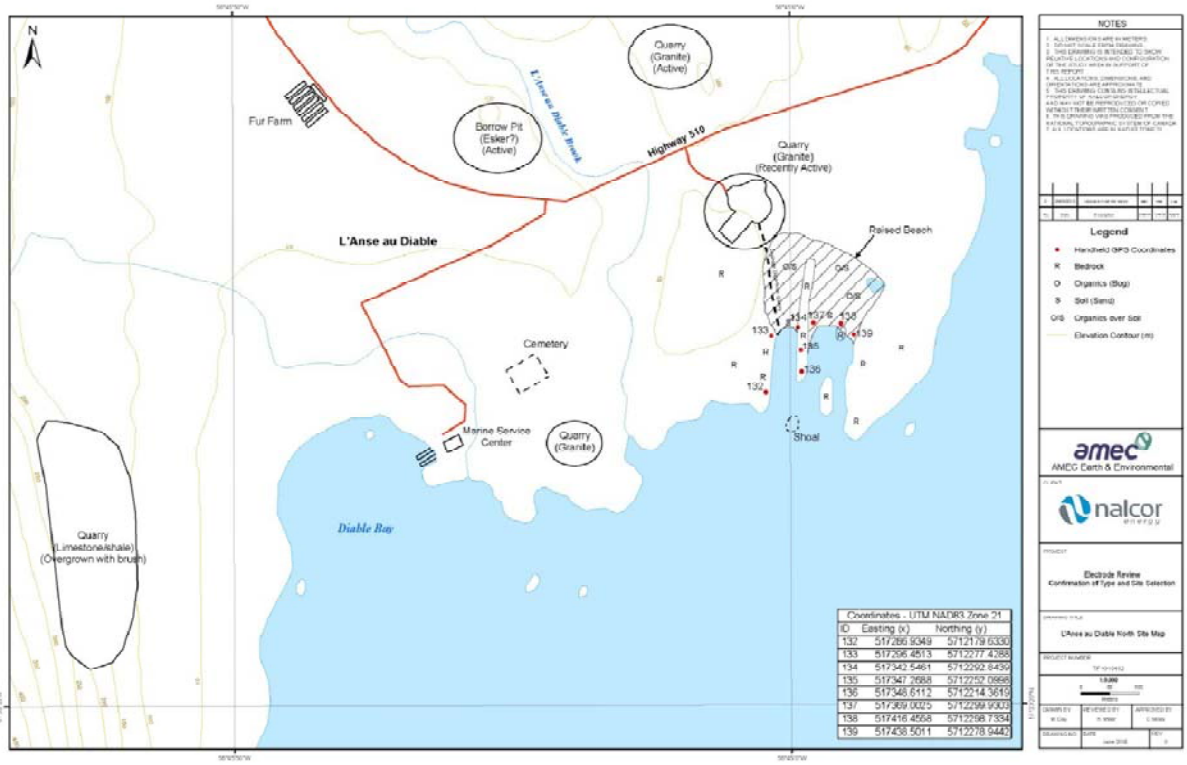

ID	Easting (x)	Northing (y)
132	517286.8349	5712179.6336
133	517356.4513	5712277.4388
134	517342.5461	5712292.8436
135	517347.2668	5712257.0668
136	517348.6112	5712214.3619
137	517369.0025	5712299.9303
138	517416.4558	5712298.7354
139	517458.5011	5712278.9442

Figure 2-2: LAD North Electrode Location

2.1.2 **Island Site**

Previous studies by Nalcor Energy have identified Dowden's Point as a suitable site for the Newfoundland shoreline electrode. The site is located on the south shore of Conception Bay, between Seal Cove Pond and Lance Cove Pond. A few operating industrial units are located in the area. Residential infrastructure is located in Seal Cove in the vicinity of Dowden's Point. Seal Cove is a part of the town of Conception Bay South, a larger major population centre that extends 15 km northeast from Seal Cove to Topsail. An abandoned railway right-of-way running parallel to the shoreline of Conception Bay (which is part of the Newfoundland T'Railway) is used by walkers and all-terrain vehicles. The key transmission and generation facilities including Holyrood Generating Station, Holyrood 230 kV Terminal Station, Seal Cove Generating Station, and NL Power Distribution Station are located within a 6 km radius from the Dowden's Point electrode location. Figure 2-3 shows a photograph taken at Dowden's Point and Figure 2-4 shows the overall map of the area.

Figure 2-3: View of Dowden's Point Looking Northeast

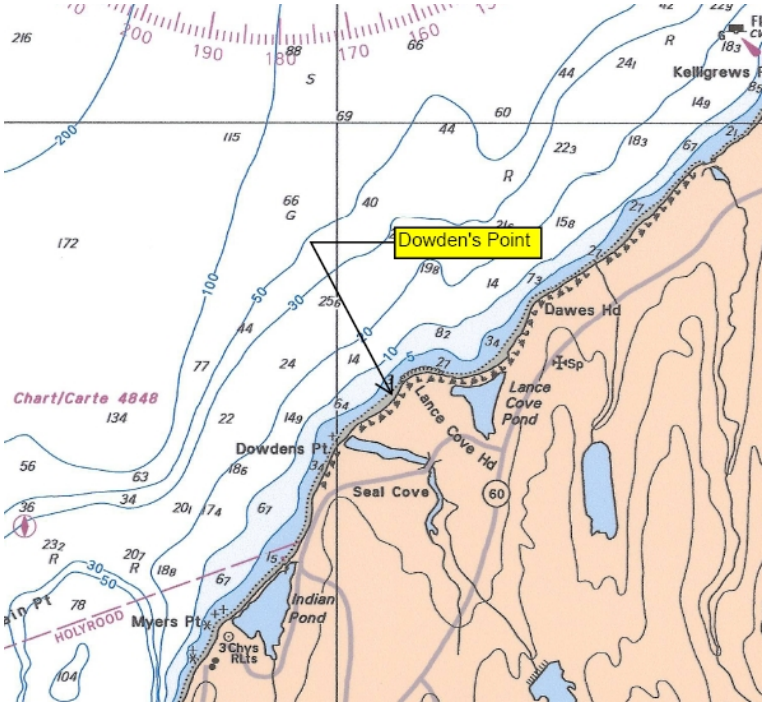

Figure 2-4: Dowden's Point Electrode Location

2.2 Electrode Design Criteria

A shoreline pond electrode must meet the electrical performance requirements of the HVdc system, the operational and maintenance requirements and the safety criteria in accessible areas. The electrode must also have minimum negative effects on the infrastructure and the environment and have a robust structure to withstand the site conditions and elements.

To ensure its electrical performance, the electrode must be sized adequately for the current duties while maintaining the electrode element current densities within the recommended limits of the manufacturer. The operation and maintenance factors to be considered include capability of the electrode element to perform without replacement during an expected pole outage, safety of the operating personnel and access to the elements for inspection and maintenance. The shoreline ponds, the breakwaters and the electrode installations are designed such that the GPR gradients on the land and in the sea of the accessible areas are within predetermined safety limits. The electrode should be located such that; ground potential rise levels do not cause stray currents that compromise equipment performance or cause corrosion that compromises the integrity of foundations, pipelines and grounding grids; vessel operations in the area if any are not affected by the electric and magnetic fields; and electric field, magnetic field, and chemical and physical emissions do not significantly affect the environment.

2.2.1 **Current Duties**

The electrode is sized adequately to meet the HVdc system monopolar operation needs including current and ampere-hour duties. The current and ampere-hour duties were reviewed with Nalcor Energy for the transmission system voltages 320 kV and 400 kV, and Table 2-1 and Table 2-2 present these data.

Table 2-1: Electrode Station Monopolar Current Duties

Parameter Description	320 kV Option	400 kV Option
Nominal Current, I_{nom} (A)	1406.25	1125.00
Maximum Continuous Current, $I_{max, cont.}$ (A)	2109.38	1687.50
Maximum 10-Minute Overload, $I_{max, 10 min.}$ (A)	2813.30	2250.00

Table 2-2: Electrode Ampere-Hour Duties Over 40 Year Life Cycle

Description	Duty (Ah) 320 kV Option	Duty (Ah) 400 kV Option	Remarks
Scheduled Outages	2,586,938	2,069,550	$I_{max, cont.}$ *0.5%*70%*8760 h/y*40 y
Forced Outages	4,927,500	3,942,000	$I_{max, 10min.}$*0.5%*8760 h/y*40 y
Continuous Imbalance	4,927,500	3,942,000	I_{nom}*1%*8760 h/y*40 y
Cable Outage (1 year)	18,478,125	14,782,500	$I_{max, cont.}$ *8760 h/y*1 y
Total Duty (40 years)	**30,920,063**	**24,736,050**	**Ampere hours**

The maximum continuous currents of 2109 A and 1688 A (150% of the normal operating currents) are considered for determining the minimum number of electrode elements required for the electrode. The number of electrode elements selected allow for continuous monopolar operation without replacement for the duration of more than one year (in the event of submarine cable damage in the Strait of Belle Isle). A design margin is considered to address any imbalances in current sharing, electrode element design tolerances and

condition of the electrode at the start of the worst case monopolar operation. Additional elements are proposed to ensure electrode performance during maintenance. The effect on the surrounding infrastructure is evaluated for 30,920,063 Ah and 24,736,050 Ah duties which are based on a very pessimistic operation of the HVdc link. For example, metallic return for the schedule outages is not considered, 70% rather than 50% probability of pole outage is assumed and a high bipolar imbalance is assumed. The electrode duty needs to be reviewed based on the manufacturer's data for equipment failure rates and bipolar imbalances, future system reliability and availability studies, maintenance practices, and planned modes of operation.

2.2.2 **Safety Limits**

The safety on the land and in the sea is a function of the GPR gradient, the sea/soil resistivity and the voltage transferred via conductive structures. Step potentials, defined as the voltage difference across a human step of 1 m and large animal step of 2 m, are the main concerns on the land side. The touch potential, defined as the voltage between a conductive body and the feet of the of the person in contact with the object, is normally not a concern for electrode installations because the metallic connections are either divided into isolated sections (e.g., fences) or grounded at location of the point of contact. The safety aspects of step potential are discussed in detail.

The tolerable current through human bodies and animal bodies is a well researched subject and is based on experimental data. A set of experiments, reported by Dalziel [12], indicates that the threshold of perception where a slight tingling sensation is felt by the hand or finger occurs at an average level of 5.2 mA dc. Consequently, the level of 5 mA dc body current is currently accepted as the threshold of annoyance for a person walking on the energized earth. The threshold for a prone human is 22 mA dc and 160 mA dc for a large, standing animal. The tolerable step potentials on the land for a standing or walking human, a prone human and an animal are shown in Table 2-3 and are based on the soil resistivities (ρ_s) considered in the models.

Table 2-3: Tolerable Body Current, Step Voltages and Voltage Gradient Near a dc Electrode

Description	Human Walking or Standing	Human Prone	Cow or Horse Standing	Remarks
Weight (kg)	70	70	500	Typical body mass
Body Resistance (Ω)	1000	1000	140	Typical values [5]
Contact Resistance (Ω)	$6\rho_s$	$3\ \rho_s$	$3\rho_s$	Typical values [5]
Sensitivity	Annoyance	Pain	Pain	
Tolerable Current (mA)	5	22	160	
Voltage (V)	$5 + 0.03\rho_s$	$22 + 0.07\rho_s$	$22 + 0.48\rho_s$	
Step (m)	1	2	2	Typical
Gradient (V/m): $\rho_s = 0$	5	11	11	In seawater or shoreline saturated soil.
Gradient (V/m): $\rho_s = 300$	14	21.5	83	Labrador Sediments (2011 Model) for shoreline
Gradient (V/m): $\rho_s = 3000$	95	116	731	Wet stone - Breakwater
Gradient (V/m): $\rho_s = 5000$	155	186	1211	Glacio Marine Top at Dowden's Point

The expected GPR gradients for all scenarios will be less than the tolerable step potentials (i.e., $5+0.03\rho_s$) of 5 V/m for the shore (saturated soil) and in the water, 95 V/m on the breakwater, and 14 V/m on the land side of the LAD North electrode and 155 V/m on the land side of the Dowden's Point electrode, shown in Table 2-3.

Sensitivity to an electric field varies for different species in the water and depends on the size and weight of the animal; the body shape and electrical resistance; the resistivity of the water; the type of current; and the electric field configuration. Typical reactions to an electrical field include attraction, narcosis, convulsions (tetanus), and death. Published literature indicates that fish might be attracted to an anode at 5 V/m, tetanus could occur at 20 V/m, and mortality is possible at 50 V/m. An average human may feel discomfort at a voltage gradient of 2.5 V/m in seawater. A value of 1.25 V/m is selected as safe design value [3] [4] [5] for large fish and humans. The contact area between the breakwater and the sea is a key factor in determining the GPR gradient; a minimum contact area between the shoreline pond and the breakwater must be achieved to ensure a safe voltage gradient on the sea side of the breakwater.

2.2.3 **Electrical Design Parameters and Pond Sizing**

The dimensions of the shoreline pond and breakwater are a function of the electrode element types, electrode element installations, seawater resistivity, tide changes, ice formation during winter, and safe GPR gradients required on the sea side. When installed along the side of the breakwater, the shoreline pond must be deep enough to fully submerse the electrode elements, and in addition account for tide changes and ice. From an operational perspective, the electrode installations should facilitate maintenance. Regular inspection of electrode elements should be achieved from the top of the breakwater, without the need of a diving team. Access to the pond will be controlled to address the safety and security; the GPR gradient in the pond would be higher than the tolerable limits and uncontrolled access to the pond would compromise the safety of public while the electrode is in operation, and the integrity of the electrode installations.

The number of electrode elements is selected such that the current densities are lower than the manufacturer's recommended values for satisfactory operation, and is such that the rate of electrode consumption allows for maximum continuous monopolar current for aduration of 3.5 years without replacement. The element composition is such that it can withstand the marine environment without corroding for long durations while the Project is operated as bipolar; chromium in high silicon chromium chill cast iron (HSCI) electrode elements provides a good corrosion resistance. The elements shall be arranged to have uniform current distribution among elements. The breakwater contact area to the sea shall be such that the GPR gradient on the sea side is less than 1.25 V/m.

Considering a current dissipation of 35 A per element for maximum continuous current (less than the manufacturer's recommended current value of 44.5 A per element and electrode consumption time period of more than 3.5 years) and a contingency of one subsection (for maintenance), the electrodes at each end of the transmission link require 60 elements (i.e., six subsections of 10 elements) for the 320 kV scenario and the electrodes require 48 elements (i.e., six subsections of 8 elements) for the 400 kV scenario. The elements are divided into six subsections to facilitate maintenance of one subsection while the electrode is in operation. Table 2-4 summarizes the pond sizes required for each scenario. Anotec type 4884H high silicon chromium chill cast iron electrode elements, used predominantly in pond electrode designs, are considered.

Table 2-4: Electrical Design Parameters Shoreline Pond Electrode and Pond Size

Description	UOM	320 kV		400 kV	
		LAD N	DP	LAD N	DP
Number of Electrode Elements (Maintenance)/ Current Dissipation per Element	ea/A	50/42	50/42	40/42	40/42
Number of Electrode Elements (Normal)/ Current Dissipation per Element	ea/A	60/35	60/35	48/35	48/35
Minimum Breakwater Length[3]	m	95	90	75	75

Notes:

1. The electrode element current at maximum continuous current is 150% of the normal current.
2. The electrode element imbalance is not considered.
3. The pond design considers additional breakwater contact area (50% or higher) to ensure safety during the maximum 10 minutes electrode current duty.

The pond sizes are selected to meet the performance requirements for the 320 kV and 400 kV HVdc system voltages. The analysis considers the maximum continuous current, and the total current is assumed to dissipate entirely through the straight section of the breakwater at low tide as a conservative design measure. Additional breakwater contact area is considered on the seaside to ensure safety during the maximum 10 minutes electrode current duty. The additional breakwater contact area in contact with the body of sea water, bottom of the pond and the land side will dissipate a portion of the current and the GPR gradient on the sea side will be less than the value calculated. Also a conservative breakwater resistivity of 3 Ωm is considered assuming a low void ratio of 19.3%; the actual design void ratio will be higher and will result in lower GPR at the electrode and lower GPR gradient in the breakwater. The electrode elements are arranged on the pond side of the breakwater with provisions of pulling out the elements for inspection and maintenance. The elements are protected from pond ice using concrete encased PVC conduits; Figures 2-5 to 2-10 show the conceptual arrangements for the LAD North and Dowden's Point designs.

2.3 Proposed Electrode Design

2.3.1 **L'Anse au Diable North Electrode Design**

The layout and section of the shoreline pond electrode, breakwater and associated installations are shown in Figure 2-5 and Figure 2-6 respectively. The breakwater extends beyond the mouth of the cove into the SOBI such that, at the land side toe of the breakwater where the elements are installed, a natural low-tide sea depth of 4 m is achieved (i.e., no excavation of the seabed). The length of the breakwater along the centerline is approximately 205 m.

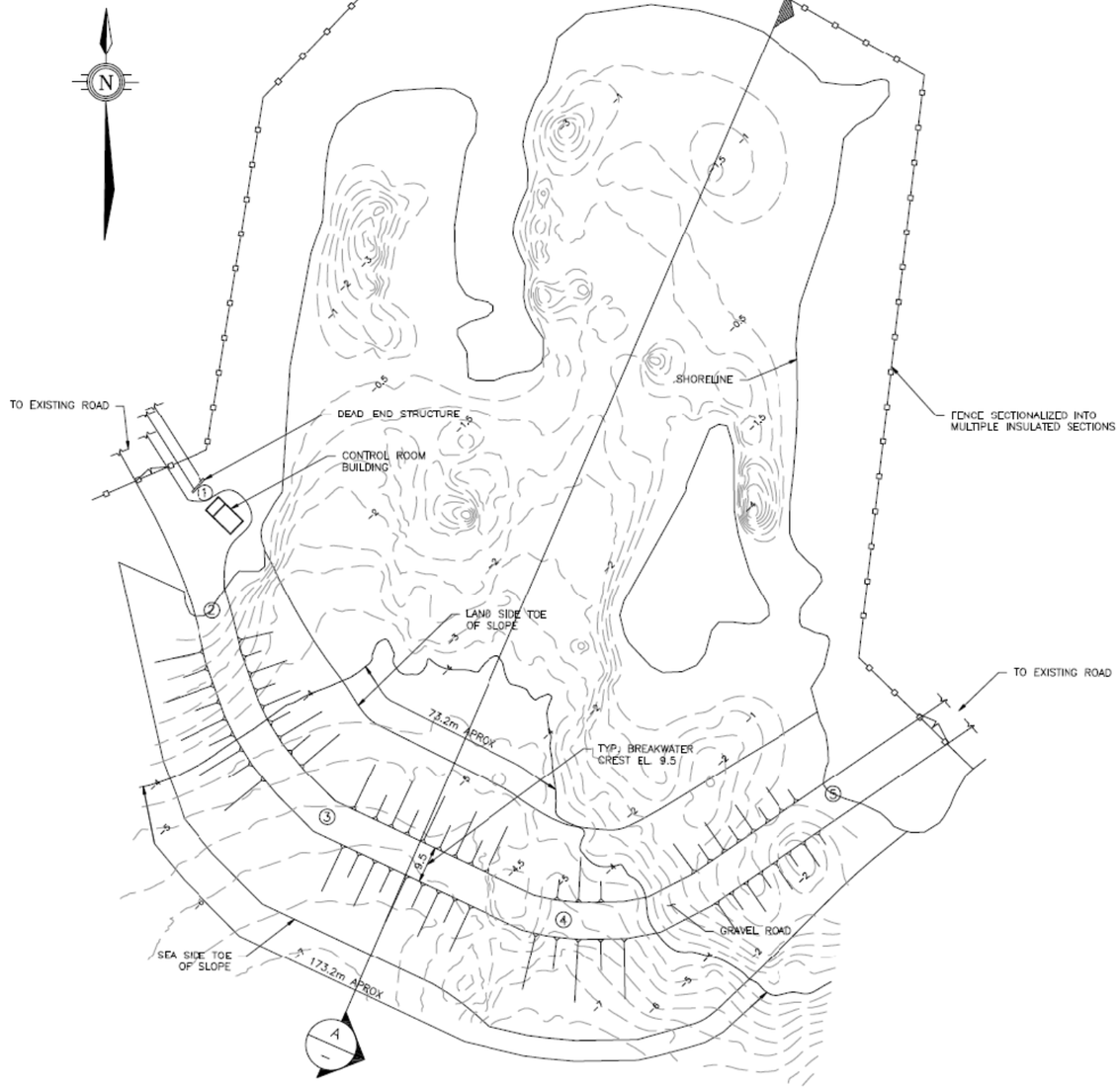

PLAN VIEW
_'ANSE–AU–DIABLE NORTH–OPTION 1 – 320kV

NOTES:

1. ELECTRODE ELEMENTS AND ASSOCIATED RACEWAYS ARE NOT SHOWN SIXTY (60) ELECTRODE ELEMENTS TO BE INSTALLED @ 1.2M SPACING ON THE POND SIDE OF THE BREAKWATER.
2. THE SHORELINE AND BATHYMETRY CONTOURS ARE BASED ON THE BATHYMETRIC SURVEY DRAWING PROVIDED BE NALCOR.
3. THE COORDINATES OF POINTS 1–5 ARE BASED ON THE BATHYMETRY CHART PROVIDED BY NALCOR AND SHOULD BE VERIFIED.
4. CREST OF BREAKWATER: EL. 9.5m.
5. HIGH WATER LEVEL: EL. 1.5m.
6. LOW WATER LEVEL: EL. 0.0m
7. BREAKWATER SLOPES ASSUMED TO BE 1.5H:1V.

COORDINATES IN UTM ZONE 21, NAD 83.		
POINT	NORTHING	EASTING
F	5712198	517409
1	5712186	517279
2	5712156	517279
3	5712103	517370
4	5712077	517370
5	5712110	517439

PRELIMINARY

DATE: FEB., 2011

HATCH™

Figure 2-5: LAD North Shoreline Pond and Breakwater Plan

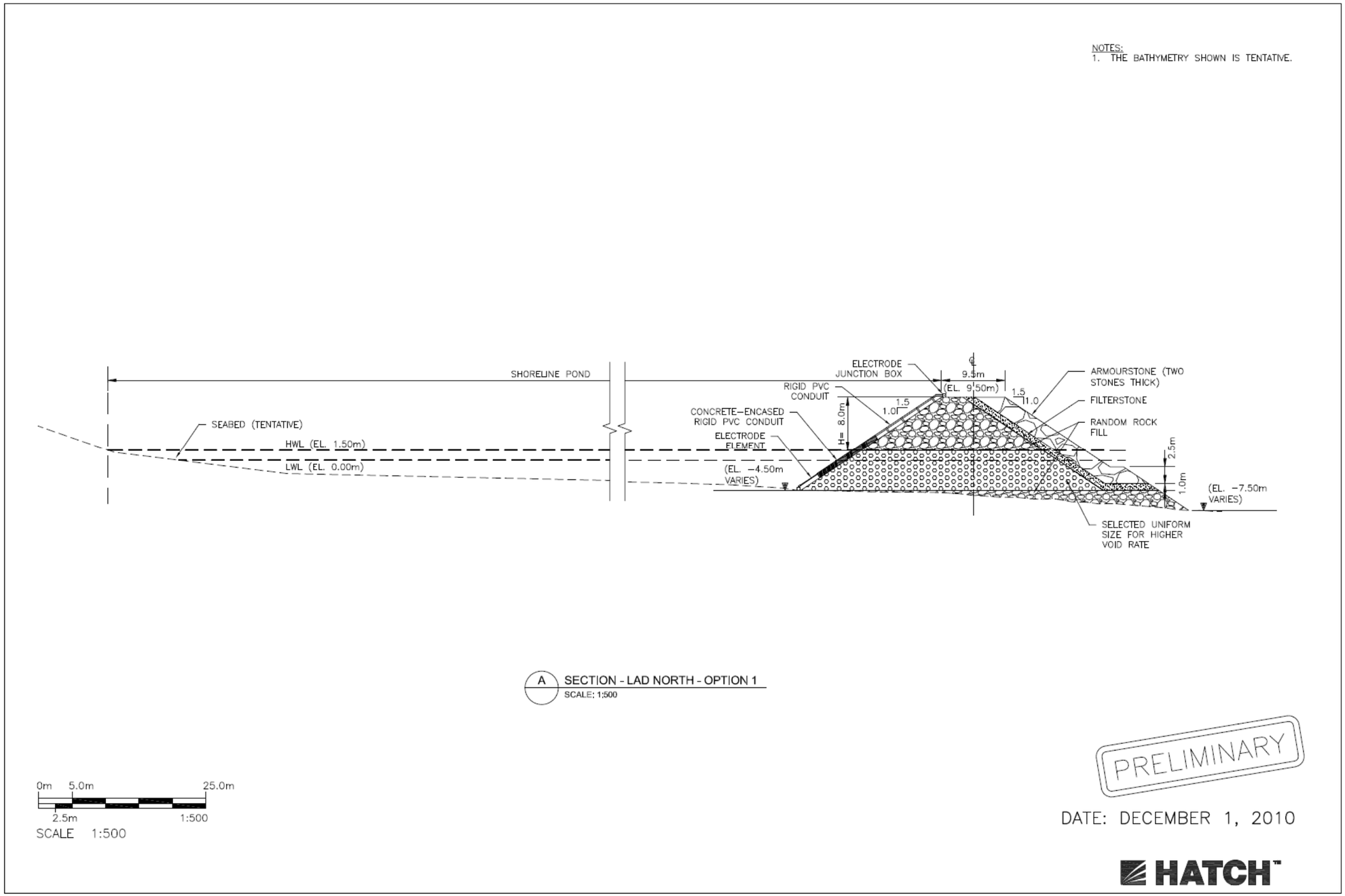

Figure 2-6: LAD North Shoreline Pond and Breakwater Cross Section

The low and high tide levels indicated in the cross sections are the worst case considered for the breakwater design. The daily change in the level will be lower than maximum tide change of 1.5 m, indicated in the breakwater sections and used for the breakwater design.

The pond and breakwater plan is based on the 320 kV scenario current duties; the same design is used for the 400 kV scenario current duties. The design for the 400 kV scenario can be optimized based on the design parameters included in this report. This optimization would only affect the field distribution in the pond and in the close vicinity of the electrode, however, not at locations farther from the electrode. Therefore, the pond design is not revised for the modelling of the 400 kV scenario.

2.3.2 **Dowden's Point Electrode Design**

The layout and section of the shoreline pond electrode, breakwater and associated installations are shown in Figure 2-7 and Figure 2-8 respectively; this design is referred to as Option 1. The breakwater extends into Conception Bay such that, at the pond side toe of the breakwater where the elements are installed, a natural low-tide sea depth of 4 m is achieved (i.e., no excavation of the seabed). The breakwater length measured along the centerline of the breakwater is approximately 385 m. The land side toe line of the breakwater is approximately 79 m from the shoreline and the sea side toe line is approximately 129 m from the shoreline.

The design is based on the 320 kV scenario current duties; the same design is used for the 400 kV scenario.

Minimizing the footprint of the breakwater is desirable to reduce issues in the environmental and regulatory processes. Also, the site is exposed to significant wave action and the design and protection of the larger breakwater extended into the sea may be a challenge. Therefore, an alternative shoreline pond electrode was designed at Dowden's Point; the layouts for Option 2 are shown in Figure 2-9 and Figure 2-10 for the 320 kV and 400 kV scenarios, respectively. The crest of the breakwater aligns with the top of the existing bank and the sea side toe line coincides with the existing low tide shoreline. A channel would be excavated to a depth of 4 m from the inside of the shoreline pond outward to the natural depth of 4 m in Conception Bay. The depth of the soil above the bedrock at Dowden's Point is anticipated to be approximately 30 m, which would permit excavation without the need to blast. The excavated area on the sea side of the breakwater would be in the shape of a wedge, increasing the electrode's exposure to the sea. A regular excavation program may be required to maintain the seabed depth requirement of 4 m to ensure the electrical resistance of the electrode does not increase significantly, the breakwater's permeable zone is not clogged, and the safety criteria of the contact area between the breakwater and the sea is complied with.

A larger breakwater contact area to the sea is required for the 320 kV scenario because of higher current density and to maintain safe GPR gradients on the sea side. Also, more electrode elements are required for the 320 kV scenario to maintain the current densities at each electrode element within the manufacturer's recommended limit and to attain a useful life suitable for the worst case monopolar operation.

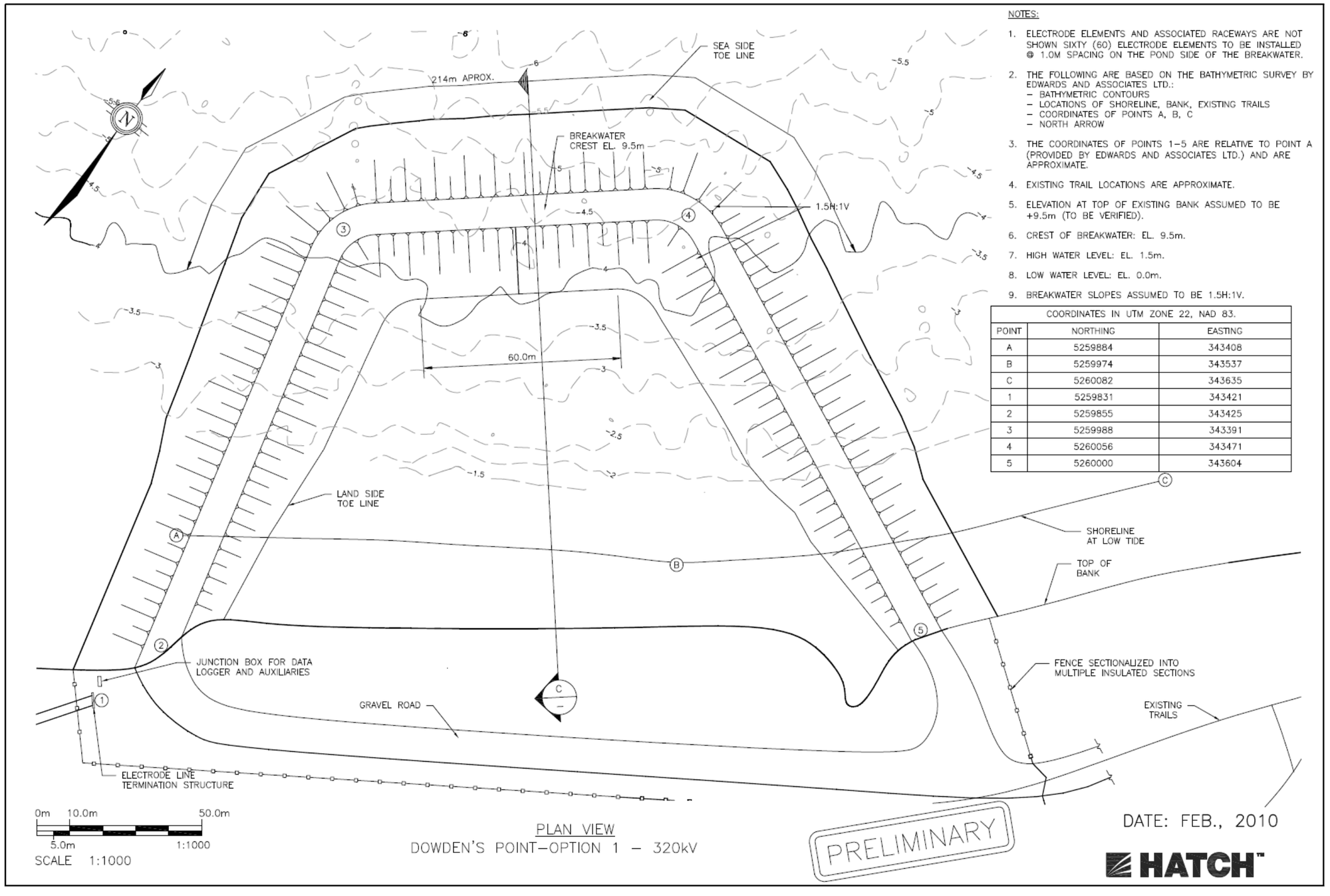

Figure 2-7: Dowden's Point Shoreline Pond and Breakwater Plan – Option 1

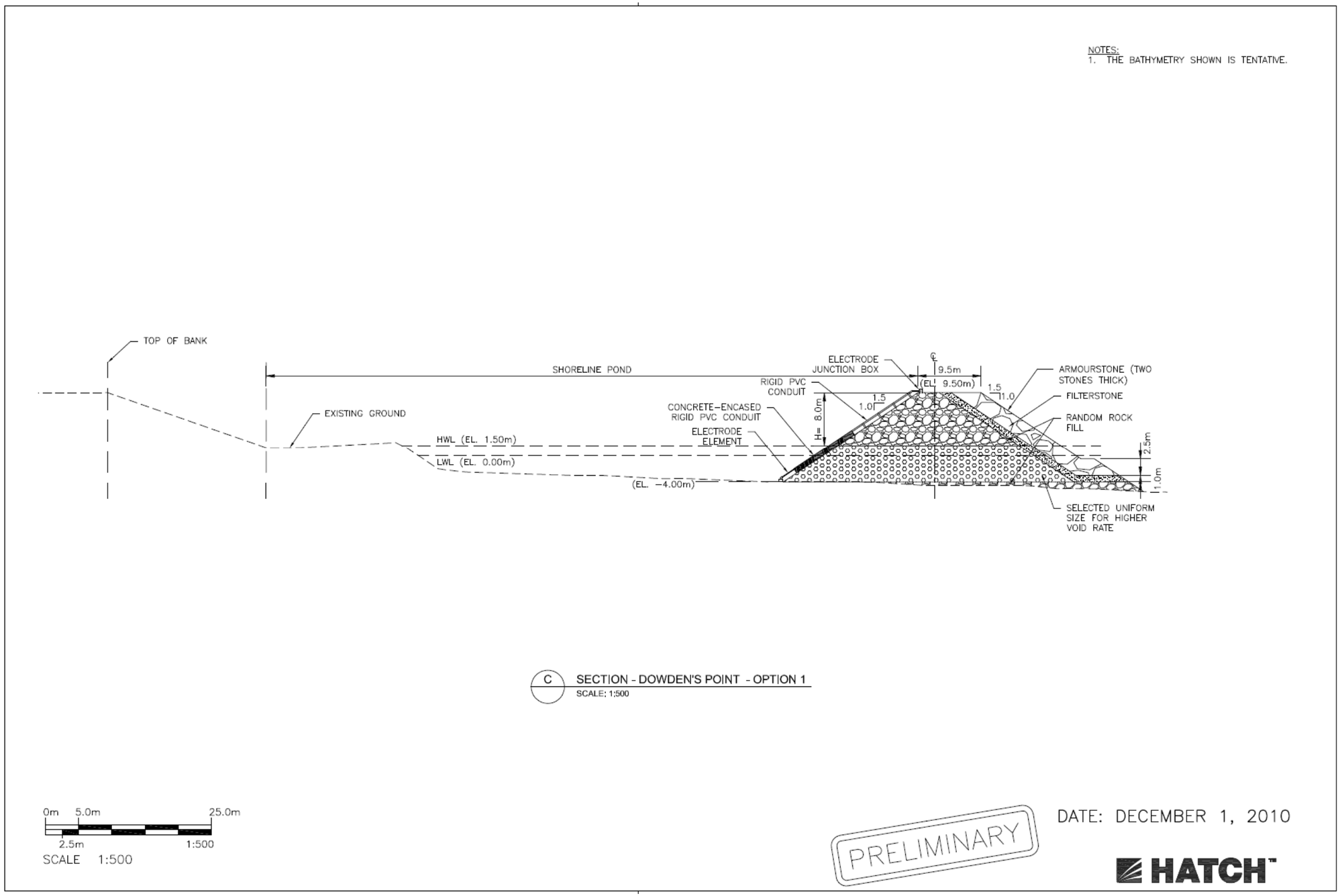

Figure 2-8: Dowden's Point Shoreline Pond and Breakwater Cross Section – Option 1

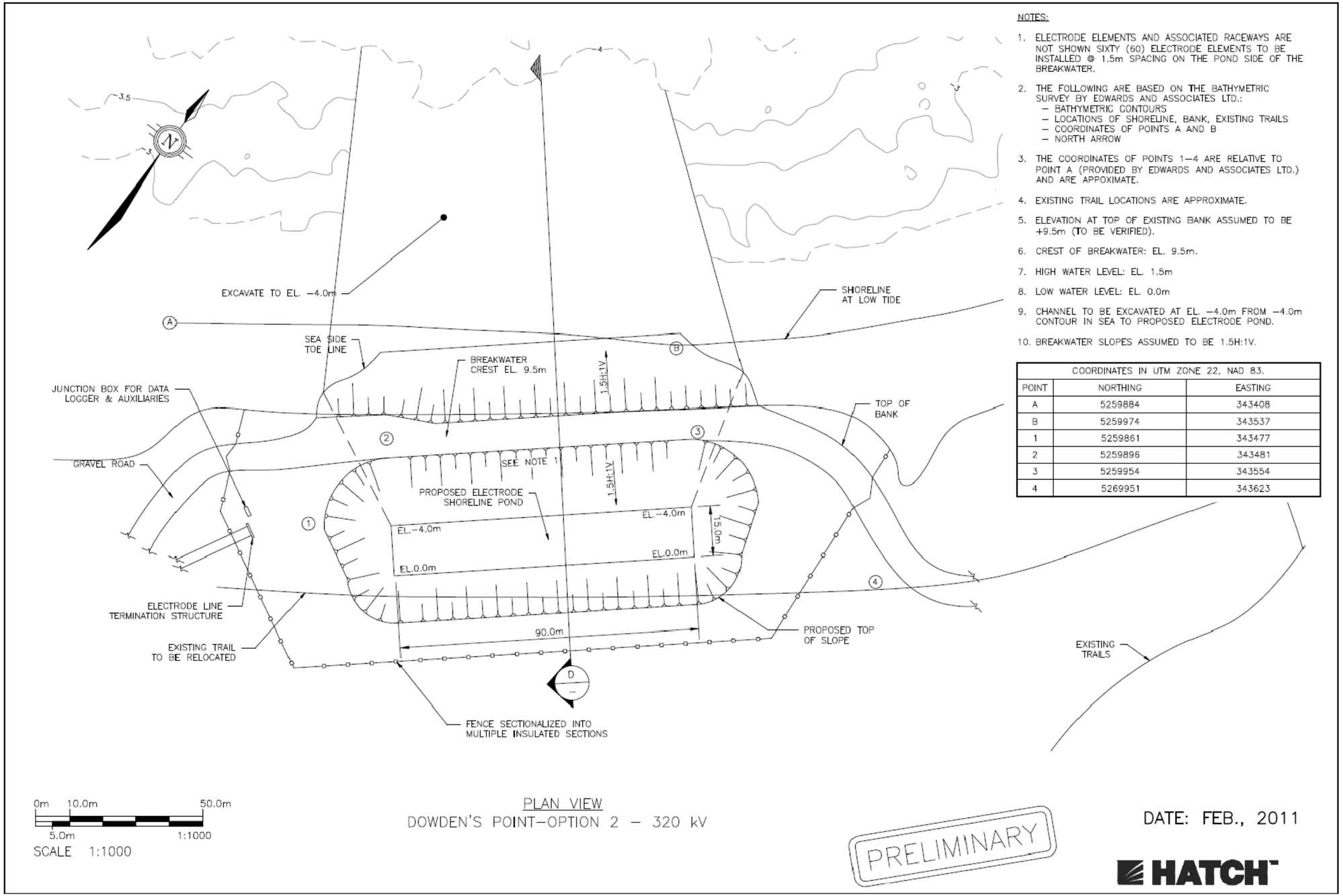

Figure 2-9: Dowden's Point Shoreline Pond and Breakwater Plan – Option 2, 320 kV Scenario

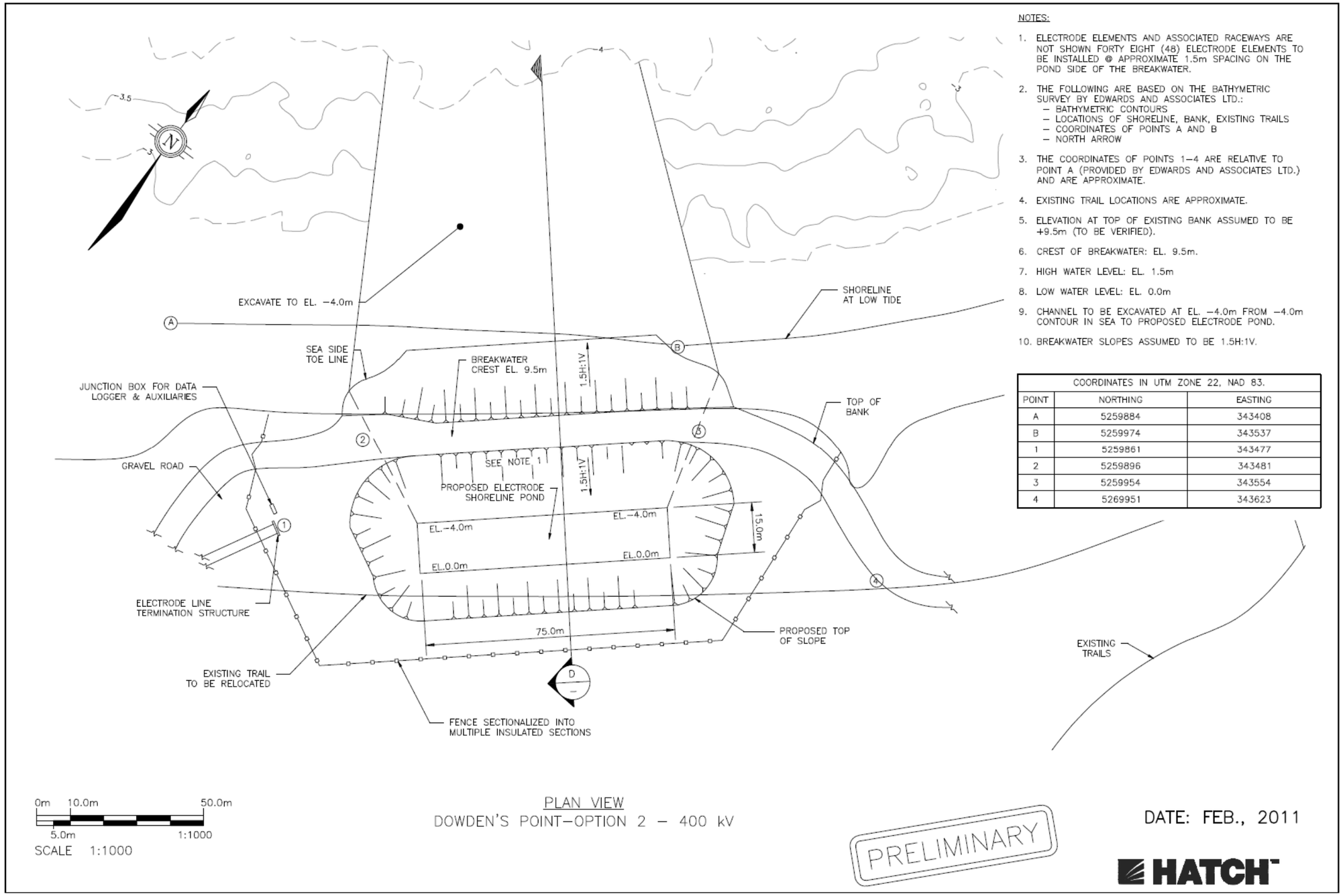

Figure 2-10: Dowden's Point Shoreline Pond and Breakwater Plan – Option 2, 400 kV Scenario

The low and high tide levels indicated in the sections are the worst case considered for the breakwater design. The daily change in the level will be lower than 1.5 m, indicated in the breakwater sections and used for the breakwater design.

2.3.3 **Civil/Structural and Geotechnical Design Review**

The breakwaters for both sites must be designed to withstand the expected worst case site conditions, including wave action, tidal effects, pack ice, and freezing inside the shoreline pond. The following review applies for the breakwaters at both sites and is independent of the HVdc system voltage.

The depth of the shoreline pond required at the land side toe line must account for the electrode element installations in the shoreline pond, changes in the water level due to tides and ice formation within the shoreline pond. The depth will be such that the electrode elements are fully immersed in the water below the ice under various tide conditions. Also, a depth on the sea side and length in contact with the sea water at low tide shall be such that the safety criteria of GPR gradient 1.25 V/m are met.

Significant wave height in the range of 6 m to 8 m is expected along the shore of the SOBI and in Conception Bay requiring a substantial breakwater structure and armour. It is anticipated that the breakwater would be a rubble mound structure consisting of embankment materials obtained from nearby quarries. The majority of the structure will be random materials from blasting in the quarry. Larger quarry rocks will be used as the armour stones, placed on the sea side slope to protect the main body of the mound from destruction by storm waves. A further selection will be made to form the embankment which must be permeable to allow natural flushing and transfer of saltwater through the embankment. Any potential landslides at the eroded shoreline fill could be mitigated by slope flattening and revetment with riprap stone. Coarser rock will be selected to form a pavement on the pond side slope in the range of expected tide and ice movement.

Access roads to the site will be constructed to link with existing local roads. The site will be fenced by chain link fencing to prevent public access from the land side to the pond, if required from sea side.

Approximate significant parameters for the rubble mound structure and pond are indicated in Table 2-5.

Table 2-5: Breakwater Civil/Structural Design Summary

Description	Unit	Value
Pond length	m	Varies[1]
Pond width	m	Varies
Pond depth at pond side toe, low tide	m	4, minimum
Water depth at sea side toe	m	Not confirmed
Assumed shore slope	H: 1V	1.5
Crest width	m	9.5
Sea side mound slope	H: 1V	1.5
Shore side mound slope	H: 1V	1.5
Approximate CL height	m	15.5
Tide height	m	1.5 [3]
Crest above low water	m	9.5
Low water level on shoreline	el m	0
Armour weight (mass)	Tonnes	4 & 12
Permeable core size	m	0.5 to 1.0

Notes:

1. The minimum lengths are determined in the pond sizing calculations for the various scenarios.
2. The minimum length corresponds to the breakwater section where the depth at the seaside toe is 4 m or more.
3. The tide height is the worst case considered for the breakwater design.

The design is proposed based on available information, site visits, published geological data, and known designs of breakwaters in the area. Items that have been identified as being of potential concern from a geotechnical perspective are: (i) the effect of large waves along the SOBI and in Conception Bay; and (ii) the effect of pack ice, shove, and vertical and horizontal movement on the armour stones.

2.4 Modelling of Electrode Effects

2.4.1 **Electric and Magnetic Fields**

Electric Fields

The current injected into or collected by an electrode results in ground potential rise (GPR) at the electrode and in the surrounding area. The magnitude of the GPR at the electrode is a function of the current and the impedance of the electrode to the remote earth. The resistivity of the local soil layers and the electrode configuration are the main determining factors of the GPR near the electrode, and define the size of the electrode zone of influence. An electrode with a large contact area will result in a lower maximum GPR, and an electrode installed in low resistivity soil or seawater will result in a smaller zone of electrode influence. However, at a significant distance from the electrode outside the zone of influence, the GPR distribution will not be affected by local soil conditions or element arrangement at the electrode. The remote earth resistivity determines the GPR distribution outside the zone of influence.

For a shoreline pond electrode, the GPR in the near vicinity is a function of the breakwater design, its exposure to the open sea, and the seawater resistivity; a higher breakwater resistivity (wider and lower void ratio) will result in higher local GPR. Typically it is difficult to model the electrode elements and the breakwater precisely

and a coarse model is used to review GPR distribution for effects assessment; the GPR distribution outside the pond will be representative of the actual using a coarse model. Analytical techniques are used to calculate the GPR gradients in the close proximity using conservative assumptions.

The electric fields resulting from electrode operation can affect nearby infrastructure. Electrolytic corrosion (applicable for buried and immersed metallic infrastructure) and electrical interference (applicable primarily for wye-grounded transformers and machines) are the two types of effects. Also, the GPR distribution in the vicinity of the electrode may have an effect on land and marine species.

Electrical interference in a system (mainly ac transmission and distribution, and dc transmission systems) is caused by the dc stray current flow through the system. DC stray current is injected into the system terminal station where equipment neutrals are connected to the ground, where equipment connections/configurations allow flow of zero sequence currents, and where terminal stations are at different potentials due to HVdc ground current flow. Electrical interference is instantaneous in nature but its effect can have lasting implications on equipment.

The flow of current between a metallic structure and the soil/water body results in oxidation or reduction reaction and consumption of the structure metal. Stray dc currents through metallic structures may appear minimal but because corrosion effects are cumulative, their long term effect can be significant.

Magnetic Fields

The flow of dc current through cables and conductors, as well as through the sea and soil, create dc magnetic field. The magnitude of the magnetic field at a point depends on the location of the point relative to the current carrying conductor/body, the magnitude of the current and the relative permeability of the medium in which the point is located. The current flow in the sea from electrode operation will produce a magnetic field, decreasing in intensity as it moves away from the electrode, and therefore a zone of magnetic influence around the electrode can be established. There are two main concerns associated with magnetic fields: 1) the effect of magnetic fields on marine operations, specifically sea navigation; and 2) the effect of magnetic fields on magneto-sensitive marine species. The zone of influence for the magnetic field is much smaller than the zone associated with electric fields because the dc magnetic fields are weak except in the close proximity of the electrode. Around shoreline electrodes, the electric current is distributed over a large area in the sea (i.e., the total surface area of breakwater). Due to this large area, the induced magnetic field surrounding the electrodes is very weak compared to the induced magnetic field of a cable or geomagnetic fields. The compass deviation is a function of the magnitude of the induced magnetic field and its orientation relative to the earth's magnetic field. The magnetic field values are calculated from the current distribution in the sea calculated in Teshmont's GPR modelling.

Compass Deviation

Current flow to and from the electrodes will induce magnetic fields, with the greatest intensity of the magnetic field present in the near vicinity of the electrodes. The magnetic fields may be a source of compass deviation for ships navigating in the proximity of the electrodes. The induced magnetic fields observed in the electrode simulations are used to establish the zones around LAD North and Dowden's Point which determine the angle of deviation in the resultant horizontal magnetic field.

Marine Species

As previously stated, current flow to and from the electrodes will create induced magnetic fields with the highest intensity of the magnetic field in the near vicinity of the electrodes. A large variety of organisms have been shown to respond to geomagnetic cues, including: magnetotactic bacteria [17], protists [18], gastropods [19], crustaceans [20], insects [21], bony fish [22], amphibians [23], sea turtles [24], birds [25], and migratory whales [26]. The values obtained from the modelling presented in the following sections will be used in the EIS for the Project to assess the effect on the marine environment.

2.4.2 **Chemical and Physical Emissions**

Chemical Emissions

The chemical emissions analysis describes the chemical reactions occurring at the anode and cathode and estimates the products from primary reactions, based on the electrode and pond designs considered for the 320 kV and 400 kV HVdc transmission options, including during bipolar and monopolar operations. The secondary and tertiary reactions including their effect on the primary reactions are reviewed qualitatively. The analysis also qualitatively describes the sensitivity of emissions to water temperature, water pH value, light, gas exchange at the surface, and electrode element current density. A conservative approach is taken to estimate the levels of emissions, especially the assumption of a chlorine selectivity of 30% (the upper limit); typically chlorine selectivity varies from 5% to 30%. The concentration of chlorine potentially produced at each site is also estimated considering the effect of tidal flushing.

Physical Emissions

The current injection (collection) at the anode (cathode) is a source of energy that is dissipated in the resistive medium through which it travels. The energy dissipated is a function of the electrode resistance and the current injected (collected) by the electrode. The distribution of energy is a function of current density in a medium and its resistivity. The bulk of the energy is dissipated in the near vicinity of the electrode where current densities are the highest. For the proposed design, the electrode current will disperse mainly through the breakwater into the open sea; therefore, the breakwater will dissipate a high proportion of the total energy. The approach of the analysis is to quantify the heat dissipation in the pond, through the breakwater, and in the sea at the interface of the breakwater. The heat dissipation density in the sea away from the breakwater will be insignificant because the large dispersion of currents and low resistivity of the seawater, and therefore it is not analyzed.

2.5 Study Team

The review and analysis were conducted by a panel consisting of experts in HVdc electrodes, local geology and geophysics, marine structures, and marine biology. The panel members and their specific areas of expertise are as follows:

- Donald Gordon and Mark Stobart, Teshmont Consultants LP – HVdc Electrodes;
- Terry Treasure, Hatch – HVdc Electrodes;
- Hugh Miller, AMEC – Geophysics;

- Calvin Miles, AMEC – Geotechnical;
- Scott Hancock, Hatch – Marine Structures;
- Michael Teasdale, AMEC – Marine Biology;
- Rauf Ahmed and Ben McLeod, Hatch – HVdc Electrodes and Panel Coordinators.

3.0 RESULTS AND ANALYSIS

The results of the modelling conducted for this report fall under two broad categories: 1) ground potential rise and magnetic field and 2) physical and chemical emissions. The ground current flow results in GPR in the soil body or sea body of water, and magnetic field above and below the earth surface. Section 3.1 presents the GPR and magnetic field simulations, which included inputs such as the sea and soil model, electrode configurations, shoreline pond, and breakwater model. The modelling results are presented as GPR contours and magnetic fields at various points in the vicinity of the electrode. This is followed by an effects analysis on the following: 1) electric fields on infrastructure; and 2) magnetic fields on compass deviations and the marine environment. The chemical and physical emissions associated with electrode operations are presented in Section 3.2.

3.1 Ground Potential Rise Simulations

GPR simulations were performed at both LAD North and Dowden's Point for both 320 kV and 400 kV options. The GPR levels at various points of interest were used as inputs for the effects analysis.

There are three aspects to the model which affect the simulation: the resistivity properties of the geological units, their spatial extents, and electrode current. The details of assigning these parameters and the development of the specific models for use in simulation are documented in the following subsections.

This analysis was carried out using Teshmont's GRELEC (GRound ELECtrode) program. This program calculates voltages and potential gradients within a 3-Dimensional model of non-homogeneous material when a current is injected at one point or at a number of points. The GRELEC program divides the soil into layers, rings and sectors, and calculates the self- and mutual-resistances of each element.

3.1.1 **L'Anse au Diable North Electrode**

Sea and Soil Model

A modelling scenario was identified based on soil resistivity models developed under previous studies conducted for Nalcor Energy. Table 3-1 describes the modelling scenario and the sea and soil units are identified in Figure 3-1.

Table 3-1: L'Anse au Diable Suggested Soil and Sea Modelling Scenarios

Unit Descriptions	Parameter Descriptions	Parameter values
SOBI Water	Resistivity (Ωm)	0.39
	Thickness (m)	per bathymetry
Labrador Sediments	Resistivity (Ωm)	1000
	Thickness (m)	150
Labrador Basement	Resistivity (Ωm)	5000
	Thickness (m)	infinite
SOBI Sediments	Resistivity (Ωm)	300
	Thickness (m)	300
SOBI Basement	Resistivity (Ωm)	5000
	Thickness (m)	infinite
NL Carbonates	Resistivity (Ωm)	300
	Thickness (m)	500
NL Dunnage	Resistivity (Ωm)	2000
	Thickness (m)	2000
NL Basement	Resistivity (Ωm)	5000
	Thickness (m)	infinite

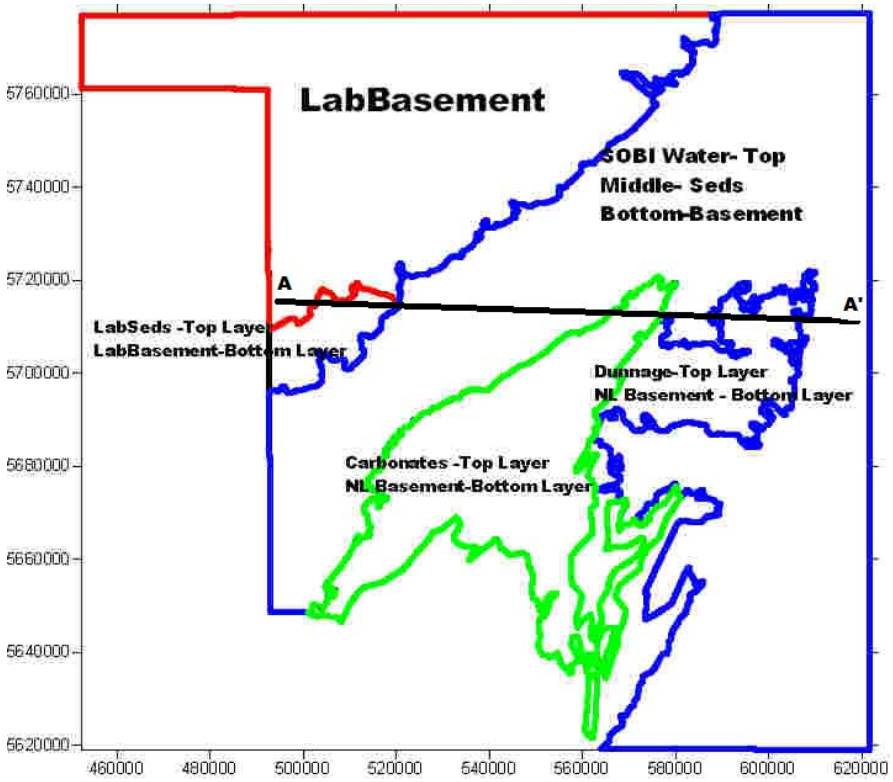

Figure 3-1: Sea and Soil Units in the Area of the Strait of Belle Isle

The details of various geological units in Table 3-1 and their spatial extents were determined by a geophysical and geological investigation completed under previous studies [1] [2] [27]. The sea depths considered in the model are low tide depths as shown in bathymetric charts from Canadian Hydrographic Services [6] and the depths in the near vicinity of LAD North are based on the bathymetric data provided by Nalcor Energy. As a

conservative design measure, the low resistivity mud or sediment atop the seabed is not considered in the model.

Electrode, Shoreline Pond and Breakwater Model

The spatial extents and resistivities were based on:

- The sea and soil model summarized above;
- The bathymetric data of the SOBI [6]; and
- The shoreline pond electrode design (void ratio of 19.3% of uniform size rock, resistivity of 3 Ωm for the breakwater and 0.01 Ωm resistivity for volumes representing the electrode elements were assumed).

A cylindrical volume of 600 km in radius and 50 km in depth was modelled; volumes outside the modelled mass will not have a significant effect on the simulation results. Figure 3-2 shows the top layer of the model in close proximity to the electrode.

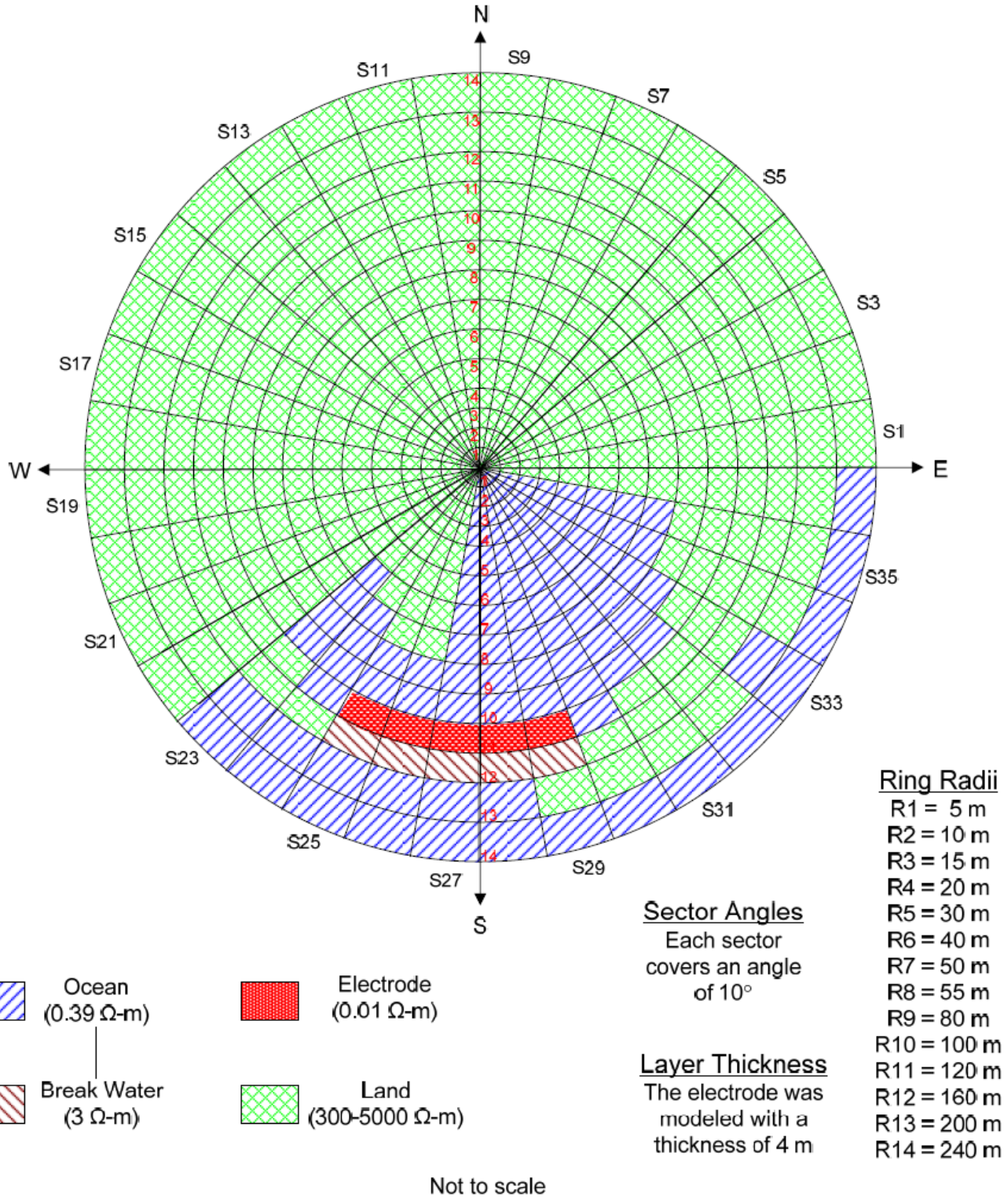

Figure 3-2: LAD North Shoreline Pond and Breakwater Model

A current of 2109 A and 1688 A, the maximum continuous electrode currents, were injected at the LAD North location (5712200N, 517350E in UTM 21). The current injected into the GRELEC model was distributed among the low resistivity volumes representing the electrode (the area shown in red in Figure 3-2). This approach will

produce a more realistic representation of the GPR distribution in the near vicinity of the shoreline pond compared to a single point source current injection method. The volumes containing electrode elements were assigned a low resistivity of 0.01 Ωm to approximate the actual resistance of the electrode element array. GPR values were also calculated for bipolar operations (i.e., 1% of the current passes through the electrode due to system imbalances).

The representation of a rectangular breakwater is approximate in cylindrical coordinate and its slopes cannot be represented. As a result, the GPR levels and gradients inside the pond are not representative of the actual values. Therefore, manual calculations are used to estimate the GPR gradients for the safety analysis and the breakwater resistance for heat dissipation.

Simulation Results

Figure 3-3 and Figure 3-5 show the GPR contours in the vicinity of the electrode for the 320 kV and 400 kV scenarios, respectively for the maximum continuous current. Figure 3-4 and Figure 3-6 show the voltage gradient plots for the 320 kV and 400 kV scenarios, respectively for the maximum continuous current. The values for bipolar imbalance current can be obtained by scaling the reported maximum continuous current values by a factor of 1/150.

L'Anse au Diable Equipotential Contours (to 2 km) (LAD_04_2109A – 0.39 ohm-m sea, 50 km depth)

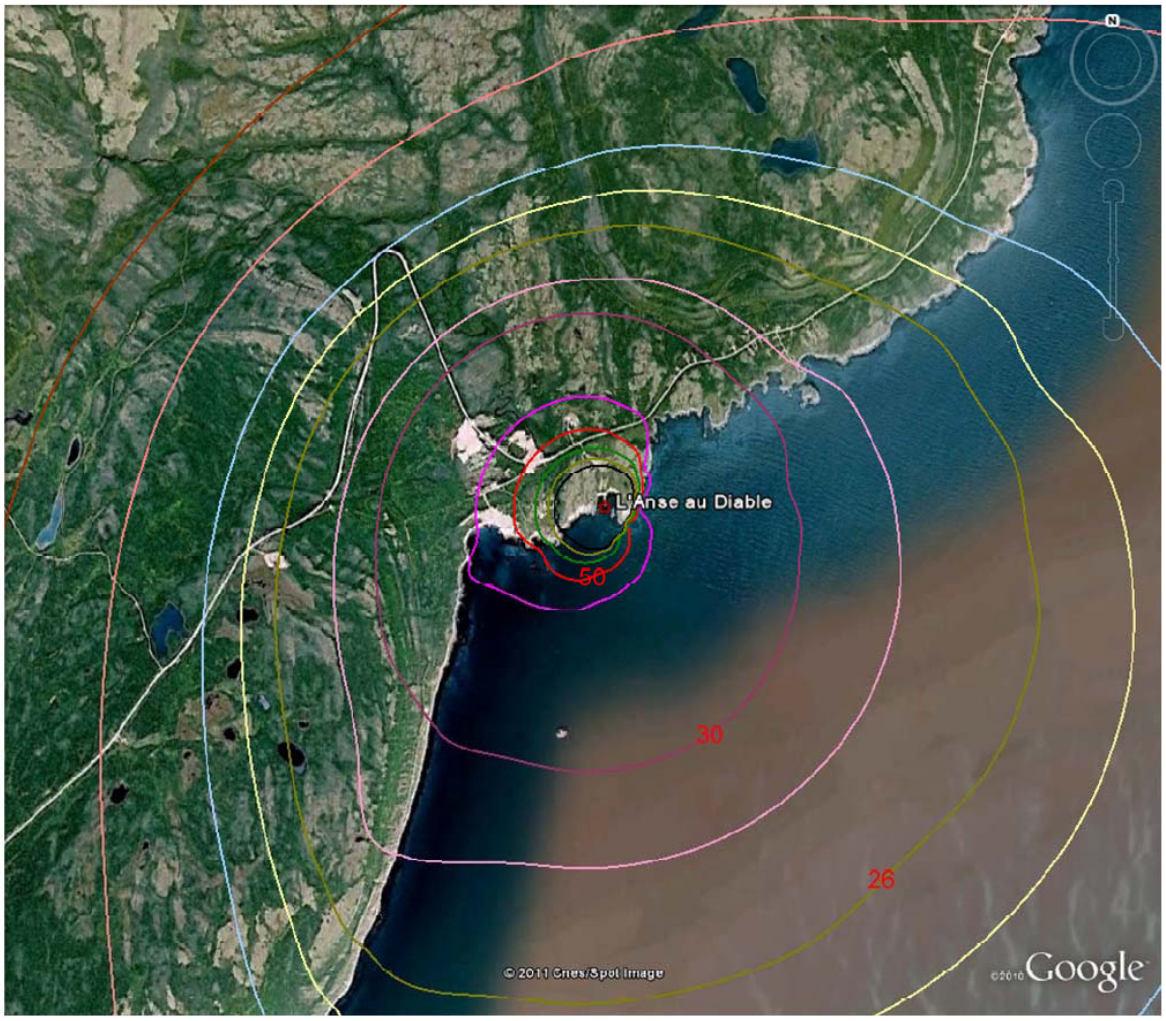

0 2km

Ground Potential Rise (V)

78	70	60	50	40	30
28	26	25	24	22	20

Teshmont

April 20, 2011

Figure 3-3: GPR Contours in the Vicinity of LAD North (320 kV Option)

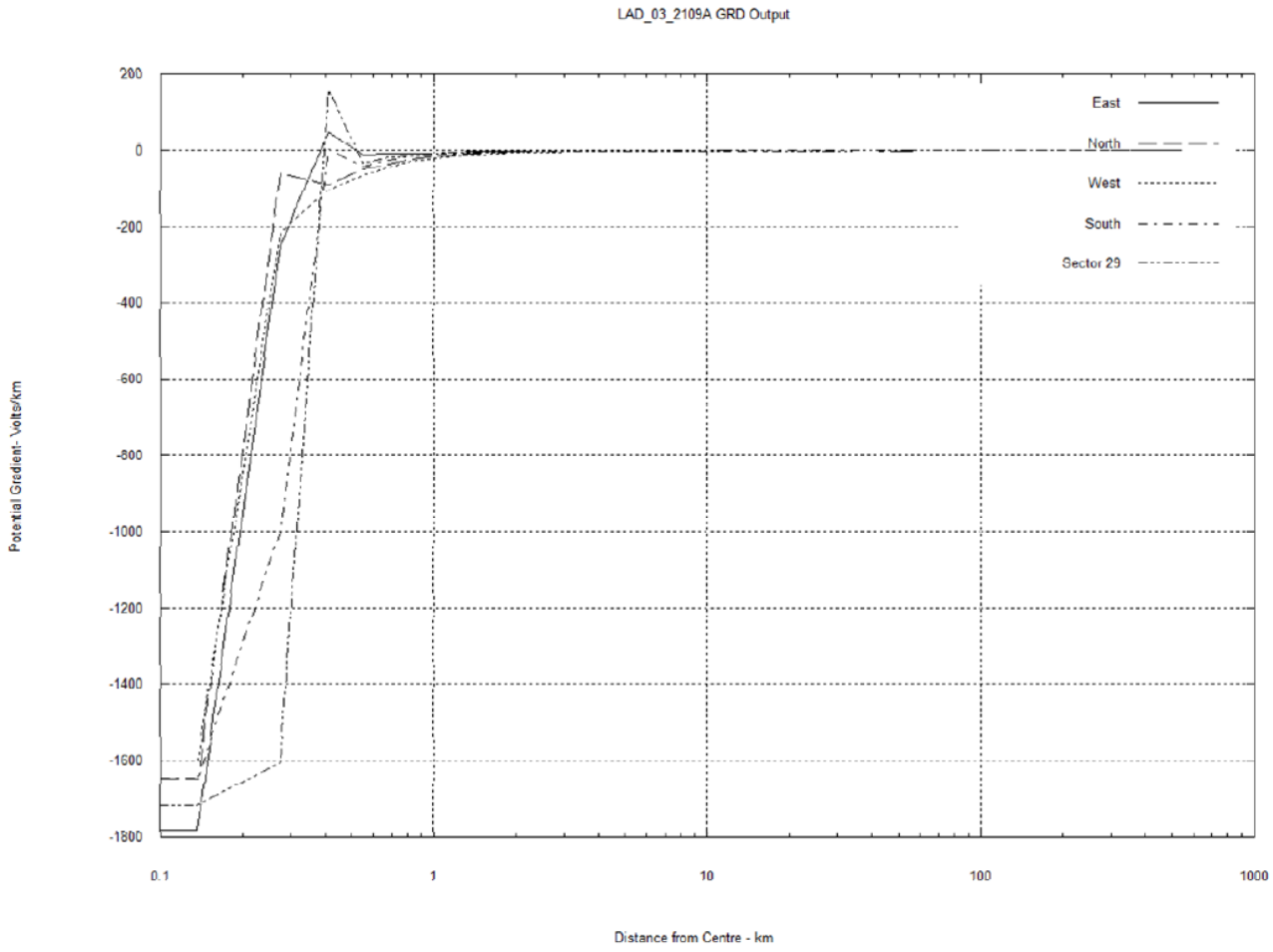

Figure 3-4: Voltage Gradients in the Vicinity of LAD North (320 kV Option)

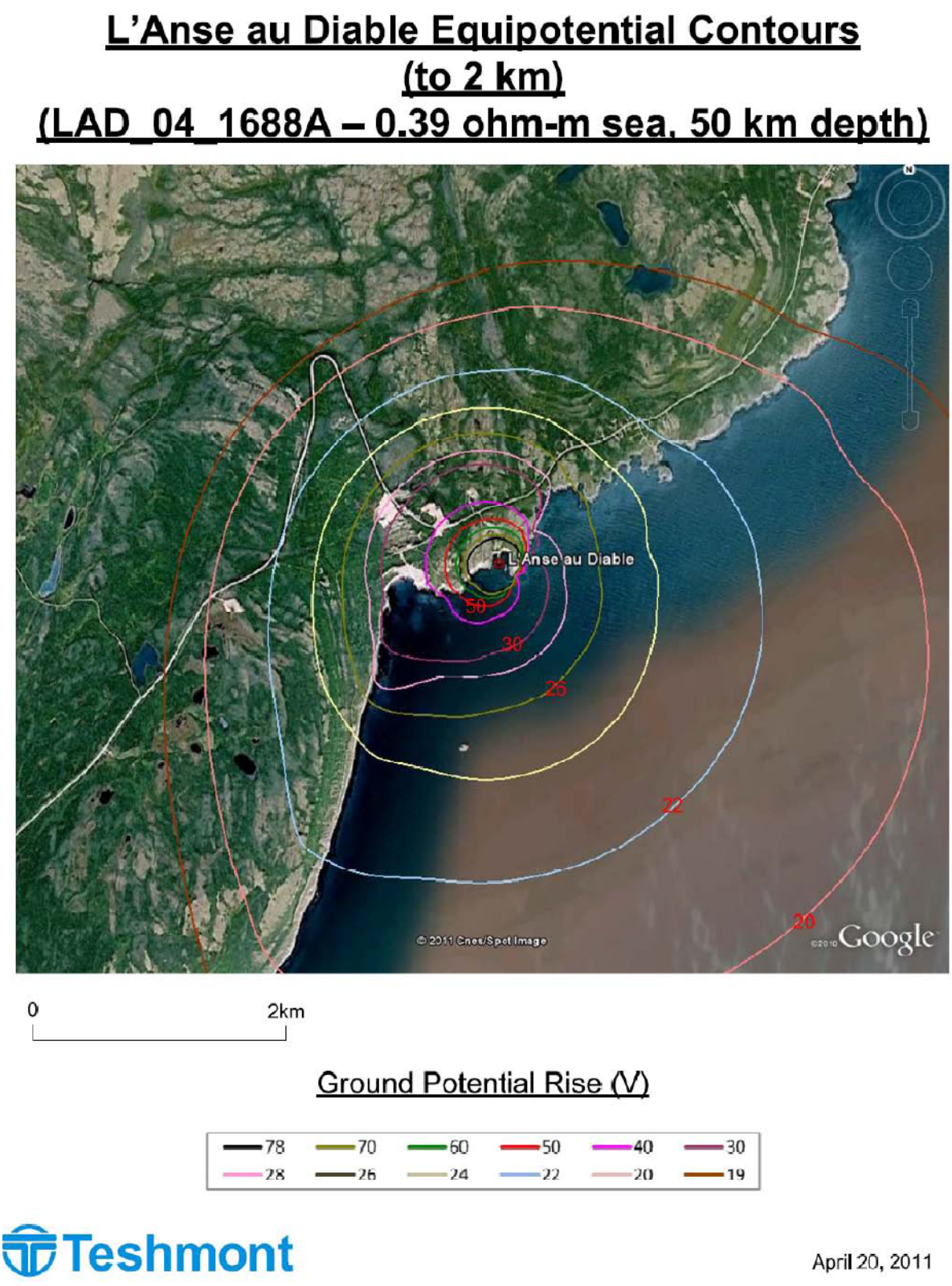

Figure 3-5: GPR Contours in the Vicinity of LAD North (400 kV Option)

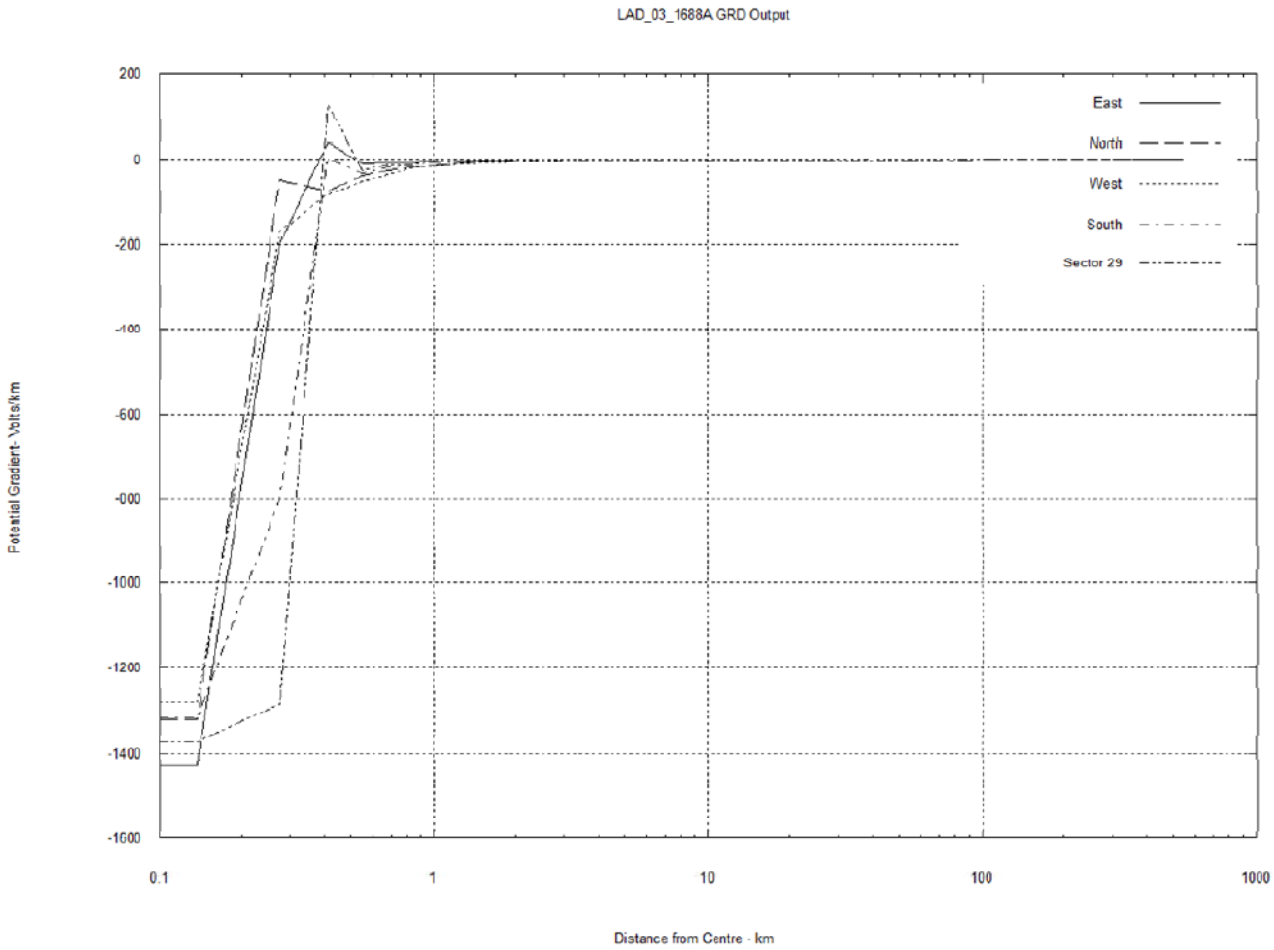

Figure 3-6: Voltage Gradients in the Vicinity of LAD North (400 kV Option)

3.1.2 **Dowden's Point Electrode**

Sea and Soil Model

The land model was developed based on the resistivity soundings near the proposed electrode location and a literature review of the geology in the area, and consideration of spatial parameters for geological units and the unit resistivities.

The modelling scenarios are presented in Table 3-2 and are based on work completed under previous studies [1] [2] [28]. Figure 3-7 shows the extents of the sea and soil units.

Table 3-2: Dowden's Point Suggested Soil and Sea Modelling Scenarios

Unit Descriptions	Parameter Descriptions	Parameter Values
Conception Bay	Resistivity (Ωm)	0.38
	Thickness (m)	per bathymetry
Seal Cove Pond	Resistivity (Ωm)	0.55
	Thickness (m)	10
Lance Cove Pond	Resistivity (Ωm)	10
	Thickness (m)	10
Indian Cove Pond	Resistivity (Ωm)	0.35
	Thickness (m)	10
Glacio-Marine Top	Resistivity (Ωm)	5000
	Thickness (m)	4
Glacio-Marine Middle	Resistivity (Ωm)	300
	Thickness (m)	3
Glacio-Marine Lower	Resistivity (Ωm)	5000
	Thickness (m)	5
Till Undifferentiated	Resistivity (Ωm)	2000
	Thickness (m)	5
Poor Till	Resistivity (Ωm)	2000
	Thickness (m)	5
Cambro-Ordovician	Resistivity (Ωm)	500
	Thickness (m)	500
Granitoid-Volcanics	Resistivity (Ωm)	5000
	Thickness (m)	infinite

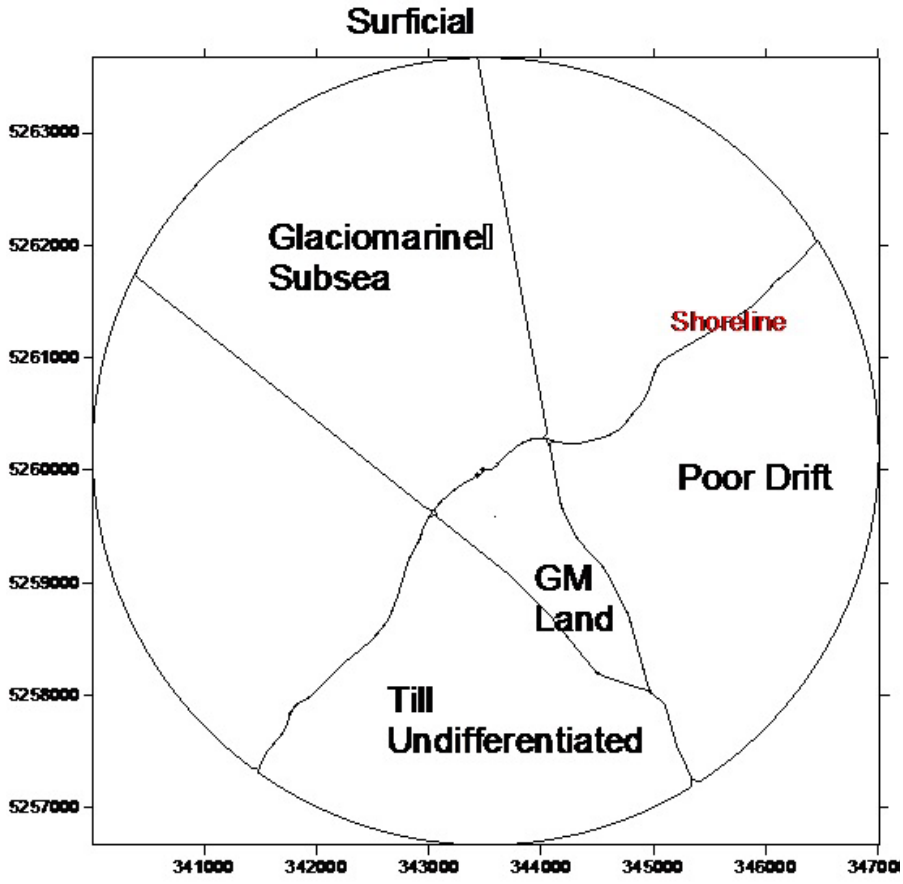

Figure 3-7: Sea and Soil Units in the Area of the Dowden's Point

The worst case seawater resistivity of winter bottom layer of 0.38 Ωm for Conception Bay is used for the model. The sea depths considered in the model are low tide depths as shown in bathymetric charts [7], and the depths in the near vicinity of Dowden's Point are based on the bathymetric data provided by Nalcor Energy. The low resistivity mud or sediment on the seabed is not considered in the model as a conservative design measure.

Electrode, Shoreline Pond and Breakwater Model

The spatial extents and resistivities were based on:

- Sea and soil model;
- The bathymetric data of Conception Bay [7]; and
- The shoreline pond electrode design (a void ratio of 19.3% and resistivity of 3 Ωm for the breakwater and 0.01 Ωm resistivity for the volumes representing the electrode elements; a lower resistivity of the water body of the pond is used to offset the effect of a point source current injection).

A cylindrical volume of 600 km in radius and 50 km in depth was modelled; volumes outside the modeled mass will not have significant effect on the simulation results.

Figure 3-8 shows the model of the recessed shoreline pond and breakwater.

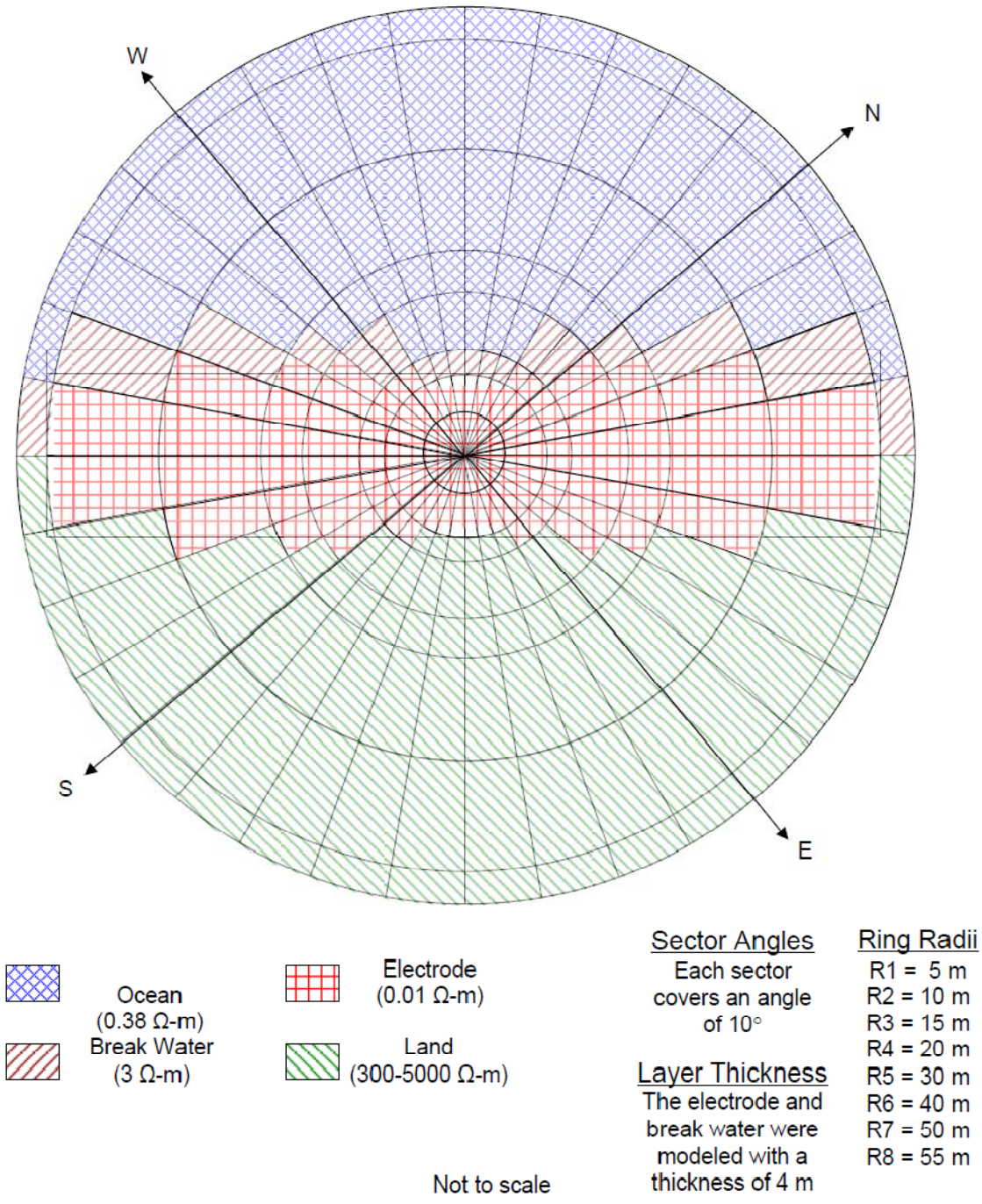

Figure 3-8: Dowden's Point Shoreline Pond and Breakwater Model

Simulation Results

Figure 3-9 and Figure 3-11 show the GPR contours in the vicinity of the electrode for the 320 kV and 400 kV scenarios respectively for the recessed breakwater model. Figure 3-10 and Figure 3-12 show the voltage gradient plots for the 320 kV and 400 kV scenarios respectively for the recessed breakwater model. The values for bipolar imbalance current can be obtained by scaling the reported maximum continuous current values by a factor of 1/150.

Dowden's Point Equipotential Contours (to 2 km) (DP_16_2109A – 0.38 ohm-m sea, 50 km depth)

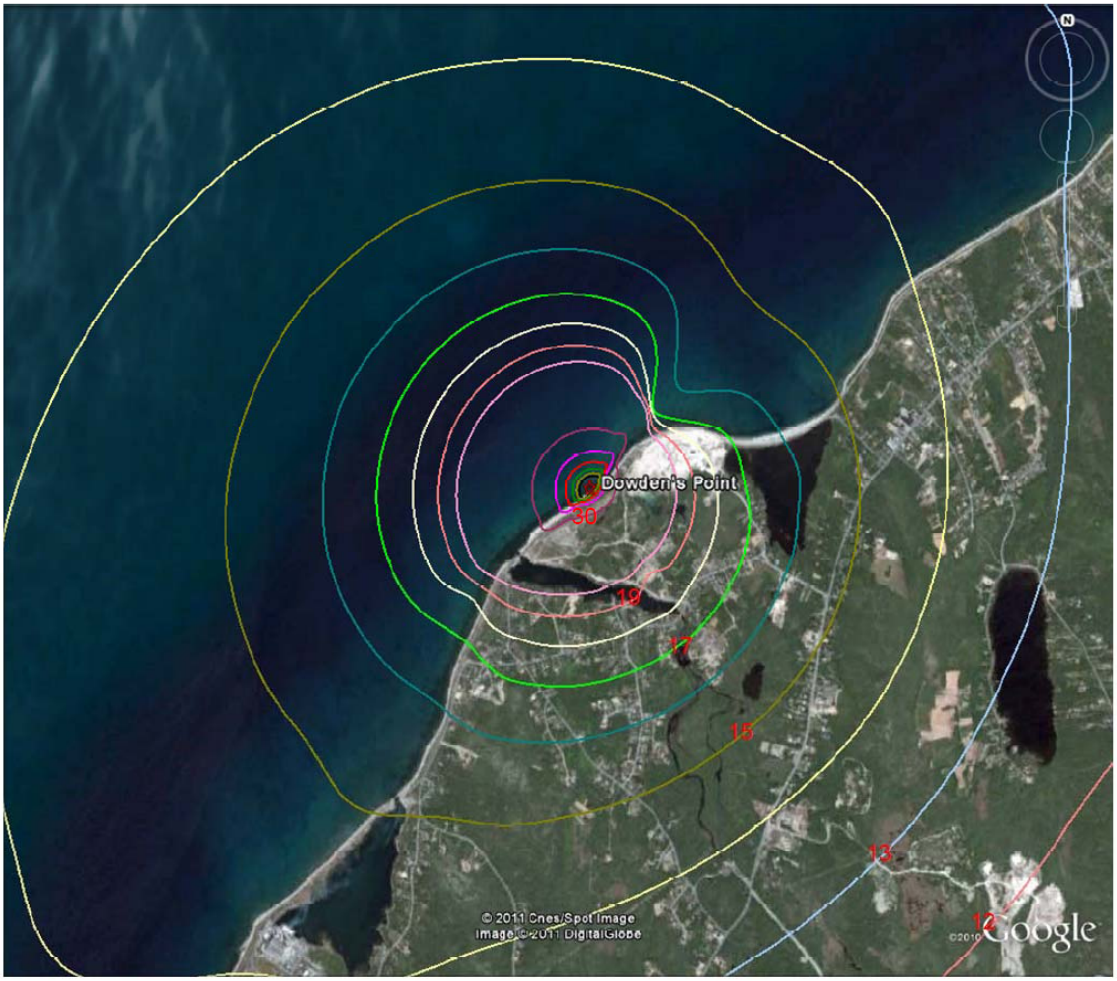

Figure 3-9: GPR Contours in the Vicinity of Dowden's Point (320 kV Option)

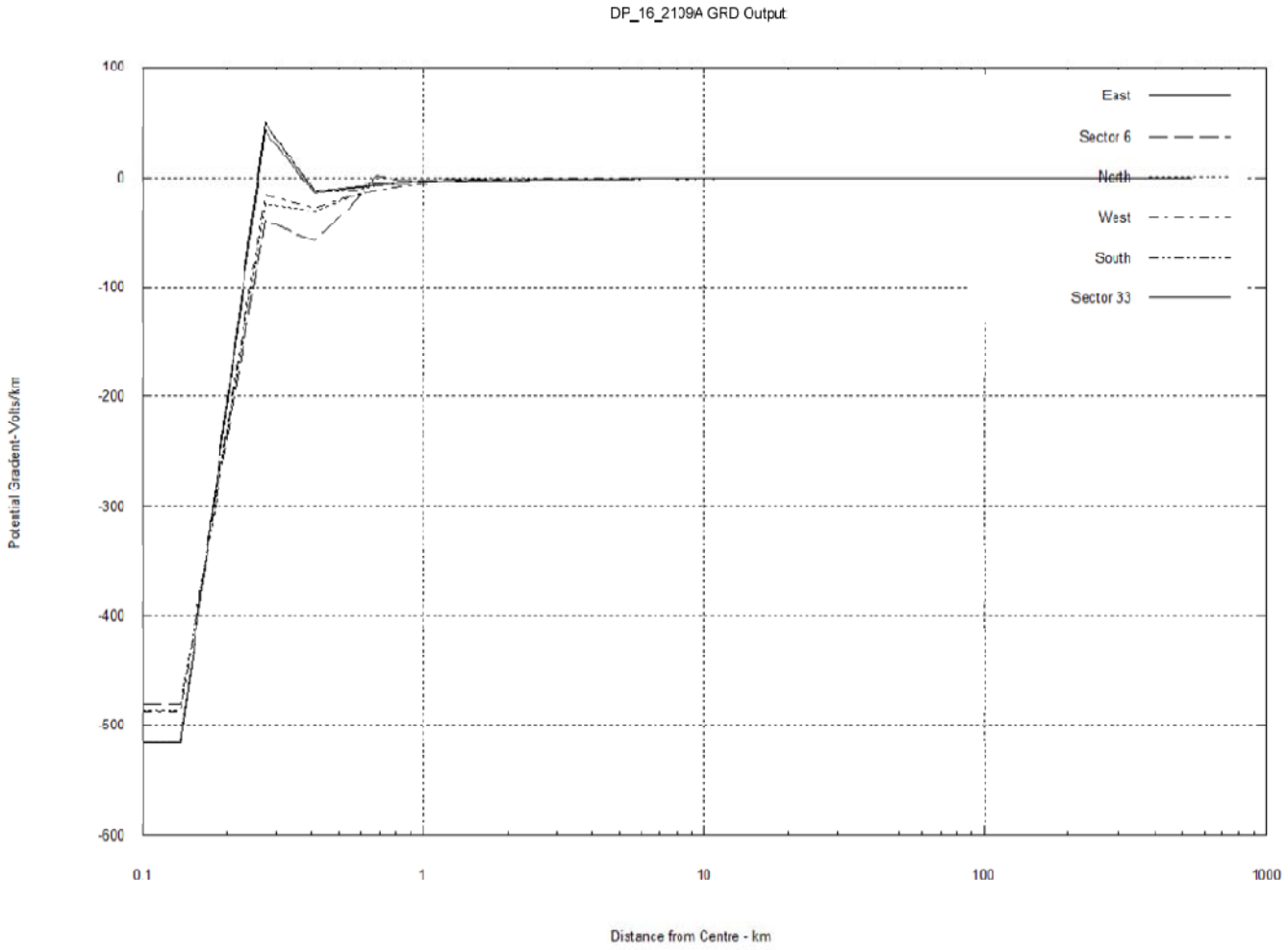

Figure 3-10: Voltage Gradients in the Vicinity of Dowden's Point (320 kV Option)

Dowden's Point Equipotential Contours (to 2 km) (DP_16_1688A – 0.38 ohm-m sea, 50 km depth)

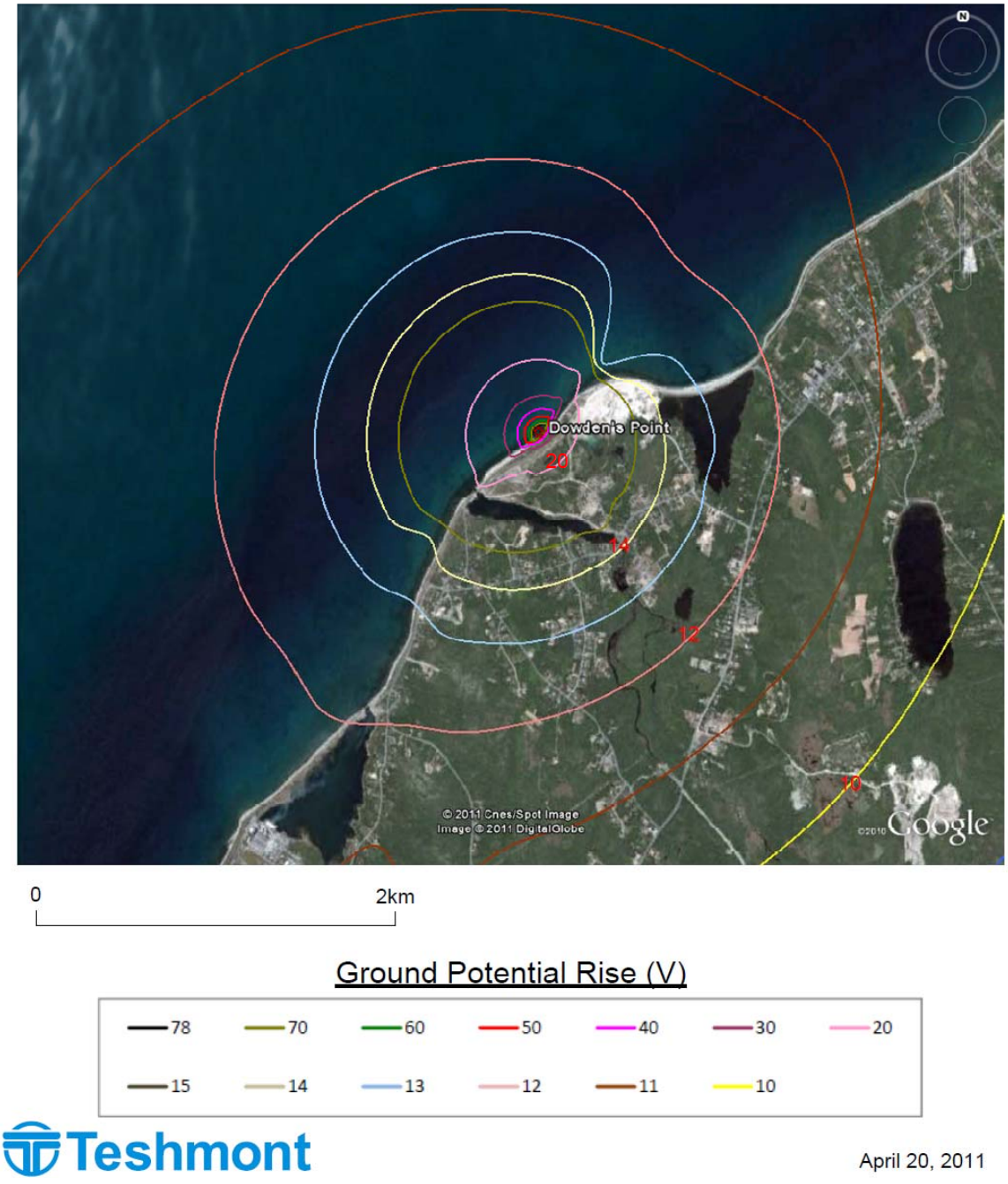

Figure 3-11: GPR Contours in the Vicinity of Dowden's Point (400 kV Option)

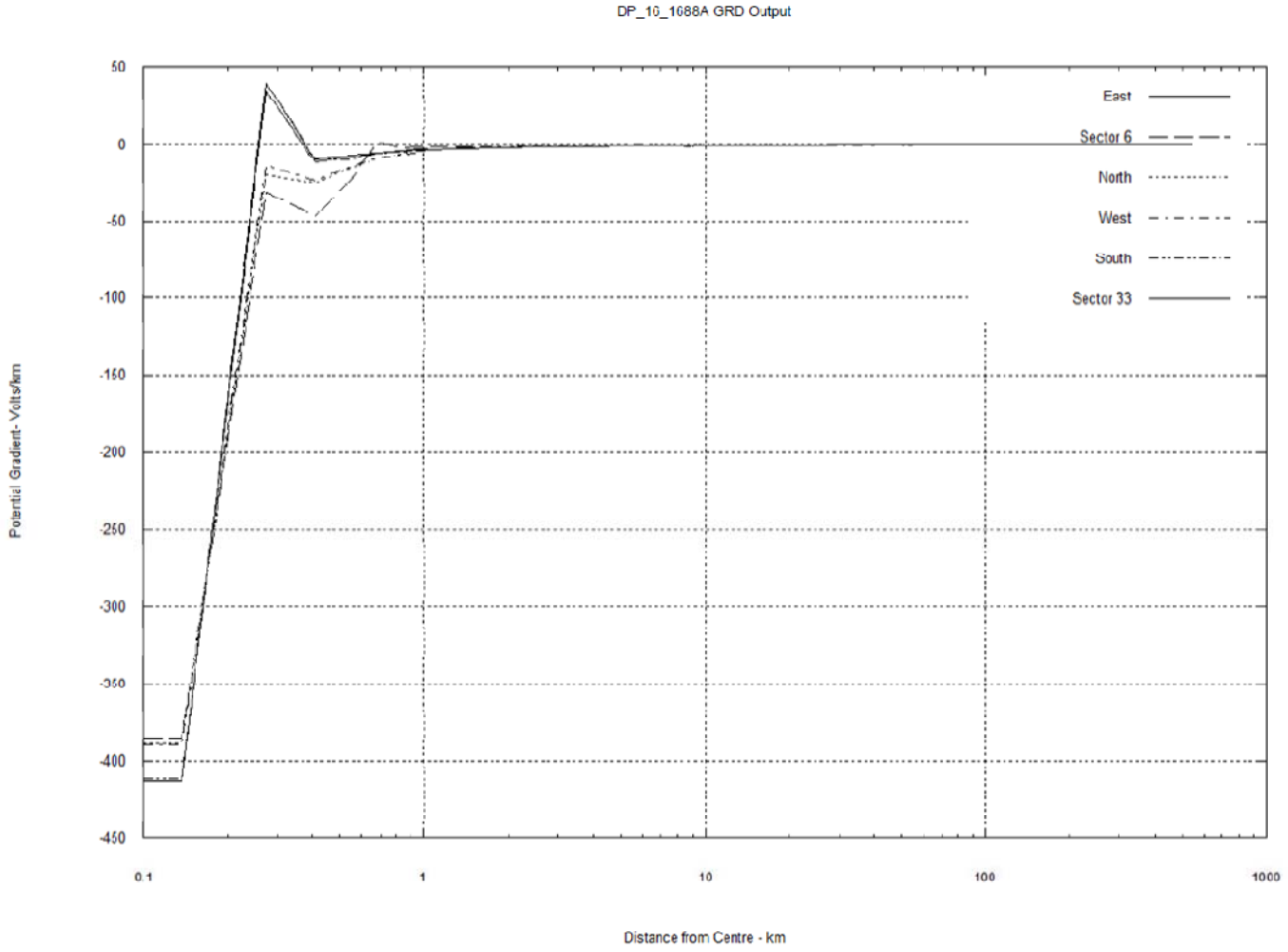

Figure 3-12: Voltage Gradients in the Vicinity of Dowden's Point (400 kV Option)

The GPR distribution outside the zone of influence for the extended breakwater design will be the same as that of the recessed breakwater design. The GPR at the electrode will be marginally lower because of better seawater exposure and a larger contact area between the breakwater and the sea. The GPR gradients will be lower on the seaside because of the lower current densities and will be lower on the landside because of the greater distance from the electrode elements. Therefore, the GPR modelling exercise is not repeated for the extended breakwater option.

3.1.3 **Safety Analysis**

The calculated GPR gradients for L'Anse au Diable in the sea, on the shoreline and on the breakwater are lower than the safe step potential defined [3] [4]. Table 3-3 compares the calculated values of GPR gradients versus the safe limits.

Table 3-3: LAD North Safety Analysis

Description	Calculated GPR Gradient [V/m]	Safe Limit [V/m]	Remarks
At the electrode elements	16.73	N/A	Access to the electrode elements is controlled.
On the breakwater	9.62	95	
In the water on the seaside of breakwater	< 1.25	1.25	

The calculated GPR gradients for Dowden's Point in the sea, on the shoreline and on the breakwater are lower than the safe step potential defined [3] [4]. Table 3-4 compares the calculated values of GPR gradients versus the safe limits.

Table 3-4: Dowden's Point Safety Analysis

Description	Calculated GPR Gradient [V/m]	Safe Limit [V/m]	Remarks
At the electrode elements	16.30	N/A	Access to the electrode elements is controlled.
On the breakwater	9.87	95	
In the water on the seaside of breakwater	< 1.25	1.25	

3.1.4 **Effect of GPR on Infrastructure**

A ground return current results in a ground potential rise in the vicinity of the electrode. DC stray currents will flow through conductive elements providing a connection between points of different potential. The magnitude of the dc stray current is a function of GPR differential and the dc resistance of the current path. DC stray currents may result in electrical interference to power system equipment and electrolytic corrosion of the immersed metallic structures in contact with the earth.

L'Anse au Diable North Electrode

The infrastructure near the LAD North electrode includes an overhead distribution system, a service marina, a few houses, a fur farm, and quarries. The future submarine cable terminal station may be located approximately 13 km southwest of the electrode location.

The potential difference across a typical structure of 100 m in length or smaller (e.g., marine service centre) will be negligible. In case the structure is connected to remote earth via a distribution circuit or any other conductive connection, the dc current will not cause significant corrosion to a large structure.

The dc stray current through the distribution system are lower than the acceptable limits of electrical interference for the distribution transformers and marginally exceed the electrolytic corrosion limits for a few distribution pole ground rods. These rods can be inspected and replaced as required and corrosion is not a concern.

Telephone lines and facilities in the area will not be affected. A ground potential of up to 70 V [4] does not cause any operational issues and does not constitute a safety hazard since the insulated telephone circuits do not allow stray current through the network, and the combined potential difference (a GPR of 70 V and a telephone loop voltage of 48 V) is a non-lethal hazard to the telephone company personnel. The actual GPR values are less than 70 V at the location of the houses and marine service centre.

Dowden's Point Electrode

The infrastructure in the vicinity of the electrode mainly includes generation, transmission and distribution systems; industrial installations; and marine infrastructure.

The dc stray currents injected into or collected from the transmission system through grounded transformer neutrals are below the typical acceptable limits that can affect the transformer's performance and it is not a concern. The currents through the transmisison line foundations and guywire anchors are below the tolerable limits that can jeopardize the integrity of these structures.

The potential difference across a typical bridge, fuel storage infrastructure associated with the Holyrood Generating Station, penstocks or structure of relatively small expanse will be negligible. If the connection to the remote earth is a concern for the system connected at the other end (e.g., distribution transformer), the system can be isolated.

3.1.5 Magnetic Field Effects

The magnetic field from the electrode cables and element will be greatest near the breakwater and the contribution of these current dipoles will diminish as one moves away from the electrode. The current through the body of sea water induces a magnetic field at the surface and is normally weak due to the low current density in the body of water.

This analysis does not take into account the electrode leads and hence the estimated magnetic field near the breakwater will not be representative of the actual magnetic field distribution. The magnetic field near the breakwater will be a function of the cable layout.

The calculation of the magnetic field is based on current values deduced from the GPR modelling between the soil volumes. The current flow between soil volumes is considered as a dipole to calculate the magnetic field contribution. As one moves into the sea where the soil volume centers are far apart, the magnetic field in the Z direction will not be representative and is not a concern since it does not contribute to the compass deviation.

The magnetic field is calculated at the surface of the water only for anodic operation. In cathodic operation, the dc magnetic field will be equal in magnitude but in the opposite direction as the field produced in anodic operation. The magnitude of the resultant field (earth magnetic intensity plus electrode magnetic intensity) will be different and will be oriented in a different direction. However, the compass deviations will be of the same order as the values reported in the tables below.

The induced magnetic effects are focussed on two aspects: compass deviations (i.e., magnetic field at 1 m above sea level) and marine life (i.e., magnetic field at 0 m above sea level).

L'Anse au Diable North Electrode – Compass Deviations

The magnetic field calculated for 320 kV and 400 kV options operating at the maximum continuous current up to a distance of 500 m are shown in Tables 3-5 and 3-6. The magnetic field beyond a distance of 500 m are insignificant, and hence are not reported. The calculations assume LAD North is operating as an anode. The observation points are identified in cylindrical coordinates (A_ρ, A_Φ, A_Z) and the magnetic field is given by (H_ρ, H_Φ, H_Z). The angles A_Φ and H_Φ are the compass headings in degrees, clockwise relative to True North.

At the time of this study, the horizontal component of the earth's magnetic field near LAD North was approximately 13.6 A/m and the field intensity was changing by approximately 0.03 A/m annually [3]. The angle of declination (between true north and magnetic north) was 338.6^o degree measured clockwise. The induced magnetic field associated with the normal bipolar imbalance are shown in Tables 3-7 and 3-8 up to a distance of 400 m.

The variables presented in the following tables are defined below:

Horizontal coordinate of observation point	A_ρ
Angle of observation point (w.r.t. True North)	A_Φ
Vertical coordinate of observation point	A_z
Horizontal component of induced magnetic field	H_ρ
Angle of induced magnetic field (w.r.t. True North)	H_Φ
Vertical component of induced magnetic field	H_z
Horizontal component of resultant magnetic field intensity (earth and induced)	$H_{res,\rho}$
Horizontal angle of deviation (w.r.t. Magnetic North)	α

Table 3-5: Magnetic Field Intensity, LAD North 320 kV, Monopolar Maximum Continuous Current

Point	Coordinates			Induced Magnetic Field Intensity			Resultant Magnetic Field Intensity	
A	A_ρ [m]	A_Φ [°]	A_z [m]	H_ρ [A/m]	H_Φ [°]	H_z [A/m]	$H_{res,\rho}$ [A/m]	α [°]
1	50	230.00	1	7.663	339.41	-5.414	21.288	0.30
2	50	207.08	1	10.915	312.26	-0.828	23.904	11.68
3	50	184.16	1	1.717	262.82	7.921	14.146	6.75
4	50	161.25	1	1.203	238.72	2.134	13.471	5.05
5	50	138.33	1	1.296	222.00	-1.511	13.097	5.08
6	50	92.49	1	2.272	175.87	-13.863	11.476	3.37
7	50	70.00	1	13.266	147.02	-8.998	2.729	76.70
8	100	230.00	1	2.455	320.14	3.936	15.973	2.79
9	100	207.08	1	1.395	292.11	6.930	14.621	3.97
10	100	184.16	1	0.749	250.30	2.554	13.668	3.14
11	100	161.25	1	0.479	235.82	0.492	13.527	1.98
12	100	138.33	1	0.459	225.61	-1.618	13.453	1.80
13	100	92.49	1	2.010	212.59	-1.413	12.550	7.45
14	100	70.00	1	2.469	164.43	-4.239	11.172	1.29
15	250	230.00	1	0.630	324.32	-3.369	14.236	0.62
16	250	207.08	1	0.647	309.35	1.155	14.194	1.28
17	250	184.16	1	0.213	235.81	0.637	13.580	0.88
18	250	161.25	1	0.098	246.79	0.056	13.622	0.41
19	250	138.33	1	0.143	232.41	-0.793	13.586	0.58
20	250	92.49	1	0.866	180.44	5.239	12.825	1.44
21	250	70.00	1	0.397	151.74	-0.334	13.230	0.20
22	500	230.00	1	0.078	325.15	-0.592	13.701	0.08
23	500	207.08	1	0.072	273.82	-0.403	13.656	0.27
24	500	184.16	1	0.045	251.99	0.109	13.628	0.19
25	500	161.25	1	0.026	239.34	0.024	13.621	0.11
26	500	138.33	1	0.029	228.04	-0.218	13.615	0.11
27	500	92.49	1	0.046	177.17	-0.255	13.581	0.06
28	500	70.00	1	0.072	153.74	-0.055	13.554	0.03

Table 3-6: Magnetic Field Intensity, LAD North 400 kV, Monopolar Maximum Continuous Current

Point	Coordinates			Induced Magnetic Field Intensity			Resultant Magnetic Field Intensity	
A	A_ρ [m]	A_Φ [°]	A_z [m]	H_ρ [A/m]	H_Φ [°]	H_z [A/m]	$H_{res,\rho}$ [A/m]	α [°]
1	50	230.00	1	6.133	339.41	-4.333	19.758	0.26
2	50	207.08	1	8.736	312.26	-0.663	21.803	10.23
3	50	184.16	1	1.374	262.82	6.340	14.026	5.45
4	50	161.25	1	0.963	238.72	1.708	13.494	4.03
5	50	138.33	1	1.037	222.00	-1.209	13.194	4.03
6	50	92.49	1	1.818	175.87	-11.095	11.901	2.60
7	50	70.00	1	10.618	147.02	-7.202	3.860	33.41
8	100	230.00	1	1.965	320.14	3.150	15.501	2.30
9	100	207.08	1	1.116	292.11	5.546	14.417	3.22
10	100	184.16	1	0.600	250.30	2.045	13.656	2.52
11	100	161.25	1	0.384	235.82	0.394	13.545	1.58
12	100	138.33	1	0.367	225.61	-1.295	13.486	1.44
13	100	92.49	1	1.609	212.59	-1.131	12.746	5.86
14	100	70.00	1	1.976	164.43	-3.393	11.661	0.99
15	250	230.00	1	0.504	324.32	-2.696	14.114	0.50
16	250	207.08	1	0.518	309.35	0.925	14.080	1.03
17	250	184.16	1	0.170	235.81	0.510	13.588	0.70
18	250	161.25	1	0.078	246.79	0.045	13.623	0.33
19	250	138.33	1	0.115	232.41	-0.635	13.594	0.46
20	250	92.49	1	0.693	180.44	4.194	12.984	1.14
21	250	70.00	1	0.318	151.74	-0.268	13.309	0.16
22	500	230.00	1	0.063	325.15	-0.474	13.686	0.06
23	500	207.08	1	0.057	273.82	-0.322	13.650	0.22
24	500	184.16	1	0.036	251.99	0.087	13.627	0.15
25	500	161.25	1	0.021	239.34	0.019	13.622	0.09
26	500	138.33	1	0.023	228.04	-0.175	13.617	0.09
27	500	92.49	1	0.037	177.17	-0.204	13.590	0.05
28	500	70.00	1	0.057	153.74	-0.044	13.568	0.02

Table 3-7: Magnetic Field Intensity, LAD North 320 kV, Bipolar 1% Imbalance Current

Point	Coordinates			Induced Magnetic Field Intensity			Resultant Magnetic Field Intensity	
A	A_ρ [m]	A_Φ [°]	A_z [m]	H_ρ [A/m]	H_Φ [°]	H_z [A/m]	$H_{res,\rho}$ [A/m]	α [°]
1	50	230.00	1	0.051	339.41	-0.036	13.676	0.00
2	50	207.08	1	0.073	312.26	-0.006	13.690	0.14
3	50	184.16	1	0.011	262.82	0.053	13.628	0.05
4	50	161.25	1	0.008	238.72	0.014	13.624	0.03
5	50	138.33	1	0.009	222.00	-0.010	13.621	0.03
6	50	92.49	1	0.015	175.87	-0.092	13.611	0.02
7	50	70.00	1	0.088	147.02	-0.060	13.538	0.07
8	100	230.00	1	0.016	320.14	0.026	13.641	0.02
9	100	207.08	1	0.009	292.11	0.046	13.631	0.03
10	100	184.16	1	0.005	250.30	0.017	13.625	0.02
11	100	161.25	1	0.003	235.82	0.003	13.624	0.01
12	100	138.33	1	0.003	225.61	-0.011	13.624	0.01
13	100	92.49	1	0.013	212.59	-0.009	13.617	0.05
14	100	70.00	1	0.016	164.43	-0.028	13.609	0.01
15	250	230.00	1	0.004	324.32	-0.022	13.629	0.00
16	250	207.08	1	0.004	309.35	0.008	13.629	0.01
17	250	184.16	1	0.001	235.81	0.004	13.625	0.01
18	250	161.25	1	0.001	246.79	0.000	13.625	0.00
19	250	138.33	1	0.001	232.41	-0.005	13.625	0.00
20	250	92.49	1	0.006	180.44	0.035	13.620	0.01
21	250	70.00	1	0.003	151.74	-0.002	13.622	0.00
22	400	230.00	1	0.001	328.19	-0.004	13.626	0.00
23	400	207.08	1	0.001	266.43	0.009	13.625	0.00
24	400	184.16	1	0.000	242.82	0.004	13.625	0.00
25	400	161.25	1	0.000	239.37	0.000	13.625	0.00
26	400	138.33	1	0.000	229.44	-0.002	13.625	0.00
27	400	92.49	1	0.000	173.94	-0.002	13.625	0.00
28	400	70.00	1	0.001	150.55	0.000	13.624	0.00

Table 3-8: Magnetic Field Intensity, LAD North 400 kV, Bipolar 1% Imbalance Current

Point	Coordinates			Induced Magnetic Field Intensity			Resultant Magnetic Field Intensity	
A	A_ρ [m]	A_Φ [°]	A_z [m]	H_ρ [A/m]	H_Φ [°]	H_z [A/m]	$H_{res,\rho}$ [A/m]	α [°]
1	50	230.00	1	0.041	339.41	-0.029	13.666	0.00
2	50	207.08	1	0.058	312.26	-0.004	13.677	0.11
3	50	184.16	1	0.009	262.82	0.042	13.627	0.04
4	50	161.25	1	0.006	238.72	0.011	13.624	0.03
5	50	138.33	1	0.007	222.00	-0.008	13.622	0.03
6	50	92.49	1	0.012	175.87	-0.074	13.613	0.02
7	50	70.00	1	0.071	147.02	-0.048	13.556	0.06
8	100	230.00	1	0.013	320.14	0.021	13.637	0.02
9	100	207.08	1	0.007	292.11	0.037	13.630	0.02
10	100	184.16	1	0.004	250.30	0.014	13.625	0.02
11	100	161.25	1	0.003	235.82	0.003	13.624	0.01
12	100	138.33	1	0.002	225.61	-0.009	13.624	0.01
13	100	92.49	1	0.011	212.59	-0.008	13.619	0.04
14	100	70.00	1	0.013	164.43	-0.023	13.612	0.01
15	250	230.00	1	0.003	324.32	-0.018	13.628	0.00
16	250	207.08	1	0.003	309.35	0.006	13.628	0.01
17	250	184.16	1	0.001	235.81	0.003	13.625	0.00
18	250	161.25	1	0.001	246.79	0.000	13.625	0.00
19	250	138.33	1	0.001	232.41	-0.004	13.625	0.00
20	250	92.49	1	0.005	180.44	0.028	13.621	0.01
21	250	70.00	1	0.002	151.74	-0.002	13.623	0.00
22	400	230.00	1	0.000	328.19	-0.003	13.625	0.00
23	400	207.08	1	0.001	266.43	0.008	13.625	0.00
24	400	184.16	1	0.000	242.82	0.003	13.625	0.00
25	400	161.25	1	0.000	239.37	0.000	13.625	0.00
26	400	138.33	1	0.000	229.44	-0.002	13.625	0.00
27	400	92.49	1	0.000	173.94	-0.002	13.625	0.00
28	400	70.00	1	0.000	150.55	0.000	13.625	0.00

The induced magnetic field from the electrode currents will interact with the natural earth magnetic field and will result in local distortions. The magnetic field in the horizontal plane will skew the earth horizontal magnetic field and can be a source of compass error. The worst case for compass error occurs along the line from the electrode parallel with the magnetic north, where the earth's magnetic field and the induced magnetic field from the electrode are orthogonal. Tables 3-5 to 3-8 above show the compass deviation error results. The angle of deviation is of concern in the radius of 500 m from the centre of the electrode installations for monopolar operation at maximum continuous current. The angles of deviation associated with bipolar imbalance currents are insignificant.

Figure 3-13 is the vector diagram of the earth magnetic field and HVdc electrode magnetic field and also illustrates the angle of deviation.

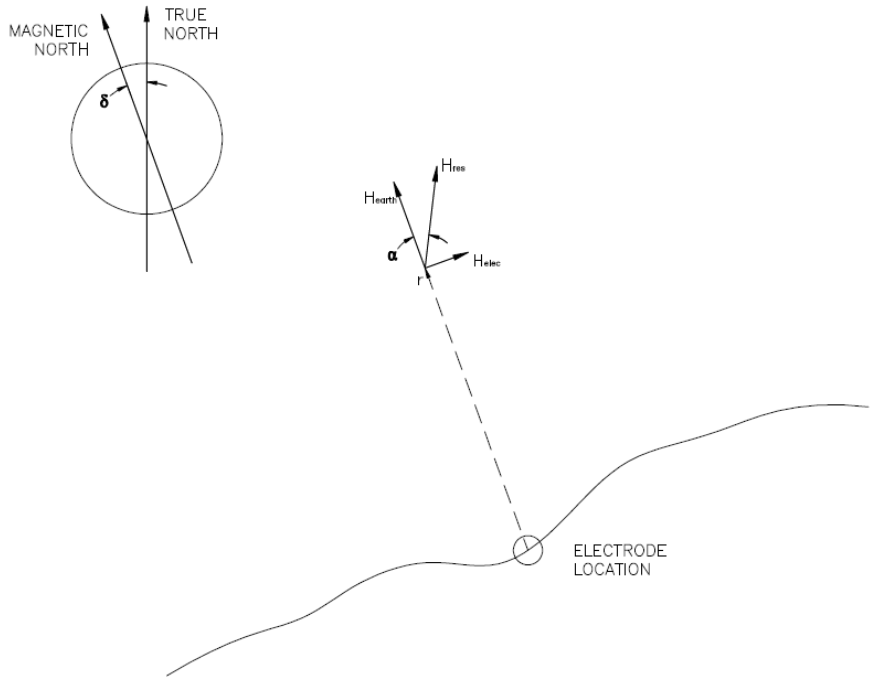

Figure 3-13: Magnetic Field and Compass Deviation

An angle of deviation of 0.5° or less is considered acceptable [10]. Nowadays, large ships and vessels use gyro compasses or GPS navigation, and magnetic compasses as back-up.

Dowden's Point Electrode – Compass Deviations

The discussions of the LAD North compass deviation are applicable to the Dowden's Point electrode installations. The calculated induced magnetic fields and the compass errors for the Dowden's Point electrode operating as an anode during maximum continuous current are shown in Table 3-9 and Table 3-10 for 320 kV and 400 kV HVdc transmission options respectively.

The induced magnetic field associated with the normal bipolar imbalance are shown in Tables 3-11 and 3-12.

At the time of this study, the horizontal component of the earth's magnetic field near Dowden's Point was approximately 15.7 A/m and was changing by approximately 0.03 A/m annually [3]. The angle of declination (between true north and magnetic north) was 340.7^{o} degree measured clockwise.

Table 3-9: Magnetic Field Intensity, Dowden's Point 320 kV, Monopolar Maximum Continuous Current

Point	Coordinates			Induced Magnetic Field Intensity			Resultant Magnetic Field Intensity	
A	A_ρ [m]	A_Φ [°]	A_z [m]	H_ρ [A/m]	H_Φ [°]	H_z [A/m]	$H_{res,\rho}$ [A/m]	α [°]
1	50	30.00	1	12.033	136.21	-40.854	6.861	46.57
2	50	7.08	1	15.345	120.77	64.792	10.588	68.40
3	50	344.16	1	1.412	94.86	18.794	15.145	4.88
4	50	321.25	1	0.680	72.12	10.269	15.666	2.49
5	50	298.33	1	0.480	41.71	6.379	15.907	1.51
6	50	275.41	1	0.439	8.10	4.052	16.060	0.72
7	50	252.49	1	0.364	343.00	2.369	16.033	0.05
8	50	230.00	1	0.300	319.63	0.843	15.949	0.39
9	100	30.00	1	3.733	124.79	-20.712	12.832	9.82
10	100	7.08	1	6.038	99.61	14.207	13.800	22.52
11	100	344.16	1	0.423	86.06	7.969	15.562	1.50
12	100	321.25	1	0.207	56.62	4.393	15.720	0.73
13	100	298.33	1	0.139	31.32	2.716	15.758	0.39
14	100	275.41	1	0.117	2.40	1.635	15.777	0.16
15	100	252.49	1	0.096	335.20	0.718	15.765	0.03
16	100	230.00	1	0.098	319.93	0.136	15.761	0.13
17	250	30.00	1	1.109	125.73	0.947	14.774	2.46
18	250	7.08	1	1.027	101.45	4.475	15.169	3.33
19	250	344.16	1	0.080	51.65	2.523	15.695	0.28
20	250	321.25	1	0.030	52.69	1.407	15.678	0.10
21	250	298.33	1	0.022	32.60	0.873	15.682	0.06
22	250	275.41	1	0.020	14.33	0.508	15.685	0.04
23	250	252.49	1	0.027	2.06	0.297	15.694	0.04
24	250	230.00	1	0.025	325.02	-0.079	15.693	0.02
25	500	30.00	1	0.111	121.97	-0.161	15.583	0.25
26	500	7.08	1	0.079	105.34	1.933	15.624	0.24
27	500	344.16	1	0.018	75.51	0.874	15.667	0.07
28	500	321.25	1	0.008	52.25	0.515	15.671	0.03
29	500	298.33	1	0.006	31.17	0.333	15.673	0.02
30	500	275.41	1	0.005	9.42	0.195	15.674	0.01
31	500	252.49	1	0.005	344.73	0.088	15.674	0.00
32	500	230.00	1	0.006	320.57	-0.028	15.674	0.01

Table 3-10: Magnetic Field Intensity, Dowden's Point 400 kV, Monopolar Maximum Continuous Current

Point	Coordinates			Induced Magnetic Field Intensity			Resultant Magnetic Field Intensity	
A	A_ρ [m]	A_Φ [°]	A_z [m]	H_ρ [A/m]	H_Φ [°]	H_z [A/m]	$H_{res,\rho}$ [A/m]	α [°]
1	50	30.00	1	9.630	136.21	-32.697	7.972	30.01
2	50	7.08	1	12.281	120.77	51.856	10.055	51.58
3	50	344.16	1	1.130	94.86	15.042	15.241	3.88
4	50	321.25	1	0.545	72.12	8.218	15.665	1.99
5	50	298.33	1	0.384	41.71	5.105	15.859	1.22
6	50	275.41	1	0.351	8.10	3.243	15.981	0.58
7	50	252.49	1	0.291	343.00	1.896	15.960	0.04
8	50	230.00	1	0.240	319.63	0.675	15.893	0.31
9	100	30.00	1	2.988	124.79	-16.577	13.363	7.53
10	100	7.08	1	4.833	99.61	11.371	13.986	17.60
11	100	344.16	1	0.339	86.06	6.378	15.582	1.20
12	100	321.25	1	0.166	56.62	3.516	15.710	0.59
13	100	298.33	1	0.111	31.32	2.174	15.740	0.31
14	100	275.41	1	0.094	2.40	1.308	15.756	0.13
15	100	252.49	1	0.077	335.20	0.574	15.746	0.03
16	100	230.00	1	0.079	319.93	0.109	15.743	0.10
17	250	30.00	1	0.888	125.73	0.758	14.950	1.95
18	250	7.08	1	0.822	101.45	3.581	15.265	2.65
19	250	344.16	1	0.064	51.65	2.020	15.690	0.22
20	250	321.25	1	0.024	52.69	1.126	15.676	0.08
21	250	298.33	1	0.017	32.60	0.699	15.680	0.05
22	250	275.41	1	0.016	14.33	0.407	15.682	0.03
23	250	252.49	1	0.021	2.06	0.238	15.689	0.03
24	250	230.00	1	0.020	325.02	-0.063	15.688	0.02
25	500	30.00	1	0.089	121.97	-0.129	15.600	0.20
26	500	7.08	1	0.063	105.34	1.547	15.633	0.19
27	500	344.16	1	0.014	75.51	0.700	15.668	0.05
28	500	321.25	1	0.006	52.25	0.412	15.671	0.02
29	500	298.33	1	0.005	31.17	0.267	15.672	0.01
30	500	275.41	1	0.004	9.42	0.156	15.673	0.01
31	500	252.49	1	0.004	344.73	0.071	15.673	0.00
32	500	230.00	1	0.005	320.57	-0.023	15.673	0.01

Table 3-11: Magnetic Field Intensity, Dowden's Point 320 kV, Bipolar 1% Imbalance Current

Point	Coordinates			Induced Magnetic Field Intensity			Resultant Magnetic Field Intensity	
A	A_ρ [m]	A_Φ [°]	A_z [m]	H_ρ [A/m]	H_Φ [°]	H_z [A/m]	$H_{res,\rho}$ [A/m]	α [°]
1	50	30.00	1	0.120	136.21	-0.409	15.559	0.18
2	50	7.08	1	0.153	120.77	0.648	15.551	0.36
3	50	344.16	1	0.014	94.86	0.188	15.663	0.05
4	50	321.25	1	0.007	72.12	0.103	15.669	0.02
5	50	298.33	1	0.005	41.71	0.064	15.671	0.02
6	50	275.41	1	0.004	8.10	0.041	15.673	0.01
7	50	252.49	1	0.004	343.00	0.024	15.673	0.00
8	50	230.00	1	0.003	319.63	0.008	15.672	0.00
9	100	30.00	1	0.037	124.79	-0.207	15.639	0.08
10	100	7.08	1	0.060	99.61	0.142	15.640	0.19
11	100	344.16	1	0.004	86.06	0.080	15.668	0.01
12	100	321.25	1	0.002	56.62	0.044	15.669	0.01
13	100	298.33	1	0.001	31.32	0.027	15.670	0.00
14	100	275.41	1	0.001	2.40	0.016	15.670	0.00
15	100	252.49	1	0.001	335.20	0.007	15.670	0.00
16	100	230.00	1	0.001	319.93	0.001	15.670	0.00
17	250	30.00	1	0.011	125.73	0.009	15.660	0.02
18	250	7.08	1	0.010	101.45	0.045	15.664	0.03
19	250	344.16	1	0.001	51.65	0.025	15.669	0.00
20	250	321.25	1	0.000	52.69	0.014	15.669	0.00
21	250	298.33	1	0.000	32.60	0.009	15.669	0.00
22	250	275.41	1	0.000	14.33	0.005	15.669	0.00
23	250	252.49	1	0.000	2.06	0.003	15.669	0.00
24	250	230.00	1	0.000	325.02	-0.001	15.669	0.00
25	400	30.00	1	0.002	120.89	-0.001	15.667	0.00
26	400	7.08	1	0.001	105.29	0.030	15.668	0.00
27	400	344.16	1	0.000	73.62	0.012	15.669	0.00
28	400	321.25	1	0.000	51.39	0.007	15.669	0.00
29	400	298.33	1	0.000	31.51	0.005	15.669	0.00
30	400	275.41	1	0.000	9.91	0.003	15.669	0.00
31	400	252.49	1	0.000	345.38	0.001	15.669	0.00
32	400	230.00	1	0.000	320.58	0.000	15.669	0.00

Table 3-12: Magnetic Field Intensity, Dowden's Point 400 kV, Bipolar 1% Imbalance Current

Point	Coordinates			Induced Magnetic Field Intensity			Resultant Magnetic Field Intensity	
A	A_ρ [m]	A_Φ [°]	A_z [m]	H_ρ [A/m]	H_Φ [°]	H_z [A/m]	$H_{res,\rho}$ [A/m]	α [°]
1	50	30.00	1	0.064	136.21	-0.218	15.610	0.10
2	50	7.08	1	0.082	120.77	0.346	15.606	0.19
3	50	344.16	1	0.008	94.86	0.100	15.666	0.03
4	50	321.25	1	0.004	72.12	0.055	15.669	0.01
5	50	298.33	1	0.003	41.71	0.034	15.670	0.01
6	50	275.41	1	0.002	8.10	0.022	15.671	0.00
7	50	252.49	1	0.002	343.00	0.013	15.671	0.00
8	50	230.00	1	0.002	319.63	0.004	15.670	0.00
9	100	30.00	1	0.020	124.79	-0.110	15.653	0.04
10	100	7.08	1	0.032	99.61	0.076	15.653	0.10
11	100	344.16	1	0.002	86.06	0.043	15.668	0.01
12	100	321.25	1	0.001	56.62	0.023	15.669	0.00
13	100	298.33	1	0.001	31.32	0.014	15.669	0.00
14	100	275.41	1	0.001	2.40	0.009	15.669	0.00
15	100	252.49	1	0.001	335.20	0.004	15.669	0.00
16	100	230.00	1	0.001	319.93	0.001	15.669	0.00
17	250	30.00	1	0.006	125.73	0.005	15.664	0.01
18	250	7.08	1	0.005	101.45	0.024	15.666	0.02
19	250	344.16	1	0.000	51.65	0.013	15.669	0.00
20	250	321.25	1	0.000	52.69	0.008	15.669	0.00
21	250	298.33	1	0.000	32.60	0.005	15.669	0.00
22	250	275.41	1	0.000	14.33	0.003	15.669	0.00
23	250	252.49	1	0.000	2.06	0.002	15.669	0.00
24	250	230.00	1	0.000	325.02	0.000	15.669	0.00
25	400	30.00	1	0.001	120.89	-0.001	15.668	0.00
26	400	7.08	1	0.001	105.29	0.016	15.668	0.00
27	400	344.16	1	0.000	73.62	0.007	15.669	0.00
28	400	321.25	1	0.000	51.39	0.004	15.669	0.00
29	400	298.33	1	0.000	31.51	0.002	15.669	0.00
30	400	275.41	1	0.000	9.91	0.001	15.669	0.00
31	400	252.49	1	0.000	345.38	0.001	15.669	0.00
32	400	230.00	1	0.000	320.58	0.000	15.669	0.00

The induced magnetic field modelling presented above was completed for Option 2, a breakwater at the shoreline. This analysis also applies to Option 1, a breakwater extended into the sea. However the induced magnetic field profile will extend into the sea by a distance equal to the breakwater extension into the sea.

L'Anse au Diable North Electrode – Marine Environment

The magnetic fields calculated for the 320 kV and 400 kV scenarios operating at the maximum continuous current up to a distance of 500 m are shown in Tables 3-13 and Table 3-14. The magnetic fields calculated for the 320 kV and 400 kV scenarios operating during bipolar operations for normal system imbalances up to a distance of 400 m are shown in Tables 3-15 and Table 3-16. The calculations assume LAD North is operating as an anode. The magnetic field is presented as magnetic flux density for ease of comparison with the published literature on the effects of magnetic fields on marine life. The induced magnetic field density at the surface is higher than at any other point in the water because of partial cancellation of flux from the top layer of water. The induced flux densities will be zero at a point where currents in the water above and below the point are equal. The flux intensity at the bottom of the sea will be less than at the surface and in the opposite direction (about the z-axis). The resultant magnetic field, vector sum of the induced electrode and the natural earth field, reported in these tables include resultant horizontal magnetic field and its angle of deviation, vertical (z-axis) magnetic field, and absolute resultant magnetic field at the sea surface corresponding to the low tide elevation.

The variables presented in the following tables are defined below:

Horizontal coordinate of observation point	A_ρ
Angle of observation point (w.r.t. True North)	A_Φ
Vertical coordinate of observation point	A_z
Horizontal component of induced magnetic field	B_ρ
Angle of induced magnetic field (w.r.t. True North)	B_Φ
Vertical component of induced magnetic field	B_z
Horizontal component of resultant magnetic field	$B_{res,\rho}$
Veritcal component of resultant magnetic field	$B_{res,z}$
Magnitude of resultant magnetic field (Earth and Induced)	$\lvert \mathbf{B}_{res} \rvert$
Horizontal component of resultant magnetic field intensity	$B_{res,\rho}$
Horizontal angle of deviation (w.r.t. Magnetic North)	α

Table 3-13: Magnetic Flux Density, LAD North 320 kV, Monopolar Maximum Continuous Current

Point	Coordinates			Induced Magnetic Flux Density			Resultant Magnetic Flux Density			
	A_ρ [m]	A_Φ [°]	A_z [m]	B_ρ [μT]	B_Φ [°]	B_z [μT]	$B_{res,\rho}$ [μT]	$B_{res,z}$ [μT]	$\lvert B_{res}\rvert$ [μT]	α [°]
1	50	230.00	0	1.046	347.85	-6.885	18.154	43.869	47.48	0.53
2	50	207.08	0	1.140	311.17	-3.485	18.141	47.269	50.63	1.66
3	50	184.16	0	1.401	247.78	10.120	17.159	60.874	63.25	4.68
4	50	161.25	0	1.283	233.76	2.721	16.839	53.475	56.06	4.22
5	50	138.33	0	1.375	222.92	-1.952	16.572	48.802	51.54	4.29
6	50	92.49	0	1.513	187.67	-17.414	15.816	33.340	36.90	2.67
7	50	70.00	0	1.758	146.31	-12.392	15.408	38.362	41.34	1.39
8	100	230.00	0	0.551	332.58	5.053	17.669	55.807	58.54	0.19
9	100	207.08	0	0.606	284.13	8.561	17.481	59.315	61.84	1.62
10	100	184.16	0	0.800	245.76	3.239	17.100	53.993	56.64	2.68
11	100	161.25	0	0.550	233.46	0.625	16.986	51.379	54.11	1.79
12	100	138.33	0	0.463	219.95	-2.046	16.904	48.708	51.56	1.38
13	100	92.49	0	0.619	194.77	-1.317	16.625	49.437	52.16	1.26
14	100	70.00	0	0.658	157.89	-5.443	16.463	45.311	48.21	0.03
15	250	230.00	0	0.317	335.36	-4.245	17.437	46.509	49.67	0.06
16	250	207.08	0	0.603	327.85	1.414	17.714	52.168	55.09	0.36
17	250	184.16	0	0.251	236.26	0.794	17.069	51.548	54.30	0.82
18	250	161.25	0	0.118	246.56	0.071	17.117	50.825	53.63	0.40
19	250	138.33	0	0.144	241.99	-0.999	17.105	49.755	52.61	0.48
20	250	92.49	0	0.284	166.16	6.690	16.840	57.444	59.86	0.13
21	250	70.00	0	0.167	154.16	-0.430	16.955	50.324	53.10	0.04
22	500	230.00	0	0.087	329.42	-0.744	17.207	50.010	52.89	0.05
23	500	207.08	0	0.074	282.03	-0.506	17.162	50.248	53.10	0.21
24	500	184.16	0	0.046	254.14	0.137	17.126	50.891	53.70	0.15
25	500	161.25	0	0.032	239.58	0.030	17.116	50.784	53.59	0.11
26	500	138.33	0	0.032	228.78	-0.275	17.110	50.479	53.30	0.10
27	500	92.49	0	0.041	178.97	-0.321	17.083	50.433	53.25	0.05
28	500	70.00	0	0.066	153.54	-0.069	17.055	50.685	53.48	0.02

Table 3-14: Magnetic Flux Density, LAD North 400 kV, Monopolar Maximum Continuous Current

Point	Coordinates			Induced Magnetic Flux Density			Resultant Magnetic Flux Density			
	A_ρ [m]	A_Φ [°]	A_z [m]	B_ρ [µT]	B_Φ [°]	B_z [µT]	$B_{res,\rho}$ [µT]	$B_{res,z}$ [µT]	$\lvert B_{res}\rvert$ [µT]	α [°]
1	50	230.00	0	0.837	347.85	-5.510	17.948	45.244	48.67	0.43
2	50	207.08	0	0.913	311.17	-2.789	17.936	47.965	51.21	1.34
3	50	184.16	0	1.121	247.78	8.099	17.142	58.853	61.30	3.75
4	50	161.25	0	1.027	233.76	2.178	16.888	52.932	55.56	3.37
5	50	138.33	0	1.100	222.92	-1.563	16.674	49.191	51.94	3.41
6	50	92.49	0	1.211	187.67	-13.938	16.074	36.816	40.17	2.10
7	50	70.00	0	1.407	146.31	-9.918	15.749	40.836	43.77	1.09
8	100	230.00	0	0.441	332.58	4.044	17.560	54.798	57.54	0.15
9	100	207.08	0	0.485	284.13	6.852	17.408	57.606	60.18	1.30
10	100	184.16	0	0.640	245.76	2.593	17.102	53.347	56.02	2.14
11	100	161.25	0	0.440	233.46	0.500	17.012	51.254	54.00	1.43
12	100	138.33	0	0.371	219.95	-1.637	16.946	49.117	51.96	1.10
13	100	92.49	0	0.496	194.77	-1.054	16.724	49.700	52.44	1.00
14	100	70.00	0	0.527	157.89	-4.356	16.594	46.398	49.28	0.02
15	250	230.00	0	0.253	335.36	-3.398	17.374	47.356	50.44	0.05
16	250	207.08	0	0.482	327.85	1.132	17.595	51.886	54.79	0.29
17	250	184.16	0	0.201	236.26	0.636	17.079	51.390	54.15	0.66
18	250	161.25	0	0.095	246.56	0.057	17.118	50.811	53.62	0.32
19	250	138.33	0	0.116	241.99	-0.800	17.108	49.954	52.80	0.38
20	250	92.49	0	0.227	166.16	5.355	16.896	56.109	58.60	0.10
21	250	70.00	0	0.134	154.16	-0.344	16.988	50.410	53.20	0.03
22	500	230.00	0	0.069	329.42	-0.595	17.189	50.159	53.02	0.04
23	500	207.08	0	0.059	282.03	-0.405	17.154	50.349	53.19	0.17
24	500	184.16	0	0.037	254.14	0.110	17.125	50.864	53.67	0.12
25	500	161.25	0	0.026	239.58	0.024	17.117	50.778	53.59	0.08
26	500	138.33	0	0.026	228.78	-0.220	17.112	50.534	53.35	0.08
27	500	92.49	0	0.033	178.97	-0.257	17.090	50.497	53.31	0.04
28	500	70.00	0	0.053	153.54	-0.056	17.068	50.698	53.49	0.02

Table 3-15: Magnetic Flux Density, LAD North 320 kV, Bipolar 1% Imbalance Current

Point	Coordinates			Induced Magnetic Flux Density			Resultant Magnetic Flux Density			
	A_ρ [m]	A_Φ [°]	A_z [m]	B_ρ [μT]	B_Φ [°]	B_z [μT]	$B_{res,\rho}$ [μT]	$B_{res,z}$ [μT]	$\lvert B_{res}\rvert$ [μT]	α [°]
1	50	230.00	0	0.007	347.85	-0.046	17.128	50.708	53.52	0.00
2	50	207.08	0	0.008	311.17	-0.023	17.128	50.731	53.54	0.01
3	50	184.16	0	0.009	247.78	0.067	17.121	50.821	53.63	0.03
4	50	161.25	0	0.009	233.76	0.018	17.119	50.772	53.58	0.03
5	50	138.33	0	0.009	222.92	-0.013	17.117	50.741	53.55	0.03
6	50	92.49	0	0.010	187.67	-0.116	17.112	50.638	53.45	0.02
7	50	70.00	0	0.012	146.31	-0.083	17.110	50.671	53.48	0.01
8	100	230.00	0	0.004	332.58	0.034	17.125	50.788	53.60	0.00
9	100	207.08	0	0.004	284.13	0.057	17.123	50.811	53.62	0.01
10	100	184.16	0	0.005	245.76	0.022	17.121	50.776	53.58	0.02
11	100	161.25	0	0.004	233.46	0.004	17.120	50.758	53.57	0.01
12	100	138.33	0	0.003	219.95	-0.014	17.120	50.740	53.55	0.01
13	100	92.49	0	0.004	194.77	-0.009	17.118	50.745	53.55	0.01
14	100	70.00	0	0.004	157.89	-0.036	17.117	50.718	53.53	0.00
15	250	230.00	0	0.002	335.36	-0.028	17.123	50.726	53.54	0.00
16	250	207.08	0	0.004	327.85	0.009	17.125	50.763	53.57	0.00
17	250	184.16	0	0.002	236.26	0.005	17.121	50.759	53.57	0.01
18	250	161.25	0	0.001	246.56	0.000	17.121	50.754	53.56	0.00
19	250	138.33	0	0.001	241.99	-0.007	17.121	50.747	53.56	0.00
20	250	92.49	0	0.002	166.16	0.045	17.119	50.799	53.61	0.00
21	250	70.00	0	0.001	154.16	-0.003	17.120	50.751	53.56	0.00
22	400	230.00	0	0.001	337.61	-0.004	17.122	50.750	53.56	0.00
23	400	207.08	0	0.001	271.20	0.012	17.121	50.766	53.58	0.00
24	400	184.16	0	0.000	243.79	0.005	17.121	50.759	53.57	0.00
25	400	161.25	0	0.000	239.37	0.000	17.121	50.754	53.56	0.00
26	400	138.33	0	0.000	230.45	-0.002	17.121	50.752	53.56	0.00
27	400	92.49	0	0.000	177.17	-0.003	17.121	50.751	53.56	0.00
28	400	70.00	0	0.000	151.31	0.000	17.121	50.754	53.56	0.00

Table 3-16: Magnetic Flux Density, LAD North 400 kV, Bipolar 1% Imbalance Current

Point	Coordinates			Induced Magnetic Flux Density			Resultant Magnetic Flux Density			
	A_ρ [m]	A_Φ [°]	A_z [m]	B_ρ [μT]	B_Φ [°]	B_z [μT]	$B_{res,\rho}$ [μT]	$B_{res,z}$ [μT]	$\lvert B_{res}\rvert$ [μT]	α [°]
1	50	230.00	0	0.006	347.85	-0.037	17.127	50.717	53.53	0.00
2	50	207.08	0	0.006	311.17	-0.019	17.126	50.735	53.55	0.01
3	50	184.16	0	0.007	247.78	0.054	17.121	50.808	53.62	0.03
4	50	161.25	0	0.007	233.76	0.015	17.119	50.769	53.58	0.02
5	50	138.33	0	0.007	222.92	-0.010	17.118	50.744	53.55	0.02
6	50	92.49	0	0.008	187.67	-0.093	17.114	50.661	53.47	0.01
7	50	70.00	0	0.009	146.31	-0.066	17.112	50.688	53.50	0.01
8	100	230.00	0	0.003	332.58	0.027	17.124	50.781	53.59	0.00
9	100	207.08	0	0.003	284.13	0.046	17.123	50.800	53.61	0.01
10	100	184.16	0	0.004	245.76	0.017	17.121	50.771	53.58	0.01
11	100	161.25	0	0.003	233.46	0.003	17.120	50.757	53.57	0.01
12	100	138.33	0	0.002	219.95	-0.011	17.120	50.743	53.55	0.01
13	100	92.49	0	0.003	194.77	-0.007	17.118	50.747	53.56	0.01
14	100	70.00	0	0.004	157.89	-0.029	17.117	50.725	53.54	0.00
15	250	230.00	0	0.002	335.36	-0.023	17.123	50.731	53.54	0.00
16	250	207.08	0	0.003	327.85	0.008	17.124	50.762	53.57	0.00
17	250	184.16	0	0.001	236.26	0.004	17.121	50.758	53.57	0.00
18	250	161.25	0	0.001	246.56	0.000	17.121	50.754	53.56	0.00
19	250	138.33	0	0.001	241.99	-0.005	17.121	50.749	53.56	0.00
20	250	92.49	0	0.002	166.16	0.036	17.120	50.790	53.60	0.00
21	250	70.00	0	0.001	154.16	-0.002	17.120	50.752	53.56	0.00
22	400	230.00	0	0.000	337.61	-0.004	17.121	50.750	53.56	0.00
23	400	207.08	0	0.001	271.20	0.010	17.121	50.764	53.57	0.00
24	400	184.16	0	0.000	243.79	0.004	17.121	50.758	53.57	0.00
25	400	161.25	0	0.000	239.37	0.000	17.121	50.754	53.56	0.00
26	400	138.33	0	0.000	230.45	-0.002	17.121	50.752	53.56	0.00
27	400	92.49	0	0.000	177.17	-0.002	17.121	50.752	53.56	0.00
28	400	70.00	0	0.000	151.31	0.000	17.121	50.754	53.56	0.00

Dowden's Point Electrode – Marine Environment

The magnetic fields calculated for the 320 kV and 400 kV scenarios operating at the maximum continuous current up to a distance of 500 m are shown in Tables 3-17 and Table 3-18. The magnetic field calculated for 320 kV and 400 kV options operating during bipolar operations for normal system imbalances up to a distance of 400 m are shown in Tables 3-19 and Table 3-20. The calculations assume Dowden's Point is operating as an anode. The magnetic field is presented as magnetic flux density for comparison with the published literature on

the effects of magnetic fields on marine life. The induced magnetic field density at the surface is higher than at any other point in the water because of partial cancellation of flux from the top layer of water.

Table 3-17: Magnetic Flux Density, Dowden's Point 320 kV, Monopolar Maximum Continuous Current

Point	Coordinates			Induced Magnetic Flux Density			Resultant Magnetic Flux Density			
	A_ρ [m]	A_Φ [°]	A_z [m]	B_ρ [μT]	B_Φ [°]	B_z [μT]	$B_{res,\rho}$ [μT]	$B_{res,z}$ [μT]	$\lvert B_{res}\rvert$ [μT]	α [°]
1	50	30.00	0	2.955	131.54	-53.007	17.169	-5.575	18.05	4.81
2	50	7.08	0	5.393	105.69	85.286	17.173	132.718	133.82	14.90
3	50	344.16	0	0.834	73.31	23.711	19.669	71.143	73.81	2.43
4	50	321.25	0	0.587	49.17	12.936	19.913	60.368	63.57	1.57
5	50	298.33	0	0.535	22.55	8.010	20.092	55.442	58.97	1.02
6	50	275.41	0	0.543	355.67	5.088	20.215	52.520	56.28	0.40
7	50	252.49	0	0.489	333.68	2.996	20.176	50.428	54.31	0.17
8	50	230.00	0	0.428	314.20	1.059	20.074	48.491	52.48	0.54
9	100	30.00	0	1.357	123.67	-26.432	18.624	21.000	28.07	2.51
10	100	7.08	0	2.310	100.62	17.078	18.645	64.510	67.15	6.16
11	100	344.16	0	0.348	71.18	10.044	19.690	57.476	60.76	1.01
12	100	321.25	0	0.226	40.90	5.526	19.803	52.958	56.54	0.57
13	100	298.33	0	0.174	18.41	3.413	19.828	50.845	54.57	0.31
14	100	275.41	0	0.153	354.37	2.048	19.839	49.480	53.31	0.10
15	100	252.49	0	0.123	336.23	0.899	19.813	48.331	52.23	0.03
16	100	230.00	0	0.116	318.12	0.171	19.798	47.603	51.56	0.13
17	250	30.00	0	0.719	126.46	1.208	19.099	48.640	52.26	1.21
18	250	7.08	0	0.580	103.45	5.586	19.382	53.018	56.45	1.44
19	250	344.16	0	0.090	43.18	3.167	19.732	50.599	54.31	0.23
20	250	321.25	0	0.035	40.21	1.769	19.708	49.201	53.00	0.09
21	250	298.33	0	0.028	22.58	1.097	19.711	48.529	52.38	0.05
22	250	275.41	0	0.026	6.50	0.639	19.713	48.071	51.96	0.03
23	250	252.49	0	0.024	340.03	0.376	19.714	47.808	51.71	0.00
24	250	230	0	0.024	322.90	-0.099	19.713	47.333	51.27	0.02
25	500	30	0	0.085	122.35	-0.203	19.623	47.229	51.14	0.15
26	500	7.081688	0	0.069	103.93	2.430	19.652	49.862	53.60	0.17
27	500	344.1634	0	0.019	67.79	1.099	19.691	48.531	52.37	0.06
28	500	321.2451	0	0.010	44.29	0.648	19.694	48.080	51.96	0.03
29	500	298.3268	0	0.008	24.52	0.419	19.696	47.851	51.75	0.02
30	500	275.4084	0	0.007	4.45	0.245	19.696	47.677	51.59	0.01
31	500	252.4901	0	0.007	342.33	0.111	19.697	47.543	51.46	0.00
32	500	230	0	0.007	321.10	-0.036	19.697	47.396	51.33	0.01

Table 3-18: Magnetic Flux Density, Dowden's Point 400 kV, Monopolar Maximum Continuous Current

Point	Coordinates			Induced Magnetic Flux Density			Resultant Magnetic Flux Density			
	A_ρ [m]	A_Φ [°]	A_z [m]	B_ρ [μT]	B_Φ [°]	B_z [μT]	$B_{res,\rho}$ [μT]	$B_{res,z}$ [μT]	$\lvert B_{res}\rvert$ [μT]	α [°]
1	50	30.00	0	2.365	131.54	-42.424	17.662	5.008	18.36	3.74
2	50	7.08	0	4.317	105.69	68.258	17.572	115.690	117.02	11.61
3	50	344.16	0	0.668	73.31	18.977	19.671	66.409	69.26	1.94
4	50	321.25	0	0.470	49.17	10.353	19.867	57.785	61.11	1.26
5	50	298.33	0	0.428	22.55	6.411	20.011	53.843	57.44	0.82
6	50	275.41	0	0.435	355.67	4.072	20.110	51.504	55.29	0.32
7	50	252.49	0	0.392	333.68	2.398	20.079	49.830	53.72	0.14
8	50	230.00	0	0.343	314.20	0.848	19.997	48.280	52.26	0.44
9	100	30.00	0	1.086	123.67	-21.155	18.834	26.277	32.33	1.99
10	100	7.08	0	1.849	100.62	13.669	18.835	61.101	63.94	4.88
11	100	344.16	0	0.278	71.18	8.039	19.690	55.471	58.86	0.81
12	100	321.25	0	0.181	40.90	4.423	19.781	51.855	55.50	0.46
13	100	298.33	0	0.139	18.41	2.731	19.800	50.163	53.93	0.25
14	100	275.41	0	0.123	354.37	1.639	19.809	49.071	52.92	0.08
15	100	252.49	0	0.099	336.23	0.720	19.788	48.152	52.06	0.02
16	100	230.00	0	0.093	318.12	0.137	19.776	47.569	51.52	0.10
17	250	30.00	0	0.576	126.46	0.966	19.217	48.398	52.07	0.97
18	250	7.08	0	0.464	103.45	4.471	19.443	51.903	55.43	1.15
19	250	344.16	0	0.072	43.18	2.534	19.723	49.966	53.72	0.19
20	250	321.25	0	0.028	40.21	1.416	19.704	48.848	52.67	0.07
21	250	298.33	0	0.022	22.58	0.878	19.706	48.310	52.17	0.04
22	250	275.41	0	0.021	6.50	0.511	19.709	47.943	51.84	0.03
23	250	252.49	0	0.020	340.03	0.301	19.710	47.733	51.64	0.00
24	250	230.00	0	0.019	322.90	-0.079	19.708	47.353	51.29	0.02
25	500	30.00	0	0.068	122.35	-0.162	19.637	47.270	51.19	0.12
26	500	7.08	0	0.055	103.93	1.945	19.660	49.377	53.15	0.13
27	500	344.16	0	0.015	67.79	0.879	19.691	48.311	52.17	0.04
28	500	321.25	0	0.008	44.29	0.518	19.693	47.950	51.84	0.02
29	500	298.33	0	0.006	24.52	0.335	19.694	47.767	51.67	0.01
30	500	275.41	0	0.006	4.45	0.196	19.695	47.628	51.54	0.01
31	500	252.49	0	0.005	342.33	0.089	19.695	47.521	51.44	0.00
32	500	230.00	0	0.006	321.10	-0.028	19.695	47.404	51.33	0.01

Table 3-19: Magnetic Flux Density, Dowden's Point 320 kV, Bipolar 1% Imbalance Current

Point	Coordinates			Induced Magnetic Flux Density			Resultant Magnetic Flux Density			
	A_ρ [m]	A_Φ [°]	A_z [m]	B_ρ [μT]	B_Φ [°]	B_z [μT]	$B_{res,\rho}$ [μT]	$B_{res,z}$ [μT]	$\lvert B_{res}\rvert$ [μT]	α [°]
1	50	30.00	0	0.030	131.54	-0.530	19.664	46.902	50.86	0.04
2	50	7.08	0	0.054	105.69	0.853	19.659	48.285	52.13	0.13
3	50	344.16	0	0.008	73.31	0.237	19.690	47.669	51.58	0.02
4	50	321.25	0	0.006	49.17	0.129	19.692	47.561	51.48	0.02
5	50	298.33	0	0.005	22.55	0.080	19.694	47.512	51.43	0.01
6	50	275.41	0	0.005	355.67	0.051	19.695	47.483	51.41	0.00
7	50	252.49	0	0.005	333.68	0.030	19.695	47.462	51.39	0.00
8	50	230.00	0	0.004	314.20	0.011	19.694	47.443	51.37	0.01
9	100	30.00	0	0.014	123.67	-0.264	19.679	47.168	51.11	0.02
10	100	7.08	0	0.023	100.62	0.171	19.678	47.603	51.51	0.06
11	100	344.16	0	0.003	71.18	0.100	19.690	47.532	51.45	0.01
12	100	321.25	0	0.002	40.90	0.055	19.691	47.487	51.41	0.01
13	100	298.33	0	0.002	18.41	0.034	19.691	47.466	51.39	0.00
14	100	275.41	0	0.002	354.37	0.020	19.691	47.452	51.38	0.00
15	100	252.49	0	0.001	336.23	0.009	19.691	47.441	51.37	0.00
16	100	230.00	0	0.001	318.12	0.002	19.691	47.434	51.36	0.00
17	250	30.00	0	0.007	126.46	0.012	19.684	47.444	51.37	0.01
18	250	7.08	0	0.006	103.45	0.056	19.687	47.488	51.41	0.01
19	250	344.16	0	0.001	43.18	0.032	19.690	47.464	51.39	0.00
20	250	321.25	0	0.000	40.21	0.018	19.690	47.450	51.37	0.00
21	250	298.33	0	0.000	22.58	0.011	19.690	47.443	51.37	0.00
22	250	275.41	0	0.000	6.50	0.006	19.690	47.438	51.36	0.00
23	250	252.49	0	0.000	340.03	0.004	19.690	47.436	51.36	0.00
24	250	230.00	0	0.000	322.90	-0.001	19.690	47.431	51.36	0.00
25	400	30.00	0	0.001	120.62	-0.002	19.689	47.430	51.35	0.00
26	400	7.08	0	0.001	104.15	0.037	19.689	47.469	51.39	0.00
27	400	344.16	0	0.000	62.85	0.016	19.690	47.448	51.37	0.00
28	400	321.25	0	0.000	41.86	0.009	19.690	47.441	51.37	0.00
29	400	298.33	0	0.000	23.73	0.006	19.690	47.438	51.36	0.00
30	400	275.41	0	0.000	4.48	0.003	19.690	47.435	51.36	0.00
31	400	252.49	0	0.000	342.43	0.001	19.690	47.433	51.36	0.00
32	400	230.00	0	0.000	321.14	-0.001	19.690	47.431	51.36	0.00

Table 3-20: Magnetic Flux Density, Dowden's Point 400 kV, Bipolar 1% Imbalance Current

Point	Coordinates			Induced Magnetic Flux Density			Resultant Magnetic Flux Density			
	A_ρ [m]	A_Φ [°]	A_z [m]	B_ρ [μT]	B_Φ [°]	B_z [μT]	$B_{res,\rho}$ [μT]	$B_{res,z}$ [μT]	$\lvert B_{res}\rvert$ [μT]	α [°]
1	50	30.00	0	0.016	131.54	-0.283	19.676	47.149	51.09	0.02
2	50	7.08	0	0.029	105.69	0.455	19.674	47.887	51.77	0.07
3	50	344.16	0	0.004	73.31	0.126	19.690	47.558	51.47	0.01
4	50	321.25	0	0.003	49.17	0.069	19.691	47.501	51.42	0.01
5	50	298.33	0	0.003	22.55	0.043	19.692	47.475	51.40	0.01
6	50	275.41	0	0.003	355.67	0.027	19.693	47.459	51.38	0.00
7	50	252.49	0	0.003	333.68	0.016	19.693	47.448	51.37	0.00
8	50	230.00	0	0.002	314.20	0.006	19.692	47.438	51.36	0.00
9	100	30.00	0	0.007	123.67	-0.141	19.684	47.291	51.22	0.01
10	100	7.08	0	0.012	100.62	0.091	19.684	47.523	51.44	0.03
11	100	344.16	0	0.002	71.18	0.054	19.690	47.486	51.41	0.01
12	100	321.25	0	0.001	40.90	0.029	19.691	47.461	51.38	0.00
13	100	298.33	0	0.001	18.41	0.018	19.691	47.450	51.37	0.00
14	100	275.41	0	0.001	354.37	0.011	19.691	47.443	51.37	0.00
15	100	252.49	0	0.001	336.23	0.005	19.691	47.437	51.36	0.00
16	100	230.00	0	0.001	318.12	0.001	19.691	47.433	51.36	0.00
17	250	30.00	0	0.004	126.46	0.006	19.687	47.438	51.36	0.01
18	250	7.08	0	0.003	103.45	0.030	19.688	47.462	51.38	0.01
19	250	344.16	0	0.000	43.18	0.017	19.690	47.449	51.37	0.00
20	250	321.25	0	0.000	40.21	0.009	19.690	47.441	51.37	0.00
21	250	298.33	0	0.000	22.58	0.006	19.690	47.438	51.36	0.00
22	250	275.41	0	0.000	6.50	0.003	19.690	47.435	51.36	0.00
23	250	252.49	0	0.000	340.03	0.002	19.690	47.434	51.36	0.00
24	250	230.00	0	0.000	322.90	-0.001	19.690	47.431	51.36	0.00
25	400	30.00	0	0.001	120.62	-0.001	19.689	47.431	51.36	0.00
26	400	7.08	0	0.001	104.15	0.020	19.690	47.452	51.37	0.00
27	400	344.16	0	0.000	62.85	0.008	19.690	47.440	51.36	0.00
28	400	321.25	0	0.000	41.86	0.005	19.690	47.437	51.36	0.00
29	400	298.33	0	0.000	23.73	0.003	19.690	47.435	51.36	0.00
30	400	275.41	0	0.000	4.48	0.002	19.690	47.434	51.36	0.00
31	400	252.49	0	0.000	342.43	0.001	19.690	47.433	51.36	0.00
32	400	230.00	0	0.000	321.14	0.000	19.690	47.432	51.36	0.00

3.2 Chemical and Physical Emissions

3.2.1 **Chemical Emissions**

The objective of this section is to evaluate the electrolysis emissions produced during electrode operations, for both monopolar (maximum continuous current) and bipolar operations (system imbalances). These emissions include chlorine and other by-products at the anode, and hydrogen at the cathode. The section also includes a review of the sensitivity of emissions to temperature, water pH value, water turnover rate, gas exchange at the surface, electrode element material, and electrode element current density.

The analysis of emissions from high silicon chromium chill cast iron electrode elements (elements used predominantly for a pond electrode design) was performed at two sites (LAD North and Dowden's Point) for 320 kV and 400 kV HVdc transmission options. One shoreline pond option for LAD North and two pond options for Dowden's Point were considered. Both anodic and cathodic operation were reviewed for the above six scenarios.

3.2.2 **Anodic and Cathodic Reactions**

The reactions that produce the chemicals of concern in sea or brackish water are listed below, with the main products being chlorine gas (Cl_2), oxygen (O_2), water (H_2O), hydrogen (H_2) and sodium hypochlorite (NaOCl) [9] [11].

Primary Anode Reactions

$2H_2O \rightarrow 4H^+ + O_2(g) + 4e^-$ (1)

$2Cl^- \rightarrow Cl_2(g) + 2e^-$ (2)

Primary Cathode Reaction

$2H_2O + 2e^- \rightarrow 2OH^- + H_2(g)$ (3)

Secondary Anode Reactions

$Cl_2(g) + H_2O \rightarrow HCl + HOCl$ (4)

$HOCl \rightarrow H^+ + OCl^-$ (5)

$OCl^- + Na^+ \rightarrow NaOCl$ (6)

Secondary Cathode Reactions

$OH^- + HCO_3^- \rightarrow CO_3^{2-} + H_2O$ (7)

$Mg^{2+} + 2OH^- \rightarrow Mg(OH)_2$ (8)

$Ca^{2+} + 2OH^- \rightarrow Ca(OH)_2$ (9)

Oxygen evolution at the anode is the preferred reaction since it requires less energy than the chlorine evolution reaction. Chlorine evolution has a selectivity in the range of 5% to 30% for the manufacturer recommended electrode current density. Oxygen evolution selectivity is in the range of 70% to 95%. The selectivity is a function of electrode current density, spacing between the electrode elements and pH value. Chlorine selectivity could exceed 30% if a high current density is used [9], however this is not anticipated.

While these equations represent the individual reactions that take place, the reality is that they take place nearly simultaneously, and also nearly instantaneously. It is likely that the much of the acid (HCl) formed in equation (4) is neutralized by the base (OH^-) formed.

Some of the hydrogen undoubtedly leaves solution, but it is unlikely any chlorine does, unlike in a conventional chloralkali process using concentrated brines.

Tertiary Reactions (Other Pathways)

The hypochlorite solution can then follow a myriad of pathways as shown in Figure 3-14. The figure does not account for chlorine analogs of these compounds which may form at higher concentrations. It is important to note that many of these compounds illustrated have been documented to occur in natural seawater [13].

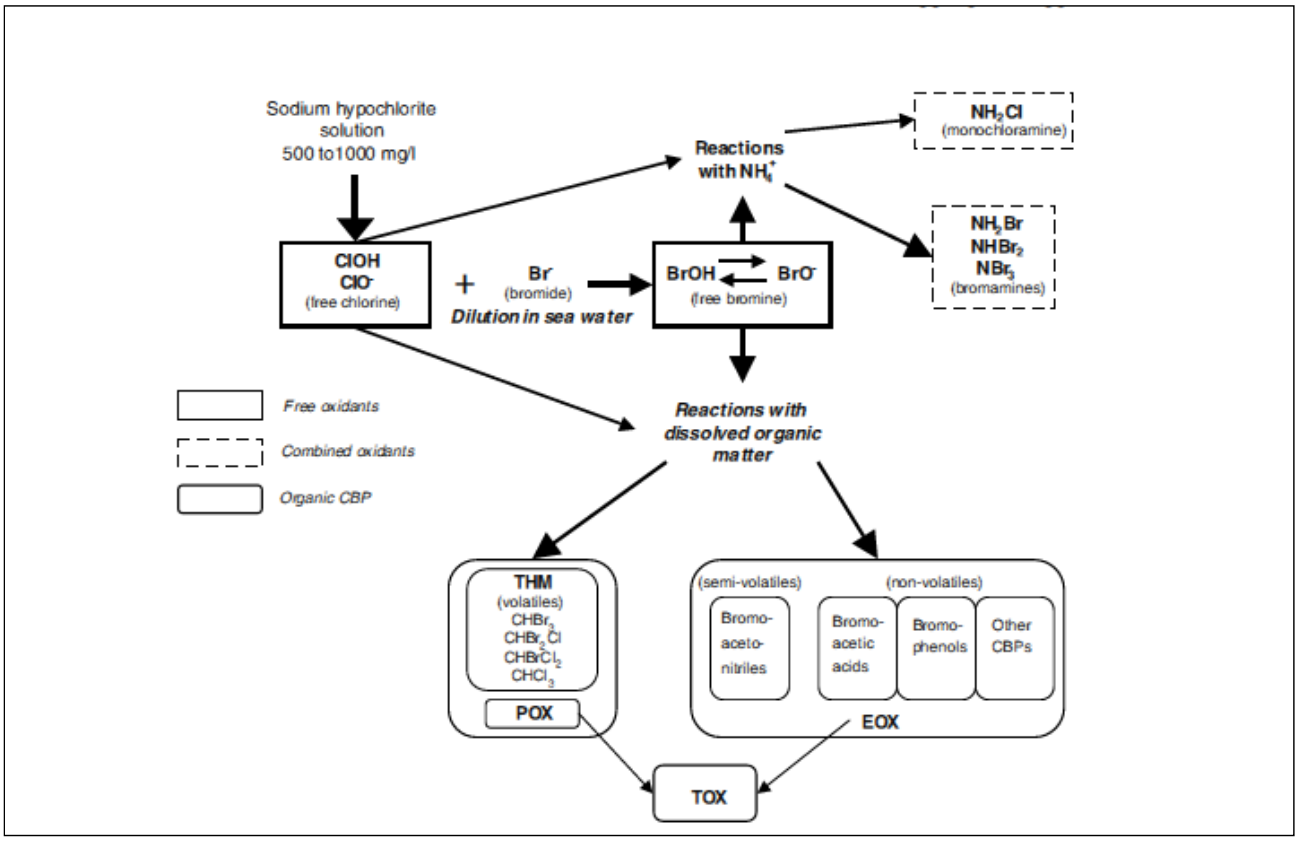

Figure 3-14: Potential Hypochlorite Pathways [14]

3.2.3 Estimates of Products

Primary Reactions

The concentrations of products from reactions (2) and (3) have been estimated based on Faraday's Law (10).

$$n = \frac{(T * I)}{(z * F)} \quad (10)$$

where:

T = Operating time (s).

I = Total current (A).

z = Stoichiometric number of electrons transferred from anodic or cathodic reaction.

F = Faraday constant (96485 C/mol).

n = products evolved (mol/s).

Estimate of Electrode Pond Volumes

To calculate the concentration of the emissions produced in the shoreline electrode ponds, the following estimates of the pond volumes were performed for all design scenarios, presented in Table 3-21.

Table 3-21: Estimates of Low Tide Pond Volumes and Volumes Displaced due to Tidal Flushing

Pond Scenario	Estimated Volume [m^3]	Estimated Surface Area [m^2]	Estimated Volume Displaced in One Half Tide Cycle (6 hrs) [m^3]	Average Flow Rate in One Half Tide Cycle (6 hrs) [L/s]	Remarks
DP Option 1	2.24E+04	9.35E+03	1.27E+04	587	
DP Option 2, 400 kV	2.25E+03	1.13E+03	9.86E+02	46	75 m long, 15 m wide, average depth of 2 m
DP Option 2, 320 kV	2.70E+03	1.35E+03	1.18E+03	55	90 m long, 15 m wide, average depth of 2 m
LAD North Pond	2.92E+04	1.44E+04	8.65E+03	401	

Notes:

1. Estimated volumes consider the low tide water depths.
2. Displaced water volumes and flow rates are considered equal for low-to-high tide transition (6 hours) and high-to-low tide transition (6 hours).
3. Conservative tide levels are considered based on data from Fisheries and Oceans Canada (0.8 m at DP and 0.6 m at LAD N). Tide levels will vary on a daily basis.
4. The flow rates assume unobstructed water flow through the breakwater.
5. Volume displaced considers the surface area of the pond at low tide plus 6500 m^2 accounting for water along slopes of breakwater and shoreline.

Table 3-22 presents the estimated yields for LAD North electrode for anodic and cathodic operation during monopolar operations at maximum continuous current. Table 3-23 presents the estimated yields for LAD North electrode operating during bipolar operations (i.e., system imbalances).

Table 3-24 and Table 3-26 present the estimated yields for Dowden's Point Option 1 (breakwater extended into Conception Bay) and Option 2 (shoreline pond electrode) during monopolar operations at maximum continuous current, respectively. Table 3-25 and Table 3-27 present the estimated yields for Dowden's Point electrode operating during bipolar operations (i.e., system imbalances).

The chlorine estimates below consider a worst case expected selectivity of 30%. For the best case expected selectivity of 5%, the chlorine estimates will be approximately on the order of 17% of the emissions reported in the tables below.

Table 3-22: Emissions Estimates for LAD North, Monopolar Maximum Continuous Current

Variable	Unit	320 kV (Anode)	320 kV (Cathode)	400 kV (Anode)	400 kV (Cathode)
T	s	1	1	1	1
I	A	2109	2109	1688	1688
z	#	2	0.5	2	0.5
F	C/mol	96485	96485	96485	96485
n	mol/s	1.09E-02	4.37E-02	8.75E-03	3.50E-02
n	mol/yr	3.45E+05	1.38E+06	2.76E+05	1.10E+06
Cl_2 (30%)	kg/s	2.32E-04	-	1.86E-04	-
Cl_2 (30%)	kg/yr	7.33E+03	-	5.87E+03	-
H_2 (100%)	kg/s	-	8.83E-05	-	7.07E-05
H_2 (100%)	kg/yr	-	2.78E+03	-	2.23E+03
Pond volume	L	2.92E+07	2.92E+07	2.92E+07	2.92E+07
[Cl_2] one day	g/L	6.89E-04	-	5.51E-04	-
[H_2] one day	g/L	-	2.62E-04	-	2.09E-04

Table 3-23: Emissions Estimates for LAD North, Bipolar 1% Imbalance Current

Variable	Unit	320 kV (Anode)	320 kV (Cathode)	400 kV (Anode)	400 kV (Cathode)
T	s	1	1	1	1
I	A	14.06	14.06	11.25	11.25
z	#	2	0.5	2	0.5
F	C/mol	96485	96485	96485	96485
n	mol/s	7.29E-05	2.91E-04	5.83E-05	2.33E-04
n	mol/yr	2.30E+03	9.19E+03	1.84E+03	7.35E+03
Cl_2 (30%)	kg/s	1.55E-06	-	1.24E-06	-
Cl_2 (30%)	kg/yr	4.89E+01	-	3.91E+01	-
H_2 (100%)	kg/s	-	5.89E-07	-	4.71E-07
H_2 (100%)	kg/yr	-	1.86E+01	-	1.49E+01
Pond volume	L	2.92E+07	2.92E+07	2.92E+07	2.92E+07
[Cl_2] one day	g/L	4.59E-06	-	3.67E-06	-
[H_2] one day	g/L	-	1.74E-06	-	1.40E-06

Table 3-24: Emissions Estimates for Dowden's Point (Extended), Monopolar Maximum Continuous Current

Variable	Unit	320 kV Extended Breakwater (Anode)	320 kV Extended Breakwater (Cathode)	400 kV Extended Breakwater (Anode)	400 kV Extended Breakwater (Cathode)
T	s	1	1	1	1
I	A	2109	2109	1688	1688
z	#	2	0.5	2	0.5
F	C/mol	96485	96485	96485	96485
n	mol/s	1.09E-02	4.37E-02	8.75E-03	3.50E-02
n	mol/yr	3.45E+05	1.38E+06	2.76E+05	1.10E+06
Cl_2 (30%)	kg/s	2.32E-04	-	1.86E-04	-
Cl_2 (30%)	kg/yr	7.33E+03	-	5.87E+03	-
H_2 (100%)	kg/s	-	8.83E-05	-	7.07E-05
H_2 (100%)	kg/yr	-	2.78E+03	-	2.23E+03
Pond volume	L	2.24E+07	2.24E+07	2.24E+07	2.24E+07
[Cl_2] one day	g/L	8.97E-04	-	7.18E-04	-
[H_2] one day	g/L	-	3.41E-04	-	2.73E-04

Table 3-25: Emissions Estimates for Dowden's (Extended), Bipolar 1% Imbalance Current

Variable	Unit	320 kV Extended Breakwater (Anode)	320 kV Extended Breakwater (Cathode)	400 kV Extended Breakwater (Anode)	400 kV Extended Breakwater (Cathode)
T	s	1	1	1	1
I	A	14.06	14.06	11.25	11.25
z	#	2	0.5	2	0.5
F	C/mol	96485	96485	96485	96485
n	mol/s	7.29E-05	2.91E-04	5.83E-05	2.33E-04
n	mol/yr	2.30E+03	9.19E+03	1.84E+03	7.35E+03
Cl_2 (30%)	kg/s	1.55E-06	-	1.24E-06	-
Cl_2 (30%)	kg/yr	4.89E+01	-	3.91E+01	-
H_2 (100%)	kg/s	-	5.89E-07	-	4.71E-07
H_2 (100%)	kg/yr	-	1.86E+01	-	1.49E+01
Pond volume	L	2.24E+07	2.24E+07	2.24E+07	2.24E+07
[Cl_2] one day	g/L	5.98E-06	-	4.78E-06	-
[H_2] one day	g/L	-	2.27E-06	-	1.82E-06

Table 3-26: Emissions Estimates for Dowden's Point (Recessed), Monopolar Maximum Continuous Current

Variable	Unit	320 kV Recessed Breakwater (Anode)	320 kV Recessed Breakwater (Cathode)	400 kV Recessed Breakwater (Anode)	400 kV Recessed Breakwater (Cathode)
T	s	1	1	1	1
I	A	2109	2109	1688	1688
z	#	2	0.5	2	0.5
F	C/mol	96485	96485	96485	96485
n	mol/s	1.09E-02	4.37E-02	8.75E-03	3.50E-02
n	mol/yr	3.45E+05	1.38E+06	2.76E+05	1.10E+06
Cl_2 (30%)	kg/s	2.32E-04	-	1.86E-04	-
Cl_2 (30%)	kg/yr	7.33E+03	-	5.87E+03	-
H_2 (100%)	kg/s	-	8.83E-05	-	7.07E-05
H_2 (100%)	kg/yr	-	2.78E+03	-	2.23E+03
Pond volume	L	2.70E+06	2.70E+06	2.25E+06	2.25E+06
[Cl_2] one day	g/L	7.44E-03	-	7.14E-03	-
[H_2] one day	g/L	-	2.83E-03	-	2.71E-03

Table 3-27: Emissions Estimates for Dowden's Point (Recessed), Bipolar 1% Imbalance Current

Variable	Unit	320 kV Recessed Breakwater (Anode)	320 kV Recessed Breakwater (Cathode)	400 kV Recessed Breakwater (Anode)	400 kV Recessed Breakwater (Cathode)
T	s	1	1	1	1
I	A	14.06	14.06	11.25	11.25
z	#	2	0.5	2	0.5
F	C/mol	96485	96485	96485	96485
n	mol/s	7.29E-05	2.91E-04	5.83E-05	2.33E-04
n	mol/yr	2.30E+03	9.19E+03	1.84E+03	7.35E+03
Cl_2 (30%)	kg/s	1.55E-06	-	1.24E-06	-
Cl_2 (30%)	kg/yr	4.89E+01	-	3.91E+01	-
H_2 (100%)	kg/s	-	5.89E-07	-	4.71E-07
H_2 (100%)	kg/yr	-	1.86E+01	-	1.49E+01
Pond volume	L	2.70E+06	2.70E+06	2.25E+06	2.25E+06
[Cl_2] one day	g/L	4.96E-05	-	4.76E-05	-
[H_2] one day	g/L	-	1.88E-05	-	1.81E-05

Secondary Reactions

The secondary reactions consist of primary products reacting with sea water and elements in the sea water to produce hypochlorites. The reactions involved are shown in reactions (4) through (9).

Reaction (4) in seawater (average pH ≈ 8) will tend to move to the right [9] yielding a minimum amount of Cl_2 at equilibrium and a large amount of product (HCl and HOCl).

Reaction (5) will have a similar result. Using the $K_{eq} = 3.5 \times 10^{-8}$ and taking $[H^+] = 10^{-8}$ for ambient seawater, then the ratio of the concentration of [HOCl] to [OCl^-] can be calculated from the equilibrium equation:

K_{eq} = [Products]/[Reactants]

$$K_{eq} = \frac{[H^+] * [OCl^-]}{[HOCl]} \qquad (11)$$

NaOCl (occurring when free Na^+ reacts with OCl^-) will be the main chemical of concern in the electrode reactions. This product in laboratory studies, however, degrades rapidly in seawater with a half-life (t_{50}) of one hour [13]. It is difficult to predict the emissions associated with these reactions further.

Tertiary Reactions

As can be seen from Figure 3-14, the tertiary reactions can follow a number of different pathways that are not easy to predict. These reactions are dependent upon numerous variables and characteristics of the water including but not limited to: water temperature, pH, salinity, light penetration, current density, dissolved organic matter concentrations, and coordination complexes (ligands and chelates).

3.2.4 Emission Losses to Gas Exchange

An increase in gas exchange between the pond and the ocean, and between the pond and air could have several effects on the anode products. For example, more of the H_2 gas from reaction (3) and Cl_2 gas from reaction (2) could be released into the air. The reduction in chlorine will then decrease the residual chlorine concentration in the water column, and therefore potentially reduce the amount of toxic chlorinated byproducts. Using Faraday's Law to calculate chlorine and hydrogen yield [9], the calculations presented are based on assumed Standard Temperature and Pressure (20° C, 1 atm).

Gas Exchange between Pond and Ocean

The gas exchange between the two water bodies is dependent upon three processes: diffusion (Fick's First Law), advection (Fick's Second Law), and turbulent mixing (Fick's Second Law). Molecular diffusion has a relatively minor effect compared to advection and turbulent mixing [15]. The exact effect of gas exchange between the pond and the ocean is not presented in this report as it would require detailed modelling. Based on Fick's First and Second Laws, there will be an increase in chlorine exchange (i.e., more dilution of chlorine in the pond) with an increase in water flow (advection), turbulence, and chlorine concentration gradient between the two water bodies.

Gas Exchange between Pond and Air

The gas exchange between the pond and the air is dependent upon Fick's First and Second Laws and can be described in terms of a diffusion film model with two diffusion films, one in liquid phase and one in the gas phase [16]. This again is controlled by the molecular diffusion coefficient of the compound and the concentration gradient between the water column and the air, wind, and water surface disturbance (e.g., waves, tides). It should be noted that gas exchange between the pond and the air will be severely curtailed if ice is present.

3.2.5 Effect of Tidal Flushing on Emission Estimates

As the chemical of concern is chlorine, only residual chlorine is considered in this section. Tables 3-22 to 3-27 provide conservative estimates and do not take into consideration the tidal flushing between the pond water and the ocean (twice per day), chlorine evaporating from the pond into the atmosphere, chlorine escaping into the sea through the breakwater permeable zone due to concentration differential, and chlorine reaction with water. In addition, the shoreline pond volumes are conservative estimates based on the conceptual breakwater plans and sections proposed, and consider the pond depths at low tide; the actual shoreline pond volumes considered in the design of the LAD North and Dowden's Point electrodes are larger than those stated in the tables. Therefore the concentrations of chlorine and hydrogen in the pond will be lower than the conservative values presented in Tables 3-22 to 3-27.

This section analyzes the effect of tidal flushing on the chlorine concentration in each of the design scenarios. The tidal flushing rates have been estimated and concentrations within the pond are presented. The calculations presented in the table have been simplified and do not take into account accumulative iterative dilutions.

Table 3-28 presents the chlorine concentrations associated with monopolar operations at maximum continuous current, followed by Table 3-29 which presents the chlorine concentrations associated with bipolar operations.

Table 3-28: Chlorine Estimates considering Tidal Flushing, Monopolar Maximum Continuous Current

Site	Current (A)	Cl_2 Produced (kg/day)	Volume of Pond (L)	Estimated Tidal Flushing (L/s)	Estimated chlorine concentration without flushing $[Cl_2]_{w/o\ Flushing}$ (g/L)	Estimated chlorine concentration with flushing $[Cl_2]_{w/\ Flushing}$ (g/L)
LAD North(320 kV)	2109	20.1	2.92E+07	401	6.89E-04	3.15E-04
LAD North (400 kV)	1688	16.1	2.92E+07	401	5.51E-04	2.52E-04
Dowden's Point (320 kV) Extended Breakwater	2109	20.1	2.24E+07	587	8.97E-04	2.75E-04
Dowden's Point (400 kV) Extended Breakwater	1688	16.1	2.24E+07	587	7.18E-04	2.20E-04
Dowden's Point (320 kV) Recessed Breakwater	2109	20.1	2.70E+06	55	7.44E-03	2.70E-03
Dowden's Point (400 kV) Recessed Breakwater	1688	16.1	2.25E+06	46	7.14E-03	2.58E-03

Table 3-29: Chlorine Estimates considering Tidal Flushing, Bipolar 1% Imbalance Current

Site	Current (A)	Cl_2 Produced (kg/day)	Volume of Pond (L)	Estimated Tidal Flushing (L/s)	Estimated chlorine concentration without flushing $[Cl_2]_{w/o\ Flushing}$ (g/L)	Estimated chlorine concentration with flushing $[Cl_2]_{w/\ Flushing}$ (g/L)
LAD North(320 kV)	14.06	0.13	2.92E+07	401	4.59E-06	2.10E-06
LAD North (400 kV)	11.25	0.11	2.92E+07	401	3.67E-06	1.68E-06
Dowden's Point (320 kV) Extended Breakwater	14.06	0.13	2.24E+07	587	5.98E-06	1.83E-06
Dowden's Point (400 kV) Extended Breakwater	11.25	0.11	2.24E+07	587	4.78E-06	1.47E-06
Dowden's Point (320 kV) Recessed Breakwater	14.06	0.13	2.70E+06	55	4.96E-05	1.80E-05
Dowden's Point (400 kV) Recessed Breakwater	11.25	0.11	2.25E+06	46	4.76E-05	1.72E-05

3.2.6 **Emission Sensitivities to Other Environmental Factors**

The concentration and ratio of the products may change based on environmental conditions such as changes in pH, light, gas exchange at the water surface, water temperature, electrode element type, and current density of electrode elements. According to Poleo and others [11], the proportion of Cl_2 versus O_2 formed at the anode depends primarily on current density, and secondarily on water temperature, salinity, and electrode material. A qualitative review of some of these parameters in relation to chlorine production is presented below.

Current Density

Increasing the electrode size (i.e., reducing the current density) would reduce the concentrations of the contaminants, and reduce the selectivity of chlorine evolution at the anode. The current densities recommended by the manufacturer for anodic operation does not result in chlorine evolution sensitivity higher than 30%; however, an exceptionally higher current density could result in higher chlorine evolution selectivity [9]. Current density also affects the ground potential rise (GPR) at the electrode; a higher current density results in higher GPR and GPR gradient in the electrode vicinity.

pH

As H^+ ions are a product of reaction (1), an increase in ambient H^+ (decreased pH) will tend to push the reaction backwards with less oxygen gas production. For secondary reactions, an increase in H^+ ions will tend to push reaction (8) to the left and less free OCl^- will be produced and more Cl_2 will remain as gas and diffuse out of the water column. This in turn, will reduce the amount of sodium hypochlorite produced (9). It is important to note, however, that the existing carbonate in the seawater will buffer any effects that the reaction has on the pH [9]. For seawater, pH is normally ~8.

Light

Hypochlorite may be converted to chloride ions and oxygen gas under the influence of ultraviolet light [11]. This would essentially take the chlorine out of the marine system.

Water Temperature

Temperature could affect the chlorine production and toxicity in opposing ways. Increased temperature will increase molecular diffusion and gas exchange across the air-water interface with similar effects to what is described directly above taking more of the chlorine out of the system. Increased temperature, however, has also been shown to increase chlorine toxicity in laboratory studies [14]. As mentioned above, it is assumed that the calculations presented here are based on Standard Temperature and Pressure (20° C, 1 atm).

Electrode Material

A number of materials are suitable for the anode (graphite/carbon, high silicon iron, magnetite and mixed metal oxide) and the cathode (graphite/carbon, high silicon iron, and copper) elements. The key consideration for the anode is the selectivity of chlorine for a particular element type. Mixed metal oxide elements can be designed for low chlorine selectivity but are not suitable for a typical pond installation [9].

3.2.7 Physical Emissions

The only physical emission considered in the analysis was the dissipation of energy in the form of heat. The heat loss calculations are theoretical and wherever assumptions were made, these were pessimistic.

The energy produced at the electrode is directly proportional to the current flowing into or out of the electrode and to the resistivity of the medium surrounding the electrode. Heat dissipation densities through the breakwater were calculated for both system voltage scenarios (320 kV and 400 kV) and for the duties of all three electrode operating modes for monopolar operations (nominal, maximum continuous and maximum 10 minutes) and during bipolar operations (1% of the current during normal operations accounting for system imbalances). Also the worst case heat dissipation through the seawater density was calculated at the seaside interface of the breakwater. The minimum area of breakwater required to achieve a safe voltage gradient is the only section considered in the analysis; in reality the breakwater surface area will be larger than the area considered on the sea side and the heat dissipation density will be proportionally lower. Also as a conservative

approach, 100% of the current in each case is assumed to flow through the minimum breakwater section in question and the water in the pond and sea side. In reality, some current will flow through the adjacent sections of the breakwater and some will flow inland.

The voltage gradient across the breakwater is established by multiplying the equivalent resistivity of the breakwater by the current density at the section of the breakwater.

Table 3-30 presents the volumetric heat dissipation through the breakwater for both LAD North and Dowden's Point, and Table 3-31 presents the volumetric heat dissipation in the seawater.

Table 3-30: Volumetric Heat Dissipation through the Breakwater

Location	System Voltage	$H_{bw, nom}$ Nominal (W/m^3)	$H_{bw, cont}$ Max, Continuous (W/m^3)	$H_{bw, 10 min.}$ Max, 10 Minute (W/m^3)	$H_{bw, 1\% imb}$ 1% imbalance (W/m^3)
LAD North	320 kV	13.7	30.8	54.8	0.001
LAD North	400 kV	8.8	19.7	35.1	0.001
Dowden's Point (Extended)	320 kV	< 14.4	< 32.5	< 57.8	< 0.001
Dowden's Point (Extended)	400 kV	< 14.4	< 32.5	< 57.7	< 0.001
Dowden's Point (Recessed)	320 kV	14.4	32.5	57.8	0.001
Dowden's Point (Recessed)	400 kV	< 14.4	< 32.5	< 57.7	< 0.001

Table 3-31: Volumetric Heat Dissipation in the Sea and Pond at the Breakwater

Location	System Voltage	$H_{sw, nom}$ Nominal (W/m^3)	$H_{sw, cont}$ Max, Continuous (W/m^3)	$H_{sw, 10 min.}$ Max, 10 Minute (W/m^3)	$H_{sw, 1\% imb}$ 1% imbalance (W/m^3)
LAD North	320 kV	1.8	4.0	7.1	< 0.001
LAD North	400 kV	1.1	2.6	4.6	< 0.001
Dowden's Point (Extended)	320 kV	< 1.8	< 4.1	< 7.8	< 0.001
Dowden's Point (Extended)	400 kV	< 1.8	< 4.1	< 7.8	< 0.001
Dowden's Point (Recessed)	320 kV	1.8	4.1	7.8	< 0.001
Dowden's Point (Recessed)	400 kV	< 1.8	< 4.1	< 7.8	< 0.001

The heat volumetric heat dissipation in the sea away from the breakwater will be insignificant because of the large water cross-section. The heat dissipation in the breakwater and in the pond results in heat gain in the pond water and this heat gain tends to increase the pond water temperature. The pond water temperature rise was estimated using a conservative approach assuming,

- Half of the heat dissipated in the breakwater is gained by the pond and the other half by the sea body of water. The elements are installed on the breakwater and heat dissipation in the pond water is minor.
- Heat is exchanged between the pond and the sea body of water as a result of tidal flushing only. Conductive, radiation and evaporation losses of the heat are not considered.

Table 3-32 presents the summary of the temperature rise in the ponds for LAD North and Dowden's Point for the maximum monopolar continuous current.

Table 3-32: Estimated Maximum Temperature Rise in Pond, Monopolar Maximum Continuous Current

Location	System Voltage	Estimated Maximum Temperature Rise in Pond [°C]
LAD North	320 kV	0.47
LAD North	400 kV	0.37
Dowden's Point (Extended)	320 kV	0.33
Dowden's Point (Extended)	400 kV	0.26
Dowden's Point (Recessed)	320 kV	3.51
Dowden's Point (Recessed)	400 kV	3.36

The temperature rises are less than 0.5°C, except for the recessed pond option at Dowden's Point which has a smaller pond volume. The actual temperature rise in the ponds will be lower than the temperature reported here because the conductive heat loss to the sea and evaporation are not considered in the analysis. The breakwater temperature rise will be less than the temperature rise of the pond.

The heat dissipated into the sea body of water is small and the temperature rise of the water adjacent to the breakwater will not be noticeable. An efficient mixing due to wave action is expected.

4.0 SUMMARY

4.1 L'Anse au Diable North Electrode

For L'Anse au Diable North electrode, the key design data, modelling and effects include:

- The number of high silicon chromium chill cast iron electrode elements required is 60 for the 320 kV scenario and 48 for the 400 kV scenario.
- The proposed breakwater is approximately 205 m along the centerline and is sized to meet the safety limits for marine life and humans. The permeable zone of the breakwater will consist of stones in the range of 0.5 m to 1.0 m in diameter. The pond water exchange rate is estimated to be 401 L/s due to tidal flushing.
- The calculated dc stray currents through the transformer windings of the distribution circuit near LAD North associated with monopolar operation of the electrode are lower than the permissible limits. The calculated dc stray currents through the pole grounding rods of this distribution network are higher than the permissible level for a few pole grounding rods near the shoreline pond electrode. Corrosion of the grounding rods is not a major concern because the rods can be inspected and replaced as required. The dc stray currents associated with the bipolar operation are insignificant and will not affect the infrastructure.
- The zone extending into the sea in which the magnetic compass deviation exceeds 0.5° as a result of maximum continuous electrode operation is limited to 500 m from the electrode for the 320 kV and 400 kV scenarios; the induced horizontal magnetic field interacts with earth horizontal magnetic field (13.6 A/m at LAD N location) and the resultant horizontal magnetic field deviates from the true magnetic north which is the cause of compass deviation. During normal bipolar operation, the compass deviation is estimated to be less than 0.1° at a distance of 100 m from the electrode.
- The estimated difference between the resultant magnetic field at the surface of the sea and that of the earth's natural magnetic field (53.6 µT near LAD North) is less than 0.8 µT and 0.6 µT at a distance of 500 m from the electrode for the continuous maximum currents of the 320 kV and 400 kV scenarios, respectively. During normal bipolar operation, the estimated difference is less than 0.2 µT and 0.1 µT at a distance of 50 m from the electrode for the 320 kV and 400 kV scenarios, respectively.
- When operating at maximum continuous duty as an anode, the estimated chlorine produced per day is 6.89×10^{-4} g/L for the 320 kV scenario and 5.51×10^{-4} g/L for the 400 kV scenario, assuming the worst case chlorine selectivity of 30%. For operation as a cathode, the estimated hydrogen produced per day is 2.62×10^{-4} g/L for the 320 kV scenario and 2.09×10^{-4} g/L for the 400 kV scenario, assuming 100% hydrogen selectivity. It is important to note these values do not consider gas exchange with the air or through the breakwater.
- When operating as an anode during normal bipolar operation and assuming a current imbalance of 1% of the nominal electrode duty, the estimated chlorine produced per day is 4.59×10^{-6} g/L for the 320 kV scenario and 3.67×10^{-6} g/L for the 400 kV scenario, assuming the worst case chlorine selectivity of 30%. For operation as a cathode during normal bipolar operation, the estimated hydrogen produced per day is 1.74×10^{-6} g/L for the 320 kV scenario and 1.40×10^{-6} g/L for the 400 kV scenario, assuming 100% hydrogen selectivity. These values do not consider gas exchange with the air or through the breakwater or account for tidal flushing.

- Tidal flushing continuously reduces the emission concentrations in the pond. The expected maximum chlorine concentration from a day of electrode operation as anode is 3.15 x 10^{-4} g/L for 320 kV scenario and 2.52 x 10^{-4} g/L for 400 kV scenario. During the bipolar operation, the expected chlorine concentration is 2.10x10^{-6} g/L and 1.68 x10^{-6} for the 320 kV and 400 kV scenarios respectively. The values do not consider gas exchange with the air or exchange with the sea water due to concentration differential.
- At the maximum continuous electrode current duties, the heat emissions from the electrode for the 320 kV scenario will be less than 4.0 W/m^3 in the water in contact with the breakwater on the sea and the pond side, and 30.8 W/m^3 in the breakwater. The corresponding temperature rise in the pond will be less than 0.5°C. The corresponding dissipation levels for the 400 kV scenario are expected to be approximately 64% of the 320 kV scenario levels. During normal bipolar operation, assuming a current imbalance of 1% of the nominal electrode duty, the heat emissions are expected to be 0.01% of the values stated above.

4.2 Dowden's Point Electrode

For Dowden's Point electrode, the key design data, modelling and effects include:

- The number of high silicon chromium chill cast iron elements required is 60 for the 320 kV scenario and 48 for the 400 kV scenario.
- Option 1: The size of the extended breakwater option is selected to meet the safety criteria and the length of the breakwater along the centerline is approximately 385 m. The land side toe of the breakwater is approximately 79 m from the shoreline and the sea side toe is approximately 129 m from the shoreline. The stone size of the permeable zone will be in the range of 0.5 m to 1.0 m in diameter and the pond water exchange rate due to tidal flushing is estimated to be 587 L/s.
- Option 2: The length of the recessed breakwater measures 90 m for the 320 kV scenario and 75 m for the 400 kV scenario. In this option, the seabed needs to be excavated to a depth of 4 m in the pond and on the sea side of the breakwater to meet the electrical and safety requirements. The permeable zone stone size will be 0.5 m to 1.0 m in diameter and the pond water exchange rate is estimated to be 55 L/s for the 320 kV scenario and 46 L/s for the 400 kV scenario.
- The calculated dc stray currents associated with the electrode operation through the transmission infrastructure equipment and structures adjacent to the electrode locations or connected via transmission lines are less than the published permissible values for both options. The dc stray currents associated with the bipolar operation are insignificant and will not affect the infrastructure.
- The zone extending into the sea in which the magnetic compass deviation exceeds 0.5° as a result of maximum continuous electrode operation is limited to 500 m from the electrode for the 320 kV and 400 kV scenarios. During normal bipolar operation, the compass deviation is estimated to be less than 0.1° at a distance of 100 m from the electrode.
- The estimated difference between the resultant magnetic field at the surface of the sea and that of the earth's natural magnetic field (51.4 µT near Dowden's Point) is less than 2.2 µT and 1.9 µT at a distance of 500 m from the electrode for the continuous maximum currents of the 320 kV and 400 kV scenarios, respectively. During normal bipolar operation, the estimated difference is less than 0.3 µT and 0.2 µT at a distance of 100 m from the electrode for 320 kV and 400 kV scenarios, respectively.

- When operating at maximum continuous duty as an anode, the estimated chlorine produced in the extended pond option (Option 1) per day is 8.97 x 10^{-4} g/L for the 320 kV scenario and 7.18 x 10^{-4} g/L for the 400 kV scenario, assuming the worst case chlorine selectivity of 30%. For operation as a cathode, the estimated hydrogen produced per day is 3.41 x 10^{-4} g/L for the 320 kV scenario and 2.73 x 10^{-4} g/L for the 400 kV scenario, assuming 100% hydrogen selectivity. These values do not consider the gas exchange with the air or through the breakwater.

- When operating at maximum continuous duty as an anode, the estimated chlorine produced in the recessed pond option (Option 2) per day is 7.44 x 10^{-3} g/L for the 320 kV scenario and 7.14 x 10^{-3} g/L for the 400 kV scenario, assuming the worst case chlorine selectivity of 30%. When operating at maximum continuous duty as a cathode, the estimated hydrogen produced per day is 2.83 x 10^{-3} g/L for the 320 kV scenario and 2.71 x 10^{-3} g/L for the 400 kV scenario, assuming 100% hydrogen selectivity. It is important to note these values do not consider gas exchange with the air or through the breakwater.

- When operating as an anode during normal bipolar operation, the estimated chlorine produced in the extended pond option (Option 1) per day is 5.98 x 10^{-6} g/L for the 320 kV scenario and 4.78 x 10^{-6} g/L for the 400 kV scenario, assuming the worst case chlorine selectivity of 30%. For operation as a cathode, the estimated hydrogen produced per day is 2.27 x 10^{-6} g/L for the 320 kV scenario and 1.82 x 10^{-6} g/L for the 400 kV scenario, assuming 100% hydrogen selectivity. These values do not consider gas exchange with the air or through the breakwater or account for tidal flushing.

- When operating as an anode during normal bipolar operation, the estimated chlorine produced in the recessed pond option (Option 2) per day is 4.96 x 10^{-5} g/L for the 320 kV scenario and 4.76 x 10^{-5} g/L for the 400 kV scenario, assuming the worst case chlorine selectivity of 30%. When operating as a cathode, the estimated hydrogen produced in the recessed pond option per day is 1.88 x 10^{-5} g/L for the 320 kV scenario and 1.81 x 10^{-5} g/L for the 400 kV scenario, assuming 100% hydrogen selectivity. These values do not consider gas exchange with the air or through the breakwater or account for tidal flushing.

- Tidal flushing continuously reduces the gas concentration in the pond. For the extended breakwater option (Option 1) when operating at maximum continuous duty as an anode, the expected maximum chlorine concentration in one day is 2.75 x 10^{-4} g/L for 320 kV scenario and 2.20 x 10^{-4} g/L for 400 kV scenario. For the recessed breakwater option (Option 2) the expected maximum chlorine concentration in one day is 2.70 x 10^{-3} g/L for 320 kV scenario and 2.58 x 10^{-3} g/L for 400 kV scenario. The values do not consider gas exchange with the air or exchange with the sea water due to concentration differential.

- For the extended breakwater option (Option 1) during normal bipolar operation as an anode, the expected maximum chlorine concentration in one day considering the tidal flushing is 1.83 x 10^{-6} g/L for 320 kV scenario and 1.47 x 10^{-6} g/L for 400 kV scenario. For the recessed breakwater option (Option 2), the expected maximum chlorine concentration in one day is 1.80 x 10^{-5} g/L for 320 kV scenario and 1.72 x 10^{-5} g/L for 400 kV scenario. The values do not consider gas exchange with the air or exchange with the sea water due to concentration differential.

- At the maximum continuous electrode current duties, the heat emissions from the recessed electrode for the 320 kV scenario will be less than 4.1 W/m^3 in the water in contact with the breakwater on the sea and the pond side, and at most 32.5 W/m^3 in the breakwater for 320 kV and 400 kV scenarios. The heat loss for the extended breakwater option will be lower than the values for the recessed breakwater because of larger breakwater area in contact with the sea. The corresponding temperature rise from electrode operation only in the pond will not exceed 0.5°C for the extended breakwater option, and will not exceed 4°C for the recessed breakwater option. During normal bipolar operation, assuming a

current imbalance of 1% of the nominal electrode duty, the heat emissions from the electrode is expected to be 0.03% of the values stated above.

5.0 REFERENCES

1. Hatch Ltd., "DC1500 – Electrode Review – Confirmation of Types and Site Selection", December 2010.
2. Hatch Ltd., "DC1250 – Electrode Review – Types and Location", March 2010.
3. Kimbark, E.W., "Direct Current Transmission, Vol. 1", Wiley Interscience, 1971.
4. CIGRÉ Working Group 14.21 – TF2, "General Guidelines for the Design of Ground Electrodes for HVDC Links", July 1998.
5. EPRI EL-2020, Project 1467-1, "HVDC Ground Electrode Design", August 1981.
6. Canadian Hydrographic Service, Bathymetric Chart 4020, "Newfoundland and Labrador, Strait of Belle Isle".
7. Canadian Hydrographic Service, Bathymetric Chart 4847, "Newfoundland, Southeast Coast, Conception Bay."
8. EPRI, TR-100450, "Proceedings: Geomagnetically Induced Current Conference", June 1992.
9. Tykeson, K., A. Nyman, and H. Carlsson, 1996, Environmental and Geographical Aspects in HVdc Electrode Design. IEEE Transactions on Power Delivery, v. 11, p. 1948-1954.
10. National Geospatial-Intelligence Agency, Handbook of Magnetic Compass Adjustment, Bethesda, MD, 2004.
11. Poleo, A. B. S., H. F. Johannessen and M. Harboe Jr., 2001. High Voltage Direct Current (HVDC) Sea Electrodes: Effects on Marine Life. Department of Biology, University of Oslo.
12. Dalziel, C.F., "The Threshold of Perception Currents", IEEE Paper 54-209, No. 13, June 1954.
13. Lopez-Galindo, C., M. C. Garrido, J. F. Casanueva, and E. Nebot, 2010, Degradation models and ecotoxicity in marine waters of two antifouling compounds: Sodium hypochlorite and an alkylamine surfactant.: Scie. Tot. Environ., v. 408, p. 1779-1785.
14. Taylor, C. J. L., 2006, The effects of biological fouling control at coastal and estuarine power stations. Mar. Poll. Bull., v. 53, p. 30-48.
15. Libes, S. M., 1992, An introduction to marine biogeochemistry. Toronto, John Wiley & Sons, Inc.
16. Stumm, W., and J. J. Morgan, 1996, Aquatic chemistry: chemical equilibria and rates in natural waters. Toronto, John Wiley & Sons, Inc.
17. Kirschvink. J.L. 1980. South Seeking Magnetic Bacteria. Journal of Experimental Biology. 86: 345-347.
18. Bazylinski, D.A., D.R. Schlezinger, B.H. Howes, R.B. Frankel and S.S. Epstein. 2000. Occurrence and Distribution of Diverse Populations of Magnetic Protists in a Chemically Stratified Coastal Salt Pond. Chemical Geology. 169: 319-328. DOI:10.1016/S0009-2541(00)(00211-4).
19. Lohmann, K.J. and A.O.D. Willows. 1987. Lunar-modulated Geomagnetic Orientation by a Marine Mollusk. Science. 235: 331-334.
20. Lohmann, K.J., N.D. Pentcheff, G.A. Nevitt, G.D. Stetten, R.K. Zimmer-Faust, H.E. Jarrard and L.C. Boles. 1995. Magnetic Orientation of Spiny Lobsters in the Ocean: Experiments with Undersea Coil Systems. The Journal of Experimental Biology. 198: 2041-2048.
21. Riveros, A.J and R.B. Srygley. 2010. Magnetic Compasses in Insects. Encyclopedia of Animal Behaviour. 2: 305-313.
22. Walker, M.M. 1984. Learned Magnetic Field Discrimination in Yellowfin Tuna, Thunnus albacares. Journal of Comparative Physiology A. 155: 673-679.

23. Diego-Rasilla, F.J., R.M. Luengo and J.B. Phillips. 2010. Light-dependent Magnetic Compass in Iberian Green Frog Tadpoles. Naturwissenschaften. 97: 1077-1088.

24. Goff, M., M. Salmon and K.J. Lohmann. 1995. The Magnetic Compass of Loggerhead Sea Turtle Hatchlings: Calibration by Surface Waves. In Proceedings of the Fifteenth Annual Symposium on Sea Turtle Biology and Conservation. NOAA Technical memorandum NMFS-SEFCS-387. p. 105.

25. Wiltschko, R., D. Gehring, S. Denzau and O. Güntürkün. 2010. Interaction of Magnetite Based Receptors in the Beak with the Visual System Underling 'Fixed Direct' Responses in Birds. Frontiers in Zoology. 7: 24-29.

26. Kirschvink, J.L., A.E. Dizon and J.A. Westphal. 1986. Evidence from Strandings for Geomagnetic Sensitivity in Cetaceans. Journal of Experimental Biology. 120: 1-24.

27. Hugh G. Miller P. Geo. February 2011. L'Anse au Diable, Ground Potential Simulation for EIS suggested Models.

28. Hugh G. Miller P. Geo. February 2011. Dowden's Point Electrode, Ground Potential Simulation for EIS suggested Models.